Structures Research
Report 2014/101350-
102056

University of Florida
Civil and Coastal Engineering

University of Florida
Civil and Coastal Engineering

Final Report April 2014

Determination of Brace Forces Caused by Construction Loads and Wind Loads During Bridge Construction

Principal investigators:
Gary R. Consolazio, Ph.D.

Graduate research assistant:
Samuel T. Edwards

Department of Civil and Coastal Engineering
University of Florida
P.O. Box 116580
Gainesville, Florida 32611

Sponsor:
Florida Department of Transportation (FDOT)

Contract:
UF Project Nos. 101350 and 102056
FDOT Contract No. BDK75-977-70

DISCLAIMER

The opinions, findings, and conclusions expressed in this publication are those of the authors and not necessarily those of the State of Florida Department of Transportation.

SI (MODERN METRIC) CONVERSION FACTORS

*APPROXIMATE CONVERSIONS **TO** SI UNITS*

SYMBOL	WHEN YOU KNOW	MULTIPLY BY	TO FIND	SYMBOL
LENGTH				
in	inches	25.4	millimeters	mm
ft	feet	0.305	meters	m
yd	yards	0.914	meters	m
mi	miles	1.61	kilometers	km
AREA				
in^2	square inches	645.2	square millimeters	mm^2
ft^2	square feet	0.093	square meters	m^2
yd^2	square yard	0.836	square meters	m^2
ac	acres	0.405	hectares	ha
mi^2	square miles	2.59	square kilometers	km^2
VOLUME				
fl oz	fluid ounces	29.57	milliliters	mL
gal	gallons	3.785	liters	L
ft^3	cubic feet	0.028	cubic meters	m^3
yd^3	cubic yards	0.765	cubic meters	m^3
NOTE: volumes greater than 1000 L shall be shown in m^3				
MASS				
oz	ounces	28.35	grams	g
lb	pounds	0.454	kilograms	kg
T	short tons (2000 lb)	0.907	Megagrams	Mg (or "t")
TEMPERATURE (exact degrees)				
^oF	Fahrenheit	5(F-32)/9 or (F-32)/1.8	Celsius	^oC
ILLUMINATION				
fc	foot-candles	10.76	lux	lx
fl	foot-Lamberts	3.426	$candela/m^2$	cd/m^2
FORCE and PRESSURE or STRESS				
kip	1000 pounds force	4.45	kilonewtons	kN
lbf	pounds force	4.45	newtons	N
lbf/in^2	pounds force per square inch	6.89	kilopascals	kPa
psf	pounds force per square foot	47.88	pascals	Pa

1. Report No.	2. Government Accession No.	3. Recipient's Catalog No.

4. Title and Subtitle	5. Report Date
Determination of Brace Forces Caused by Construction Loads and Wind Loads During Bridge Construction	April 2014
	6. Performing Organization Code
Gary R. Consolazio, Samuel T. Edwards	8. Performing Organization Report No. 2014/101350-102056
9. Performing Organization Name and Address University of Florida Department of Civil and Coastal Engineering 365 Weil Hall, P.O. Box 116580 Gainesville, FL 32611-6580	10. Work Unit No. (TRAIS)
	11. Contract or Grant No. BDK75-977-70
12. Sponsoring Agency Name and Address Florida Department of Transportation Research Management Center 605 Suwannee Street, MS 30 Tallahassee, FL 32399-0450	13. Type of Report and Period Covered Final Report May 2012 – April 2014
	14. Sponsoring Agency Code

15. Supplementary Notes

16. Abstract

The first objective of this study was to develop procedures for determining bracing forces during bridge construction. Numerical finite element models and analysis techniques were developed for evaluating brace forces induced by construction loads acting on precast concrete girders (Florida-I Beams) in systems of multiple girders braced together. A large-scale parametric study was performed with both un-factored (service) and factored (strength) construction loads (in total, more than 600,000 separate three-dimensional (3-D) structural analyses were conducted). The parametric study included consideration of different Florida-I Beam cross-sections, span lengths, girder spacing, deck overhang widths, skew angles, number of girders, number of braces, and bracing configurations (K-brace and X-brace). Additionally, partial coverage of wet (non-structural) concrete load and variable placement of deck finishing machine loads were considered. A MathCad calculation program was developed for quantifying brace forces using a database approach that employs multiple-dimensional linear interpolation. The accuracy of the database program was assessed by using it to predict end-span and intermediate-span brace forces for parameter selections not directly contained within the database, and then comparing the interpolated predictions to results obtained from finite element analyses of corresponding verification models. In a majority of cases, the database-predicted brace forces were found to be less than ten percent (10%) in error.

The second objective of this study was to experimentally determine wind load coefficients (drag, torque, and lift) for common bridge girder shapes with stay-in-place (SIP) formwork and overhang formwork in place, and then to develop recommended global (system) pressure coefficients (e.g., for strength design of substructures). Wind tunnel tests were performed on reduced-scale models of Florida-I Beam (FIB), plate girder, and box girder cross-sectional shapes to measure aerodynamic forces acting on individual girders in the bridge cross-section. Tests were conducted at multiple wind angles, and corresponding tests with and without overhang formwork were conducted. Data from the wind tunnel tests were used to develop conservative procedures for calculating global pressure coefficients suitable for use in bridge design.

17. Key Words	18. Distribution Statement
Bridge construction, girders, bracing, construction loads, wind loads, brace forces, drag coefficients, wind tunnel testing	No restrictions.

19. Security Classification. (of this report)	20. Security Classif. (of this page)	21. No. of Pages	22. Price
Unclassified	Unclassified	191	

Form DOT F 1700.7 (8-72). Reproduction of completed page authorized

ACKNOWLEDGEMENTS

The authors thank the Florida Department of Transportation (FDOT) for providing the funding that made this research possible.

EXECUTIVE SUMMARY

The first objective of this study was to develop procedures for determining bracing forces during bridge construction. Numerical finite element models and analysis techniques were developed for evaluating brace forces induced by construction loads acting on precast concrete girders (Florida-I Beams) in systems of multiple girders braced together. A large-scale parametric study was performed with both un-factored (service) and factored (strength) construction loads (in total, more than 600,000 separate three-dimensional (3-D) structural analyses were conducted). The parametric study included consideration of different Florida-I Beam cross-sections, span lengths, girder spacing, deck overhang widths, skew angles, number of girders, number of braces, and bracing configurations (K-brace and X-brace). Additionally, partial coverage of wet (non-structural) concrete load and variable placement of deck finishing machine loads were considered. A MathCad calculation program was developed for quantifying brace forces using a database approach that employs multiple-dimensional linear interpolation. The accuracy of the database program was assessed by using it to predict end-span and intermediate-span brace forces for parameter selections not directly contained within the database, and then comparing the interpolated predictions to results obtained from finite element analyses of corresponding verification models. In a majority of cases, the database-predicted brace forces were found to be less than ten percent (10%) in error.

The second objective of this study was to experimentally determine wind load coefficients (drag, torque, and lift) for common bridge girder shapes with stay-in-place (SIP) formwork and overhang formwork in place, and then to develop recommended global (system) pressure coefficients (e.g., for strength design of substructures). Wind tunnel tests were performed on reduced-scale models of Florida-I Beam (FIB), plate girder, and box girder cross-sectional shapes to measure aerodynamic forces acting on individual girders in the bridge cross-section. Tests were conducted at multiple wind angles, and corresponding tests with and without overhang formwork were conducted. Data from the wind tunnel tests were used to develop conservative procedures for calculating global pressure coefficients suitable for use in bridge design.

TABLE OF CONTENTS

LIST OF FIGURES

Figure Page

LIST OF TABLES

Table Page

CHAPTER 1
INTRODUCTION

1.1 Overview

During the process of constructing a highway bridge, both the structure and the applied loading conditions will transition through several distinct stages, each of which warrants consideration from a structural safety perspective. Initially, individual girders are lifted by crane and placed into position atop flexible elastomeric bearing pads located on the bridge supports (e.g., abutments or piers). Placement of all girders into their final positions constitutes one of the earliest distinct structural stages that must be assessed for safety. In this structural configuration, it is typical for braces to be installed between the individual girders (Figure 1.1). Additionally, one or more girders may also be anchored to the bridge supports.

Structurally, the system at this stage consists of individual girders, bearing pads, braces, potentially anchors, and support structures (i.e., substructures). Loading conditions consist primarily of vertical gravity loads and horizontal wind loads (for individual girders as well for the collection of all girders as a whole). Primary structural design and safety concerns at this stage of construction focus on girder stability, adequate strength (and stiffness) of braces, and adequate global capacity of the substructure. Addressing these concerns requires that engineering calculation methods be available for quantifying girder buckling capacity, quantifying wind loads on the individual girders (due to predominantly horizontal wind), quantifying brace forces due to the same wind loads, and quantifying global wind-induced lateral loads on the bridge substructure (e.g., for strength design). All of these areas of concern were addressed in a previous study funded by the FDOT (BDK75-977-33, Consolazio et al., 2013) that involved the development of analytical methods for predicting structural forces and capacities, and experimental wind tunnel testing to quantify aerodynamic girder wind load coefficients (drag, torque, and lift), including the effects of aerodynamic shielding.

Figure 1.1 Prestressed concrete girders braced together for stability

After continued construction progress, another key stage will be reached wherein stay-in-place (SIP) forms have been installed between the girders and overhang formwork (and associated overhang support brackets) have been eccentrically attached to the exterior (fascia) girders of the bridge. Loading conditions at this stage consist primarily of horizontal wind loads and vertical ‘construction loads’ that are primarily associated with the process of placing the wet

(plastic) concrete deck (Figure 1.2) and finishing it with a finishing machine (or a 'bridge paver'). During the deck placement process, most of the construction loads are applied eccentrically to overhang formwork and to stay-in-place forms. Consequently, torsional moments acting on the girders produce axial forces in the bracing system (diagonal and horizontal elements) that must be considered in the brace design process. Several geometric parameters influence the magnitude of brace forces caused by construction loads. A major component of the research presented in this report was carried out to quantify bracing forces caused by construction loads over a wide range of geometric parameters (i.e., span lengths, girder spacings, deck overhang widths, etc.).

Also of concern at this stage of construction are wind-induced lateral loads acting globally on the entire bridge cross section. Such loads generate lateral forces on the bridge substructure that must be considered in the design process. While the issue of global lateral wind load was addressed in the previous BDK75-977-33 study, the 'wind configuration' (or 'wind profile') of the bridge considered in the present study was distinctly different due to the aerodynamic blockage (between girders) that results from installation of SIP forms and overhangs. Therefore, in the study presented in this report, wind tunnel testing was once again used quantify wind load coefficients (drag, torque, and lift) for multiple-girder systems, but this time *with* SIP forms (and possibly overhangs) present. The goal of measuring this data was to develop conservative methods for calculating global pressure coefficients and global lateral wind loads for substructure design.

Figure 1.2 Bridge construction loads

1.2 Objectives

One objective of this research was to use finite element analysis of partially constructed bridge systems—consisting of multiple braced prestressed concrete girders (Florida-I beams)—to develop calculation procedures for quantifying brace forces caused by eccentric construction loads. A related objective was to experimentally determine wind load coefficients (drag, torque, and lift) for common bridge girder shapes with stay-in-place (SIP) forms and overhang formwork in place, and then to develop recommended global (system) pressure coefficients (e.g., for use in the strength design of substructures).

1.3 Scope of work

- Construction loads: Numerical finite element bridge models and analysis techniques were developed for evaluating brace forces induced by construction loads acting on precast concrete girders (Florida-I Beams) in systems of multiple girders braced together. The construction loads considered were: wet concrete deck load, stay-in-place (SIP) form weight, overhang formwork weight, live load, worker line loads, and concentrated loads representing a deck finishing machine. A large-scale parametric study, involving more than 600,000 separate three-dimensional structural analyses, was performed to compute maximum brace forces for un-factored (service) and factored (strength) construction load conditions. The parametric study included consideration of different Florida-I Beam cross-sections, span lengths, girder spacings, deck overhang widths, skew angles, number of girders, number of braces, and bracing configurations (K-brace and X-brace). Maximum end-span brace forces and intermediate-span brace forces quantified from the parametric study were stored into a database and an 'interpolated database approach' to brace force prediction was developed and coded into a MathCad program for ease of use.
- Wind loads: Wind tunnel testing was used to quantify wind load coefficients (drag, torque, and lift) for systems of multiple bridge girders (FIB, plate girder, and box) with stay-in-place (SIP) forms and overhang formwork in place. Tests were conducted at multiple wind angles, and corresponding tests with and without overhang formwork were conducted so that the effects of overhang formwork on drag, lift, and torque coefficients could be quantified for bridges with I-shaped girders and box girders. Drag coefficients measured at each girder position were used to develop conservative methods for computing global (system) pressure coefficients suitable for use in bridge design (particularly, for use in calculating global lateral substructure load due to wind).

CHAPTER 2
STRUCTURAL CONFIGURATION AND LOADING CONDITIONS DURING BRIDGE CONSTRUCTION

2.1 Introduction

Braces used to stabilize girders during bridge construction must be designed to resist forces that are generated by construction loads and wind loads. The manner in which brace forces are distributed to the elements of the bracing system depends on geometric parameters (span length, girder spacing, deck overhang width, etc.), bracing configurations, and cross-sectional properties of the girders. In the present study, the girders under investigation are Florida-I Beams (FIBs), a group of standard cross-sectional shapes of varying depths that are commonly employed in Florida bridge designs. These beams are typically cast offsite, transported to the construction site by truck, then lifted into position one-at-a-time by crane, where they are placed on elastomeric bearing pads and braced together for stability. Formwork systems are then added to support the wet concrete deck and other construction loads encountered during the deck pouring process. In this chapter, a physical description of the 'construction-stage' structures under consideration will be provided along with the definition of relevant terminology.

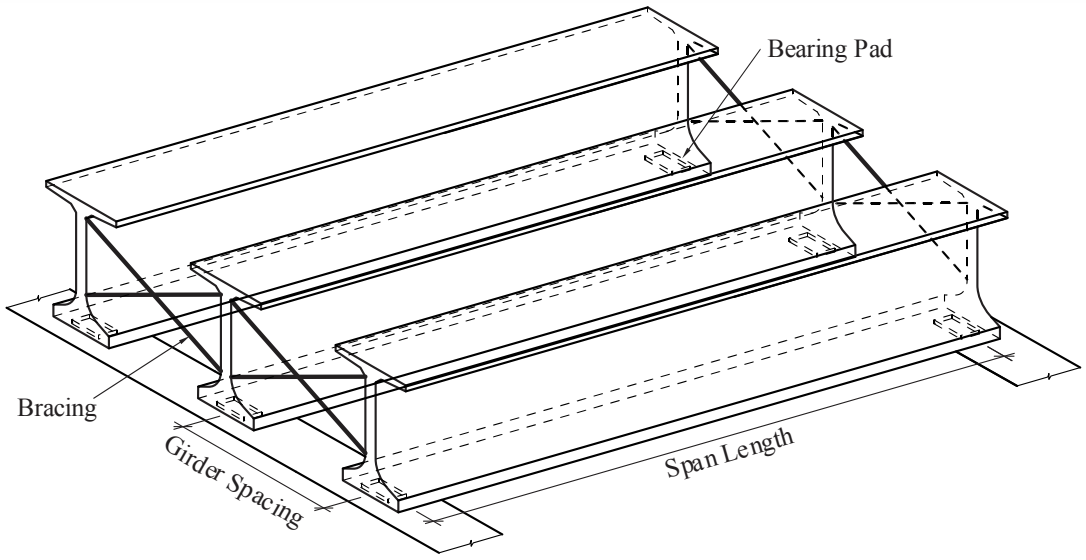

Figure 2.1 Girder system

2.2 Geometric parameters

The term *girder system* will be used to refer to a group of two or more FIBs braced together in an evenly spaced row (Figure 2.1). In addition to span length and lateral spacing, there are several geometric parameters that define the shape and placement of the girders within a system:

- Grade: Longitudinal incline of the girders, typically expressed as a percentage of rise per unit of horizontal length (Figure 2.2).

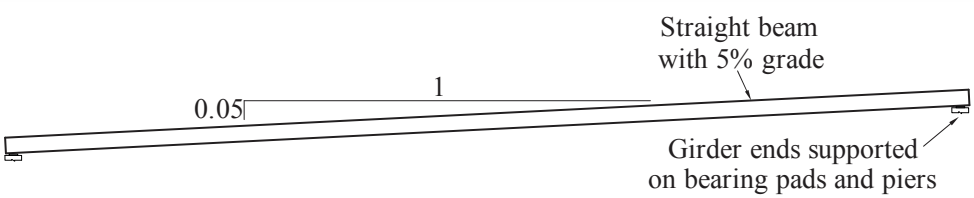

Figure 2.2 Definition of grade (elevation view)

- Cross-slope: The transverse incline (slope) of the deck, expressed as a percentage, which results in girders that are staggered vertically (Figure 2.3).

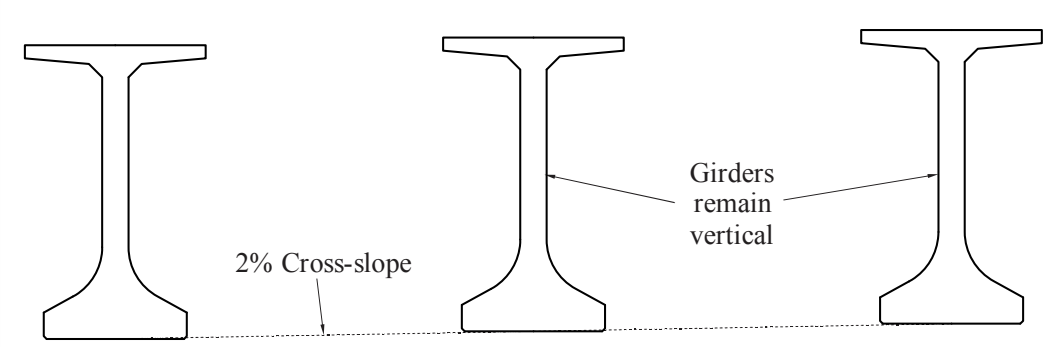

Figure 2.3 Definition of cross-slope (section view)

- Skew angle: Longitudinal staggering of girders, due to pier caps that are not perpendicular to the girder axes (Figure 2.4).

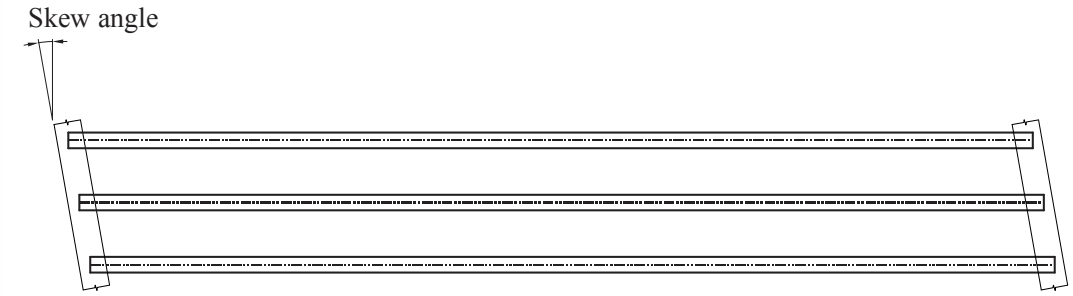

Figure 2.4 Definition of skew (plan view)

- Camber: Vertical bowing of the girder (Figure 2.5) due to prestressing in the bottom flange; expressed as the maximum vertical deviation from a perfectly straight line connecting one end of the girder to the other.

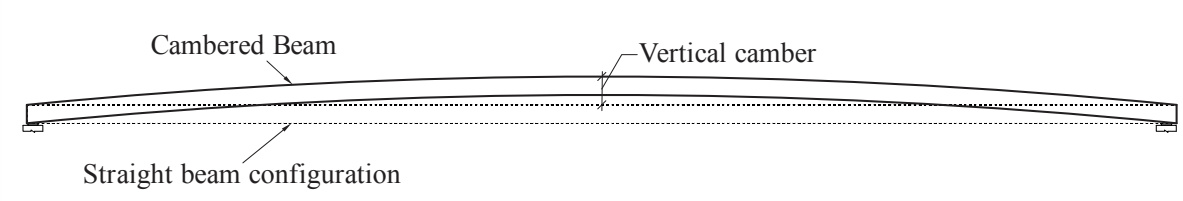

Figure 2.5 Definition of camber (elevation view)

- Sweep: Lateral bowing of the girder (Figure 2.6) due to manufacturing imperfections, expressed as the maximum horizontal deviation from a perfectly straight line connecting one end of the girder to the other.

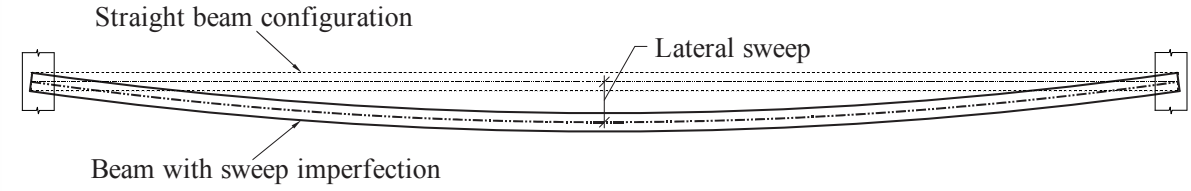

Figure 2.6 Definition of sweep (plan view)

2.3 Bearing pads

FIB bridge girders rest directly on steel-reinforced neoprene bearing pads which are the only points of contact between the girder and the substructure. There is generally sufficient friction between the pad and other structural components so that any movement of a girder relative to the substructure (with the exception of vertical uplift) must displace the top surface of the pad relative to the bottom surface. As a result, the girder support conditions in all six degrees of freedom (three translations, and three rotations) can be represented as finite stiffnesses that correspond to the equivalent deformation modes of the pad. These deformation modes fall into four categories: shear, compression (axial), rotation (e.g., roll), and torsion. Bearing pad stiffnesses in this study were quantified using calculation procedures developed and experimentally validated in a previous study (BDK75-977-33, Consolazio et al., 2013) for typical Florida bridge bearing pads.

2.4 Bracing

As adjacent girders are erected during the bridge construction process, girder-to-girder braces (henceforth referred to simply as *braces*) are used to connect the girders together into a single structural unit. At a minimum, braces are installed near the ends of the girders (close to the supporting piers); such braces are referred to as *end-span braces*. In addition, *intermediate-span braces* spaced at unit fractions (1/2, 1/3, 1/4) of the girder length may also be included. For example, quarter-point (1/4 span) bracing divides the girder into four equal unbraced lengths (Figure 2.7).

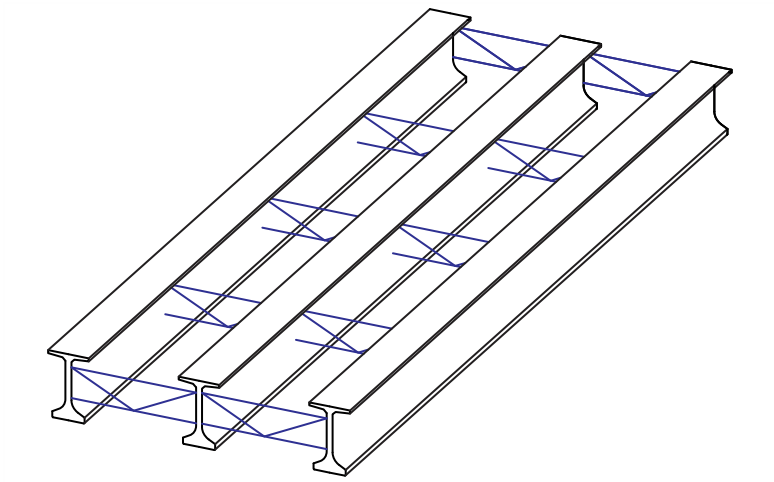

Figure 2.7 Girder system with quarter-point bracing

When skew is present, brace point locations are longitudinally offset (Figure 2.8) between adjacent girders because *FDOT Design Standard No. 20005: Prestressed I-Beam Temporary Bracing* (FDOT, 2014a) requires that all braces be placed perpendicular to the girders.

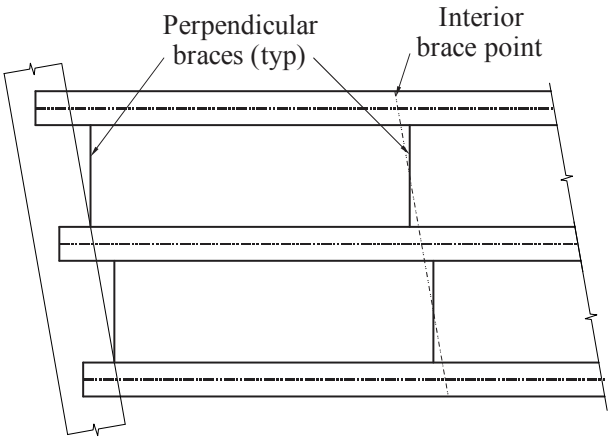

Figure 2.8 Perpendicular brace placement on skewed bridge (plan view)

Braces are typically constructed from timber or steel members, but individual brace designs are left to the discretion of the contractor, so a variety of different bracing configurations are possible. The most common types of braces used in practice in Florida are X-braces (Figure 2.9a) and K-braces (Figure 2.9b). Therefore, in the present study, only these brace types are considered. Braces are typically attached to the girders using bolted connections or welded to cast-in steel plates.

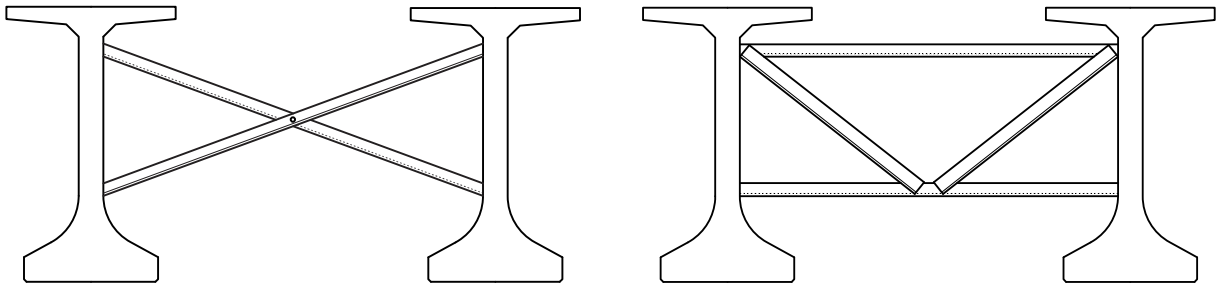

a) b)

Figure 2.9 Common brace types:
a) X-brace; b) K-brace

2.5 Bridge construction loads

A major objective this study was to determine axial brace forces induced by bridge construction loads. In particular, the bridge deck placement (concrete application and finishing) process was the construction stage considered. Components of the bridge construction loads considered in this study were as follows:

- Wind loads: During bridge construction, wind loads are an important design consideration. However, severe wind loads and active construction loads (i.e., deck placement loads) are not likely to be encountered simultaneously. According to the *FDOT Structures Design Guidelines* (SDG; FDOT, 2013), the basic wind speed for active construction is specified as 20 mph. In this study, wind loads and construction loads were treated as separate design load cases. Wind loads on girders with stay-in-place forms were quantified experimentally with wind tunnel testing.
- Concrete deck: Throughout the deck pouring and finishing process, wet (plastic) concrete has *negligible stiffness*, which is beneficial for shaping the concrete into a smooth finished surface. Consequently, a non-composite girder system must support these construction loads. However, in the final bridge condition, the bridge deck works together with the girders as a composite system to resist and distribute loads to the supporting girders. Since the wet (nonstructural) concrete load is incrementally applied to bridges in the longitudinal direction, this load is treated as a variable length load in the finite element analyses. Partial application of concrete deck loads to the girder system will be further explained later in this report.
- Stay-in-place formwork: Stay-in-place (SIP) formwork systems support intra-girder loads (wet concrete) that span transversely between girder top flanges (Figure 2.10). Stay-in-place forms consist of corrugated metal panels that are attached to the tips of the top flange of adjacent girders. The connection between the SIP forms and the girder flange is considered to be incapable of transmitting moments, therefore the SIP forms are essentially treated as being 'simply supported' on the girder flange tips.

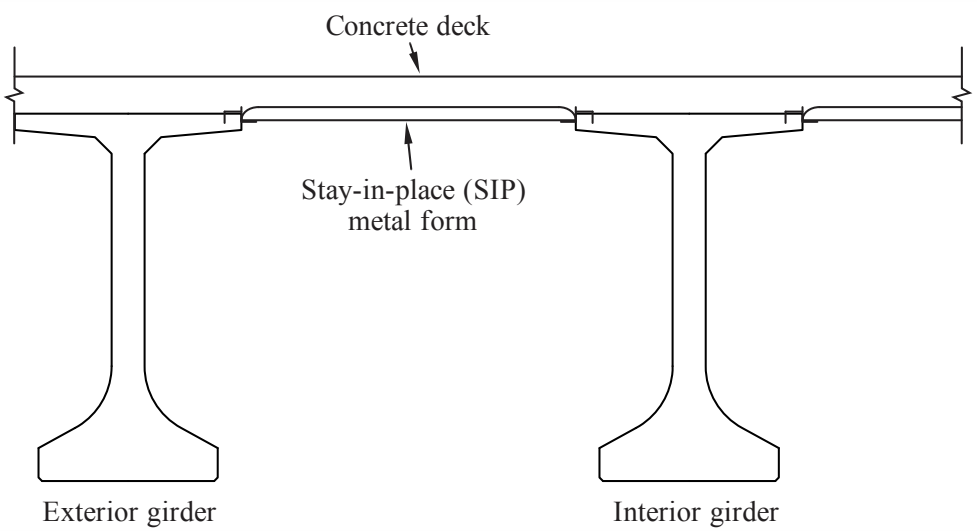

Figure 2.10 Stay-in-place formwork (section view)

- Overhang formwork: It is typical for the deck of a bridge to extend past the exterior (fascia) girder, thereby producing a cantilevered overhang (Figure 2.11). During construction, *overhang brackets* (Figure 2.12) are used to temporarily support the cantilever portion of the wet deck slab that extends beyond exterior girders. These temporary structural bracket systems support the overhang formwork, wet concrete, construction walkway, workers and concrete finishing machine. A survey of representative literature from overhang bracket manufacturers was conducted to quantify representative cross-sectional properties and longitudinal spacing requirements. Most commercially available formwork systems consist of timber joists and sheathing supported on steel bridge overhang brackets (Figure 2.13). It is important to note that all of the gravity loads supported by the overhang brackets are eccentric relative to the exterior girders, and as such apply torque loads to the exterior girders in the overall cross-sectional system.

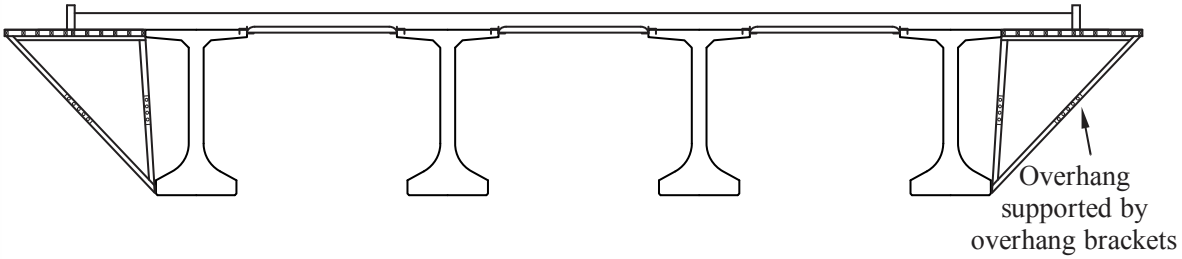

Figure 2.11 Temporary support brackets used to support deck overhangs during construction

Figure 2.12 Cantilever overhang supported by overhang brackets
(Photo credit: Clifton and Bayrak (2008))

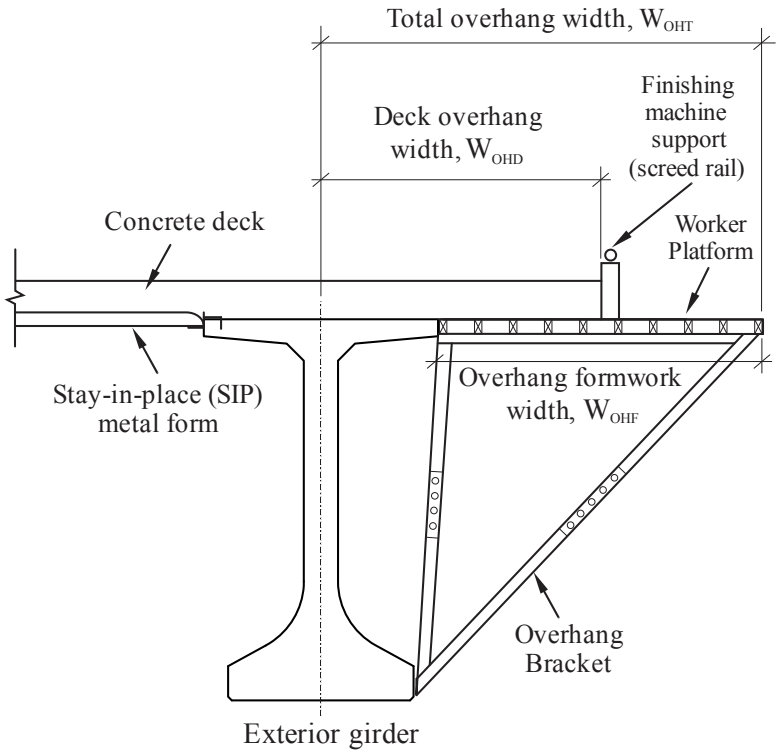

Figure 2.13 Details of overhang formwork support brackets and loads

- Finishing machine: Bridge deck finishing machines (Figure 2.14) spread, compact, and finish the freshly placed wet concrete deck surface. The finishing machine is an open steel frame that is supported at the extremities of the bridge width on the overhang brackets described

above. Drive wheels (commonly referred to as bogies) move the paver longitudinally along the length of the bridge and are eccentrically supported by screed rails (Figure 2.13) on each side of the bridge. A suspended paving carriage with augers, drums, and floats finishes the concrete surface as it moves transversely from side to side across the width of the bridge (perpendicular to the longitudinal movement of the finishing machine along the length of the bridge). Concrete is typically placed just ahead of the travelling finishing machine using separate equipment, such as a pump. The most common finishing machine manufacturers are Terex Bid-Well and Gomaco.

Figure 2.14 Typical bridge deck finishing machine in operation
(Photo credit: Gomaco)

- Live loads: Live loads that are present during the deck finishing process consist of workers, temporary materials, and supplementary construction equipment. For brace force calculation purposes, these loads are treated as either uniform pressure loads, or as line loads, as will be discussed in greater detail later in this report.

CHAPTER 3
DEVELOPMENT OF STRUCTURAL ANALYSIS MODELS

3.1 Introduction

To calculate brace forces induced by construction loads, braced systems of FIB girders were modeled and structurally analyzed using the ADINA (2012) finite element analysis code. The models were capable of capturing overall system-level behavior of braced FIB systems (including the influence of brace configuration, bearing pad stiffness, etc.), while remaining computationally efficient enough that hundreds of thousands of parametric analyses could be performed for the purpose of quantifying braces forces. In all cases, brace forces were determined using large-displacement (geometrically nonlinear) analyses, in which static loads were applied to the models in incremental steps, taking into account the deformed state of the structure at each step.

The parametric construction-stage bridge models analyzed in this study were developed in a semi-automated fashion by extending a modeling methodology developed in a previous study (BDK75-977-33, Consolazio et al., 2013) to further include the effects of construction loads and overhang brackets. In the following sections, key aspects of the model development process are summarized, and noteworthy modifications to the previously developed modeling methodology are described in detail.

3.2 Modeling of bridge girders

In the global coordinate system established for each bridge model, the X-axis corresponded to the transverse (lateral) direction; the Y-axis corresponded to the longitudinal (span) direction, and the Z-axis corresponded to the vertical direction. Bridge girders were modeled (Figure 3.1) using 'warping beam elements' which use an advanced beam element formulation type provided in ADINA that possess an additional degree of freedom at each end node to represent the torsionally-induced out-of-plane warping of the cross-section. Warping beam elements are generally superior to standard Hermitian beam elements in that the bending and torsional deformation modes of the warping element are fully coupled together at the element formulation level. However, as a consequence, the use of warping beam elements requires the calculation of a comprehensive set of cross-sectional properties—many more than standard Hermitian beam elements—several of which require knowledge of the section 'warping function', which cannot be calculated in closed form and must instead be solved for numerically. Details relating to the section properties that were calculated in this study for the catalog of FDOT FIB cross-sectional shapes are provided in Appendix A. Throughout this study, material properties assumed for the prestressed concrete FIB girders were f_c' = 8.5 ksi, unit weight = 150 pcf, and Poisson's ratio = 0.2. Using these values and the PCI Design Handbook (PCI, 2010), the concrete elastic modulus was computed to be E = 5589 ksi.

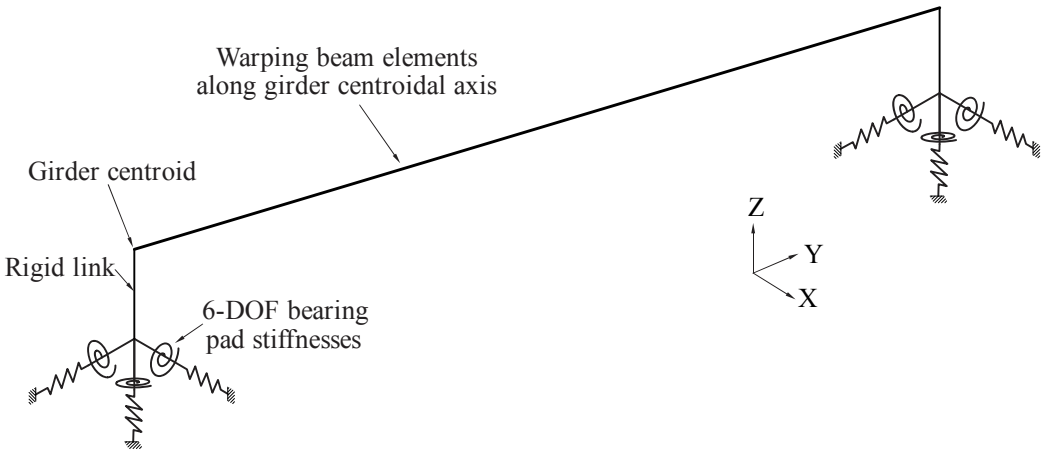

Figure 3.1 Finite element model of a single FIB (isometric view)

Support conditions at each end of each girder were modeled with six (6) springs to represent the stiffnesses of the bearing pad in each degree of freedom. Each of the six (6) springs corresponded to one of four different pad deformation modes: shear, axial, torsion, and roll (Figure 3.2). Pad stiffnesses were determined using the calculation methods developed and validated in a previous study (BDK75-977-33, Consolazio et al., 2013). The roll stiffness springs (in both the overturning and bending directions) were assigned nonlinear moment-rotation curves that captured the softening effects of partial girder liftoff from the pad. All remaining pad stiffnesses were treated as linear.

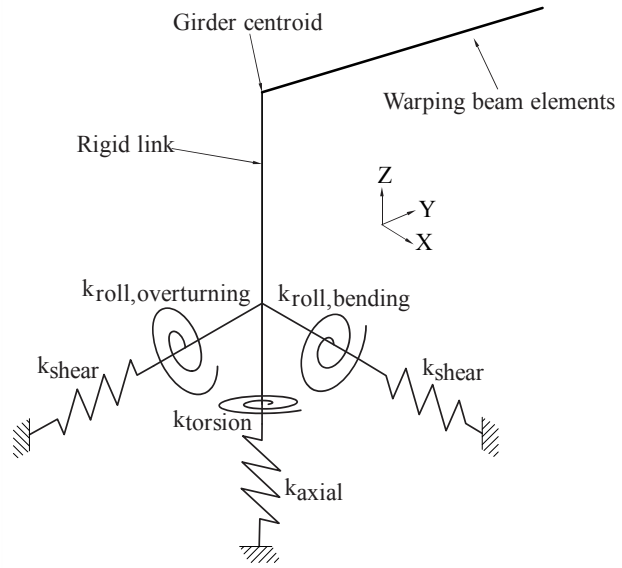

Figure 3.2 Modeling of bearing pad stiffness springs at end of girder

3.2.1 Bearing pad selection

Seven (7) standard types of elastomeric bearing pad are described in *FDOT Design Standard No. 20510: Composite Elastomeric Bearing Pads – Prestressed Florida-I Beams*

(FDOT, 2014c) for use with FIB girders. During the design process, selection of the type of pad that will be used in a particular bridge project is based on thermal expansion and live load deflection limit states of the completed bridge, neither of which can be predicted based solely on girder dimensions (cross-sectional properties or span length). As such, it is not appropriate to assume that for each unique type of FIB, there is a corresponding single type of bearing pad that would always be utilized.

In this study, bearing pad selection was instead based on ensuring that conservatively large values of *brace force* would be obtained for all analyses conducted. As bearing pad rotational stiffness decreases, the portion of the acting eccentric construction loads that is carried by a pad also decreases, thereby moderately increasing the forces that are developed in the braces. Consequently, the bearing pad with the minimum practical roll stiffness will produce the most conservative brace forces. Therefore, the FDOT Type J bearing pad was selected for use throughout this study. As documented in Consolazio et al. (2013), as the acting axial compressive load on a pad decreases, so does a component of the roll stiffness of the pad. Hence, for each FIB girder type considered in the present study, the *minimum* practical span length for that girder type was used to compute an axial pad load (equal to half of the total weight of a single girder). For each such axial load, the roll stiffness of the Type J pad was then computed and then subsequently used for all parametric analyses involving that type of FIB girder. Hence, a single minimized roll stiffness curve was calculated for each type of FIB, resulting in a total of seven (7) bearing pad moment-rotation curves. (For additional details on the bearing pad stiffness calculation procedures, see Consolazio et al., 2013, Chapter 6).

3.3 Modeling of braces

In bridge construction, a wide variety of different bracing configurations are used in practice, consequently it was not possible for every possible configuration of brace to be included in the parametric studies that were conducted in this study. After carrying out a survey of bracing designs used in the construction of bridges throughout Florida, two (2) representative brace configurations were identified:

- X-brace (Figure 3.3a): Two diagonal members that cross in the middle to form an ‘X’ shape. A steel bolt typically passes through both members at the crossing point to create a hinge.
- K-brace (Figure 3.3b): Steel members (typically steel angles) welded together into a ‘K’-shaped frame and welded or bolted to steel plates that are cast into the webs of the concrete girders.

Additionally, only the X-brace and K-brace configurations are currently recommended in the *FDOT Design Standard No. 20005: Prestressed I-Beam Temporary Bracing* (FDOT, 2014a) for end-span and intermediate-span bracing applications. For structural analysis purposes, all braces were modeled with beam elements, with each brace member represented by a single element. At the girder connection points, rigid links were used to connect the brace elements to the girder elements (i.e., the warping beam elements positioned at the centroid of the girders). Pins and hinges were modeled with beam moment end-releases and nodal constraints, respectively. Both X-brace and K-brace members included in the parametric studies were modeled as 4 in. x 4 in. x ⅜ in. steel angles, with an elastic modulus of E = 29000 ksi.

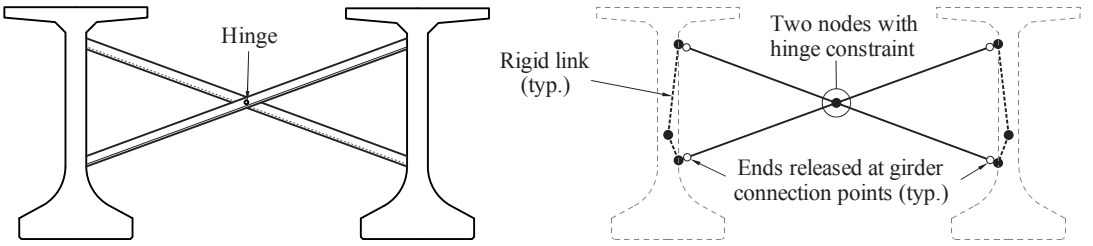

a)

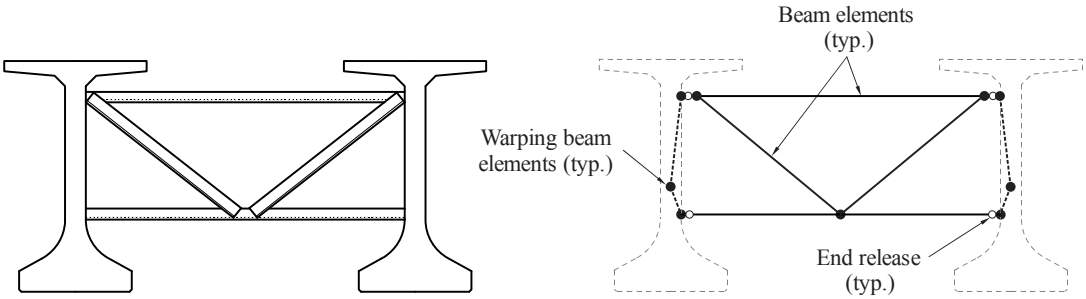

b)

Figure 3.3 Modeling of brace configurations in FIB system models:
a) X-brace; b) K-brace

3.4 Modeling of overhang brackets

Construction loads applied beyond the lateral extents of an exterior girder are structurally supported during construction by *overhang brackets*. Specifically, the finishing machine, formwork, overhang wet concrete, and construction worker live loads are typical components of the supported overhang loads. To define the lateral eccentricity of the overhang construction loads, two offset parameters had to be established. To be consistent with the *FDOT Instructions for Design Standard No. 20010: Prestressed Florida-I Beams* (FDOT, 2014b), the concrete finishing machine was offset 2.5 in. from the overhang edge (Figure 3.4). In the *FDOT Concrete I-girder Beam Stability Program*, in addition to providing calculations for determining bracing adequacy and girder stability, several recommended values for the overhang geometry are specified, including a 2-ft worker platform width. Therefore, for all the parametric studies conducted herein, the worker platform was assumed to extend 2-ft beyond the finishing machine supports (Figure 3.4).

In the girder system models, all components of the overhang brackets were modeled with beam elements, with representative cross-sectional properties that were obtained from a survey of overhang bracket manufacturers. To represent the offset eccentricities between the girder centroid and the bracket connection points, the deformable overhang bracket elements were connected to girder warping beam elements using rigid links (Figure 3.5). In order to model interaction between the overhang bracket and the girder bottom flange, two co-located but separate nodes were used: one at the bottom vertex of the metal overhang bracket, and a second at the end of the rigid link representing the surface of the girder bottom flange. At this location,

the overhang bracket bears against (i.e., is in compressive contact with) the girder bottom flange. To model this behavior structurally, a constraint condition is defined such that the lateral (X-direction) translations of the two co-located nodes are constrained to match, while permitting independent movements (relative slip) in the vertical direction.

Overhang bracket nodes are positioned (Figure 3.5) to define: the three corners of the triangular system; and all locations of load discontinuities (i.e., deck overhang edge) and load application points (i.e., finishing machine and worker line load application points). The worker line load is conservatively applied to the center of the worker platform width. Thus, the load application of the worker line load is laterally offset in the X-direction 12 in. from the assumed finishing machine application point and 14.5 in. from the deck overhang edge (Figure 3.5).

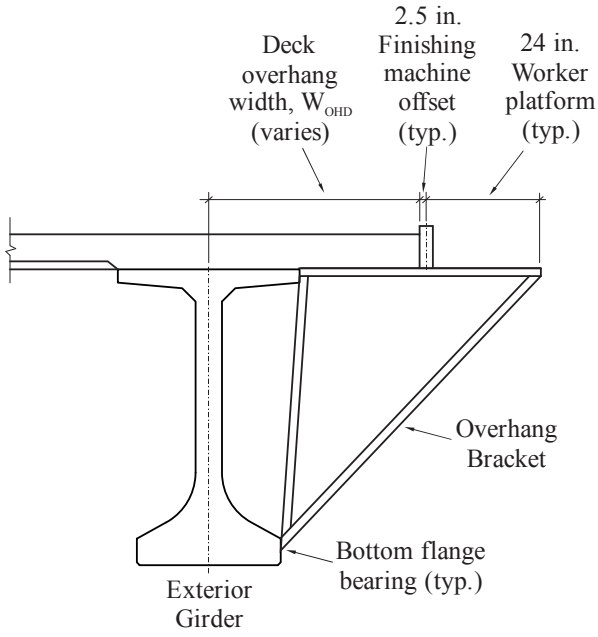

Figure 3.4 Overhang bracket components and geometry

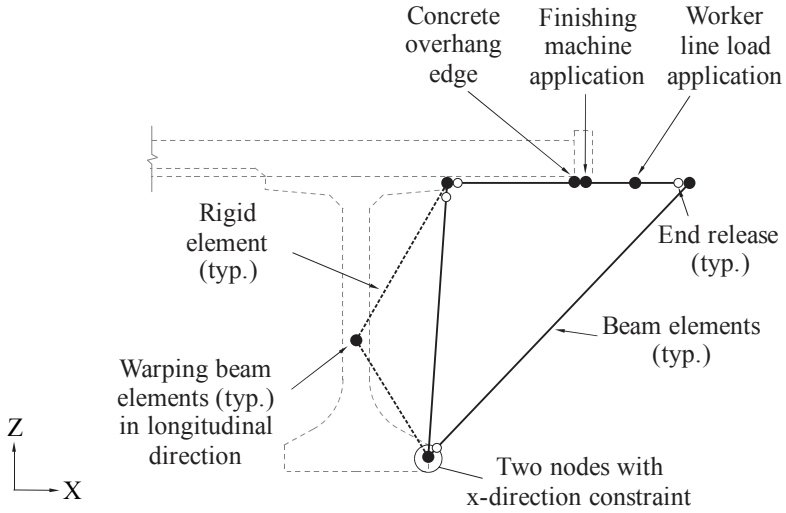

Figure 3.5 Details of overhang bracket model

By combining each of the previously mentioned modeling components, an overall illustration of a typical FIB system model is presented in Figure 3.6. Based on a review of literature obtained from typical overhang bracket manufacturers, brackets are commonly spaced between 4 ft and 6 ft on center longitudinally along the span length of a bridge. In the present study, therefore, an average longitudinal spacing of 5 ft was used for all brackets (Figure 3.7).

Also noted in the Figure 3.6 and Figure 3.7 are rigid vertical elements (links)—extending from girder centroid to girder top surface—which are included in the model for application of construction loads on each girder. These rigid elements account for the vertical eccentricity between the girder centroid and the girder top surface (where loads are applied). It was determined that brace forces induced by construction loads were not sensitive to changes in the longitudinal spacing of the rigid vertical elements, consequently the rigid links were given an arbitrary longitudinal spacing of 1-ft in the span direction.

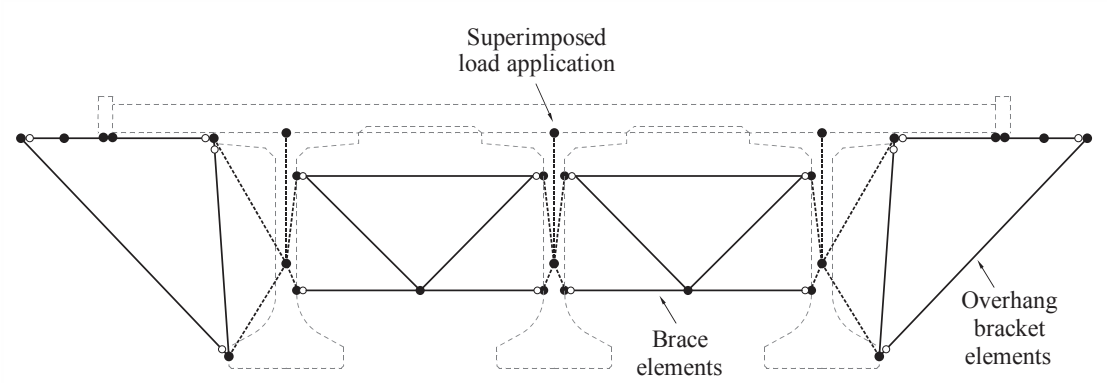

Figure 3.6 Cross-sectional view of overall braced girder system model

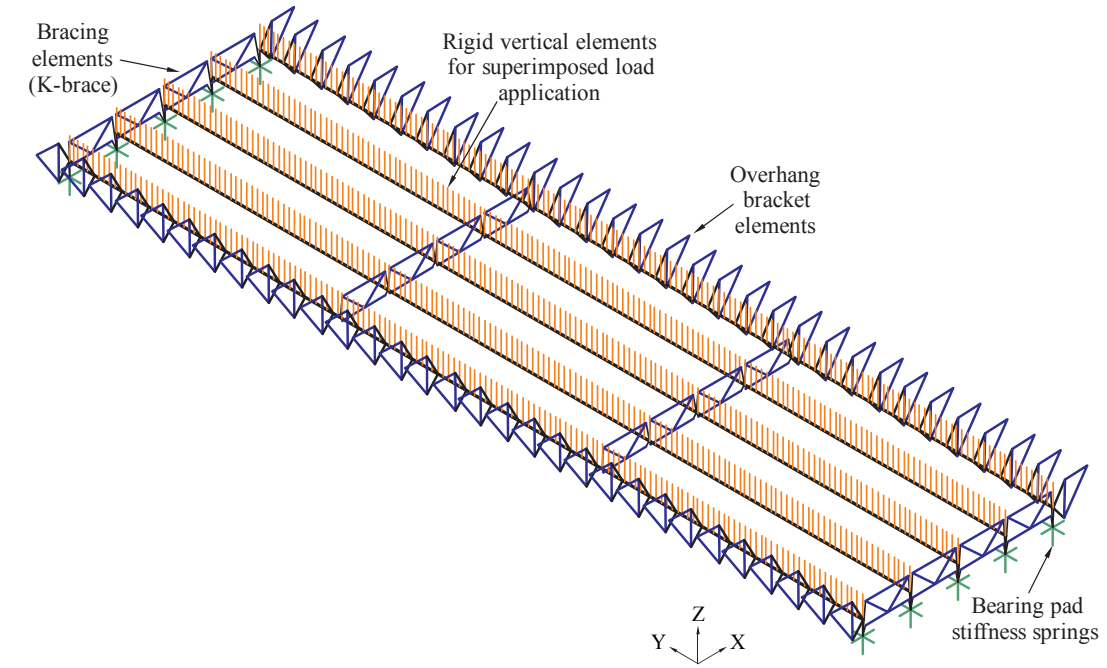

Figure 3.7 Isometric view of overall braced girder system model

3.5 Application of construction loads

In this section, the magnitudes and methods of application for construction loads considered in this study are described. In Figure 3.8, a summary of the superimposed construction loads that will be described in more detail below is provided. Additionally, self-weight (i.e., gravity loads from girders, braces, and overhang brackets) were included in the models.

An important consideration in this study was the application of the concrete finishing machine loads. Finishing machines are supported near the extremities of the bridge width by several wheels. The common Terex Bid-Well 4800 machine has a total wheel base of approximately 8 feet in the longitudinal (bridge span) direction. Since this wheel base is small relative to the typical span lengths of prestressed girder bridges, the finishing machine wheel reaction forces were idealized as single concentrated loads (one load on each side of the bridge equal to half the total machine weight).

During bridge deck placement, a concentration of live load will be located at the extremities of the bridge deck. To account for this loading, the *AASHTO Guide Design Specifications for Bridge Temporary Works* (2008) recommends that a worker line load be applied along the outside edge of all deck overhangs. In addition, the line load shall be applied as a moving load but with a fixed length of 20-ft so as to not introduce excessive conservatism. In the girder system models analyzed in this study, the worker line load was centered longitudinally at the concrete finishing machine such that the line load extended 10-ft behind and ahead of the finishing machine.

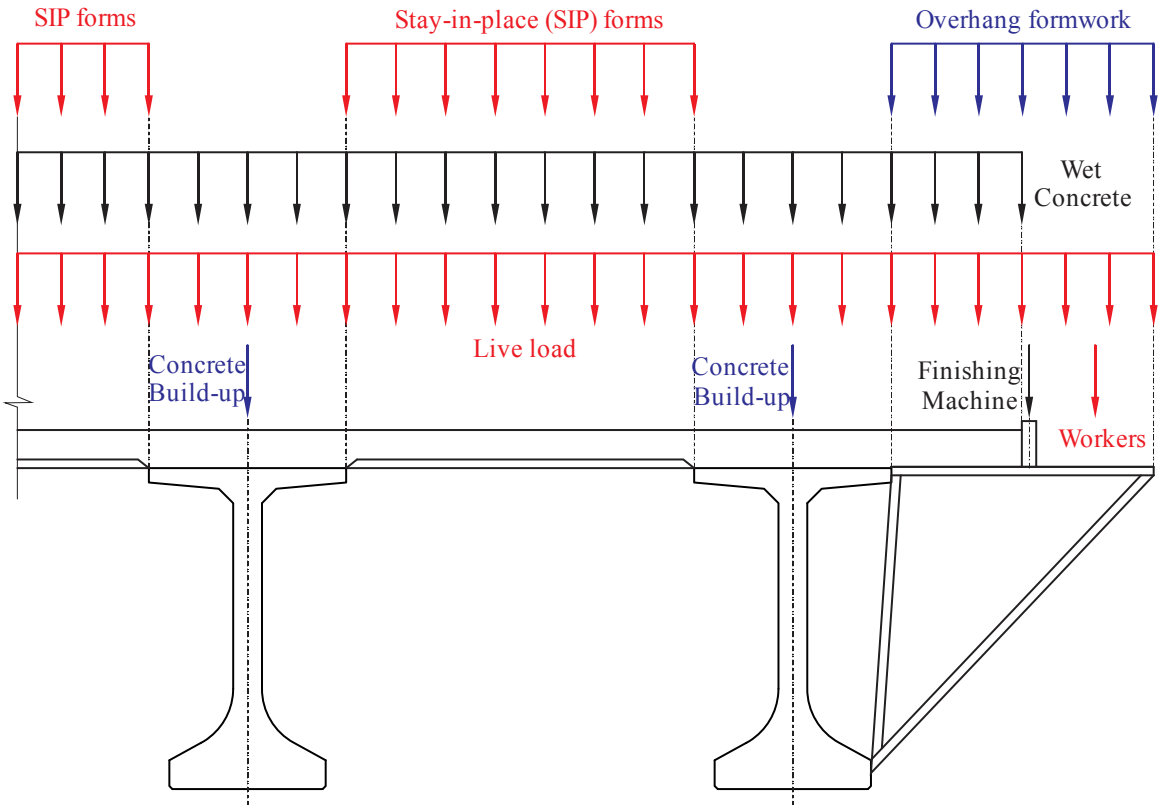

Figure 3.8 Summary of construction loads considered

Since temporary bracing must be designed for service and strength limit states, two separate parametric studies were conducted: un-factored (service) loads and factored (strength) loads. A summary of un-factored and factored construction loads is provided in Table 3.1 along with applicable references.

Table 3.1 Summary of construction loads applied in parametric studies

Construction loads	Load type	Un-factored loads	Load factor	Factored loads	Reference
Wet concrete deck	Permanent	106.25 psf (8.5" thick, 150 pcf)	1.25	132.8 psf (8.5" thick, 150 pcf)	I
Wet concrete build-up	Permanent	50 lb/ft	1.25	62.5 lb/ft	I
Stay-in-place forms	Permanent	20 psf	1.25	25 psf	I
Overhang formwork	Temporary	10 psf	1.5	15 psf	II
Live load	Temporary	20 psf	1.5	30 psf	III
Worker line load	Temporary	75 lb/ft for 20 ft	1.5	112.5 lb/ft for 20 ft	III
Finishing machine	Temporary	10 kip total (5 kip each side)	1.5	15 kip total (7.5 kip each side)	II

I: per FDOT Structures Design Guidelines (2013)
II: per FDOT recommendations
III: per AASHTO Guide Design Specifications for Bridge Temporary Works

Construction loads that are applied between adjacent girders (i.e., on the stay-in-place forms) produce vertical reaction forces that act on the tips of the girder top flanges. Since all Florida-I beams have a top flange width of 48 in., the lateral eccentricity between the girder centroid and the formwork reaction force (Figure 3.9) is 24 inches (half of the girder top flange width). For analysis purposes, each eccentric reaction forces of this type was converted into a statically equivalent combination of force and moment (Figure 3.9) which were then applied along the centerlines of the girders.

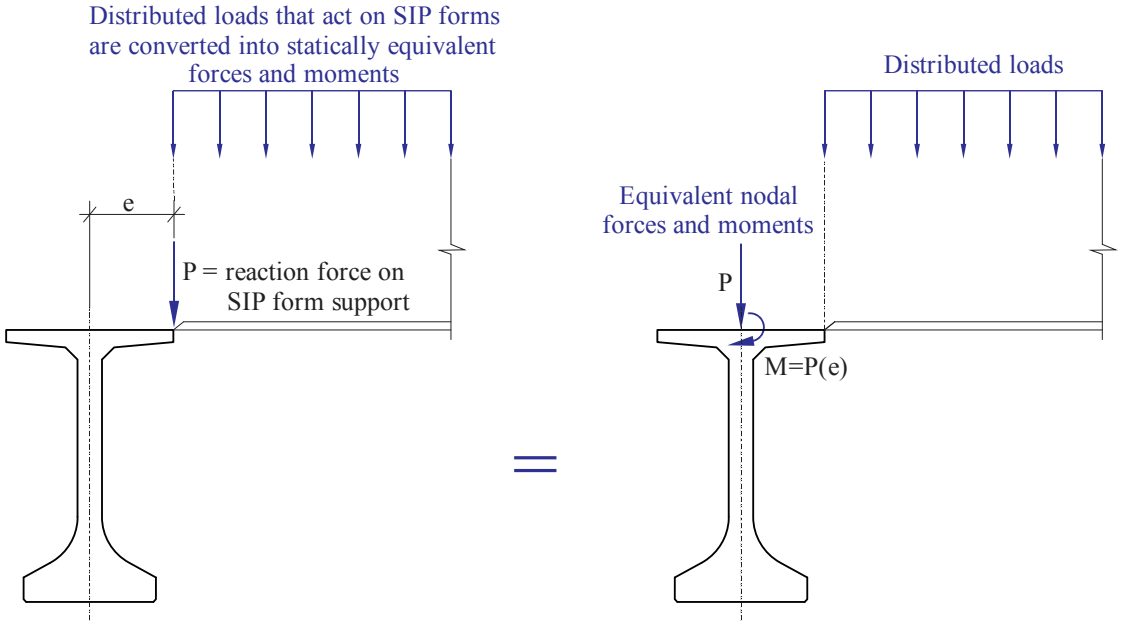

Figure 3.9 Eccentric reaction forces from loads applied to SIP forms, and statically equivalent nodal force and moment applied to top of girder

Consequently, all intra-girder distributed loads that were applied over the width of the stay-in-place formwork were converted into equivalent nodal forces and moments. Other types of construction loads, such as the overhang loads (overhang formwork, worker line load, etc.), were applied directly to nodes in the structural model based on the appropriate tributary areas (Figure 3.10).

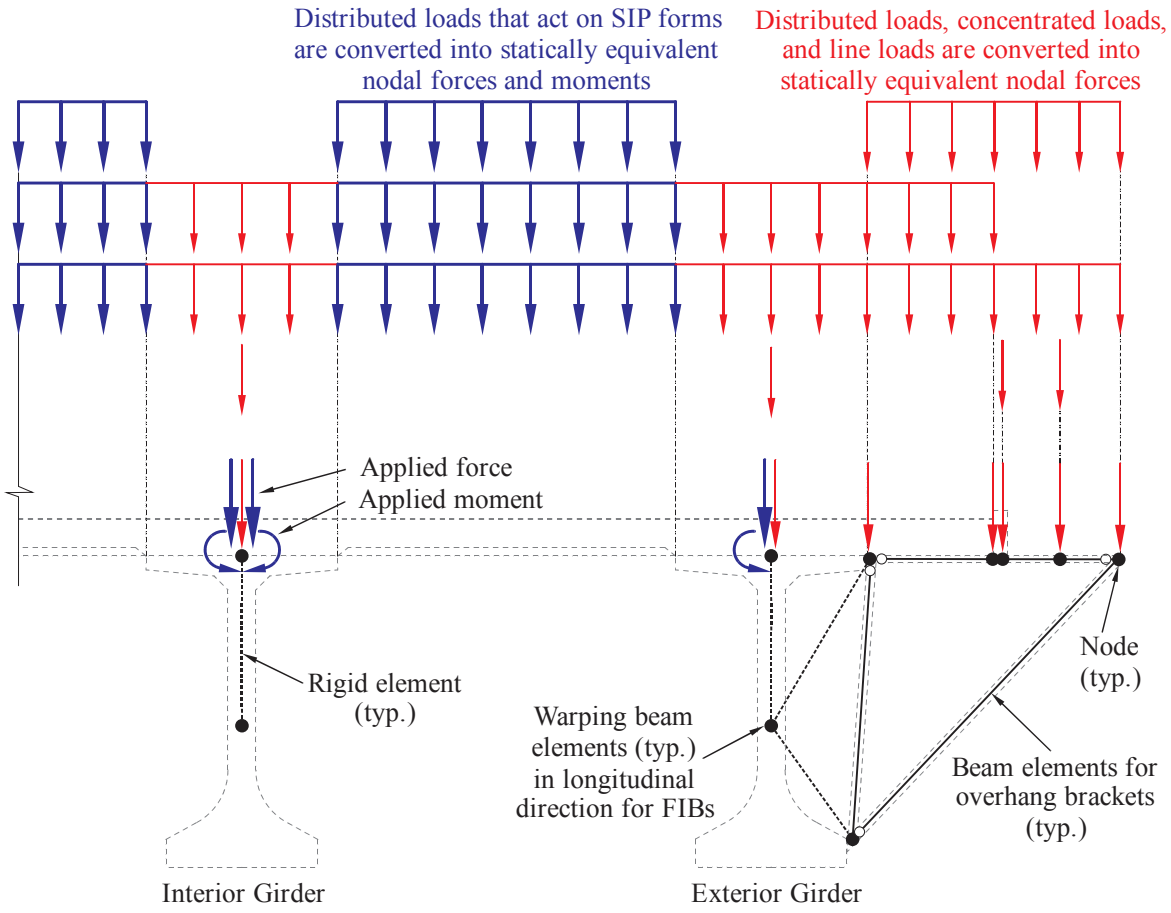

Figure 3.10 Construction loads converted to equivalent nodal loads

During the process of placing and finishing of a concrete bridge deck, wet concrete pressure load is applied to the bridge (by way of SIP forms) over incrementally increasing lengths of the structure. Consequently, loading conditions corresponding to the placement of concrete deck loads over *partial lengths* of the bridge—less than the total span length—were considered in this study. For all such partial coverage cases, the position of the finishing machine was taken to coincide with the location of the furthest placed concrete. Wet concrete is typically placed just ahead of the moving finishing machine (Figure 2.14) using a pump, therefore, in vast majority of paving situations, the location of the finishing machine and the end of the concrete coverage will generally coincide. (Although it is feasible for a finishing machine to be moved to a location other than then end of the placed concrete, it was determined that such situations are generally rare and/or non-controlling, and thus were not considered in this study). By analyzing several 'test' bridge models in which the finishing machine and the end of the concrete deck

coverage area were moved in small increments along the bridge length, it was determined that maximum end-span brace and intermediate-span brace forces occurred when the web slab load terminated at one of the bracing points (e.g., end point, 1/2 point, 1/3 point, 1/4 point). However, depending on the bridge configuration parameters (deck overhang width, girder spacing, etc.) the controlling coverage of concrete loads and finishing machine loads that produced the maximum brace forces varied from case to case. For example, full span concrete coverage with the finishing machine at the end-span often produced the highest end-span brace forces. However, a partially placed deck terminating at an interior brace point typically produced the largest interior brace forces. To ensure that maximum brace forces were quantified from the parametric studies, multiple load cases were analyzed (Figures 3.11 - 3.14) for each bridge, depending on the number of interior bracing lines that were present. Note that for each geometric configuration (span length, girder spacing, deck overhang width, etc.), maximum end-span brace and intermediate-span brace forces were quantified for each loading condition.

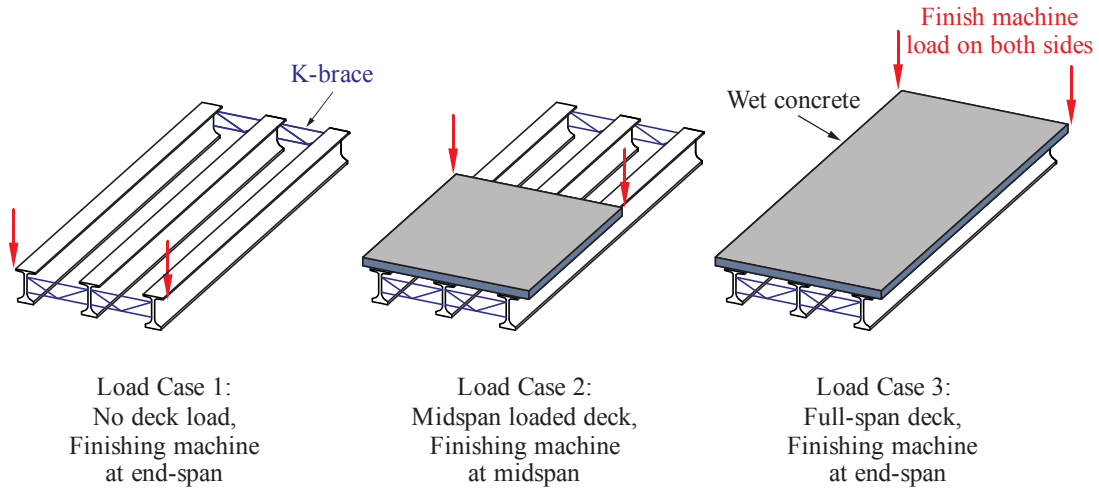

Figure 3.11 Coverage of deck loads as a function of finishing machine location (Bridge with only end-span braces; no interior braces)

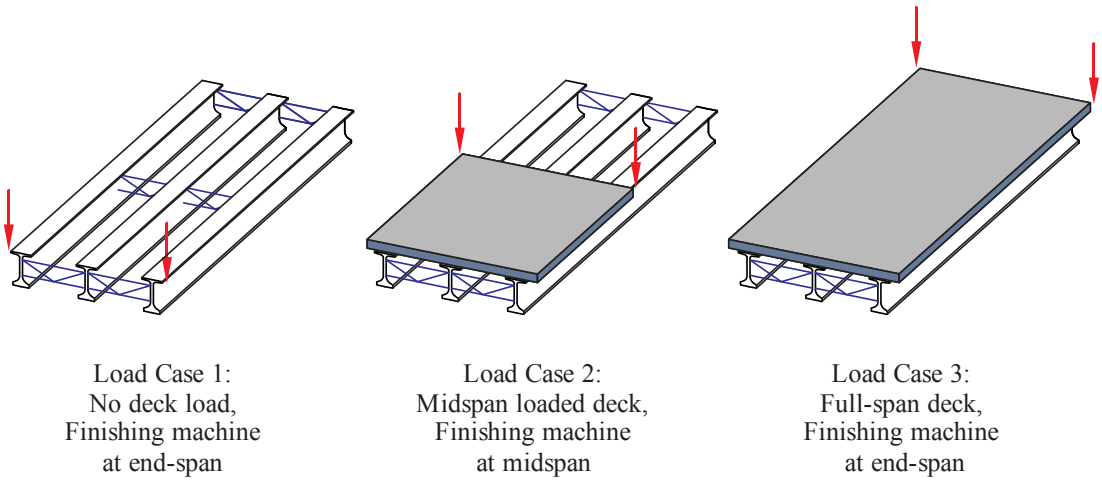

Figure 3.12 Coverage of deck loads as a function of finishing machine location (Bridge with end-span and midspan bracing)

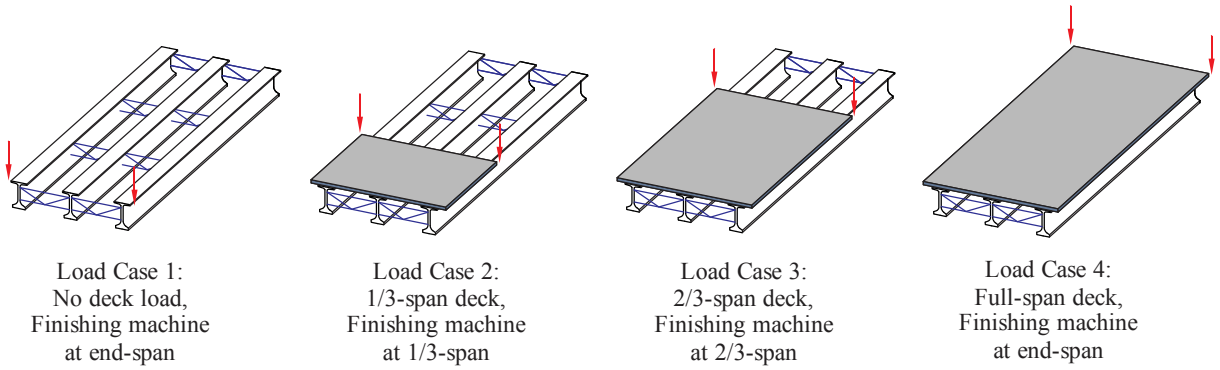

Figure 3.13 Coverage of deck loads as a function of finishing machine location (Bridges with third-point bracing)

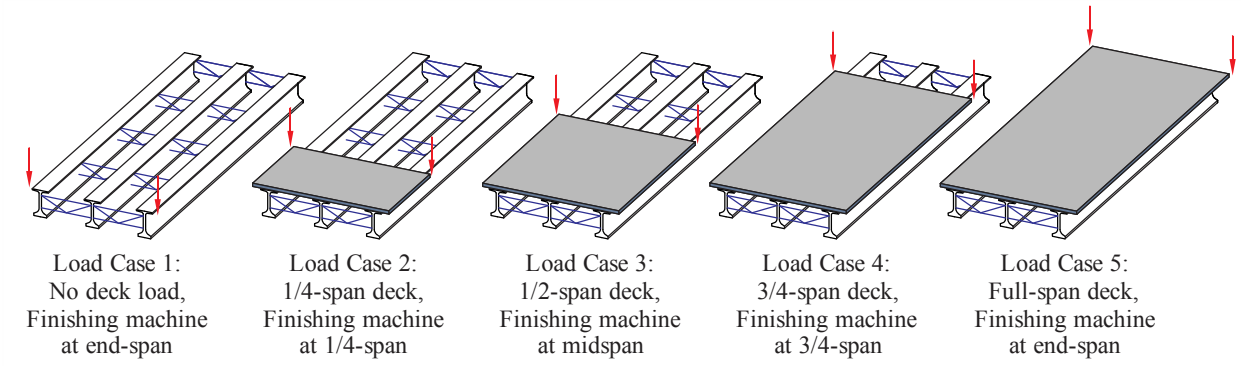

Figure 3.14 Coverage of deck loads as a function of finishing machine location (Bridges with quarter-point bracing)

According to *AASHTO Guide Design Specifications for Bridge Temporary Works* (2008), a worker line load (75 lb/ft [un-factored] over a length of 20 ft) should be included as a design load during the deck placement. This line load accounts for additional workers that are standing on the overhang platform during deck placement. For load cases where the finishing machine was at either the start or the end of the bridge, the worker line load was applied over the first or last 20 ft of the structure. For all other cases, where the concrete deck terminated at an interior brace point, the 20 ft line load extended longitudinally 10 ft to either side of the brace point (and finishing machine location).

CHAPTER 4
DEVELOPMENT OF BRACE FORCE PREDICTIONS

4.1 Introduction

To investigate brace forces caused by eccentric construction loads, a large-scale parametric study was performed using finite element models of braced systems of Florida-I Beams (FIBs). As discussed in the previous chapter, several load cases were considered depending on the number of bracing lines present in the bridge. From the parametric study, maximum end-span brace forces and intermediate-span brace forces (if present) were quantified for both factored and un-factored construction loads. In bridge construction, different types of bracing may be provided at the end-span versus at intermediate-span (interior) bracing points due to relative differences in brace forces at these locations. However, it is also typical practice to use a consistent type of bracing throughout the interior portion of the bridge (i.e., longitudinally away from the ends). Therefore, for each bridge analyzed in the parametric study, maximum brace forces were quantified once for all end-span braces, and a second time for all intermediate-span (interior) braces.

For X-brace (cross-brace) models, the maximum diagonal brace forces were quantified at end-span and intermediate-span bracing locations. However, K-braces typically have smaller diagonal element forces as compared to the top and bottom horizontal element forces. Therefore, for K-brace models, maximum diagonal forces were quantified separately from the maximum horizontal element forces (and, as noted above, separately for end-span and intermediate-span bracing locations).

Ultimately, the goal in performing the parametric study was to develop a method by which engineers can rapidly compute brace forces for varying system parameters (girder type, span length, number of bracing locations, etc.). One approach to achieving this goal would be to perform a moderate size parametric study, use the resulting brace force data to attempt to identify key relationships between forces and system parameters, and then form empirical brace force prediction equations. Such an approach must balance several—often competing—issues: the need for the empirical prediction equations to be mathematically simple in form; conservative in their prediction of brace force; but not *overly* conservative (since this outcome could lead to uneconomical bracing designs). The alternative approach taken here was to conduct a large-scale (and relatively 'fine-grain') parametric study (in total, approximately 600,000 three-dimensional (3-D) structural analyses of FIB bridges were conducted); store the summarized results data into a simple database; and then subsequently access and interpolate that database whenever brace forces need to be computed (i.e., predicted for design). By including a sufficiently large number of incremental values of each system parameter (e.g., span length, skew angle, number of braces, etc.), the error introduced in brace force prediction by database interpolation was kept to an acceptably small level. In verification tests demonstrated later in this chapter, it will be shown that the interpolated database approach yields results which are, in a majority of cases, less than ten percent (10%) in error.

4.2 Limited-scope sensitivity studies

Fully characterizing a braced multi-girder bridge system requires a large number of geometric parameters. Consequently, conducting a parametric study in which *all possible* combinations of these parameters were considered (even if only a few discrete values were

selected per parameter) would require millions of individual structural analyses to be performed. To avoid such a situation, several limited-scope sensitivity studies were performed to help guide the design of an efficient final 'database-production' parametric study. As a result of these preliminary investigations, several geometric parameters were identified as having negligible influence on bracing forces due to construction loads and were therefore excluded from the database-production parametric study. Additionally, sensitivity studies were performed to address the influence of K-brace configuration type (i.e., inverted K-brace, horizontally offset diagonal connections, etc.) on brace forces so that a conservative, representative brace type could be selected for use in the database-production parametric study. Also, in order to achieve an efficient number of construction load cases (due to the longitudinal variability of the finishing machine and concrete deck loads), the critical loading conditions to be used in the database-production parametric study were also determined.

4.2.1 Effect of geometric imperfections on brace forces

Geometric deviations (i.e., deviations from perfectly horizontal, straight girders) were considered in several limited-scope sensitivity studies to quantify the effects of the geometric deviations on maximum brace forces. In total, approximately 500 analyses were conducted for a variety of FIB bridge configurations. Bridge geometric parameters that did not have a significant effect on brace forces were not included in the database-production parametric study. Similar trends of brace force sensitivity—for both maximum end-span and intermediate-span bracing—were observed for all tested cases. Therefore, representative results for an example girder system [three (3) 78" FIB girders, quarter-point K-braces, 9 ft girder spacing, 4 ft deck overhang, 0 deg. bridge skew, service construction loads (no load factors)] are provided below for each geometric imperfection parameter:

- Grade: Longitudinal incline of the girders (recall Figure 2.2), typically expressed as a percentage of rise per unit of horizontal length. As evident in the example presented in Figure 4.1, the increase of grade by 2% had no effect on brace forces. Consequently, 0% grade was assumed for all cases in the database-production parametric study.

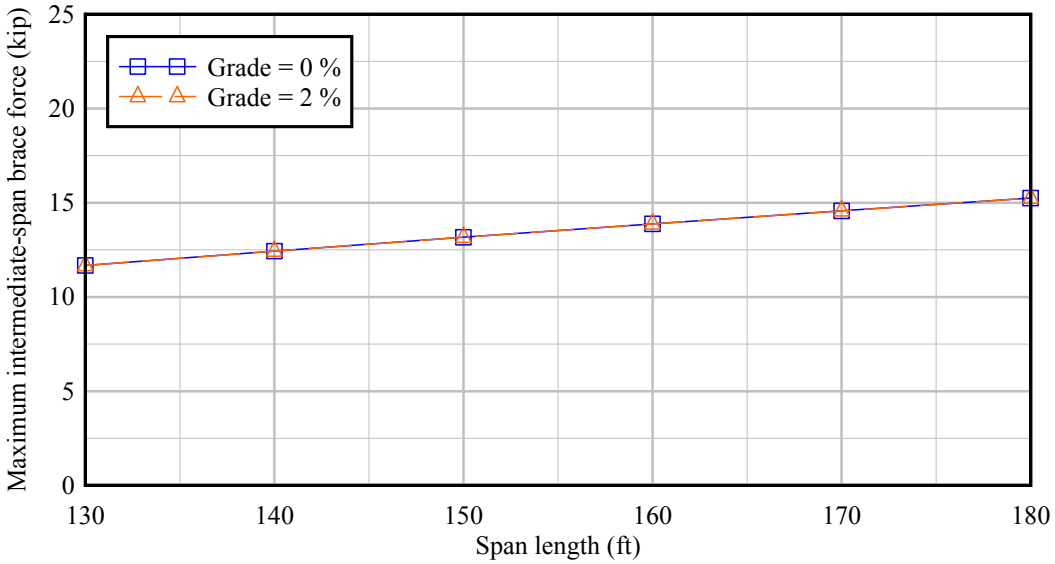

Figure 4.1 Effect of bridge grade on brace forces for an example 78" FIB system

- Cross-slope: Transverse incline (slope) of the deck (recall (Figure 2.3)), typically expressed as a percentage, which results in girders that are staggered vertically. As evident in the example presented in Figure 4.2, an increase of cross-slope by 2% had a negligible effect on brace forces. Other girder systems with higher and lower cross-slopes showed similarly negligible influences on brace forces (for both end-span and intermediate-span brace forces). Therefore, a cross-slope of 0% was assumed for all cases in the database-production parametric study.

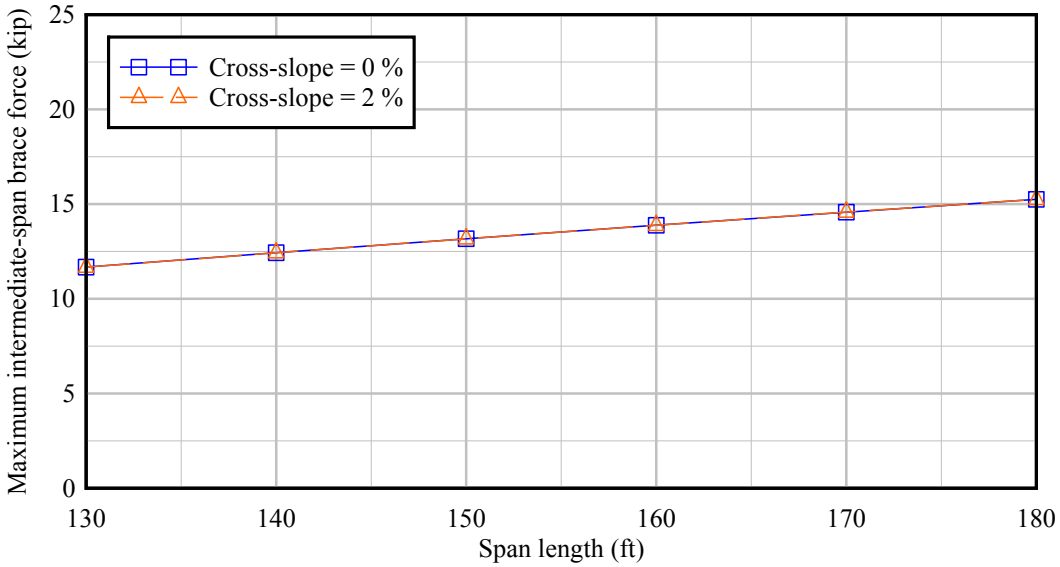

Figure 4.2 Effect of cross-slope on brace forces for an example 78" FIB system

- Camber: Vertical bowing of the girder (recall Figure 2.5) due to prestressing in the bottom flange, expressed as the maximum vertical deviation from a perfectly straight line connecting one end of the girder to the other. Girder camber was implemented as a vertical parabolic shape with a maximum vertical deviation at midspan. As evident in the example presented in Figure 4.3, an increase of camber of 6 inches (at midspan) for all girders in the system had no effect on maximum end-span brace and intermediate-span brace forces. Note that camber sensitivities for other girder systems with higher and lower maximum cambers were similar. Therefore, zero inches of camber was assumed in the database-production parametric study.

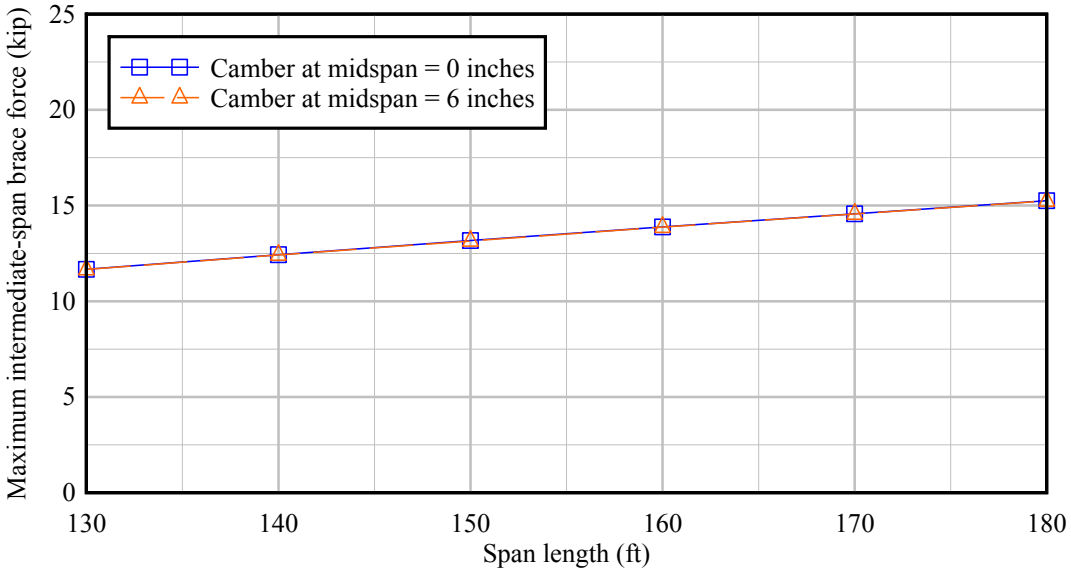

Figure 4.3 Effect of camber on brace forces for an example 78" FIB system

- Sweep: Lateral bowing of the girder (recall Figure 2.6) due to manufacturing imperfections, expressed as the maximum horizontal deviation from a perfectly straight line connecting one end of the girder to the other. Construction tolerances for FIBs are specified in the *FDOT Standard Specifications for Road and Bridge Construction* (FDOT, 2010), which limits girder sweep to ⅛ in. for every 10 ft of girder length, but not to exceed 1.5 in. Therefore, both maximum end-span and intermediate-span brace forces were compared between girder systems without sweep and girder systems with the *maximum* possible sweep of 1.5 inches (applied to all girders). By extending the modeling methodology developed in BDK75-977-33 (Consolazio et al., 2013), sweep was implemented using a half-sine function, with the maximum allowable sweep at midspan. In the example presented in Figure 4.4, increasing sweep from zero to the maximum permitted value increased the intermediate-span brace forces by approximately five percent (5%). In all tested cases, the percent differences of end-span and intermediate-span brace forces—caused by maximum girder sweep—were less than 5%. Due to the relatively small influence of sweep on brace forces, girder sweep imperfections were omitted from the database-production parametric study (i.e., lateral girder sweep was assumed to be zero at midspan).

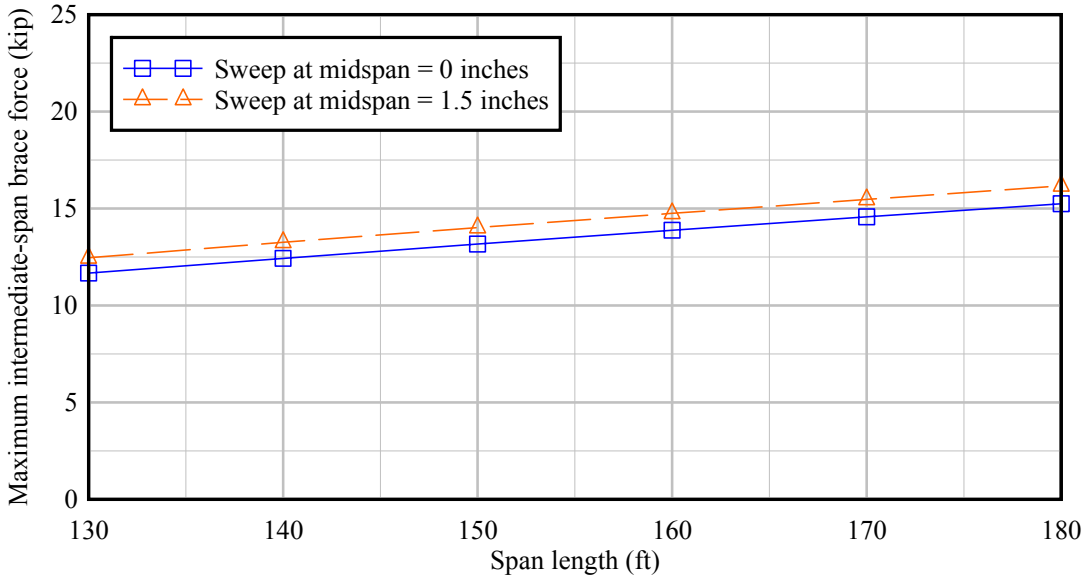

Figure 4.4 Effect of sweep on brace forces for an example 78" FIB system

4.2.2 Effect of K-brace configuration on brace forces

Sensitivity studies were performed to assess the influence of K-brace configuration (inverted K-brace, horizontally offset diagonal connections, etc.) on brace forces so that a conservative, representative brace type could be selected for the database-production parametric study. In total, approximately 300 sensitivity analyses were conducted for a variety of different bridge configurations. From a survey of typical bracing types used in modern Florida bridges, four typical K-brace types were selected (Figure 4.5). Each K-brace configuration was given a letter designation (*Type-A*, *Type-B*, etc.) for comparison purposes.

This limited-scope sensitivity study assessed the effects of K-bracing configuration on brace forces for a broad range of geometric parameters (e.g., span length, girder spacing, deck overhang width, etc.). In the *FDOT Design Standard No. 20005: Prestressed I-Beam Temporary Bracing* (FDOT, 2014a), the *Type-A* K-brace configuration (Figure 4.5) is recommended for both end-span and intermediate-span bracing applications. Therefore, it was used as a *reference brace*, by which other K-brace forces in the sensitivity study could be compared by normalization.

As evident in Figure 4.6, the *Type-A* K-brace had normalized maximum brace force results that were approximately equal to *Type-C* (i.e., normalized values were approximately 1.0 indicating that the brace forces were very similar). Additionally, the *Type-A* K-brace had conservatively higher, but not overly-conservative, maximum brace forces compared to the offset diagonal configurations of *Type-B* and *Type-D* (Figure 4.7, normalized values were slightly greater than 1.0 in most cases). Note that the average conservatism of Type A compared to both *Type-B* and *Type-D* was approximately five percent (5%). Therefore, the *Type-A* configuration was selected as the representative K-brace configuration to be used for all cases in the database-production parametric study.

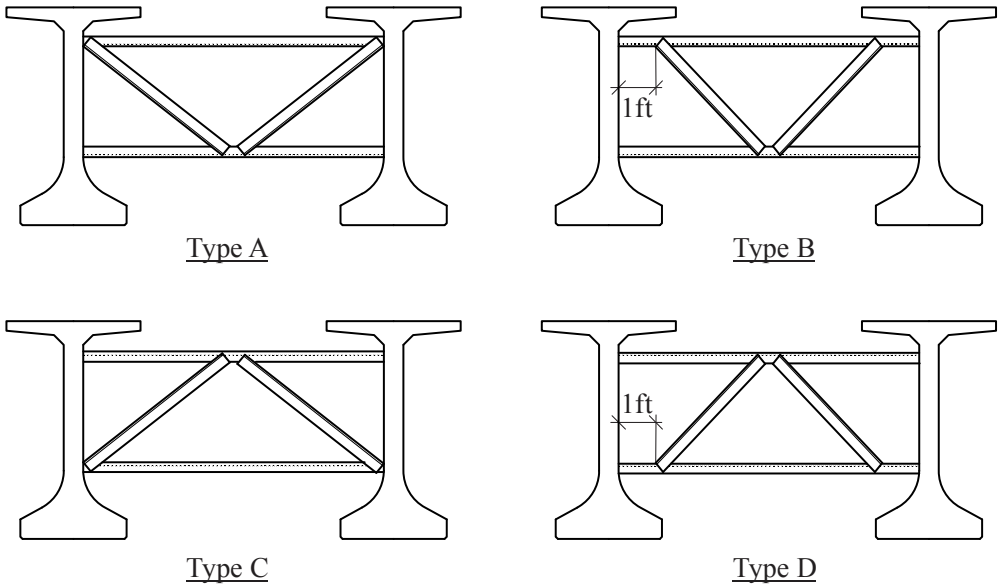

Figure 4.5 K-brace configurations analyzed in limited-scope sensitivity study

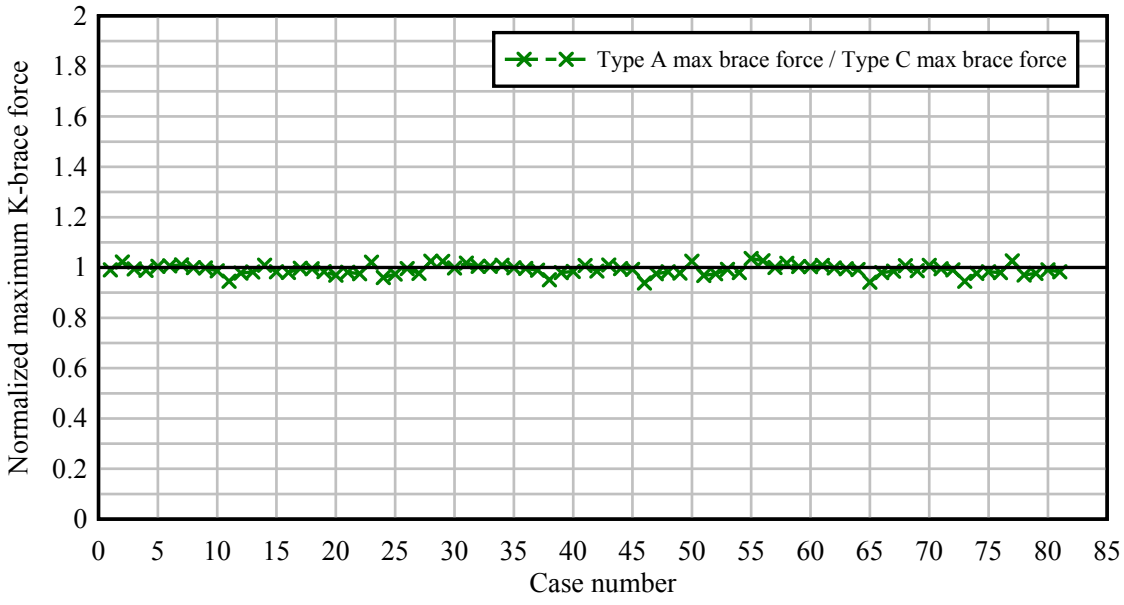

Figure 4.6 Conservatism of selected K-brace configuration (compared to inverted K-brace)

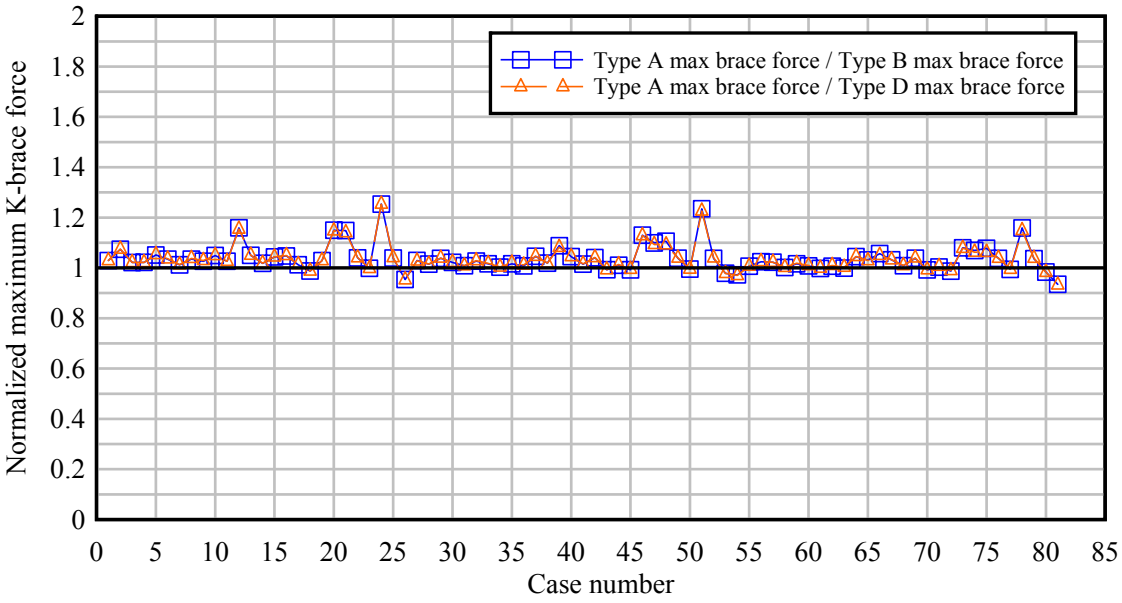

Figure 4.7 Conservatism of selected K-brace configuration (compared to offset ends)

4.2.3 Effect on brace forces of partial application of construction loads

As discussed previously, during the process of placing and finishing a concrete bridge deck, wet concrete pressure loads are applied to a bridge (by way of SIP forms) over incrementally increasing lengths of the structure. Consequently, loading conditions corresponding to the placement of concrete deck loads over *partial lengths* of the bridge—less than the total span length—were considered in the database-production parametric study. For all such partial deck coverage cases, the position of the finishing machine was taken to coincide with the location of the furthest placed concrete. As discussed in Chapter 2, wet concrete is typically placed just ahead of the finishing machine (recall Figure 2.14) using a pump, therefore, in the vast majority of paving situations, the location of the finishing machine and the end of the concrete coverage will generally coincide.

A limited-scope sensitivity study was conducted to determine the critical locations—those that cause maximum brace forces—of the wet slab and finishing machine. In total, approximately 900 analyses were conducted where the concrete deck coverage area was moved in small increments along the bridge length. For this sensitivity study, the increments corresponded to the bridge 10^{th} points (i.e., increments of ten percent (10%) of the bridge span length). In all cases, the maximum end-span brace and intermediate-span brace forces occurred when the web slab load terminated close to one of the bracing points (e.g., end point, 1/2 point, 1/3 point, 1/4 point). Conversely, it was determined that partially placed deck loads terminating *between* the locations of the braces did not control maximum end-span or intermediate-span brace forces. Therefore, for purposes of quantifying maximum brace forces in the database-production parametric study, it was found to be adequate to consider the multiple deck load cases illustrated earlier in Figures 3.11 - 3.14 for each bridge, with the specific number of load cases depending on the number of intermediate-span bracing lines present in the bridge.

4.3 Scope of the 'database-production' parametric study

To develop a comprehensive database of brace forces for use in the brace force prediction program, a final 'database production' parametric study was conducted. Three-dimensional (3-D) structural analyses were conducted to quantify maximum end-span and intermediate-span brace forces for combinations of the following parameters:

- FIB cross-section depth (in.)
- Span length (ft)
- Girder spacing (ft)
- Deck overhang width (ft)
- Skew angle (deg.)
- Brace type (K-brace or X-brace)
- Number of brace points (end-span only, 1/2 point, 1/3 point, 1/4 point)
- Number of girders
- Construction load factors (un-factored service loads; factored strength loads)

Specific parameter values that were included in the database-production parametric study—which involved 604,800 separate analyses—are listed in Table 4.1. For the factored construction load analyses, the load factors previously listed in Table 3.1 were used. (Note that seven (7) of the eight (8) standard FIB cross-sections were included in the study. The 36″ FIB, however, was excluded because the cross-section is so shallow that use of moment-resisting X-braces and K-braces is not likely to be feasible or warranted).

Table 4.1 Parameter values used in the database-production parametric study

Span length, *L* (ft)						
45″ FIB	**54″ FIB**	**63″ FIB**	**72″ FIB**	**78″ FIB**	**84″ FIB**	**96″ FIB**
40	50	60	60	70	80	80
60	80	80	90	100	110	120
80	100	110	120	130	150	160
90	110	120	130	140	160	170
100	120	130	140	150	170	180
110	130	140	150	160	180	190
120	140	150	160	170	190	200
130	150	160	170	180	200	210

Deck overhang width, (in.)	**Skew angle**	**Intermediate-span brace points, n_i**	**Girder spacing, (ft)**	**Girders, n_g**
25	0°	0	6	3
36	15°	1	9	5
48	30°	2	12	9
60	45°	3		
72				

Maximum and minimum span lengths used in the parametric study were based on design aids included in the *FDOT Instructions for Design Standard No. 20010: Prestressed Florida-I Beams* (IDS 20010; FDOT, 2014b), which provide estimated span lengths (Table 4.2) for FIBs with different lateral spacings, based on representative bridge design calculations. Maximum lengths were conservatively based on a lateral girder spacing of 6 ft and an environment classified as ‘'Moderately Aggressive’, while minimum lengths assumed a 12-ft spacing and an ‘Extremely Aggressive’ environment. To ensure that the considered length ranges included all reasonable beam designs, the basic ranges taken from FDOT IDS 20010 were extended to cover a total span range of 50 ft.

In some circumstances, design constraints unrelated to girder strength may result in the use of span lengths significantly shorter than the typical ‘design range’ minimums listed in Table 4.2. To address these situations, additional cases were included in the ‘database production’ parametric study scope in order to improve the accuracy of brace force predictions for shorter-than-typical span lengths. It was determined that span lengths of approximately 50% and 75% of the ‘typical’ minimum span lengths (from Table 4.2) would envelope the vast majority of applications involving short-span bridge girders. Therefore, the parametric study scope included span lengths from the basic design ranges (Table 4.2) as well as two additional short-span lengths (see first two rows of span lengths in Table 4.1) for each girder type. Note that for each girder type, the short span lengths were rounded to the nearest 10-ft interval.

It was also determined from a survey of typical bridges (and FDOT recommendations) that the range of other geometric parameters, such as deck overhang widths, girder spacings, and skew angles, would cover most design scenarios. Additionally, preliminary analyses indicated that as the number of interior brace points increases beyond three (3) interior braces (i.e., 1/4 point bracing), changes in maximum brace forces become small (i.e., the brace forces converged). Similarly, increasing the number of girders in the system beyond nine (9) girders did not significantly change maximum brace forces in the construction load analyses. Therefore, bridges with more than nine girders were not expected to have significantly different brace forces induced by construction loads than would a bridge with nine (9) girders.

Table 4.2 Range of typical span lengths for FIBs

	Values from FDOT IDS 20010		
	Min length (ft) (Based on 12-ft girder spacing and an ‘Extremely Aggressive’ environment)	**Max length (ft)** (Based on 6-ft girder spacing and an ‘Moderately Aggressive’ environment)	**Span length range considered**
45″ FIB	98	126	80–130
54″ FIB	113	142	100–150
63″ FIB	124	155	110–160
72″ FIB	142	173	120–170
78″ FIB	151	182	130–180
84″ FIB	159	191	150–200
96″ FIB	175	208	160–210

For each Florida-I beam in the parametric study, a single bracing depth (Figure 4.8) was assigned based on available web height. For FIB sections, as the overall girder depth increases, so does the available web depth (since the top and bottom flange dimensions remain constant).

Therefore, deeper girders in the parametric study allowed for larger brace depths. Additionally, as brace depth increases, the bracing system becomes more effective in resisting torsional moments induced by eccentric construction loads. Therefore, the representative brace depths chosen for the parametric study (Table 4.3) were selected so as to avoid producing overly-conservative brace force data.

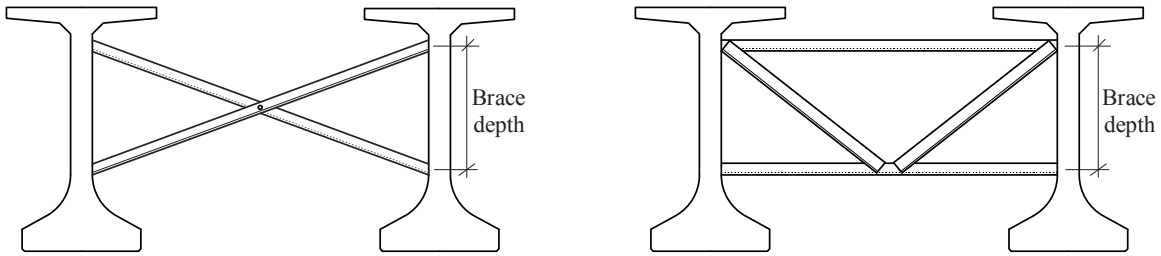

Figure 4.8 Definition of brace depth

Table 4.3 Brace depths used in construction load parametric study

Girder type	Brace depth, (in.) (For both X-brace and K-brace)
45” FIB	18
54” FIB	22
63” FIB	27
72” FIB	36
78” FIB	41
84” FIB	48
96” FIB	60

4.4 Calculation of brace forces by database interpolation

As noted earlier, the approach to brace force prediction (calculation) taken in this study was to conduct a large-scale parametric study; store the brace force results into a database; and then access and interpolate that database when forces are needed for bracing design. The overall database of information generated by the database-production parametric study was stored into two text-file ‘databases’—one for K-braced systems, and the other for X-braced systems. Within each database file, maximum brace forces were stored both for *un-factored* service loads and for *factored* strength loads. Additionally, for K-braced systems, diagonal element forces and horizontal element forces were computed and stored separately. Data contained within the database files are organized in such a manner that particular cases of interest can be efficiently located.

To make the process of accessing and interpolating the database simple and user-friendly, a MathCad-based program was developed. The program allows the user to specify the following key system parameters:

- FIB cross-section depth (in.)
- Span length (ft)

- Girder spacing (ft)
- Deck overhang width (ft)
- Skew angle (deg.)
- Brace type (K-brace or X-brace)
- Number of brace points (end-span only, 1/2 point, 1/3 point, 1/4 point)
- Number of girders

and reports back the maximum end-span and intermediate-span brace forces for un-factored (service) and for factored (strength) loading conditions. Of the eight (8) parameters listed above, three (3) are never interpolated since intermediate values are not possible—FIB depth, number of interior brace points, and brace type (K-brace or X-brace). For the five (5) remaining parameters (span length, girder spacing, deck overhang width, skew angle, and number of girders), the corresponding data are extracted directly from the database, if an exact match is available. If, however, an exact match is not available, then interpolation (and in some cases, extrapolation) is used to estimate the brace forces. To accomplish this outcome, the program implements a five-dimensional linear interpolation algorithm.

When user-specified parameter values lie outside the scope of the database-production parametric study (Table 4.1), one of three possible actions will occur: 1) data extrapolation; 2) data bounding; 3) generation of an error message. For some parameters, limited linear extrapolation outside the scope of the database is appropriate. However, for some parameters, it is more appropriate to report brace forces for the *bounding* value from Table 4.1 rather than to perform extrapolation. For example, when the number of girders exceeds nine (9), it is more appropriate to estimate the brace forces using data corresponding to a bridge with nine (9) girders than to perform linear extrapolation. Note that whenever data extrapolation or data bounding are necessary to compute brace forces, a message is generated by the program indicating to the user which process was used. Finally, selected parameter values are not permitted to be outside the range indicated in Table 4.1. Specifically, skew angles larger than 45 degrees and deck overhang widths larger than 6 ft are not permitted and will result in an error message being generated.

4.5 Verification of database approach

To evaluate the level of accuracy and conservatism produced by the interpolated database approach (and to verify correct functioning of the associated calculation program that was developed), a limited-scope sensitivity study was conducted. System parameters used in the sensitivity study (e.g., span length, deck overhang width, skew, girder spacing, number of girders) were specifically chosen to fall *between* the parameter values (Table 4.1) that were used to generate the brace force database. Additionally, for each set of intermediate system parameters that were chosen, an additional—and corresponding—finite element bridge model was constructed and analyzed to provide a datum for brace force comparison.

Approximately 200 unique geometric configurations of bridges with end-span and mid-span bracing (involving approximately 600 separate analyses with multiple construction *loading* conditions) were tested for a broad range of girder types. The level of accuracy and conservatism was quantified for each case by normalizing the database-predicted maximum brace forces by the maximum brace forces computed from the additional finite element analyses. Normalized results for K-brace cases are illustrated in Figure 4.9 for end-span braces and Figure 4.10 for intermediate-span braces. Similarly, results for X-brace cases are illustrated in Figure 4.11 for

end-span braces and Figure 4.12 for intermediate-span braces. For all four sets of data presented, the majority of the database predicted brace forces were within ±10% of the corresponding finite element computed values. Furthermore, in all four sets of data, the distributions of normalized predictions were clearly biased (skewed) toward the side of producing conservative results. Overall, the level and bias of the conservatism produced by the interpolated database approach was considered to be appropriate and reasonable for purposes of designing braces.

Note that these analyses included different combinations of intermediate parameters (i.e., parameters not in parametric study scope) from one intermediate parameter to all five parameters (skew, number of girders, span lengths, girder spacings, and deck overhang width).

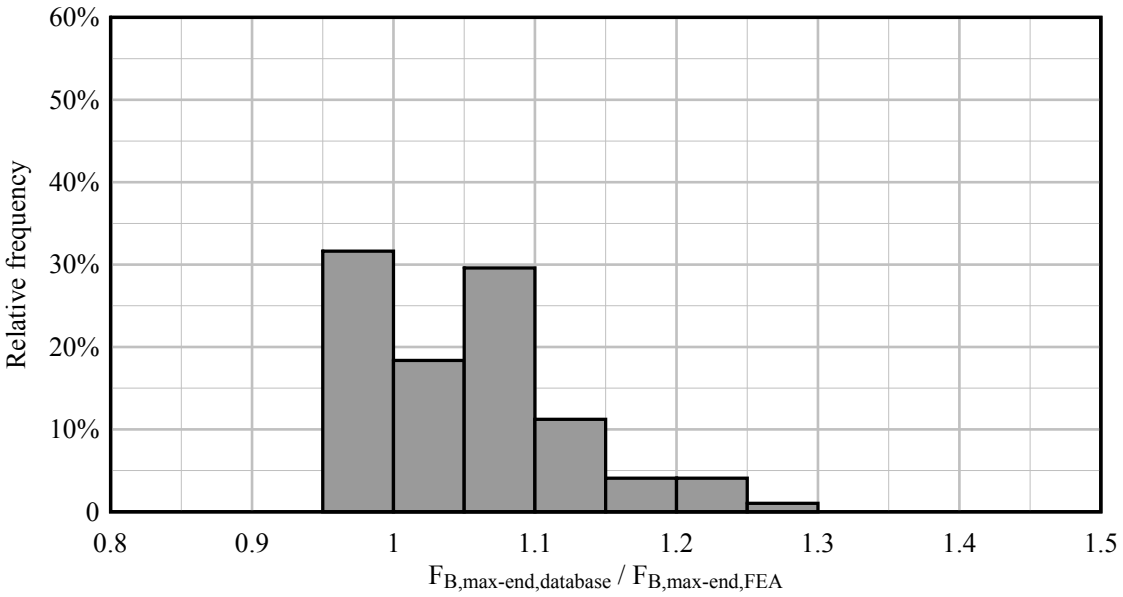

Figure 4.9 Accuracy of interpolated database approach for maximum end-span K-brace force

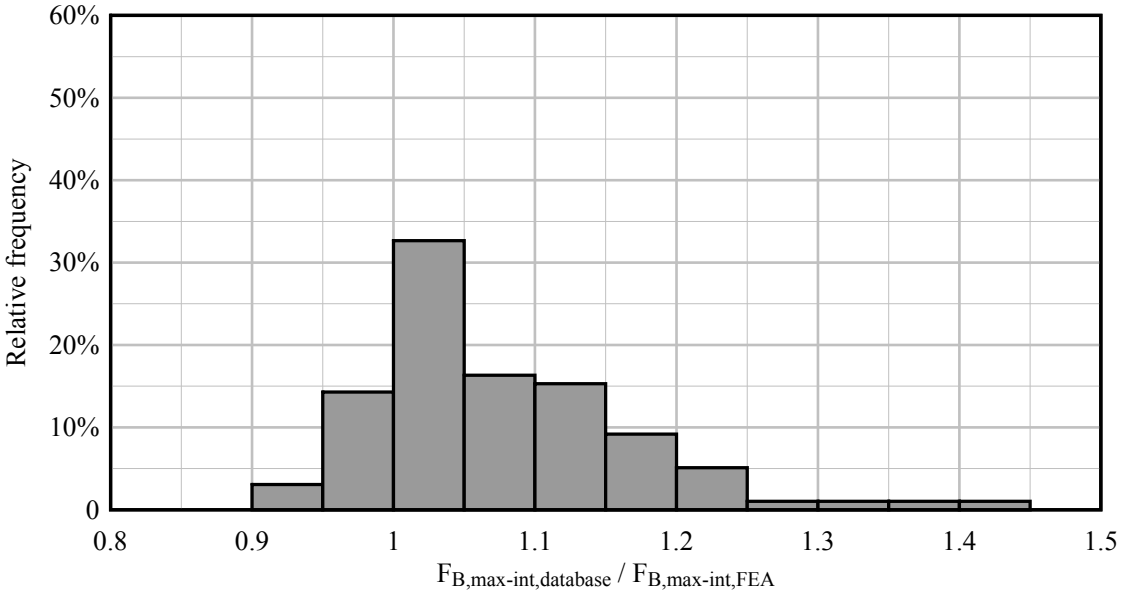

Figure 4.10 Accuracy of interpolated database approach for maximum intermediate-span K-brace force

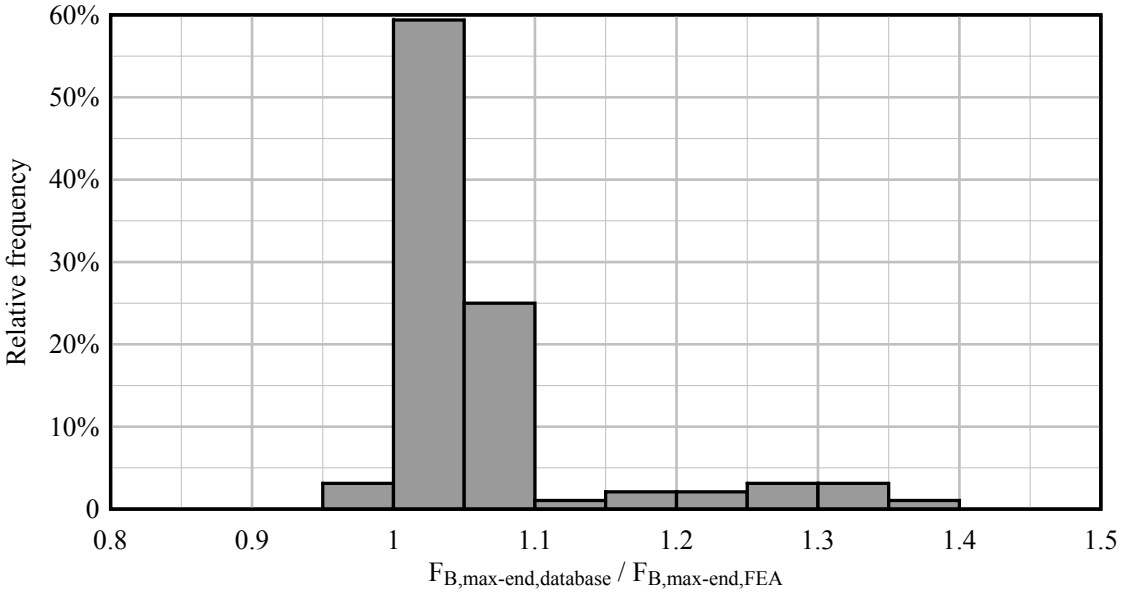

Figure 4.11 Accuracy of interpolated database approach for maximum end-span X-brace force

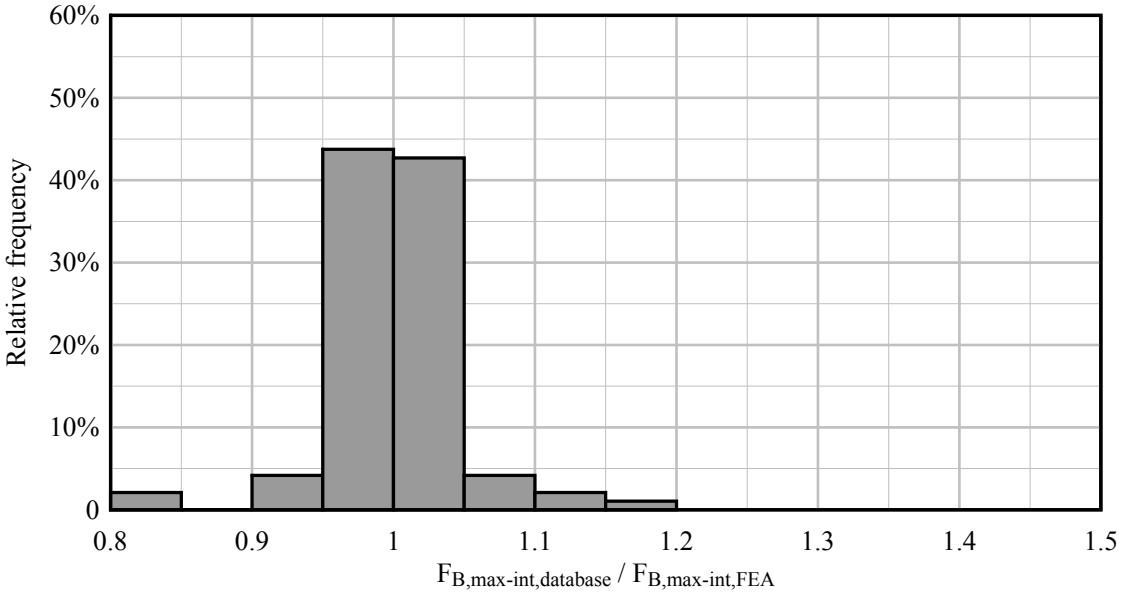

Figure 4.12 Accuracy of interpolated database approach for maximum interior-span X-brace force

CHAPTER 5
WIND TUNNEL TESTING

5.1 Introduction

In addition to the construction loads discussed in previous chapters, wind loads must also be accounted for when quantifying brace forces for bracing system design. In a previously conducted study (BDK75-977-33, Consolazio et al., 2013) wind tunnel tests were conducted to quantify girder drag coefficients for partially constructed bridges at the stage where only the girders and bracing are present. When stay-in-place forms and overhang formwork are subsequently added to the bridge—as part of the ongoing construction process—they introduce new barriers to wind flow (e.g., between adjacent girders) and therefore have the potential to alter the drag coefficients for the individual girders within the bridge cross-section. A goal of the present study was to therefore to quantify drag coefficients for individual girders in bridges that are at the construction stage where stay-in-place forms and overhang formwork have been installed. To achieve this goal, wind tunnel tests were conducted on bridges with stay-in-place forms present (and in some cases overhangs) to generate data that would complement data previously measured in BDK75-977-33. By comparing data measured in the current study to data from the previous study, the influences of stay-in-place forms and overhangs on girder drag coefficients could be quantified and appropriate drag coefficients for wind-load brace force design could be determined.

Additionally, since practical bridge structures almost always consist of *multiple* girders positioned side by side, it was also necessary to investigate the effects of *shielding* (i.e., aerodynamic interference), in which the windward girder acts as a wind break and reduces the total force on subsequent leeward girders. The wind tunnel tests conducted in this study were therefore performed on bridge cross-sections with variations in the number of girders, variations in girder spacing, and variations as to the presence of stay-in-place forms and overhangs.

5.2 Background on drag coefficients

In order to calculate wind load on a bridge girder, it is necessary to know the drag coefficient for the girder cross-sectional shape. The drag coefficient is a type of *aerodynamic coefficient*: a dimensionless factor that relates the magnitude of the fluid force on a particular geometric shape to the approaching wind speed. Drag coefficients are typically a function of the relative orientation of the object relative to the direction of the impinging wind.

5.2.1 Dimensionless aerodynamic coefficients

Fluid forces arise when a solid body is submerged in a moving fluid. As the fluid flow is diverted around the body, a combination of inertial and frictional effects generates a net force on the body. It is observed that this force—called aerodynamic force (F) when the fluid under consideration is air—is directly proportional the dynamic pressure (q) of the fluid:

$$q = \frac{1}{2}\rho V^2 \tag{5.1}$$

where ρ is the mass density of the fluid and V is the flow velocity (Çengel and Cimbala, 2006). Dynamic pressure can be considered as the *kinetic energy density* of the fluid. This offers an

intuitive explanation for its proportional relationship to aerodynamic force, which is, at the most fundamental level, the cumulative effect of innumerable microscopic collisions with individual fluid particles. Similarly, if the dimensions of the body are scaled up, it is observed that the aerodynamic force increases quadratically, reflecting the fact that the increased surface area results in a greater total number of collisions.

These proportional relationships can be combined and expressed as:

$$F = C_F q L_0 L_1 \tag{5.2}$$

where, L_0 and L_1 are arbitrary reference lengths, and C_F is a combined proportionality factor, called a *force coefficient*. The selection of L_0 and L_1 does not affect the validity of Eqn. (5.2) as long as they both scale with the structure. However, it is important to be consistent; force coefficients that use different reference lengths are not directly comparable, and a coefficient for which the reference lengths are not explicitly known is useless for predicting aerodynamic forces. In structural applications, it is common for the product $L_0 L_1$ to be expressed in the form of a reference area, A, which is typically taken as the *projected area* of the structure in the direction of wind.

By an analogous process, it is possible to derive a *moment coefficient* (C_M), which normalizes aerodynamic moment load in the same way that the force coefficient normalizes aerodynamic force. The only difference is that aerodynamic moment grows cubically with body size rather than quadratically (because the moment arms of the individual collisions grow along with the surface area). Therefore, the moment proportionality expression is:

$$M = C_M q L_0 L_1 L_2 \tag{5.3}$$

As with the force coefficient, the reference lengths must be known in order to properly interpret the value of C_M. However, with moment coefficients, it is equally important to know the center of rotation about which the normalized moment acts. Together, C_F and C_M are called *aerodynamic coefficients*, and they can be used to fully describe the three-dimensional state of aerodynamic load on a structure (for a particular wind direction).

When working with bridge girders, or other straight, slender members, it is often convenient to assume that the length of the girder is effectively infinite. This simplifies engineering calculations by reducing the girder to a two-dimensional cross-section subjected to in-plane aerodynamic line-loads (Figure 5.1). Depending on the direction of wind, out-of-plane forces and moments may exist, but they generally do not contribute to the load cases that control design and can therefore be considered negligible. In two dimensions, the proportionality expressions for the aerodynamic coefficients become:

$$F' = C_F q L_1 \tag{5.4}$$

$$M' = C_M q L_1 L_2 \tag{5.5}$$

where, F' is a distributed force (force per unit length) and M' is a distributed torque (moment per unit length). Note that two-dimensional aerodynamic coefficients can be used interchangeably in the three-dimensional formulation if the reference length L_0 is taken to be the out-of-plane length of the girder. All further discussions of aerodynamic coefficients in this report will use the two-dimensional formulation unless stated otherwise. The remaining reference lengths (L_1 and L_2)

will always be taken as the girder depth, D, so that the force and moment coefficients are defined as:

$$C_F = \frac{F'}{\frac{1}{2}\rho V^2 D} \tag{5.6}$$

$$C_M = \frac{M'}{\frac{1}{2}\rho V^2 D^2} \tag{5.7}$$

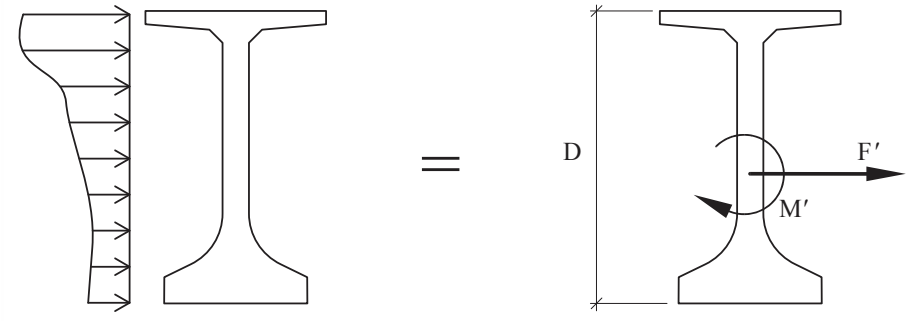

Figure 5.1 Two-dimensional bridge girder cross-section with in-plane line loads

Aerodynamic coefficients are sometimes called *shape factors* because they represent the contribution of the geometry of an object (i.e., the way airflow is diverted around it), independent of the scale of the object or the intensity of the flow. Because of the complexity of the differential equations governing fluid flow, the aerodynamic coefficients of a structure are not calculated from first principles but can, instead, be measured directly in a wind tunnel using reduced-scale models.

5.2.2 Terminology related to aerodynamic coefficients

Aerodynamic force on a body is typically resolved into two orthogonal components, drag and lift. These components have corresponding force coefficients: the *drag coefficient* (C_D) and *lift coefficient* (C_L). In this report, drag is defined as the lateral component of force and lift is defined as the vertical component of force, regardless of the angle of the applied wind.

In several subfields of fluid dynamics, it is more conventional to define drag as the component of force along the direction of the wind stream and lift as the component perpendicular to the wind stream. However, this is inconvenient when evaluating wind loads on stationary structures (e.g., bridge girders) because the angle of the wind stream can change over time. Where necessary in this report, the names *stream drag* (C_{SD}) and *stream lift* (C_{SL}) (Figure 5.2) will be used to refer to the force components that are aligned with, and perpendicular to, the wind stream.

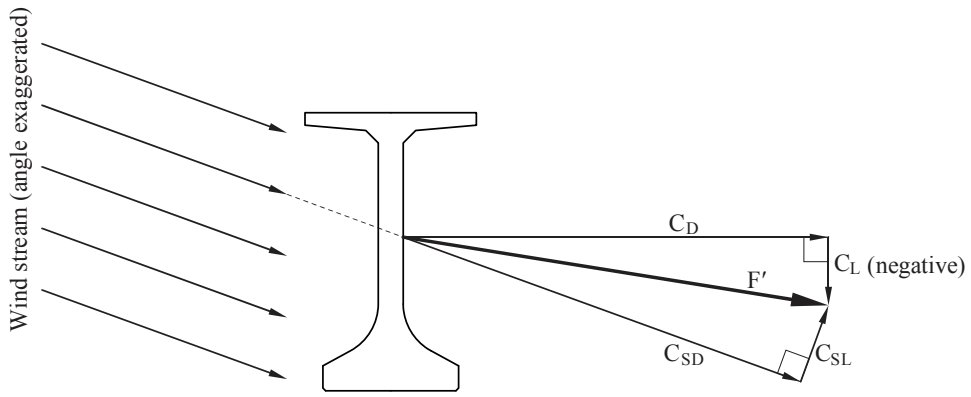

Figure 5.2 Definition of C_D, C_L, C_{SD}, and C_{SL}
(shown in positive direction except when noted)

Finally, the term *pressure coefficient* (C_P), is an alternative name for C_D, and is often used in design codes to indicate that it is to be used to calculate a wind *pressure* load (P), rather than a total force, as in:

$$P = C_P \frac{1}{2} \rho V^2 \tag{5.8}$$

This is advantageous because it obviates the need to explicitly specify the characteristic dimensions that were used to normalize the coefficient. Instead, denormalization occurs implicitly when the pressure load is applied over the projected surface area of the structure. Unfortunately, this approach breaks down when working with drag and lift coefficients together. If drag and lift are both represented as pressure loads, then the areas used to normalize the coefficients will differ (unless by chance the depth and width of the structure are equal). As a result, the magnitudes of the coefficients are not directly comparable—that is, equal coefficients will not produce loads of equal magnitude—and they cannot be treated mathematically as components of a single force vector, which complicates coordinate transformations and other operations. For this reason, the term pressure coefficient is not used in this report, except when in reference to design codes that use the term.

In this report, the term *torque coefficient* (C_T) refers to the in-plane moment that acts about the centroid of the cross-section. This is a convenient choice of axis because it coincides with the axes of beam elements in most structural analysis software. Loads calculated from C_D, C_L, and C_T can be applied directly to beam nodes (located at the centroid of the cross-section) to correctly model the two-dimensional state of aerodynamic load. However, most design codes represent wind load as a uniform pressure load that produces a resultant force acting at a location called the *center of pressure* (Figure 5.3), which is typically assumed to correspond to the mid-height of the cross-section. For such circumstances, the term *pressure torque coefficient* (C_{PT})—acting about the center of pressure—will be used to differentiate it from the C_T, which always acts about the centroid (Figure 5.4).

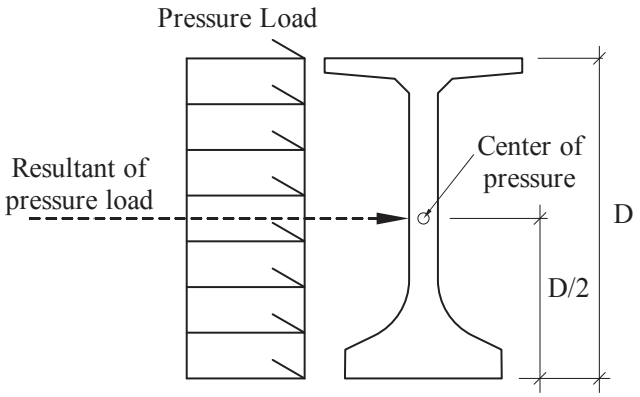

Figure 5.3 Center of pressure of a bridge girder

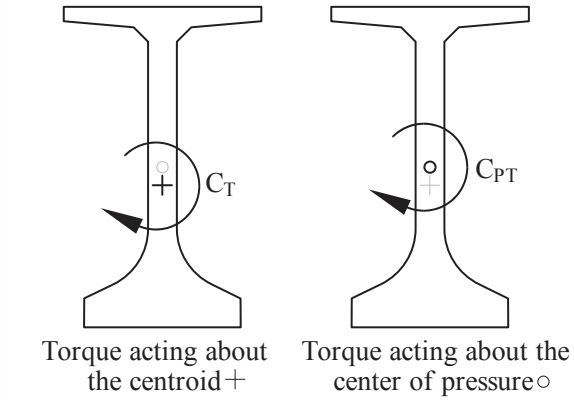

Figure 5.4 Definition of C_T and C_{PT} (shown in positive direction)

A summary of the different types of aerodynamic coefficient used in this report is presented in Table 5.1.

Table 5.1 Summary of aerodynamic coefficients

	Coefficient name	**Description**
$\mathbf{C_D}$	Drag	Component of force in horizontal (lateral) direction
$\mathbf{C_L}$	Lift	Component of force in vertical direction
$\mathbf{C_{SD}}$	Stream Drag	Component of force parallel to wind stream
$\mathbf{C_{SL}}$	Stream Lift	Component of force perpendicular to wind stream
$\mathbf{C_P}$	Pressure	Alternative name for C_D
$\mathbf{C_T}$	Torque	Torque measured about centroid
$\mathbf{C_{PT}}$	Pressure Torque	Torque measured about center of pressure

5.3 Current wind design practice in Florida

Bridge structures in Florida are designed in accordance with the provisions of the *FDOT Structures Design Guidelines* (SDG; FDOT, 2013). As with most modern design codes, the wind load provisions in the SDG are based on Eqn. (5.8), with additional scale factors included to adjust the intensity of the wind load according to the individual circumstances of the bridge. Specifically, Section 2.4 of the SDG gives the equation:

$$P_Z = 2.56\times10^{-6} K_Z V^2 G C_P \tag{5.9}$$

where P_Z is the design wind pressure (ksf, kip per square foot), K_Z is the velocity pressure exposure coefficient, V is the basic wind speed (mph), and G is the gust effect factor. The constant term, 2.56×10^{-6}, represents the quantity $\frac{1}{2}\rho$ from Eqn. (5.8) expressed in derived units of (ksf)/(mph)^2.

Each county in Florida is assigned a basic wind speed, V, adapted from wind maps published by the American Society of Civil Engineers (ASCE, 2006), which are based on statistical analyses of historical wind speed records compiled by the National Weather Service. Statistically, V represents the peak 3-second gust wind speed for a 50-year recurrence interval. In other words, if the average wind speeds during every 3-second time interval were recorded over a period of 50 years, V is the expected value of the maximum speed that would be recorded. It is important to note that this does *not* mean that Florida bridges are only designed to resist 50-year wind loads. Different load combinations use load factors for wind that effectively adjust the recurrence interval up or down. For example, the Strength III limit state, as stipulated by the SDG, includes a wind load factor of 1.4, which increases the recurrence interval to approximately 850 years (FDOT, 2009).

Basic wind speeds published by ASCE are based on measurements taken at an elevation of 33 ft and are not directly applicable to structures at other elevations. Wind that is closer to ground level is slowed by the effect of surface friction, resulting in a vertical wind gradient called the atmospheric boundary layer (Holmes, 2007). The purpose of the velocity pressure exposure coefficient, K_Z, is to modify the wind pressure load to account for differences in elevation. Because surface roughness of the terrain is known to reduce the steepness of the gradient, ASCE divides terrains into three exposure categories, B, C, and D, and provides equations for each category. However, for simplicity, the SDG conservatively assumes that all Florida structures are in the Exposure C category. As a result, the equation for K_Z in Florida is:

$$K_Z = 2.01\left(\frac{z}{900}\right)^{0.2105} \geq 0.85 \tag{5.10}$$

where z is the elevation above ground (ft). Note that K_Z is equal to unity at an elevation of 33 ft (corresponding to the wind speed measurements) and that wind speed is assumed to be constant for elevations of 15 ft or less (Figure 5.5).

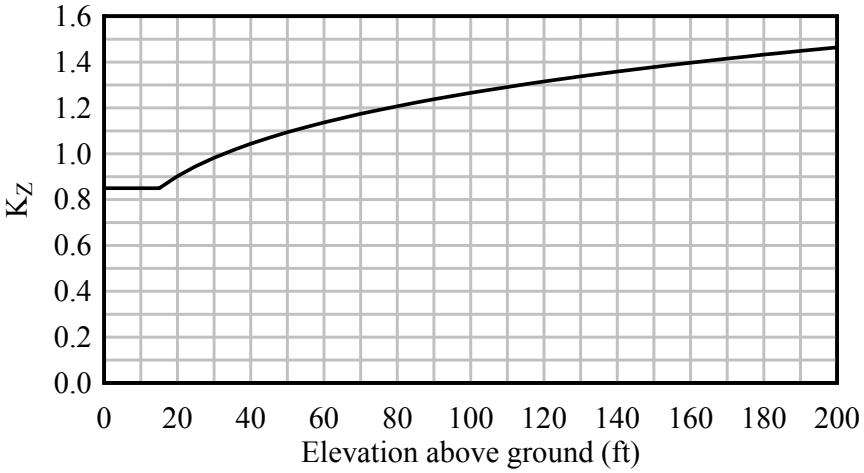

Figure 5.5 Velocity pressure exposure coefficient used by FDOT

Wind is characteristically gusty and turbulent, producing dynamic structural loads that can fluctuate significantly over short periods of time. However, it is simpler and more efficient to design structures to resist static loads. Furthermore, wind tunnel measurements of static force coefficients are typically performed in steady flow (with a major exception being site-specific wind tunnel testing, which models a proposed structure along with its surrounding terrain for the express purpose of capturing turbulent loads). The gust effect factor, G, modifies the static design wind pressure so as to envelope the effects of wind gustiness and dynamic structural response on peak structural demand. For aerodynamically rigid bridge structures, defined as those with spans less than 250 ft and elevations less than 75 ft, the SDG prescribes a gust effect factor of 0.85. By this definition, the vast majority of precast prestressed concrete girder bridges in Florida are considered aerodynamically rigid. It is noted that G actually *reduces* the design wind pressure on rigid bridges, reflecting the fact that peak gust pressures are unlikely to occur over the entire surface area of such structures simultaneously (Solari and Kareem, 1998).

The SDG further provides specific guidance on the calculation of wind loads during the bridge *construction* stage (as opposed to the calculation of wind loads on the completed bridge structure). If the exposure period of the construction stage is less than one year, a reduction factor of 0.6 on the basic wind speed is allowed by the SDG.

Calculation of wind pressure using Eqn. (5.9) requires that an appropriate pressure coefficient (C_P) be determined for the structure under consideration. Pressure coefficients are provided by the SDG for several broad categories of bridge component as indicated in Table 5.2. In the present study, the pressure coefficients of interest are those for girders *with stay-in-place forms* in place. As Table 5.2 indicates, the SDG provides a single value of C_P, regardless of girder shape, when deck forms are in place: $C_P = 1.1$. The wind tunnel testing conducted in this study was performed to help determine whether $C_P = 1.1$ is an appropriate value, and whether it should depend on the girder type.

Table 5.2 Pressure coefficients in *Structures Design Guidelines* (FDOT, 2013)

Bridge component	C_P
Substructure	1.6
Girders with deck forms in place	1.1
Completed superstructure	1.1
I-shaped bridge girders	2.2
Box and U-shaped girders	1.5

5.4 Testing configurations

To maximize the potential for comparing results from wind tunnel tests with SIP forms to those without forms, the test configurations used in a previous study (BDK75-977-33, Consolazio et al., 2013, no formwork) were used as a guide in determining the wind tunnel test program scope in the present study (with formwork). Consequently, several 'nearly-equivalent' testing configurations—with the sole difference being the presences of SIP forms—were included in the present study. Four different girder cross-sectional shapes (Figure 5.6) were selected as being representative of a wide range of modern Florida bridges:

- 78-inch-deep Florida-I Beam (*78″ FIB*): One of the most common FIB shapes used in bridge design. All FIB shapes have identical flanges, with the differences in girder depth arising from differences in the height of the web. The 78″ FIB was the deepest FIB shape considered in this study.
- 45-inch-deep Florida-I Beam (*45″ FIB*): The 45″ FIB was included in this study to quantify the effect of changing the FIB depth, and to ensure that the resulting design loads would be applicable to a range of FIB shapes.
- Wide-flange plate girder (*WF Plate*): Drag coefficients of I-shaped girders have been studied, in the literature, for width-to-depth ratios ranging from 1:1 to 2:1. However, built-up steel plate girders commonly used to support bridge decks tend to be much deeper than they are wide. The WF Plate girder considered in this study has an 8-ft deep web and 2′-8″ wide flanges, resulting in a width-to-depth ratio of 3:1, representing the approximate lower bound for bridge girders.
- Box girder (*Box*): A survey of existing box girder bridges was used to develop a representative 6-ft deep cross-section.

All of these girder sections were tested in multiple girder configurations and with addition stay-in-place formwork present (Figure 5.7a). Additionally, to quantify the influence of overhangs, all bridge cross-sections were tested both with and without maximum feasible overhangs (Figure 5.7b). Fully dimensioned drawings of the girder cross-sections and schematics of each test configuration conducted in this study are included in Appendix B.

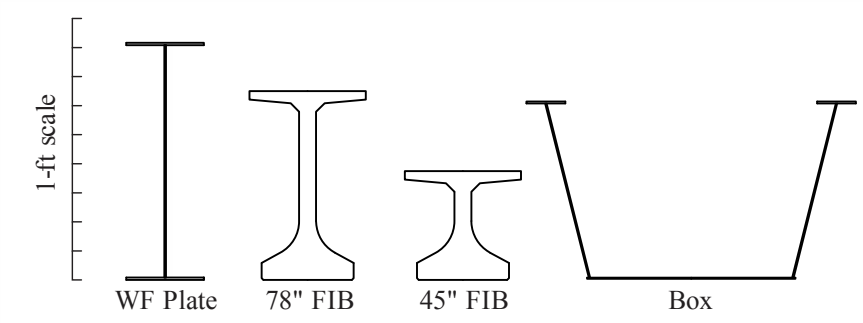

Figure 5.6 Girder cross-sections used in study

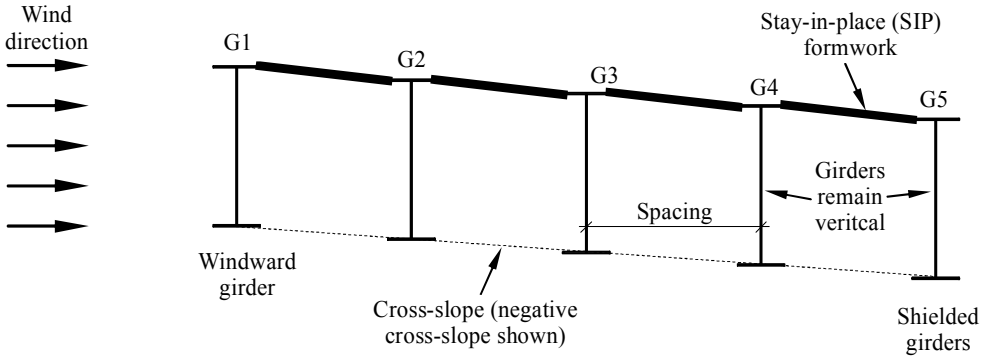

a)

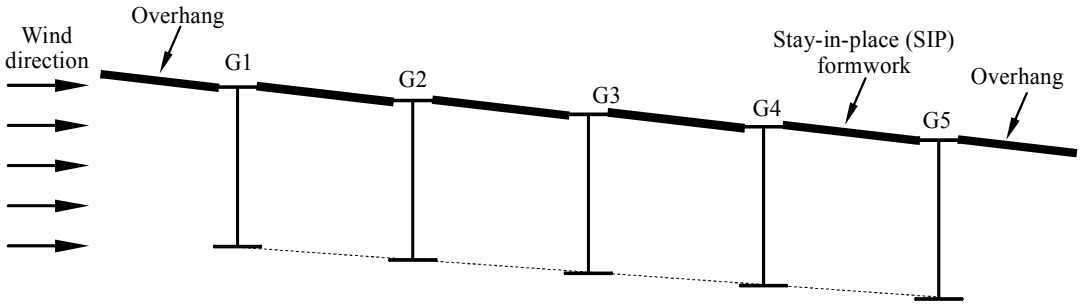

b)

Figure 5.7 Parameters definitions for each testing configuration:
a) with SIP formwork b) with SIP formwork and overhangs

Wind tunnel test configurations were defined by type of girder employed (Figure 5.6), and by the following parameters (Figure 5.7):

- Number of girders: Wind tunnel tests were performed on 2-girder, 5-girder, and 10-girder configurations.
- Spacing: Spacing refers to the horizontal center-to-center distance between girders. Results from previously conducted wind tunnel testing (Consolazio et al., 2013) indicated that girder configurations with larger spacing produced less shielding (i.e., less aerodynamic interference, and thus larger forces) on leeward girders. Therefore, to yield conservative wind tunnel results in the present study, a characteristic *maximum* spacing was determined for each

type of girder based on a survey of existing bridge designs and consultations with the FDOT. Each testing configuration for a given type of girder then used only the maximum spacing.

- Cross-slope: Most bridge decks are designed with a cross-slope that is 2% or greater in magnitude, and the girders are usually aligned vertically along that slope so that they can evenly support the deck. Therefore, the FIBs and plate girders were tested with a cross-slope that was 2% in magnitude, but negative in sign (Figure 5.7): i.e., a cross-slope of -2%. A negative cross-slope was used because when SIP forms are attached to the top flanges of the girders, the exposed bottom flanges of the girders produce a worst-case (maximum) condition in terms of drag forces generated on the shielded leeward girders.

  Generally, steel girder bridges can have a greater amount of horizontal curvature than FIB bridges, so higher cross-slopes are often included to improve vehicle handling. To account for the larger magnitude of cross-slope, the WF Plate girders were tested in configurations with -8% cross-slope.

  In contrast to the 'I-shaped' FIB and plate girders, box girders are not generally aligned vertically when supporting a cross-sloped deck. Instead, the girders are typically inclined to follow the bridge cross-slope. As a result, in this study, box girders were only tested in a 0% (un-sloped) configuration, however the range of tested wind angles was increased (relative to the I-shaped girder wind angles), as described below.

- Wind-angle: In practical bridge construction situations, the direction of wind flow will not, in general, always be perfectly horizontal. To account for the natural variation in wind angle (and at the recommendation of a commercial wind tunnel test facility), each FIB and plate girder bridge configuration was tested at five (5) different wind angles ranging from −5° to +5° in increments of 2.5° (Figure 5.8). In the case of the box girder, a change in wind angle is geometrically equivalent to rotating the girders to match the deck cross-slope (Figure 5.9). As a result, the box girder configurations were tested at −10°, −5°, 0°, +5°, and +10° angles, in order to include the *combined* effects of 5° wind angle and 5° (8.7%) of cross-slope.

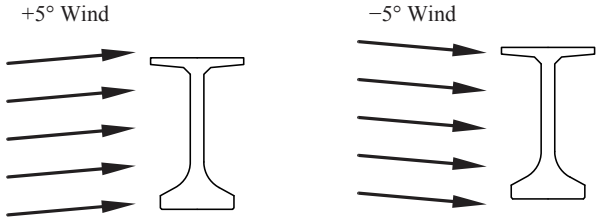

Figure 5.8 Wind angle sign convention

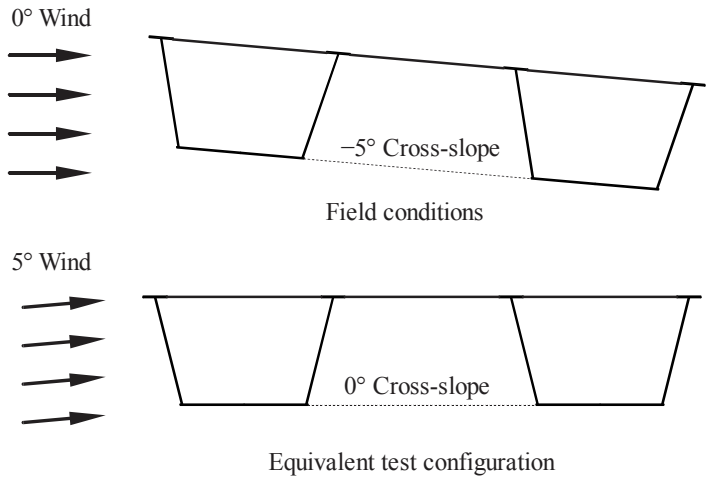

Figure 5.9 Equivalence between wind angle and cross-slope for box girders

- Overhangs: In most economical bridge designs, the bridge deck extends transversely beyond the extents of the exterior girders, thus creating an overhang of each side. Since it was desirable to quantify the effects of such overhangs on wind coefficients, overhang formwork was included in many of the configurations tested in the wind tunnel. It should be noted that the overhang formwork *support brackets* described earlier (see Section 3.4) were excluded from the wind tunnel tests because they were not expected to influence the wind coefficients. However, the top surface of the overhang formwork, which was expected to influence the wind coefficients, was included. A constant 'total overhang width' (W_{OHT}) of 5 ft (Figure 5.10), as measured from the centerline of the top girder flange to edge of the overhang formwork (*not* the edge of the concrete deck), was used for all girder types. However, due to differences in girder top flange widths, the 'overhang *formwork* width' (W_{OHF}), which was the extension of formwork *beyond* the edge of the girder top flange (Figure 5.10), varied for the girder types tested.

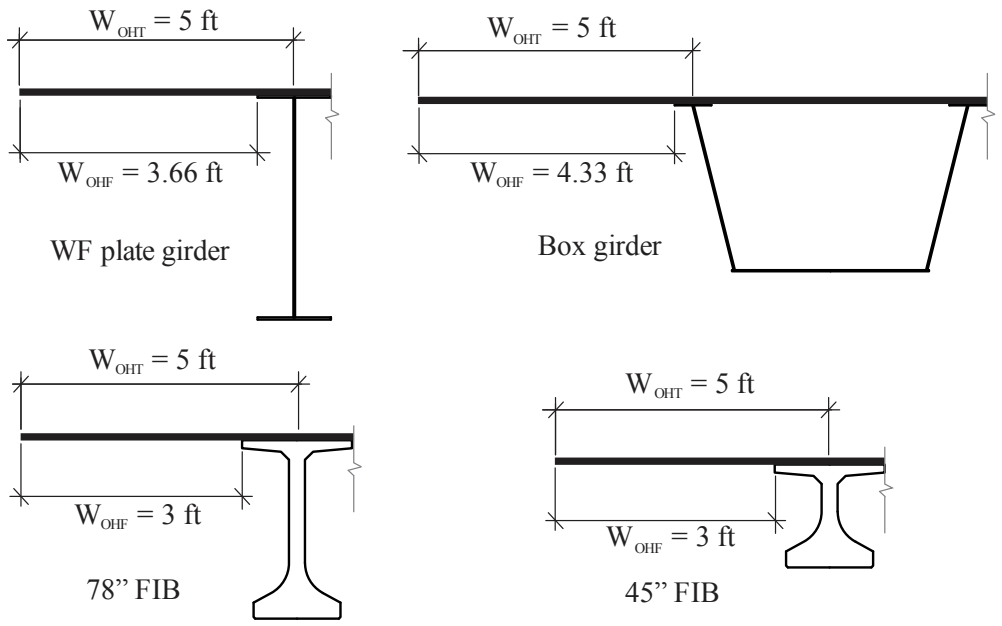

Figure 5.10 Overhang dimensions used in wind tunnel study

A summary of the scope of the wind tunnel test program is provided in Table 5.3. Note that it was not feasible to instrument (measure wind forces) at every girder position in every configuration tested. Instead, the girder positions (G1, G2 ... G10.) that were instrumented were strategically chosen to maximize the usefulness of the measured data.

Table 5.3 Summary of wind tunnel tests

Section	Overhangs included	Cross-slope	Spacing (ft)	Number of girders	Instrumented girder position	Test Angles
78" FIB	--	-2%	13	10	1, 2, 3	0°, ±2.5°, ±5°
78" FIB	Yes	-2%	13	10	1, 2, 3, 5, 10	0°, ±2.5°, ±5°
Box	--	0%	22	2	1, 2	0°, ±5°, ±10°
Box	Yes	0%	22	2	1, 2	0°, ±5°, ±10°
WF Plate	--	-8%	14	5	1, 2, 3	0°, ±2.5°, ±5°
WF Plate	Yes	-8%	14	5	1, 2, 3, 4, 5	0°, ±2.5°, ±5°
45" FIB	--	-2%	13	5	1, 2	0°, ±2.5°, ±5°
45" FIB	Yes	-2%	13	5	1, 2, 3	0°, ±2.5°, ±5°

5.5 Testing procedure

The Boundary Layer Wind Tunnel Laboratory at the University of Western Ontario (UWO) was contracted to fabricate the test specimens and to perform all wind tunnel measurements. Based on the size of the UWO wind tunnel, the girder models were constructed at reduced scale (Table 5.4), with air flow properties similarly adjusted so that the resulting forces would be applicable at full-scale. All testing was performed in smooth flow, with turbulence

intensities less than 0.5%. Because the tested cross-sections were sharp-edged, it was expected that the measured wind forces would not be sensitive to Reynolds number and the force coefficients are applicable over a broad range of wind speeds. [In a previous study (Consolazio et al., 2013), the assertion that wind forces would not be sensitive to Reynolds number was verified by UWO by performing selected tests at multiple Reynolds numbers. Results from those tests did not reveal any obvious Reynolds number sensitivities.]

Table 5.4 Wind tunnel test scaling

	Model scale	Reynolds number
WF Plate	1:25	77000
78″ FIB	1:28	56000
45″ FIB	1:28	33000
Box	1:25	58000

The scaled girder models were all 7-ft long (equivalent to 175-ft and 196-ft girders at full scale) and were constructed to be fully rigid, without exhibiting any aeroelastic effects. An adjustable frame was used to keep the girders properly oriented relative to each other in each test configuration. To measure wind-induced girder forces at varying wind angles of attack, the entire bridge cross-sectional assembly was rotated in-place relative to the wind stream.

To maximize the utility of the data collected during the wind tunnel testing, it was desirable to *individually* quantify the aerodynamic forces (drag, lift, torque) that acted on each girder within the bridge cross-section. In order to accomplish this goal, each girder in the bridge had to be structurally independent from the rest of the girders—i.e., transmission of lateral load from one girder to the next had to be prevented. Simultaneously, however, air flow between adjacent girders also had to be prevented in order to model the blockage effects associated with the presence of SIP forms.

The approach used to satisfy both of these requirements was to attach bent plates (Figure 5.11) to the top flanges of the girders in the bridge cross-section. The plates represented both the SIP forms and, where present, the overhang formwork. Structural independence was achieved by only extending the SIP form plates to the midpoint between adjacent girders (Figure 5.11) and leaving a small gap so that force transmission to the adjacent plate was not possible. As such, each SIP form plate cantilevered from a girder top flange to the midpoint of the girder spacing on each side (for an interior girder). To model the air flow blockage effects of the SIP forms, but without transmitting force across the gaps, a flexible adhesive tape (i.e., an adhesive membrane) was used to seal and span across the gaps. In tests where overhangs were present, the top plates were further extended (cantilevered) out to the extents of the overhang formwork.

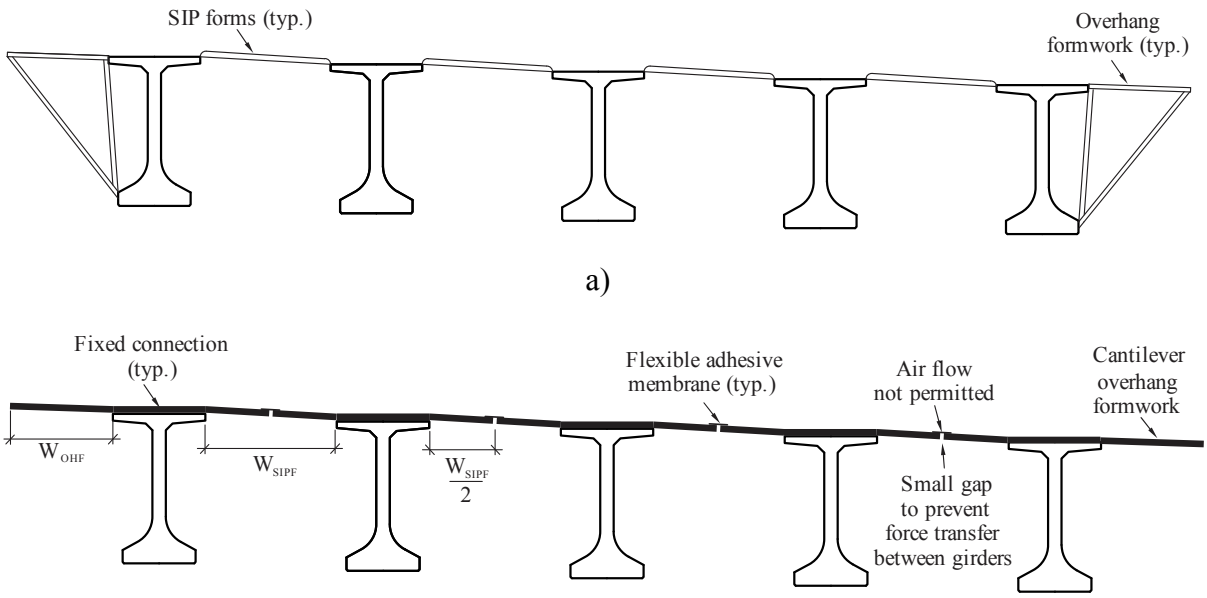

Figure 5.11 Formwork and overhang attachment methodology:
a) Typical construction schematic b) Wind tunnel testing setup

Wind forces on the girders in each test configuration were measured individually with a high-precision load balance that recorded the time-averaged horizontal load (drag), vertical load (lift), and torque (overturning moment). These loads were then normalized to produce the aerodynamic coefficients for drag (C_D), lift (C_L), and torque (C_T). Finally, the torque coefficient was adjusted so that it represented the torque about the centroid of the section, rather than the torque about the point of measurement (which was at mid-height for the I-shaped girders and at an arbitrary point for the box girders). For additional details regarding the wind tunnel test procedures and stay-in-place formwork attachment methodology, please see Appendix E.

CHAPTER 6
WIND TUNNEL TESTING RESULTS AND ANALYSIS

6.1 Introduction

Wind tunnel tests were performed on the bridge girder test configurations described in Chapter 5. Several groups of laterally spaced girders were tested to quantify shielding effects, identify trends, and evaluate the aerodynamic influence of stay-in-place formwork and overhangs. The complete set of wind tunnel test data, reported using terminology defined in Chapter 5, is available in Appendix C. From analysis of the results, simplified calculation procedures were developed for determining global drag coefficients for I-shaped girder bridges (i.e., FIBs and plate girders) and bridges constructed using box girders.

6.2 Key findings from the wind tunnel test program

After processing the wind tunnel data into a form consistent with the terminology defined in Chapter 5—which is also consistent with terminology used in a previous wind tunnel study (BDK75-977-33, Consolazio et al., 2013)—the following key findings and data trends were identified.

6.2.1 Influence of stay-in-place forms and overhangs on drag coefficients

Representative example comparisons of drag coefficients (C_D) for systems consisting *only* of bare girders and drag coefficients for systems consisting of girders with SIP forms and with overhang formwork are presented in Figure 6.1 for wide flange (WF) plate girders, and in Figure 6.2 for FIB78 girders. Data shown in these figures—which represent variations in wind angle, girder type, and bridge width (number of girders)—serve to illustrate the influence that the addition of both SIP forms and overhang formwork had on drag coefficients. (Note: data for FIB45 and box girder sections exhibit similar trends to those illustrated for the WF plate girder and FIB78 sections, but are omitted here for brevity.)

In Figure 6.1, all data presented correspond to a *magnitude* of cross-slope equal to 8%. As noted in Chapter 5, in the present study, only negative cross-slopes were investigated since these conditions produce the most conservative drag coefficients when SIP forms are present. In contrast, in study BDK75-977-33, the cross-slope was a positive value +8%. However, since these earlier tests were conducted without SIP forms or overhang formwork (bare girders only), and because the WF plate girders have doubly symmetric cross-sectional shapes, the results obtained in BDK75-977-33 for +8% also correspond to a cross-slope of -8%. Hence, the C_D data presented in Figure 6.1 from the previous study (at +8%) and the present study (at -8%) are, in fact, comparable.

In general, the data presented in Figure 6.1 and Figure 6.2 indicate that the introduction of SIP forms and overhang formwork does not alter the fundamental C_D trend that was first identified in BDK75-977-33, that is: a large positive C_D value at windward girder position G1; one or more leeward (shielded) girder positions (G2, G3, ...) with *negative* C_D values; and then subsequent increases of C_D values typically producing $+C_D$ values for girders farther downstream. With regard to the windward girder at position G1, introducing SIP forms and overhang formwork *always* produced an increase in the C_D value when corresponding cases—identical in every way except for the presence of SIP forms and overhang formwork—were

compared. For leeward (shielded) girder positions, introducing SIP forms and overhang formwork generally produced a slight decrease in the C_D values.

In Figure 6.3 and Figure 6.4, the effects on C_D values produced *only* by adding SIP forms, but *not* overhang formwork, are illustrated. For a majority of the data shown, adding SIP forms has the effect of *reducing* the C_D values for the windward girder (position G1) and for the first shielded leeward girder (position G2); both of these trends will tend to reduce the total (global) drag force on the bridge cross section. Results for shielded girders farther downwind, however, are mixed.

In Figure 6.5 and Figure 6.6, the effects on C_D values produced by adding overhang formwork to systems that already have SIP forms are illustrated. That is, Figure 6.5 and Figure 6.6 isolate solely the effects of adding overhang formwork. (This is in contrast to Figure 6.1 and Figure 6.2, which illustrated the combined effects of adding *both* SIP forms and overhang formwork). With regard to the windward girder at position G1, introducing overhang formwork *always* produced an increase in the C_D value when matched cases—identical in every way except for the presence of overhang formwork—were compared. In contrast, however, adding overhang formwork had only minor effects on the C_D values for shielded downwind girders.

6.2.2 Lift coefficients for girders and overhangs

When girder lift coefficients (C_L) from the current study, which included SIP forms in all cases, were compared to corresponding lift coefficients from study BDK75-977-33, which included only bare girders, it was found that the addition of SIP forms increased the measured lift coefficients at every girder position measured, and for every condition tested. From this observation, it is clear that the addition of SIP forms altered the flow of wind around the bridge cross-section. Further, when lift coefficients (C_L) for systems with SIP forms *and* overhangs were compared to lift coefficients for systems having only SIP forms (but without overhangs), it was evident that the addition of overhangs further increased the lift coefficients, especially for the windward girder (position G1).

In addition to quantifying lift coefficients for the girders, it was also of interest to quantify lift coefficients for the overhang formwork—i.e., the width of formwork (W_{OHF}) extending beyond the girder flange tip; recall Figure 5.10. Unfortunately, including direct measurements of uplift forces on the overhang formwork was not feasible within the scope of the wind tunnel testing program. However, it was possible to *estimate* the overhang formwork lift coefficients ($C_{L,OHF}$) from the wind tunnel data that were measured. For each condition tested (girder type and wind angle), the lift coefficient attributable to the presence of the overhang formwork ($C_{L,OHF}$) was computed as:

$$C_{L,OHF} = C_{L,G1,SIP+OH} - C_{L,G1,SIP} \tag{6.1}$$

where $C_{L,G1,SIP+OH}$ was the lift coefficient measured at the windward girder (position G1) when SIP forms and overhangs were included, and $C_{L,G1,SIP}$ was the lift coefficient measured at the windward girder when SIP forms were included, but overhangs were omitted. Overhang lift coefficients estimated in this manner are summarized in Table 6.1.

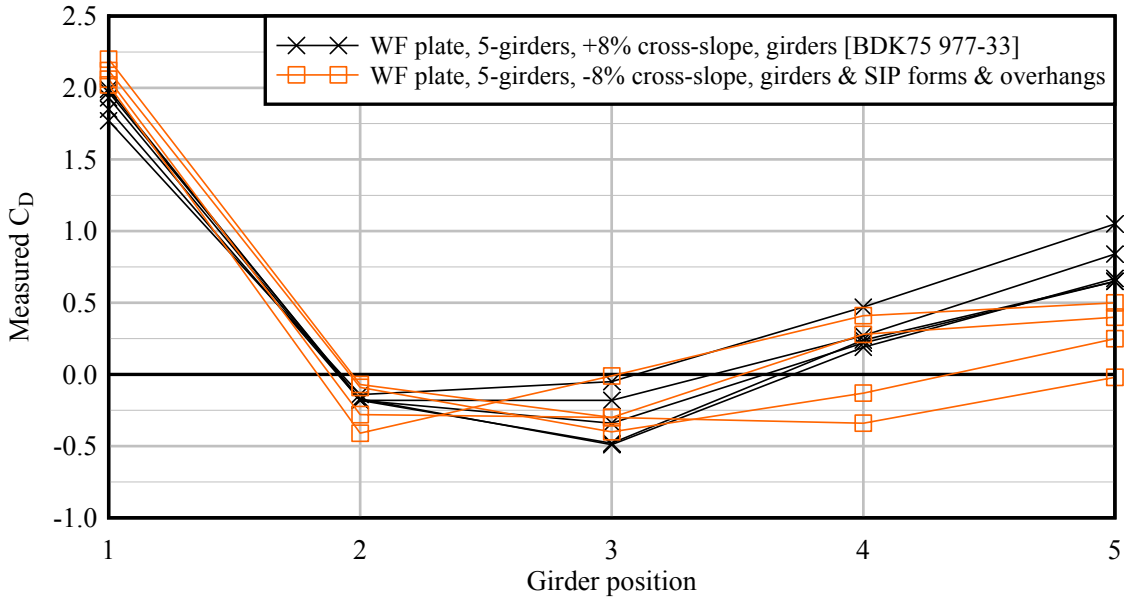

Figure 6.1 Influence on plate girder C_D values from addition of SIP forms and overhangs (All tested wind angles shown)

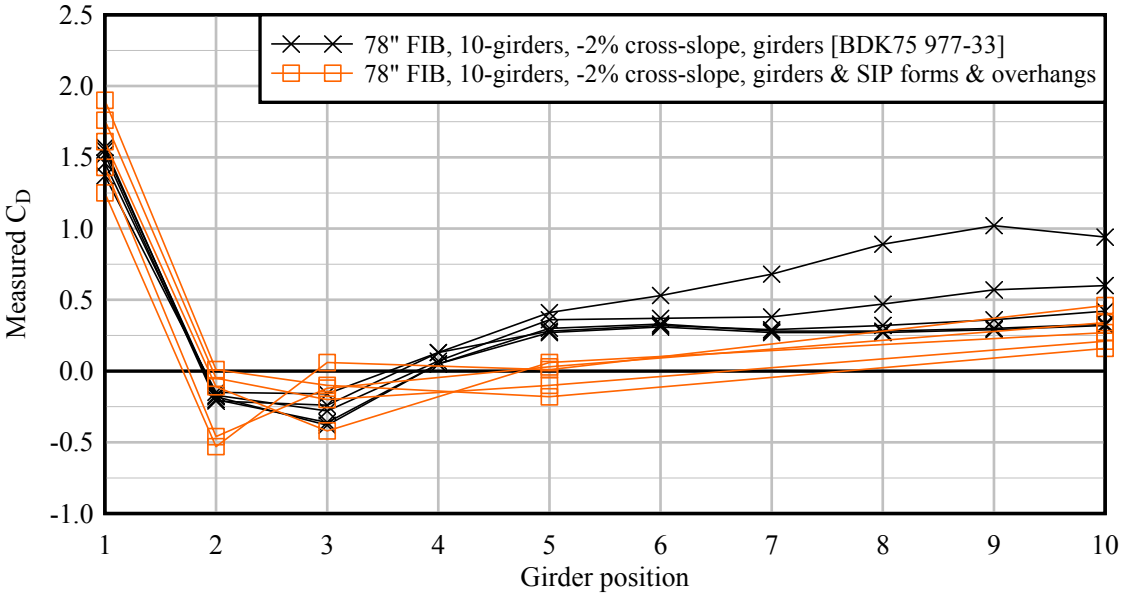

Figure 6.2 Influence on FIB78 C_D values from addition of SIP forms and overhangs (All tested wind angles shown)

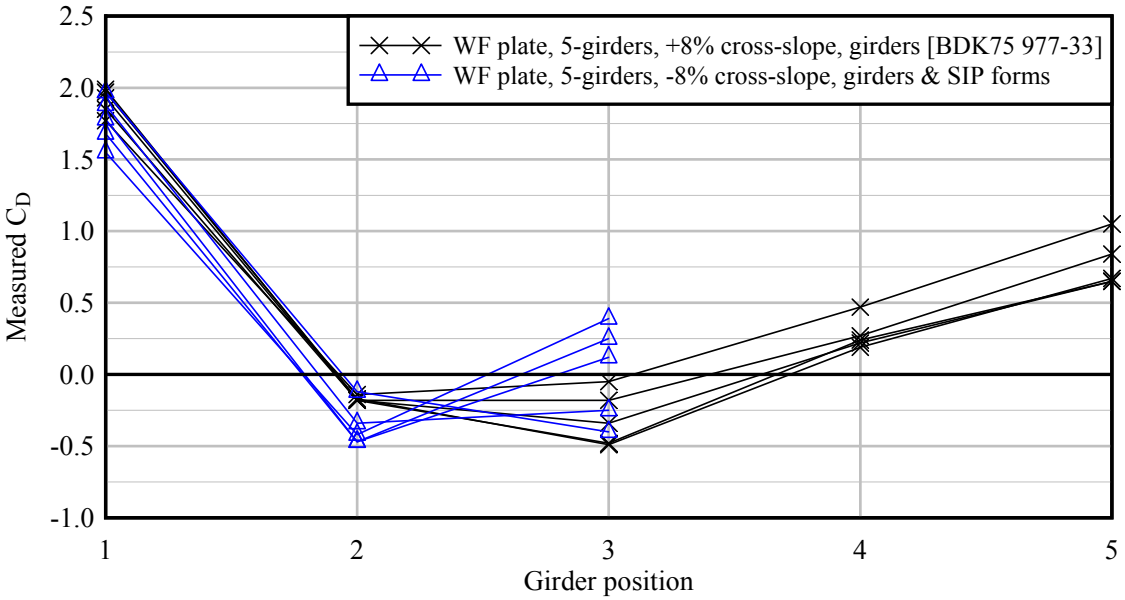

Figure 6.3 Influence on plate girder C_D values from addition of SIP forms
(All tested wind angles shown)

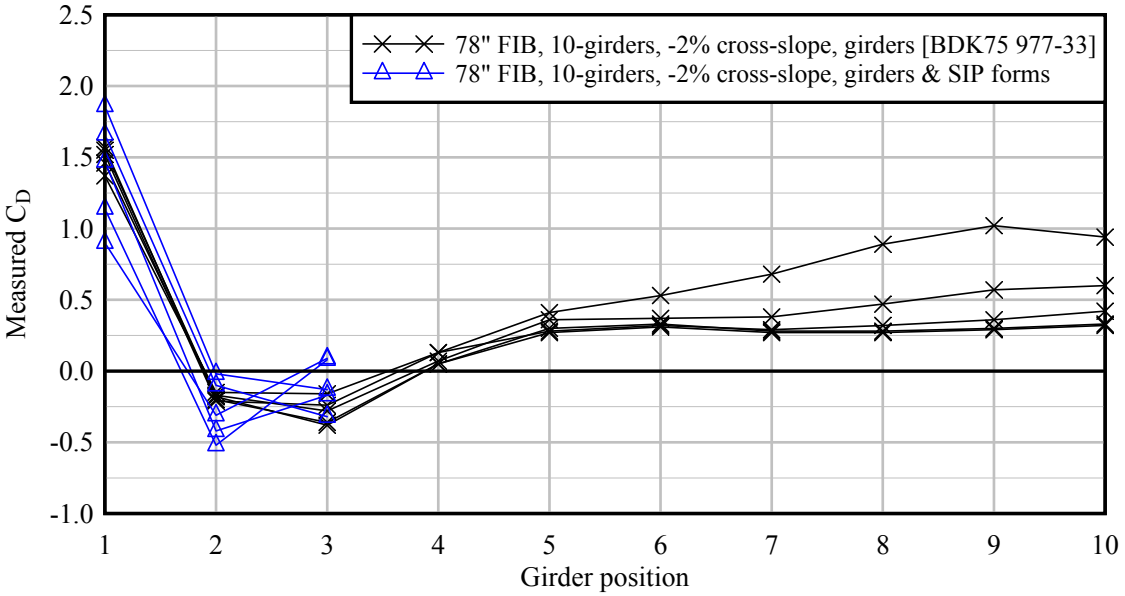

Figure 6.4 Influence on FIB78 C_D values from addition of SIP forms
(All tested wind angles shown)

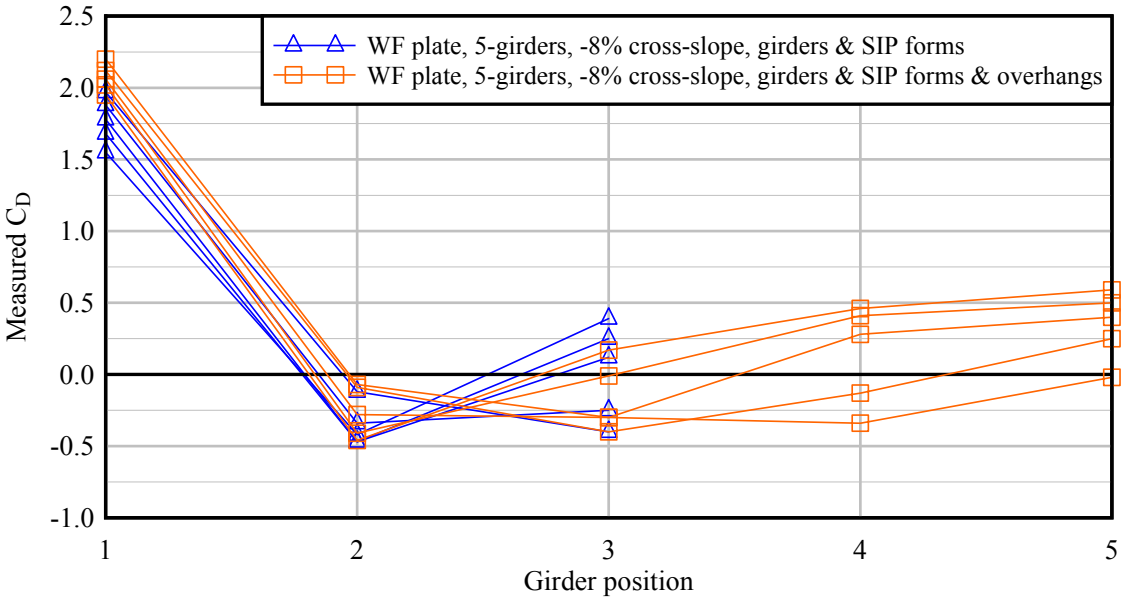

Figure 6.5 Influence on plate girder C_D values from addition of overhangs
(All tested wind angles shown)

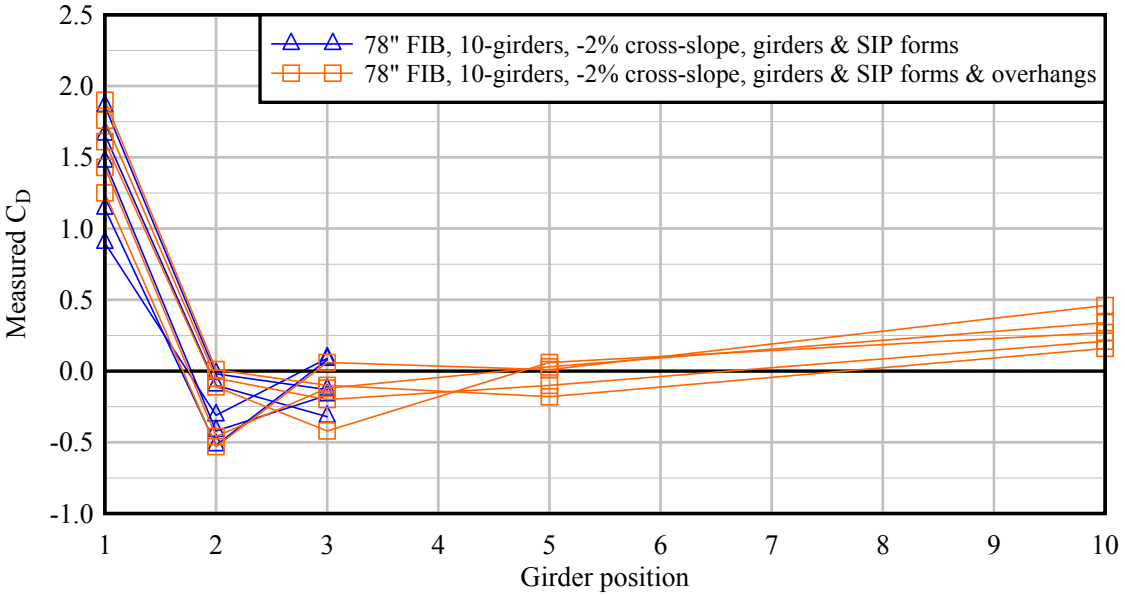

Figure 6.6 Influence on FIB78 C_D values from addition of overhangs
(All tested wind angles shown)

Table 6.1 Estimated lift coefficients ($C_{L,OHF}$) attributable to overhang formwork

	Min. $C_{L,OHF}$ across all wind angles	Max. $C_{L,OHF}$ across all wind angles	$C_{L,OHF}$ at zero-degree wind angle	Width of overhang formwork (W_{OHF}) (see Figure 5.10)
WF plate	1.32	1.51	1.51	3.66 ft
78″ FIB	0.48	1.43	1.38	3.00 ft
45″ FIB	0.12	1.80	1.68	3.00 ft
Box	0.15	1.55	1.55	4.33 ft

Since the overhang formwork lift coefficients ($C_{L,OHF}$) reported in Table 6.1 have been estimated by taking differences of *girder* lift coefficients (C_L), and since the girder lift coefficients reported throughout this study are normalized relative to the girder depth (D), by definition, the overhang formwork lift coefficients are then also normalized by the girder depth (D). Therefore, to compute overhang formwork lift forces from the coefficients reported in Table 6.1, the $C_{L,OHF}$ values must first be *de-normalized* by the girder depth (D) as:

$$F_{L,OHF} = \frac{1}{2}\rho K_Z V^2 G C_{L,OHF} D \tag{6.2}$$

or alternately, and more conveniently, expressed as:

$$F_{L,OHF} = 2.56\times10^{-6} K_Z V^2 G C_{L,OHF} D \tag{6.3}$$

where $F_{L,OHF}$ is the overhang formwork lift force per ft of girder span length, 2.56×10^{-6} represents the quantity $\frac{1}{2}\rho$ in Eqn. (6.2) expressed in units of (ksf)/(mph)^2, V is the basic wind speed (mph), K_Z is the velocity pressure exposure coefficient, G is the gust effect factor, $C_{L,OHF}$ is taken from Table 6.1, and D is the girder depth in ft. It is important to note that since only a single overhang formwork width (W_{OHF}) was tested for each girder type (Table 6.1), the lift forces computed using the coefficients provided in Table 6.1 are specific to widths tested. Additionally, the type of data measured in the wind tunnel test program does not provide insight regarding the form of the lift pressure distributions (e.g., uniform, triangular, nonlinear, etc.) that acted on the overhang formwork during testing.

6.2.3 Torque coefficients

Representative example comparisons of torque coefficients (C_T) for systems consisting *only* of bare girders, and torque coefficients for systems consisting of girders with SIP forms and with overhang formwork are presented in Figure 6.7 for wide flange (WF) plate girders, and in Figure 6.8 for FIB78 girders. (Sign convention: a positive torque induces a clockwise girder

rotation for wind moving from left to right.) The most significant trend exhibited by the data was that the addition of overhang formwork significantly increased the torque on the windward girder (position G1). For the leeward (shielded) girder positions (G2, G3, ...), torque coefficients were considerably smaller than for the windward girder. When moving from bare girders to girders with SIP forms, moderate increases in torque coefficients were produced, but they were not nearly as pronounced as when overhang formwork was added.

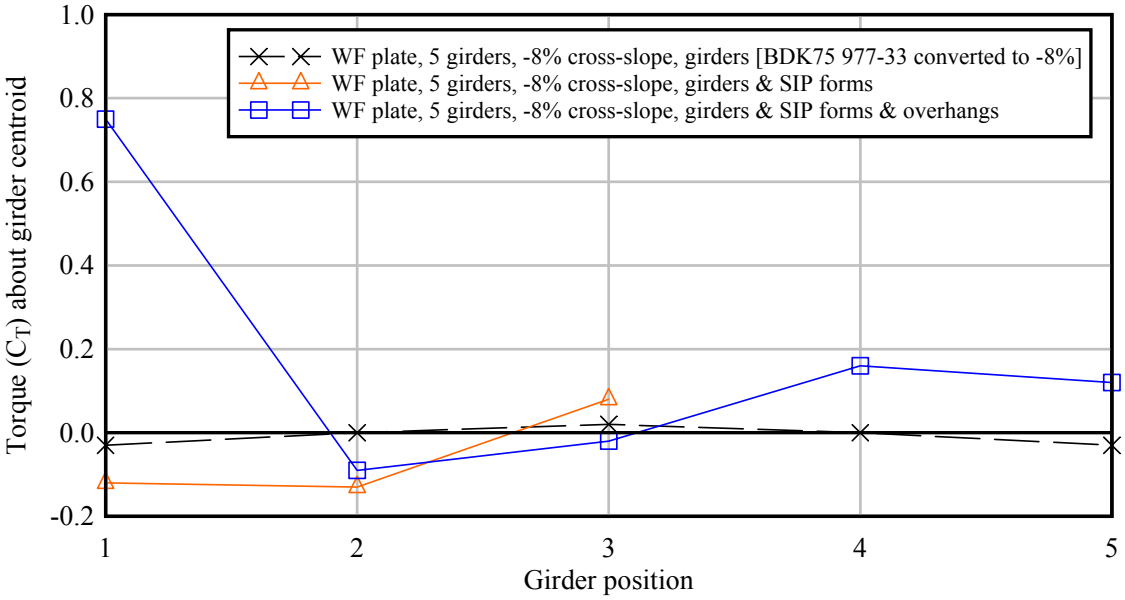

Figure 6.7 Comparison of WF plate girder torque coefficients (C_T)
(All data are for zero degree wind angle)

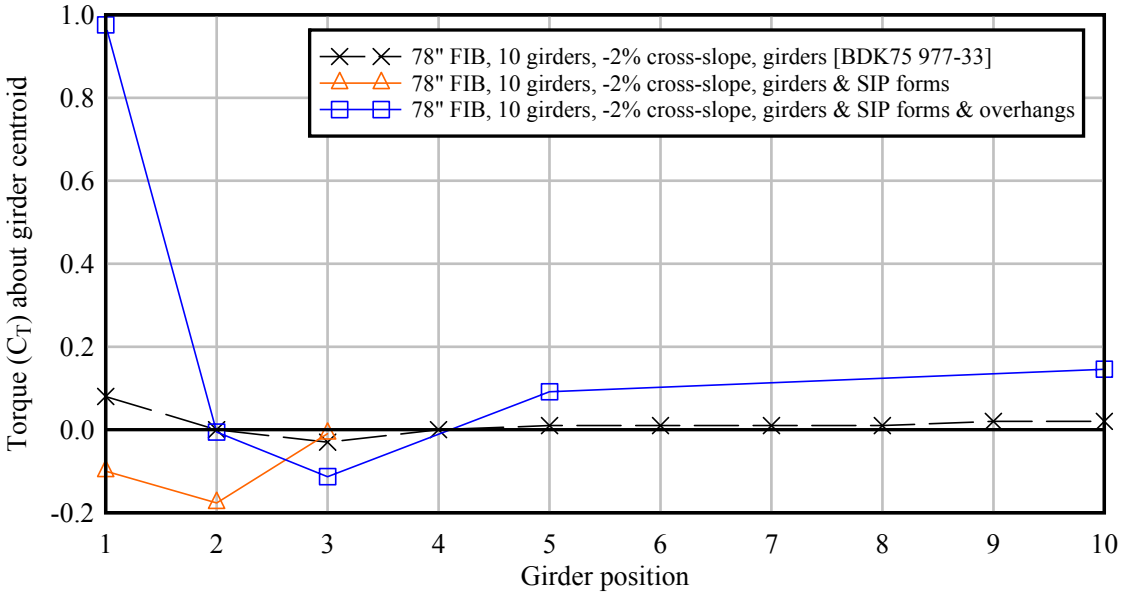

Figure 6.8 Comparison of FIB78 girder torque coefficients (C_T)
(All data are for zero degree wind angle)

6.3 Analysis of wind tunnel testing results

To quantify the full (global) wind force acting on a bridge system, the total of all girder drag coefficients must be considered. A calculation procedure was therefore developed for determining a *global pressure (drag) coefficient*—defined as the summation of the drag coefficients of all girders in the bridge cross-section. Both I-shaped girder systems (FIBs and plate girders) and box girder systems were considered in the development process.

6.3.1 Calculation of global pressure coefficient for systems with I-shaped girders

Current standard practice specified in the *FDOT Structures Design Guidelines* (SDG; FDOT, 2013) involves determining a global pressure coefficient (for a system of multiple girders with SIP forms and possibly overhang formwork), computing an applied pressure using Eqn. (5.9), and then applying that pressure to the projected area of the bridge. This method, referred to as the 'projected area method', assumes a zero degree (horizontal) wind angle. As such, the horizontal wind pressure is applied to the vertical projected depth (D_{proj}, Figure 6.9) of the bridge. The global pressure coefficient used in this process, for bridge girders with SIP formwork in place (referred to as $C_{P,SIPF}$ in this section), is specified in the FDOT SDG as 1.1 (Table 6.2).

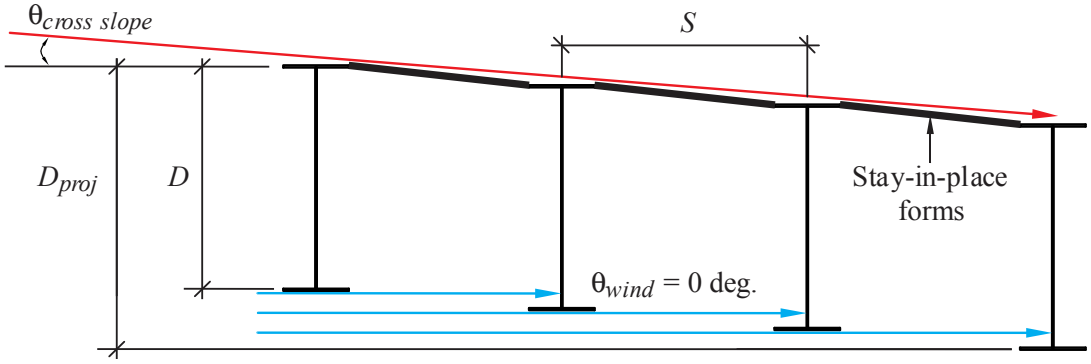

Figure 6.9 Projected area method

Table 6.2 Pressure coefficient during construction for I-shaped girders (FDOT, 2013)

Construction Condition	Pressure Coefficient
Deck forms not in place	$C_P = 2.2$
Stay-in-place (SIP) deck forms in place	$C_{P,SIPF} = 1.1$

Magnitudes of the wind loads on shielded girders are highly dependent on the interaction between the system cross-slope angle ($\theta_{cross\text{-}slope}$) and the wind angle ($\theta_{wind}$). As the absolute difference between those angles increases, a greater portion of the shielded girders are exposed to direct wind flow, resulting in a roughly proportional increase in girder drag force. Consequently, a strong predictor of total (global) wind load on a girder system is the *projected*

area of the system (i.e., the total unshielded area). To appropriately capture this trend, global drag coefficients must be a function of the *projected depth* (D_{proj}).

Because the projected depth is a function of θ_{wind}, which fluctuates randomly over time, engineering judgment must be used in selecting a design value of θ_{wind}, such that it represents the maximum expected angle during the exposure period. For conservatism, the sign of θ_{wind} must be chosen to be in opposition to that of $\theta_{cross\text{-}slope}$, so that the maximum angle difference (θ_{max}) is computed as:

$$\theta_{max} = \left|\theta_{wind}\right| + \left|\theta_{cross\text{-}slope}\right| \tag{6.4}$$

θ_{max} can then be used to calculate the *projected depth*, D_{proj}, of the girder system, as:

$$D_{proj} = D + (n-1)(S)(\tan(\theta_{max})) \tag{6.5}$$

where D is the girder depth, n is the number of girders in the system, and S is the girder spacing (Figure 6.10). In this formulation, wind streamlines are assumed to be straight and the shielding effects of girder flanges are ignored as they are not expected to significantly shield leeward girders.

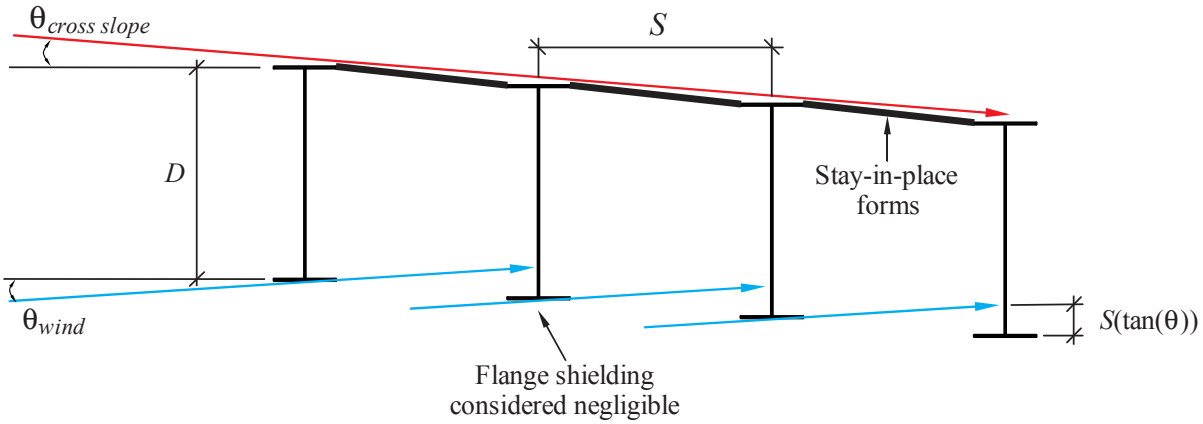

Figure 6.10 Modified projected area method

In contrast to the study BDK75-977-33 (Consolazio et al., 2013), the presence of SIP forms in the girder systems influences the controlling wind direction. For bridges with a negative cross-slope configuration, positive wind angles produce larger system level drag coefficients than do negative wind angles. (This is due to the SIP forms shielding downstream girders when the wind angles of attack are more negative than the cross-slope). Consequently, only wind angles that were in opposition to the cross-slope were considered in the cases shown below. For example, in the -8% cross-slope (-4.57 degrees) WF plate girder systems, only -2.5, 0, +2.5, and +5 degree wind angles were included. In the -2% cross-slope (-1.15 degrees) FIB systems, 0, +2.5, and +5 degree wind angles were included.

Furthermore, in addition to SIP forms, the presence of *overhang formwork* was found to marginally increase the total (global) system-level drag forces for I-shaped girders. To account

for this increase, the vertical projected depth of the *windward* overhang formwork was included in the projected depth formulation, as:

$$D_{proj} = D + (n-1)(S)(\tan(\theta_{max})) + W_{OHF}\left(\tan(\theta_{max})\right) \tag{6.6}$$

where W_{OHF} is the horizontal width of the overhang formwork (recall Figure 5.10). In the remainder of this report, using Eqn. (6.6) to compute the projected depth (instead of the D_{proj} illustrated in Figure 6.9), will be referred to as the '*modified projected area method*'.

Within the scope of the wind tunnel tests, it was not feasible to instrument every girder position for drag coefficient measurement. For reference, the following data were measured directly during the wind tunnel tests:

- WF-plate girder (5-girders): Fully instrumented for the cases with overhang formwork. Positions G1-G3 were instrumented for cases without overhang formwork.
- FIB78 (10-girders): Positions G1-G3 were instrumented in both the non-overhang and overhang formwork setups. Positions G5 and G10 were instrumented in the systems with overhang formwork.
- FIB45 (5-girders): Positions G1-G2 were instrumented in both the non-overhang and overhang formwork setups. Position G3 was instrumented in the systems with overhang formwork.

The following process was used to estimate drag coefficients at non-measured positions:

- WF-plate girder: Girder positions that were measured in overhang formwork cases were used as an estimate for non-instrumented positions in systems without overhang formwork. An example case, at zero degree wind angle, is provided in Figure 6.11 to illustrate this estimation process.

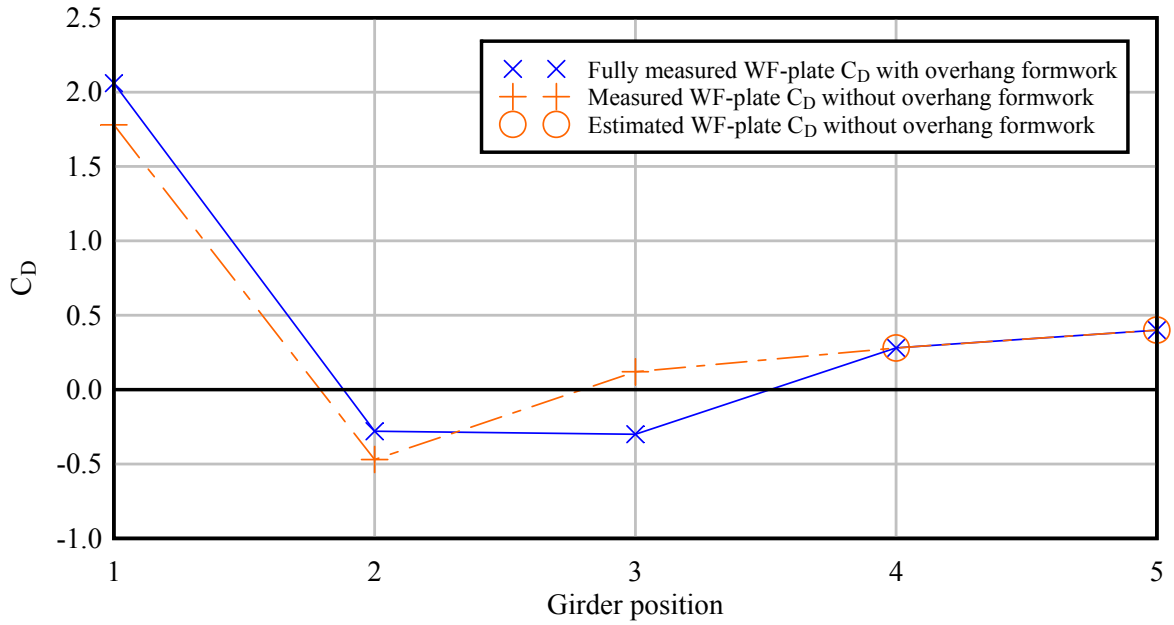

Figure 6.11 Drag coefficients for wide-flange plate girder systems (zero degree wind angle)

- FIB78: Positions G5 and G10 were experimentally measured in the systems with overhang formwork and used as estimates in the non-measured positions in systems without overhang formwork. Other intermediate drag coefficients were linearly interpolated between the range of G3-G5 and G5-G10. An example case, at zero degree wind angle, is provided in Figure 6.12 to illustrate the linear interpolation process.

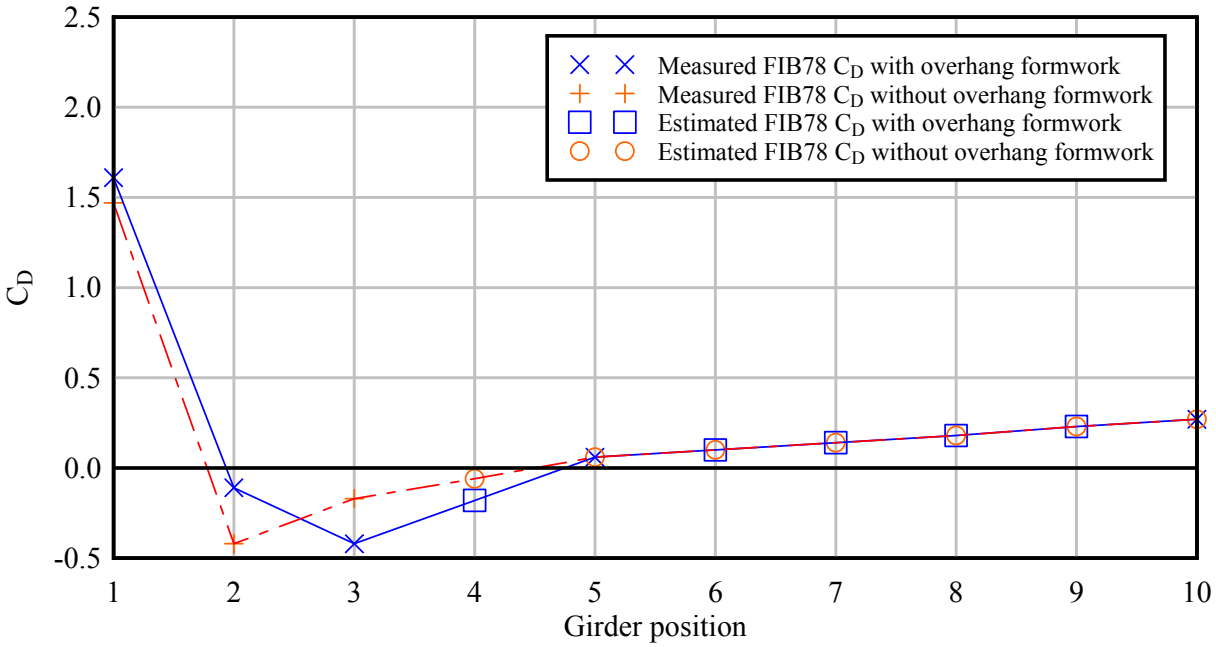

Figure 6.12 Drag coefficients for FIB78 systems (zero degree wind angle)

- FIB45: Position G3 was measured in the systems with overhang formwork and was used to estimate the corresponding position for the systems without overhang formwork. The last (most leeward) position in 5-girder FIB45 systems was estimated using the proportionality between the first to the last position (i.e., $C_{D,Last}/C_{D,First}$) experimentally measured in the FIB78 systems. When transitioning from a -5 degree wind angle to a +5 degree wind angle, the ratio of first girder to last girder drag coefficients decreases; that proportionality was reflected in the FIB45 estimations. The following calculation was performed:

$$C_{D,Last,FIB45} = C_{D,First,FIB45}\left(\frac{C_{D,Last,FIB78}}{C_{D,First,FIB78}}\right) \tag{6.7}$$

where the last position (G5) in a FIB45 system was estimated using the proportionality between the first and last measured drag coefficient in the FIB78 systems. Similar to the FIB78 estimation process, Position G4 was linearly interpolated between G3-G5 (Figure 6.13).

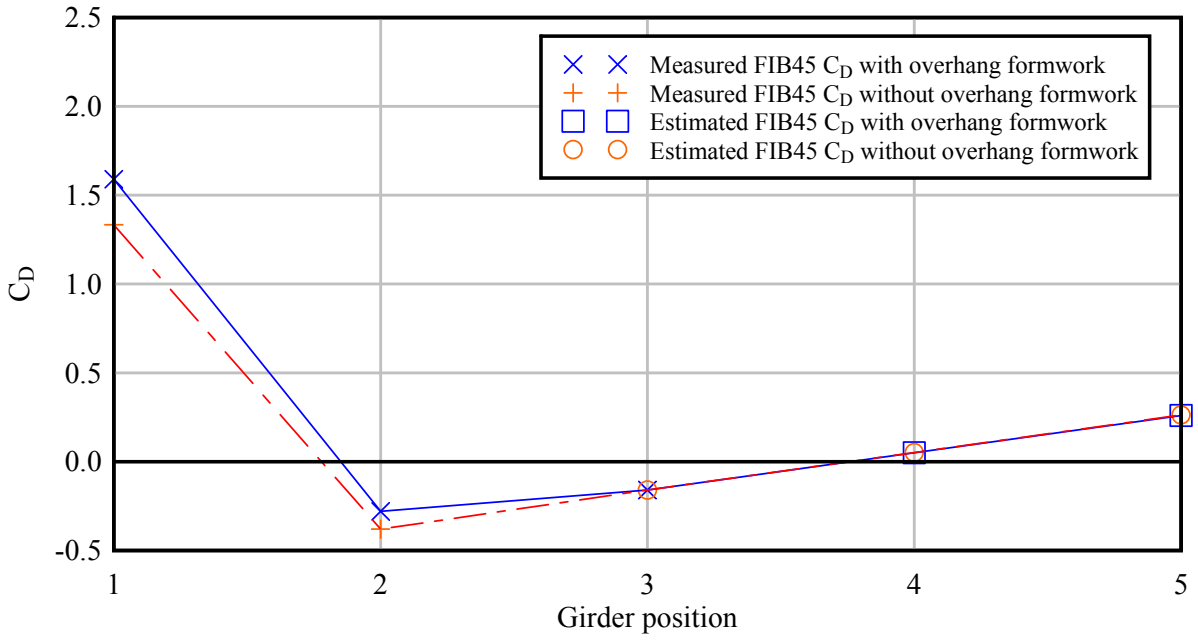

Figure 6.13 Drag coefficients for FIB45 systems (zero degree wind angle)

To assess the level of conservatism produced by use of the modified projected area calculation method (using Eqn. (6.6) to compute D_{proj}) for I-shaped girders, a 'conservatism ratio' was defined as the calculated (predicted) lateral wind force divided (normalized) by the summation of girder drag forces measured during the wind tunnel study (or estimated, for non-instrumented girders positions, as described above). Defined in this manner, the conservatism ratio was ≥ 1.0 when the modified projected area method was conservative, and < 1.0 when the method was unconservative.

However for convenience, it was desired to compute the conservatism ratio in terms of pressure (drag) coefficients rather than the total wind forces corresponding to those coefficients. To do so, it was recognized that in the modified projected area method, $C_{P,SIPF}$ is used to compute a pressure that is then applied to the *projected depth* (D_{proj}) of the structure. In contrast, the *girder* drag coefficients reported from wind tunnel testing ($C_{D,\exp}$) are normalized (referenced) to the *girder depth* (*D*), not the *projected* depth (D_{proj}). Therefore, to compute a proper conservatism ratio based on the ratio of pressure (drag) coefficients (rather than forces), it was necessary to define:

$$\delta = \left(\frac{D_{proj}}{D} \right) \tag{6.8}$$

Using this definition, the conservatism ratio could be properly defined in terms of pressure (drag) coefficients as $\left(\delta C_{P,SIPF}\right) \Big/ \left(\sum C_{D,\exp}\right)$. Ratios computed in this manner for all I-shaped girders are presented in Figure 6.14.

It is evident in the figure that using a pressure coefficient of $C_{P,SIPF}$ = 1.1 (from Table 6.2) produced *unconservative* results in many cases. Note that in some cases, the systems were tested in *horizontal wind* (zero degree wind angle), meaning that the modified projected area approach used the same assumption as currently recommended by the SDG (Figure 6.9). To ensure that conservative force predictions were obtained (i.e., normalized values greater than 1.0), it was determined—via calibration—that the pressure coefficient for girders with formwork in place ($C_{P,SIPF}$) needed to be revised to 1.4 (see again, Figure 6.14).

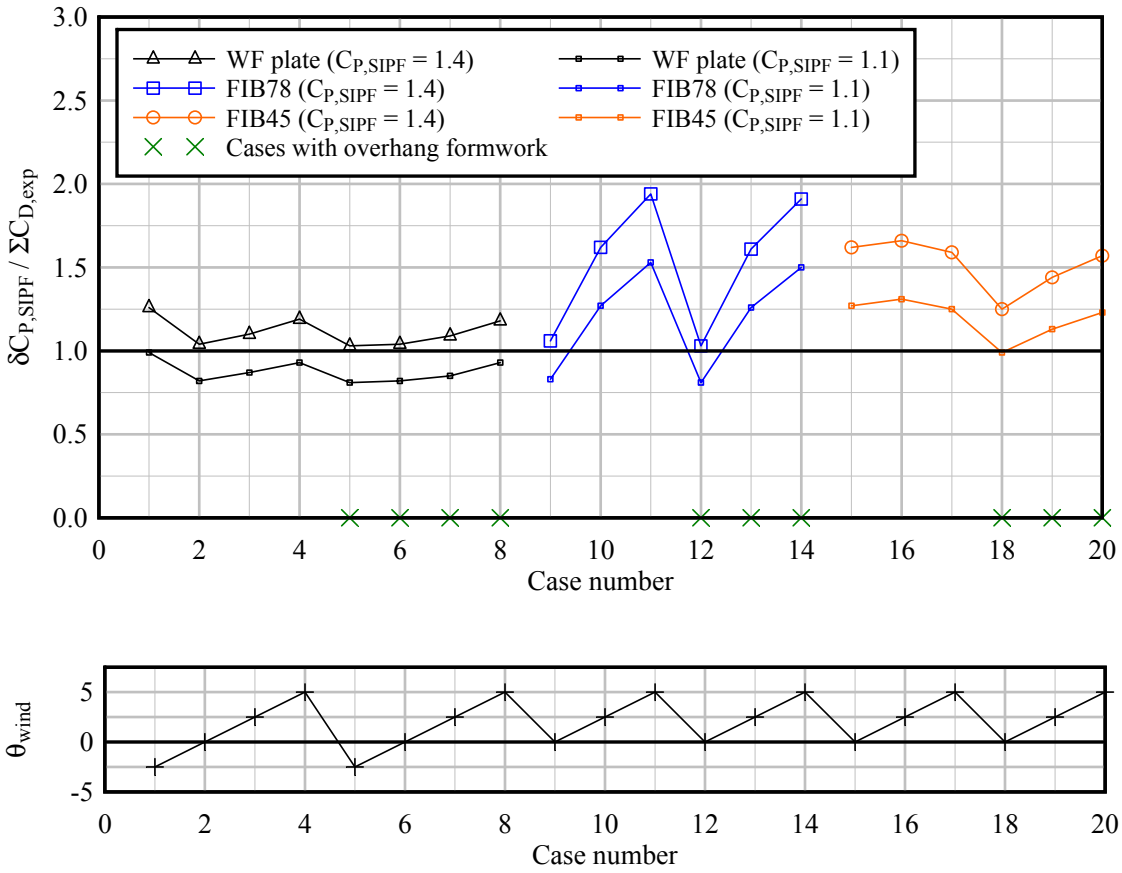

Figure 6.14 Conservatism of modified projected area calculation procedure for I-shaped girders

The goal of this method was to provide conservative predictions of global pressure coefficients. However, with a design pressure coefficient of 1.4, FIB-girder global pressure coefficients are overly-conservative in comparison to WF plate girder systems (Figure 6.14). To produce a more refined prediction of FIB-girder global pressure coefficients, a reduction factor was developed for use in the modified projected area approach. An ideal global C_P reduction factor (β_{ideal}) could be calculated as:

$$\beta_{ideal} = \frac{\Sigma C_{D,\exp}}{\delta C_{P,SIPF}} \tag{6.9}$$

where the sum of experimentally determined girder drag coefficients in a girder system ($\Sigma C_{D,exp}$) is normalized by the predicted global pressure coefficient. In Figure 6.15, ideal reduction factors are plotted against maximum angles (absolute differences between the wind angle and cross-slope). To envelope the data, an upper bound linear curve fit was applied:

$$\beta = 1.05 - 0.07(\theta_{max}) \leq 1 \tag{6.10}$$

where β is the reduction factor to be applied in the calculation of FIB-girder global pressure coefficients, and θ_{max} has units of degrees. Additionally, since β is a *reduction* factor, its computed value must be less than or equal to 1.0, thus creating a bi-linear curve.

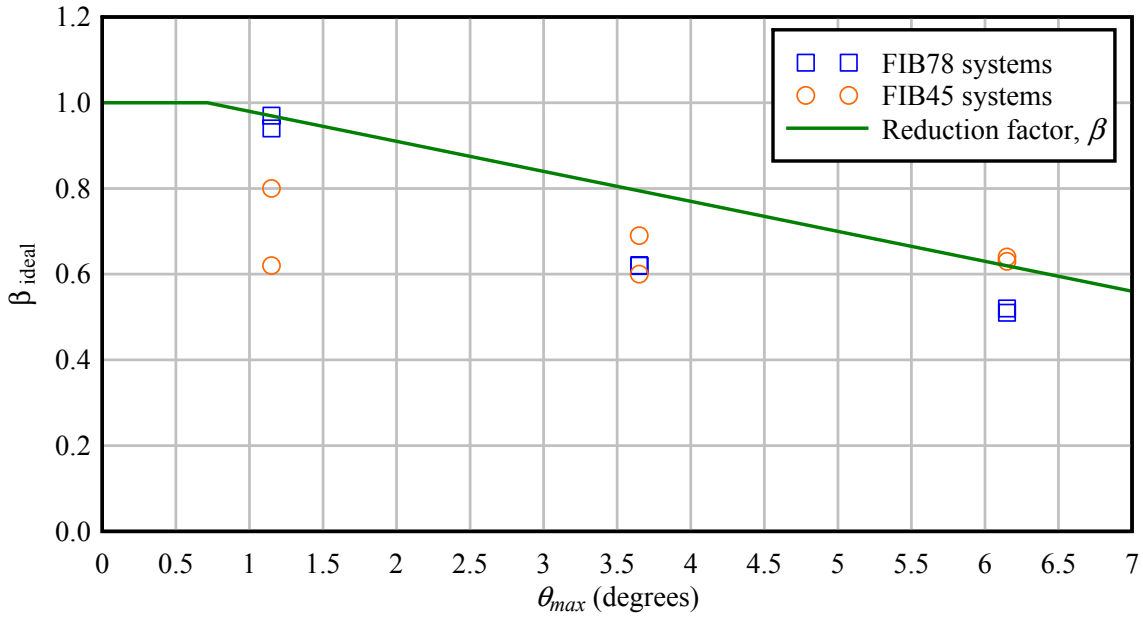

Figure 6.15 Upper bound formulation of reduction factor (β) for FIB systems

Application of the reduction factor (β) to the prediction of FIB-girder global pressure coefficients produces conservatism levels that are appropriate for design purposes (Figure 6.16) with an average conservatism ratio (across all three girder types: WF plate girder, FIB45 and FIB78) of 1.16. Note that the revised design pressure coefficient $C_{P,SIPF}$ = 1.4 was used in these calculations and wind angles (θ_{wind}) were included when computing the maximum angle difference (θ_{max}).

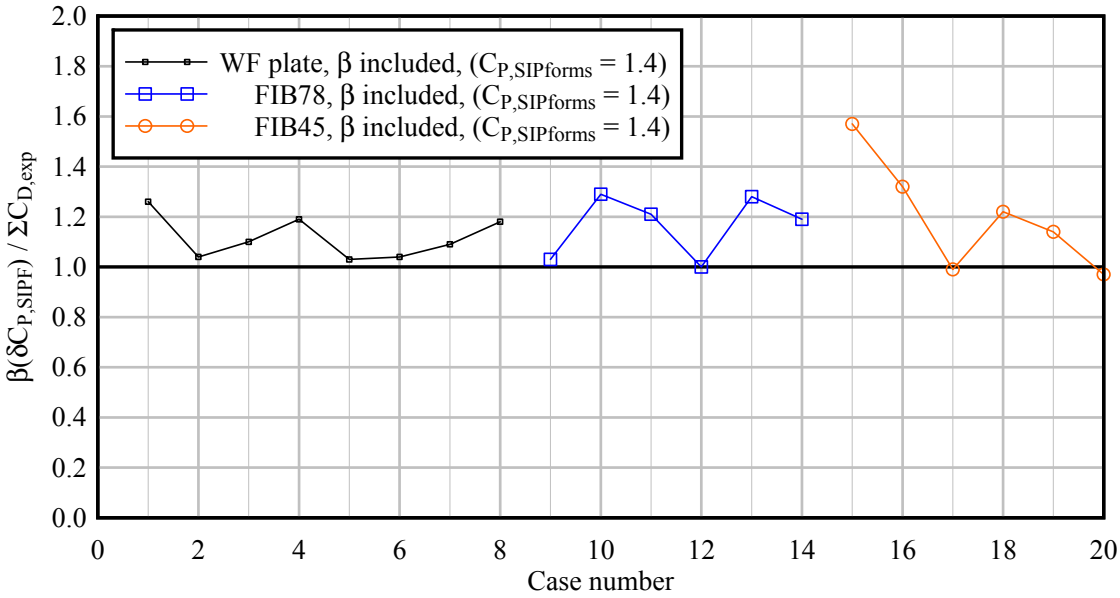

Figure 6.16 Conservatism of modified projected area calculation procedure for I-shaped girders (Reduction factor β applied to FIB systems)

An alternative calculation procedure for determining global drag coefficients was also developed by implicitly including wind angle in the projected depth calculation. Similar to the currently prescribed method in the FDOT SDG for global drag coefficients, wind load was taken as the pressure of the wind acting horizontally on a vertical projection over the exposed area of the structure. In other words, it was assumed that the maximum difference angle (θ_{max}) is equivalent to the cross-slope angle ($\theta_{cross\text{-}slope}$), and that the wind angle (θ_{wind}) was taken as zero-degrees. Then:

$$\theta_{max} = \left|\theta_{cross\text{-}slope}\right| \tag{6.11}$$

By normalizing predicted global drag coefficients (determined using Eqn. 6.11 to define θ_{max}) by measured global drag coefficients at variable wind angles, the level of conservatism was evaluated. As evident in Figure 6.17, the level of conservatism produced by this approach was not desirable when a design pressure coefficient $C_{P,SIPF} = 1.1$ was used.

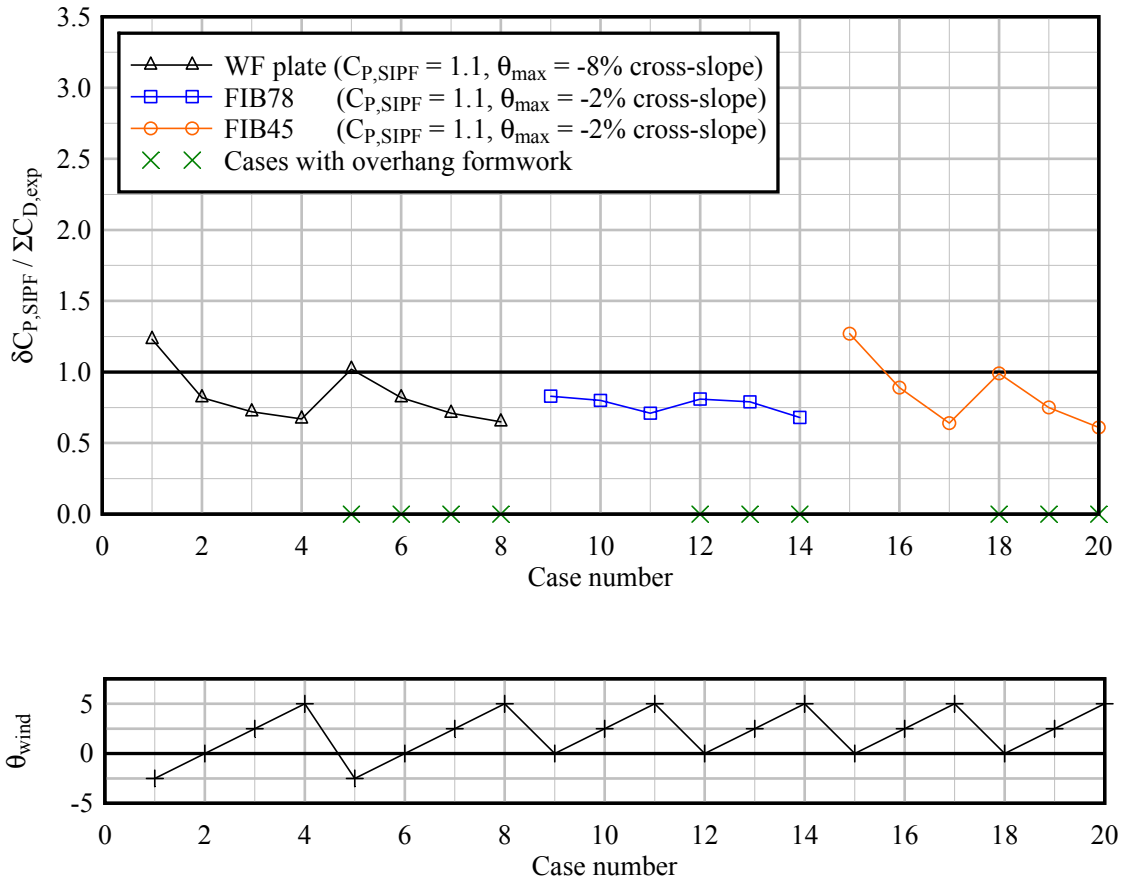

Figure 6.17 Conservatism of alternative projected area calculation procedure for I-shaped girders ($C_{P,SIPF}$ = 1.1 and wind angle not included in calculation of maximum difference angle; i.e., θ_{max}= ($\theta_{cross\text{-}slope}$))

Therefore, to ensure that conservative force predictions were achieved (i.e., normalized values greater than 1.0, Figure 6.18), it was determined through calibration that the pressure coefficient needed to be $C_{P,SIPF}$ = 1.8 (rather than the values of 1.1 or 1.4 previously noted), if wind angles are not explicitly included in the determination of maximum difference angle θ_{max}.

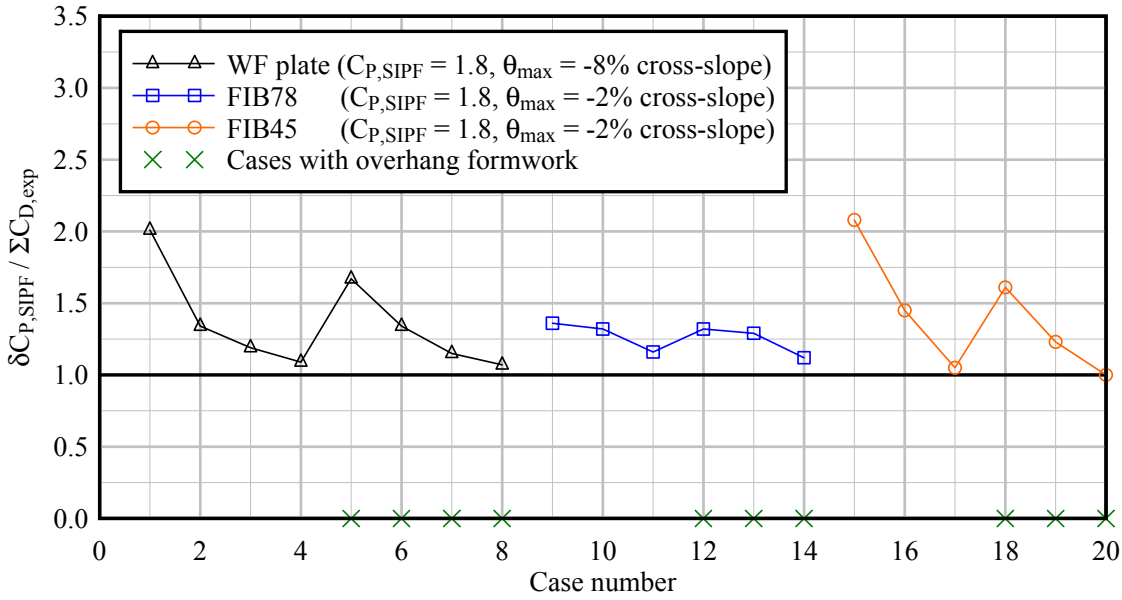

Figure 6.18 Conservatism of alternative projected area calculation procedure for I-shaped girders ($C_{P,SIPF}$ = 1.8 and wind angle not included in calculation of maximum difference angle; i.e., θ_{max}= ($\theta_{cross\text{-}slope}$))

6.3.2 Calculation of global pressure coefficient for systems with box girders

Currently, the *FDOT Structures Design Guidelines* (SDG, FDOT, 2013) specify that a $C_{P,SIPF}$ = 1.1 be applied to both I-shaped girder and box girder superstructures *when deck forms are in place* (Table 6.3). Similar to the I-shaped girder global pressure coefficient calculation procedure described in the previous section, the accuracy of the projected area method was compared to the experimentally determined global drag coefficients for box girders.

Table 6.3 Pressure coefficient during construction for box girders (FDOT, 2013)

Construction Condition	**Pressure Coefficient**
Deck forms not in place	C_P = 1.5
Stay-in-place (SIP) deck forms in place	$C_{P,SIPF}$ = 1.1

Recall from Chapter 5 that box girders were tested in the wind tunnel at 0°, ±5° and ±10° wind angles with the girders aligned with the cross-slope (Figure 6.19). Given the matching alignment of the girders and the cross-slopes, these test configurations were geometrically equivalent to zero-degree (horizontal) wind angles with 0% (0 degree), ±8.7% (±5 degree), and ±17.6% (±10 degree) cross-slopes.

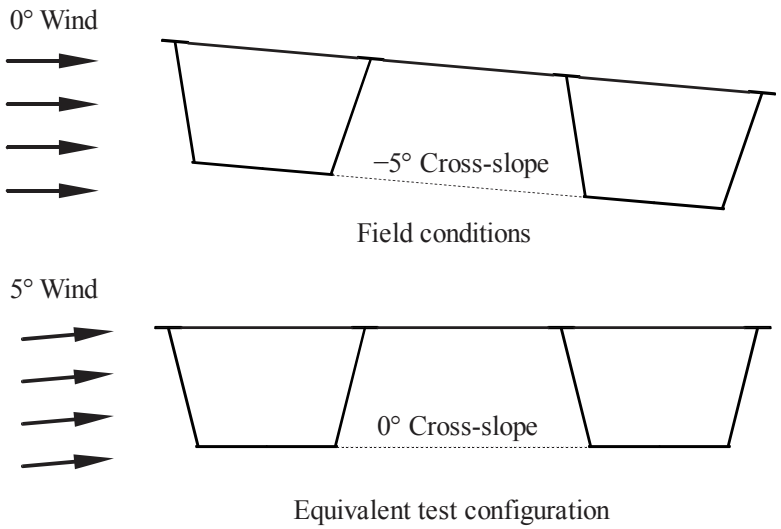

Figure 6.19 Equivalence of box girder cross-slope and wind-angle

Fully measured global drag coefficients for box girders with SIP forms are plotted as a function of wind angle in Figure 6.20. For I-shaped girders, positive wind angles (that opposed the negative cross-slope) always produced higher global drag forces. In contrast, clearly defined trends were not evident for the box girder data in terms of wind angle (i.e., positive wind angles did not necessarily produce global drag forces that exceed those produced at negative wind angles). Consequently, *all* box girder cases (positive and negative angles) with SIP forms were included in the development of a global pressure coefficient prediction method.

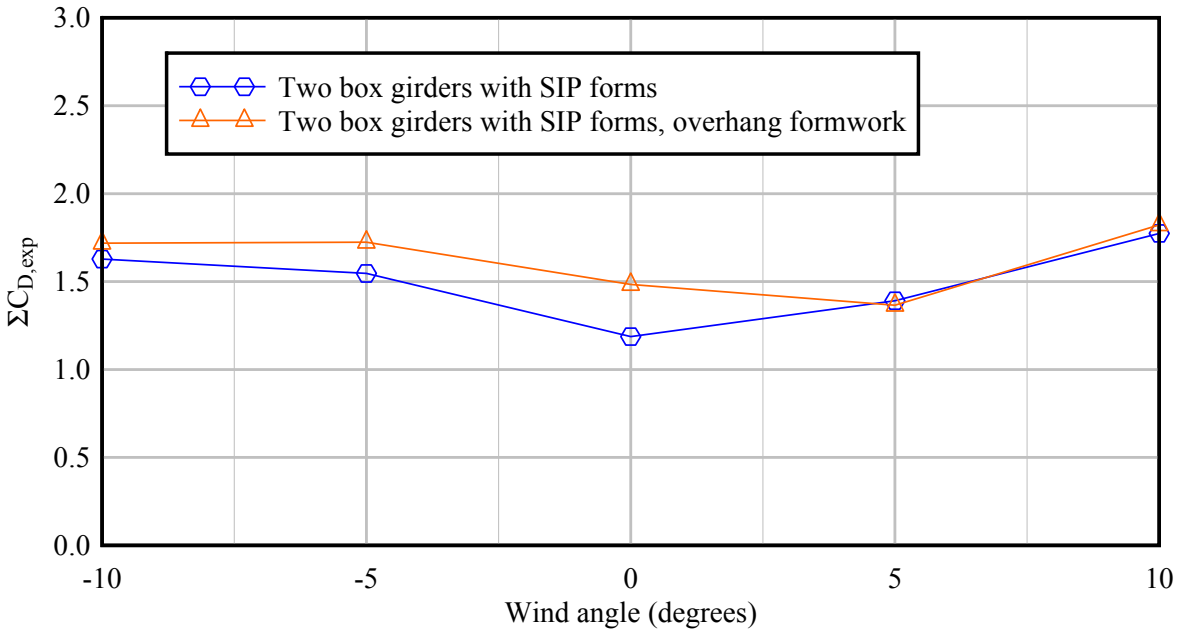

Figure 6.20 Measured global pressure coefficients for box girders

To develop such a prediction method, projected depths were calculated for each case by considering the entire superstructure. In the I-shaped girder global pressure prediction method described earlier, flange shielding was considered negligible and girders were assumed to behave as flat, vertical plates. In contrast, the equivalent 'full-scale' width of the bottom 'flange' of each box section tested was seven (7) ft across and therefore could not be idealized as a vertical plate. Consequently, the projected depth could not be defined simply in terms of girder spacing (S) and angle. Instead, the projected depth of box girder systems was defined by projecting the entire geometry of the boxes (including bottom flange width) onto a vertical plane (Figure 6.21a). Additionally, when overhang formwork was present in the cross-section (Figure 6.21b), the vertical projection of the *windward* overhang was included in the projected depth [analogously to the $W_{OHF}\left(\tan(\theta_{max})\right)$ term previously noted in Eqn. (6.6)]. The leeward overhang was omitted since it is 'hidden' behind the projected depth of the leeward box.

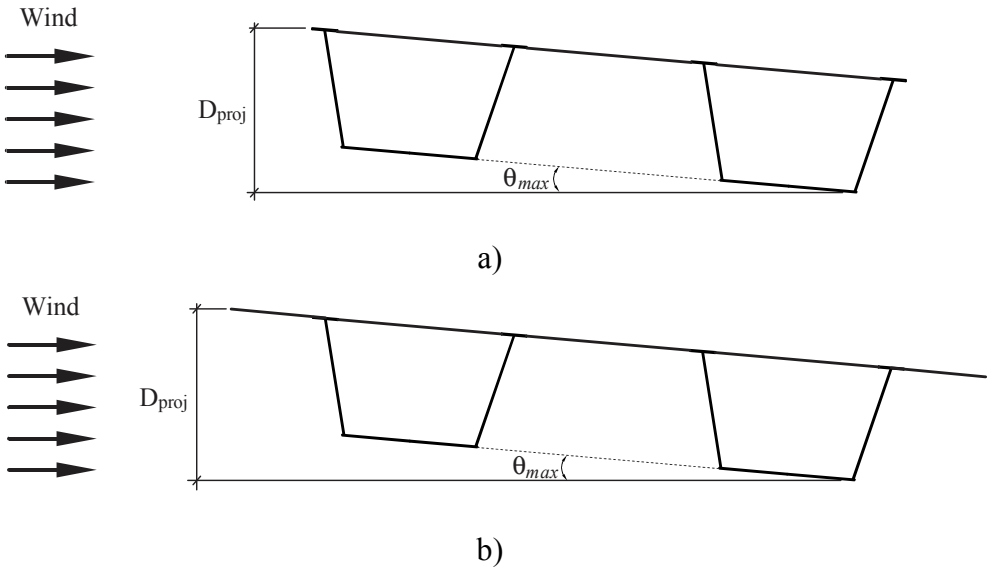

Figure 6.21 Determination of projected depth for box girder bridges:
a) without overhang formwork; b) with overhang formwork

Using this projection method, and $C_{P,SIPF}$ = 1.1, per Table 6.3, both cases (without and with formwork overhangs) at zero degree maximum difference angles (θ_{max}) were *under-predicted* (Figure 6.22), i.e., unconservative relative to measured wind tunnel data. Additionally, the predicted global drag force was significantly more *unconservative* (greater error) for the box girder bridge with overhang formwork present. This is important since at zero degree wind and 0% cross-slope, the box girder depth (D) and the projected depth (D_{proj}) and equal. Since the global drag force (and pressure coefficient) was larger when overhang formwork was present—despite the fact that the projected depth (D_{proj}) was no different than the girder depth (D)—this indicated that use of projected depth *alone* was not adequate to predict the global pressure coefficient (as was the case earlier for I-shaped girders).

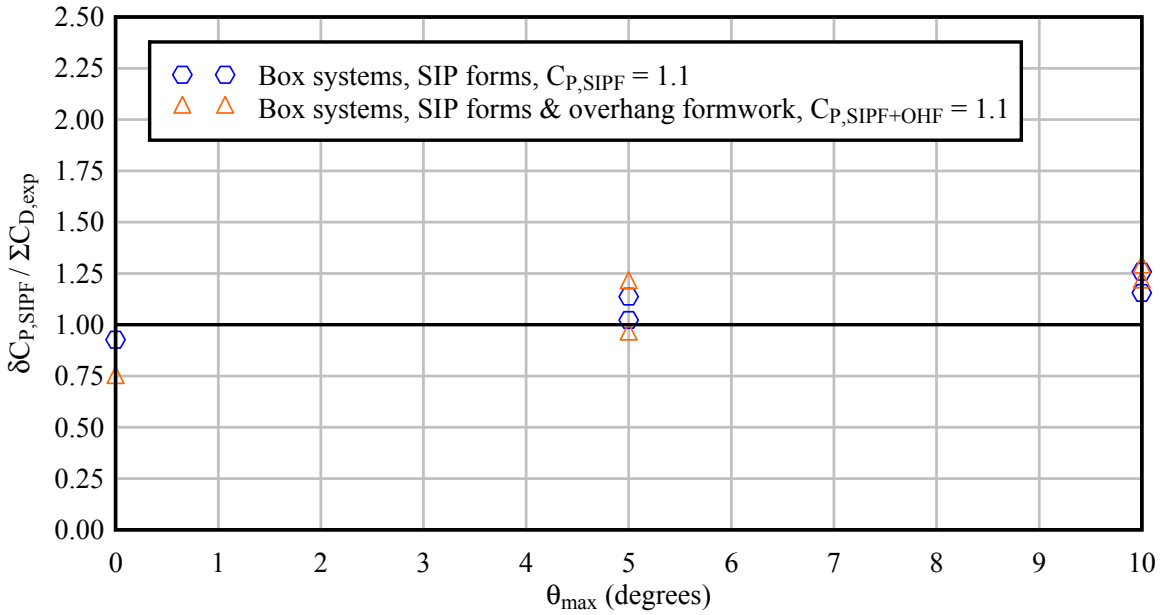

Figure 6.22 Conservatism of projected area calculation procedure for box girders (Using current FDOT $C_{P,SIPF}$ = 1.1 and $C_{P,SIPF+OHF}$ = 1.1)

Instead, the global pressure coefficient for box girder bridges was formulated to account for the presence, and width, of the overhang formwork. It was found that the minimum global pressure coefficients needed to produce conservative results at zero wind angle were $C_{P,SIPF}$ = 1.19 (SIP forms only) and $C_{P,SIPF}$=1.48 (SIP forms and overhang formwork). For convenience in design, these values were rounded to $C_{P,SIPF}$ = 1.2 and $C_{P,SIPF}$ = 1.5, respectively. In the wind tunnel test program, it was only feasible to conduct tests at a single overhang formwork width: W_{OHF}=4.33 ft (recall Figure 5.10 and Table 6.1) Therefore, to account for intermediate overhang widths that are likely to be encountered in practice, the pressure coefficient for box girder bridges with SIP forms and overhang formwork was defined using linear interpolation as:

$$C_{P,SIPF} = 1.2 + 0.3\left(\frac{W_{OHF}}{4.33\text{ ft}}\right) \tag{6.12}$$

where W_{OHF} is defined in units of ft. Using the box girder $C_{P,SIPF}$ together with projected depth (D_{proj}), to account for wind angles other than zero degrees, the normalized predicted global pressure coefficients were computed for all conditions tested in the wind tunnel (Figure 6.23) and were found to be conservative (greater than 1.0).

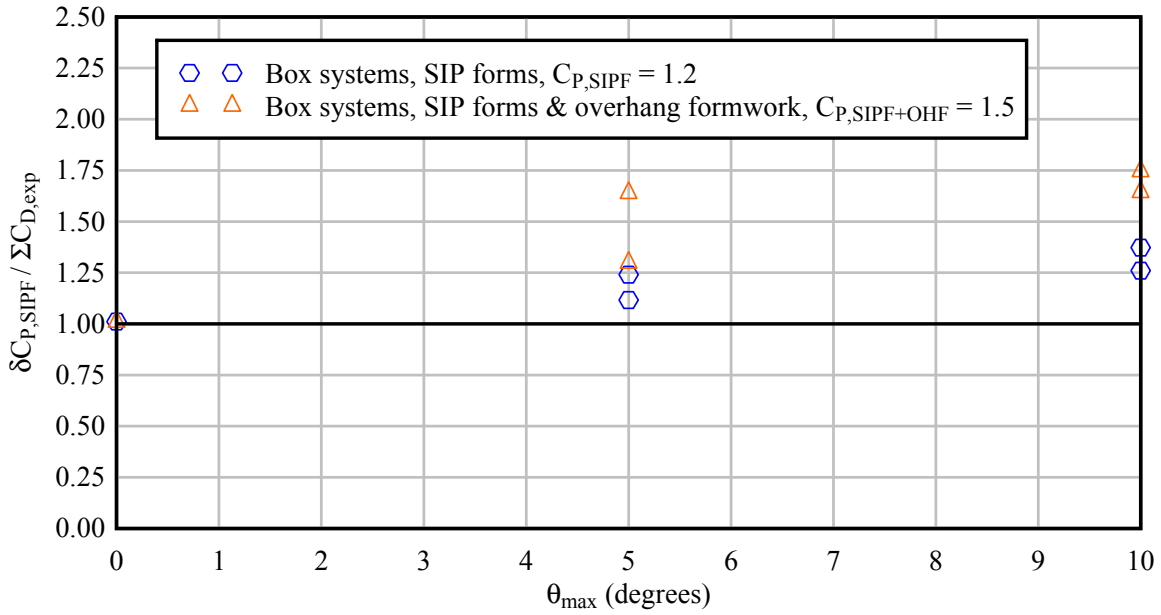

Figure 6.23 Conservatism of projected area calculation procedure for box girders (Using proposed $C_{P,SIPF}$ = 1.2 and $C_{P,SIPF+OHF}$ = 1.5)

However, for large wind angles, the degree of conservatism was greater than desirable, therefore, a reduction factor (β) was developed in a manner similar to that previously developed for FIB systems. As before, an ideal reduction factor (β_{ideal}) for each test case was determined using Eqn. (6.9), where $C_{P,SIPF}$ was computed from Eqn. (6.12) and D_{proj} as defined in Figure 6.21. In Figure 6.24, the ideal reduction factors are plotted as a function of maximum difference angle (i.e., absolute value of the difference between the wind angle and cross-slope). To envelope the data, an upper bound linear curve fit was applied:

$$\beta = 1.0 - 0.02(\theta_{max}) \tag{6.13}$$

where θ_{max} is defined in Eqn. (6.4) and has units of degrees, and β is the reduction factor for calculation of box girder global pressure coefficients. Use of the reduction factor (β) produced conservatism levels that are deemed appropriate for design purposes (Figure 6.25).

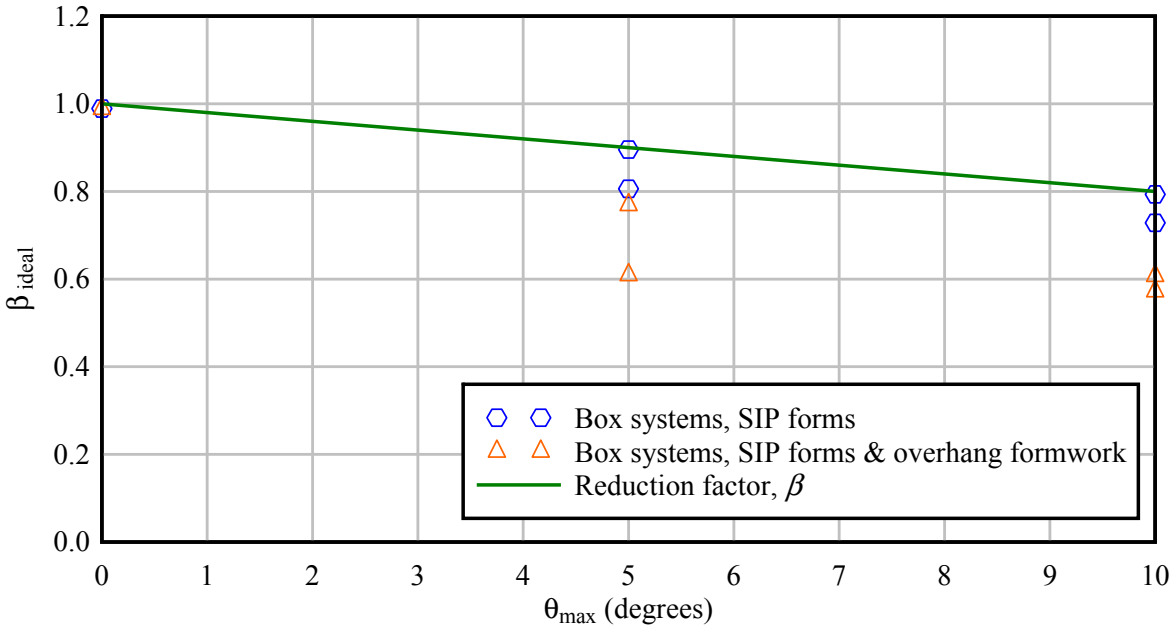

Figure 6.24 Upper bound formulation of a reduction factor (β) for box girders

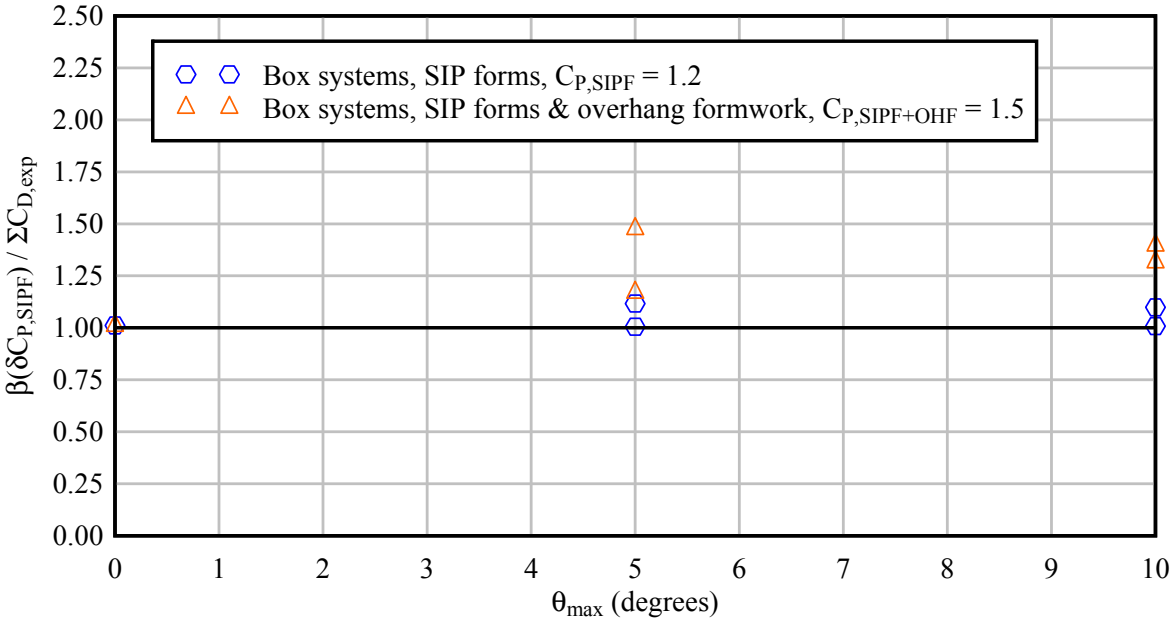

Figure 6.25 Conservatism of projected area calculation procedure for box girders (reduction factor (β) included)

6.3.3 Recommended procedure for calculation of wind loads

Using the pressure coefficients for I-shaped girders and box girders that were developed above, an overall procedure for computing lateral wind loads was developed.

1. Establish wind angle θ_{wind} and θ_{max}:

Establish the angle of wind (θ_{wind}) that will be considered. If wind will be assumed to be horizontal, then set $\theta_{wind} = 0$. Compute the maximum 'angle of difference' between the wind angle and the bridge cross-slope:

$$\theta_{max} = \left|\theta_{wind}\right| + \left|\theta_{cross-slope}\right| \tag{6.14}$$

2. Determine pressure coefficient $C_{P,SIPF}$:

For a partially constructed bridge consisting of multiple girders with SIP forms (and possibly overhang formwork), determine the pressure coefficient $C_{P,SIPF}$ from Table 6.4. For box girder bridges, the calculation of $C_{P,SIPF}$ involves the use of the overhang formwork width W_{OHF} (in units of ft.) which is defined in Figure 5.10.

Table 6.4 Recommended pressure coefficients for bridges during construction

Component type	**Pressure Coefficient**
I-shaped girders with SIP formwork	$C_{P,SIPF} = 1.4$
Box girders with SIP formwork	$C_{P,SIPF} = 1.2 + 0.3\left(\frac{W_{OHF}}{4.33\text{ ft}}\right)$

3. Determine the pressure coefficient C_P:

Compute the pressure coefficient C_P as:

$$C_P = \beta C_{P,SIPF} \tag{6.15}$$

where β is a reduction factor that takes into account the effects of wind angle:

$$\beta = \begin{Bmatrix} 1.0 & Plate\ girders \\ 1.05 - 0.07(\theta_{max}) \le 1.0 & FIB\ girders \\ 1.00 - 0.02(\theta_{max}) & Box\ girders \end{Bmatrix} \tag{6.16}$$

where θ_{max} has units of degrees.

4. Compute the design wind pressure P_Z:

Per current FDOT practice, compute the design wind pressure P_Z using Eqn. (5.9), repeated here for convenience:

$$P_Z = 2.56\times10^{-6} K_Z V^2 G C_P \tag{6.17}$$

where P_Z is the design wind pressure (ksf), K_Z is the velocity pressure exposure coefficient, V is the basic wind speed (mph), G is the gust effect factor, and the constant term 2.56×10^{-6} is in units of (ksf)/(mph)^2. [For additional details, see the *FDOT Structures Design Guidelines* (FDOT, 2013)].

5. Apply the design wind pressure over the projected area of the structure:

To compute the projected area for box girder bridges, the projected depth (D_{proj}) should be determined as indicated in Figure 6.21. To compute the projected area for I-shaped girders, the following definition of projected depth (D_{proj}) should be used:

$$D_{proj} = D + (n-1)(S)(\tan(\theta_{max})) + W_{OHF}\left(\tan(\theta_{max})\right) \tag{6.18}$$

where D is the girder depth, n is the number of girders, S is the girder spacing, $\theta_{max} = |\theta_{wind}| + |\theta_{cross-slope}|$, and W_{OHF} is the overhang formwork width (in units of ft.) as defined in Figure 5.10.

6.3.4 Alternate procedure for calculation of wind loads for I-shaped girders

For bridges constructed from I-shaped girders, the following alternate procedure for computing lateral wind loads implicitly accounts for the effects of variable wind angles (but without the need for explicitly quantifying θ_{wind}).

1. Establish θ_{max}:

Set the maximum 'angle of difference' to the bridge cross-slope: $\theta_{max} = |\theta_{cross-slope}|$.

2. Determine pressure coefficient $C_{P,SIPF}$:

For a partially constructed bridge consisting of multiple I-shaped girders with SIP forms (and possibly overhang formwork), determine the pressure coefficient $C_{P,SIPF}$ from Table 6.5.

Table 6.5 Alternate pressure coefficient for bridges during construction

Component type	Pressure Coefficient
I-shaped girders with SIP formwork	$C_{P,SIPF}$ = 1.8

3. Determine the pressure coefficient C_P:

Set the pressure coefficient:

$$C_P = C_{P,SIPF} \tag{6.19}$$

4. Compute the design wind pressure P_Z:

Per current FDOT practice, compute the design wind pressure P_Z using Eqn. (5.9), repeated here for convenience:

$$P_Z = 2.56\times10^{-6} K_Z V^2 G C_P \tag{6.20}$$

where P_Z is the design wind pressure (ksf), K_Z is the velocity pressure exposure coefficient, V is the basic wind speed (mph), G is the gust effect factor, and the constant term 2.56×10^{-6} is in units of (ksf)/(mph)^2. [For additional details, see the *FDOT Structures Design Guidelines* (FDOT, 2013)].

5. Apply the design wind pressure over the projected area of the structure:

To compute the projected area, use the following definition of projected depth (D_{proj}):

$$D_{proj} = D + (n-1)(S)(\tan(\theta_{max})) + W_{OHF}\left(\tan(\theta_{max})\right) \tag{6.21}$$

where D is the girder depth, n is the number of girders, S is the girder spacing, $\theta_{max} = \left|\theta_{cross-slope}\right|$, and W_{OHF} is the overhang formwork width (in units of ft.) as defined in Figure 5.10.

6.4 Assessment of brace forces due to wind loads

In the previous section, a methodology was developed for computing the *global* pressure (drag) coefficient and associated global wind load on a multiple-girder bridge cross-section with SIP forms (and possibly overhang formwork) in place. Such wind loads will typically be used in a *global* strength limit state evaluation for the determination of wind load reactions on the substructure. However, applied wind loads will also induce forces in the individual brace components (diagonals and horizontal elements) and, as such, have the potential to affect the brace design process. It was therefore important to determine how the magnitudes of brace forces caused by wind loads compared to those caused by construction gravity loads (e.g., eccentric construction loads, etc.). If wind-load-induced brace forces were consistently smaller in magnitude than construction-load-induced brace forces, then there would be no need to formulate wind pressure coefficients specifically for use in designing the bracing elements when SIP forms are present.

To carry out this assessment, structural analysis models of bracing systems were created for purposes of analyzing brace forces due to wind loads. Two-dimensional (2-D) bracing models were analyzed by adapting the modeling methodology previously developed in BDK75-977-33 (see Section 5.6 of Consolazio et al., 2013). In the most-windward bracing panel (i.e., between girders G1 and G2), the largest differences between the G1 and G2 drag coefficients (C_D) were observed. Since such conditions produce the most severe wind-induced brace forces, only braces forces in this panel were compared to forces induced by construction loads.

As previously noted (e.g., in Section 6.2.3), wind tunnel testing revealed that the addition of overhang formwork significantly increased the wind-induced magnitude of torque on the windward girder (G1). However, for *every* wind angle tested, the direction of wind-induced torque (related to C_T) on the overhang was found to be in *opposition* to the torque (i.e., moment) produced on the overhang by the downward acting gravity (self-weight) of the overhang

formwork (denoted M_{OHF}). Hence, for all feasible scenarios, the effect of including wind-induced overhang torque would be to *reduce* (i.e., offset) the effect that moment M_{OHF} would have on the development of brace forces. Consequently, for simplicity and conservatism, the worst case loading condition for brace force assessment was taken as the moment M_{OHF} acting without any reduction attributable to wind-induced torque. That is, wind-induced torque was conservatively omitted. [Note that because the bottom of each overhang bracket bears against (makes contact with) the bottom flange of the exterior girder (recall Section 3.4), but is *not* structurally connected to the girder, it is *not* possible for wind-induced torque to exceed M_{OHF} and cause a net increase in torque (and associated brace force). Instead, the maximum effect that wind-induced torque can achieve is to fully cancel out M_{OHF}.] Consequently, in the simplified 2-D models used to assess 'wind-related' brace forces, the maximum differences in wind-tunnel measured drag coefficients (C_D) for G1 and G2 were converted into an equivalent maximum horizontal-wind force, which was simultaneously applied to the model in conjunction with the maximum gravity-induced overhang moment M_{OHF}.

To be particularly conservative in including the effects of M_{OHF} on brace forces, the overhang formwork dead load (causing M_{OHF}) was assumed to be 20 psf (rather than the 10 psf value noted earlier in Table 3.1), and only worst-case geometric configurations were considered. Maximum feasible braced lengths were chosen for 45" FIB and 78" FIB analysis models based on an 'end-span only' bracing configuration. Consequently, wind pressures were converted into wind loads (drag forces)—for application to the structural analysis models—by multiplying them by a tributary length equal to one-half the maximum feasible girder span length. Additionally, a conservative estimate of maximum 'construction inactive' wind speed was assumed. The FDOT SDG (FDOT, 2013) allows a reduction factor (R_e) of 0.6 to be applied for structures with an exposure period of less than one year. By selecting the maximum 'construction inactive' wind speed in Florida (150 mph), and applying the reduction factor, a construction design wind speed of 90 mph was obtained and used in all analyses.

Maximum brace forces produced by the combined application of wind-induced drag force and maximum feasible overhang moment (M_{OHF}) were found to be *smaller than* the maximum brace forces caused by the application of the full set of construction loads listed in Table 3.1. That is, construction loads—*not* wind loads—were found to produce brace forces that would control the brace design process. Therefore, pressure coefficients for use specifically in determining wind-induced brace forces were not developed in this study. Instead, it is recommended that construction loads be considered the controlling load case for the design of construction-stage girder bracing when SIP formwork is in place.

CHAPTER 7
SUMMARY, CONCLUSIONS, AND RECOMMENDATIONS

7.1 Introduction

In this study, issues relating to the application of construction gravity loads and lateral wind loads, to bridges under construction, were investigated. For construction gravity loads, a brace force prediction methodology was developed. For lateral wind loads, drag coefficients were measured using wind tunnel testing and a methodology for computing global pressure coefficients and applying the associated lateral wind pressures to bridges under construction was developed.

7.2 Brace forces due to construction loads

Numerical finite element bridge models and analysis techniques were developed for evaluating brace forces induced by construction loads acting on precast concrete girders (Florida-I Beams) in systems of multiple girders braced together. Construction loads considered in this study included: wet concrete deck load, stay-in-place (SIP) form weight, overhang formwork weight, live load, worker line loads, and concentrated loads representing a deck finishing machine.

Preliminary limited-scope sensitivity studies indicated that brace forces were not particularly sensitive to bridge grade, bridge cross-slope, girder camber, or girder sweep; therefore, variations of these parameters were not included in subsequent parametric analyses. Additional sensitivity studies indicated that the typical configuration of K-brace recommended for use the FDOT generally produced marginally larger brace forces than did three alternative K-brace configurations. Consequently, for brace force determination purposes, only the FDOT recommended K-brace configuration was used in the remainder of the study.

A large-scale parametric study, involving more than 600,000 separate three-dimensional structural analyses, was performed to compute maximum brace forces for un-factored (service) and factored (strength) construction load conditions. Maximum end-span brace forces and intermediate-span brace forces quantified from the parametric study were stored into a database. The parametric study included consideration of different Florida-I Beam cross-sections, span lengths, girder spacings, deck overhang widths, skew angles, number of girders, number of braces, and bracing configurations (K-brace and X-brace). Additionally, partial coverage of wet (non-structural) concrete load and variable placement of deck finishing machine loads were considered.

To make the process of accessing and interpolating the brace force database simple and user-friendly, a MathCad-based program was developed that employed automated data-retrieval (from the database) and multiple-dimensional linear interpolation. The accuracy of the database interpolation approach to brace force prediction was found to be suitable for use in design (less than ten percent (10%) error was present in a majority of verification cases assessed). It is therefore recommended that the brace force database and database interpolation program developed in this study be deployed as a methodology for computing brace forces for bracing design in bridges under construction.

7.3 Wind pressure coefficients and corresponding lateral loads

Wind tunnel testing was used to quantify wind load coefficients (drag, torque, and lift) for systems of multiple bridge girders (FIB, plate girder, and box) with stay-in-place (SIP) forms and overhang formwork in place. Tests were conducted at multiple wind angles, and corresponding tests with and without overhang formwork were conducted so that the effects of overhang formwork on drag, lift, and torque coefficients could be quantified.

Wind tunnel tests indicated that adding SIP forms to systems of bare girders [as were investigated in a previous study (BDK75-977-33, Consolazio et al., 2013)] had only an incremental influence on individual girder drag coefficients, rather than fundamentally changing the distribution of drag coefficients across the bridge. However, it was found that adding overhang formwork significantly increased the wind-induced torque on the windward girder. Additionally, by making use of lift force data measured for the windward girder, estimates of uplift forces acting on overhang formwork were produced.

Drag coefficients measured at each girder position in bridges with I-shaped girders, and in bridges with box girders, were used to develop conservative methods for computing global (system) pressure coefficients suitable for use in bridge design (particularly, for use in calculating global lateral substructure load due to wind). The developed methodology involves computing global pressure coefficients (using newly proposed values and expressions), computing design wind pressures (using established FDOT methods), and then applying the computed wind pressure to the projected area of the bridge using a newly proposed definition of projected bridge depth.

Finally, by comparing brace forces (note: *not* global substructure forces) caused by construction loads to brace forces caused primarily by wind load, it was found that the construction loads produced significantly larger brace forces and would therefore be very likely to control the design of bracing systems and bracing elements.

REFERENCES

AASHTO (American Association of State Highway and Transportation Officials) (2008). *Guide Design Specification for Bridge Temporary Works*, AASHTO, Washington, D.C.

ADINA (2012). *Theory and Modeling Guide, Volume 1: ADINA Solids & Structures*, ADINA R&D, Inc, Watertown, MA.

ASCE (American Society of Civil Engineers) (2006). *ASCE 7–05: Minimum Design Loads for Buildings and Other Structures*, ASCE, New York, NY.

Çengel, Y. and Cimbala, J. (2006). *Fluid Mechanics: Fundamentals and Applications*, McGraw–Hill Higher Education, Boston, MA.

Clifton, S. and Bayrak, O. (2008). *Bridge Deck Overhang Construction,* Technical Report IAC: 88-5DD1A003-2, University of Texas, Austin, TX.

Consolazio, G., Gurley, K., and Harper, Z. (2013). *Bridge Girder Drag Coefficients and Wind-Related Bracing Recommendations*, Structures Research Report No. 2013/87322, University of Florida, Gainesville, FL.

FDOT (Florida Department of Transportation) (2009). *Temporary Design Bulletin C09–07*, FDOT, Tallahassee, FL.

FDOT (Florida Department of Transportation) (2010). *Standard Specifications for Road and Bridge Construction*, FDOT, Tallahassee, FL.

FDOT (Florida Department of Transportation) (2013). *Structures Manual Volume I: Structures Design Guidelines*, FDOT, Tallahassee, FL.

FDOT (Florida Department of Transportation) (2014a). *Design Standard No. 20005: Prestressed I-Beam Temporary Bracing*, FDOT, Tallahassee, FL.

FDOT (Florida Department of Transportation) (2014b). *Instructions for Design Standard No. 20010: Prestressed Florida-I Beams*, FDOT, Tallahassee, FL.

FDOT (Florida Department of Transportation) (2014c). *Design Standard No. 20510: Composite Elastomeric Bearing Pads – Prestressed Florida-I Beams*, FDOT, Tallahassee, FL.

Holmes, J. (2007). *Wind Loading of Structures: 2nd Edition*, Taylor & Francis, New York, NY.

PCI (2010). *PCI Design Handbook: 7th Edition*, Precast/Prestressed Concrete Institute, Chicago, IL.

Solari, G. and Kareem, A. (1998). "On the Formulation of ASCE 7–95 Gust Effect Factor", *Journal of Wind Engineering and Industrial Aerodynamics*, Vol. 77, pp. 673–684.

APPENDIX A
CROSS-SECTIONAL PROPERTIES OF FLORIDA-I BEAMS

In this study, finite element models Florida-I Beams (FIBs) were analyzed to evaluate temporary bracing forces caused by construction loads. In each model, the FIBs were modeled using *warping beam elements*, specialized beam elements available in the ADINA finite element code, which require the calculation of a comprehensive set of cross-sectional properties. This appendix provides mathematical definitions of all such properties and corresponding numeric values that were calculated for each FIB cross-sectional shape.

Definitions of the cross-sectional properties that are required to use the warping beam element in ADINA are listed in Table A.1. Each property requires the evaluation of an integral over the area of the cross-section, in which the integrands are written in terms of coordinates x and y, referenced to the geometric centroid of the section (Figure A.1). Some properties also require knowledge of the *warping function*, $\psi(x,y)$, which represents the torsionally-induced out-of-plane warping displacements per rate of twist at every point on the cross-section. (The units of ψ are therefore in/(rad/in) or in^2.)

Table A.1 Definitions of cross-sectional properties required for use of a warping beam element

Property	Integral form	Units	Description
A	$\int_A dA$	in^2	Cross-sectional area
I_{yy}	$\int_A y^2 dA$	in^4	Strong-axis moment of inertia
I_{xx}	$\int_A x^2 dA$	in^4	Weak-axis moment of inertia
I_{xy}	$\int_A (xy) dA$	in^4	Product of inertia
x_s	$-\frac{1}{I_{yy}} \int_A (y\psi_c)\, dA$	in	X-coordinate of shear center
y_s	$\frac{1}{I_{xx}} \int_A (x\psi_c)\, dA$	in	Y-coordinate of shear center
J	$\int_A \left(x^2 + y^2 + x\frac{d\psi}{dy} - y\frac{d\psi}{dx} \right) dA$	in^4	St. Venant torsional constant
C_ω	$\int_A \psi^2 dA$	in^6	Warping constant
I_{xr}	$\int_A x\left(x^2 + y^2\right) dA$	in^5	Twist/strong-axis bending coupling term
I_{yr}	$\int_A y\left(x^2 + y^2\right) dA$	in^5	Twist/weak-axis bending coupling term
$I_{\omega r}$	$\int_A \psi\left(x^2 + y^2\right) dA$	in^6	Twist/warping coupling term
I_{rr}	$\int_A \left(x^2 + y^2\right)^2 dA$	in^6	Wagner constant

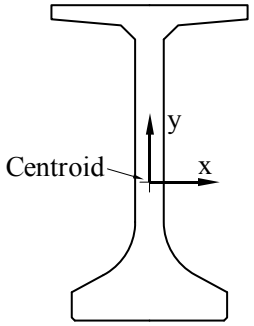

Figure A.1 Coordinate system used in the calculation of cross-sectional properties

For general cross-sectional shapes (e.g., an FIB), analytical (closed form) solutions for $\psi(x,y)$ do not exist; instead the warping field $\psi(x,y)$ must be solved numerically. In this study, the calculation of $\psi(x,y)$ for each FIB shape was accomplished by discretizing the cross-sectional shape into a high-resolution mesh of thousands of two-dimensional triangular elements, and then employing a finite element approach to solve the governing differential equation.

In general, solutions for $\psi(x,y)$ change depending on the assumed location of the center of twist. In the literature, the term 'warping function' typically refers to a particular solution (ψ in Table A.1) corresponding to a state of *pure torsion*, i.e., torsion about the shear center. As a result, prior knowledge of the location of the shear center is required to compute several of the warping beam properties. However, it is possible to calculate the coordinates of the shear center, x_S and y_S (Table A.1), using an alternative solution to the warping function (ψ_C), where the center of twist is assumed to be located at the centroid of the section. Therefore, two different warping functions were computed for each FIB section: first the section centroid was used to compute ψ_C and then the location of the shear center, obtained from ψ_C, was used to compute ψ as well as the remaining cross-sectional properties.

Because all FIB cross-sections are symmetric about the y-axis, I_{xy}, x_S, I_{xr}, and $I_{\omega r}$ have a value of zero (0) by definition. The remaining cross-sectional properties calculated for each FIB shape are summarized in Table A.2.

Table A.2. Cross-sectional properties of Florida-I Beams

Section	A (in^2)	I_{yy} (in^4)	I_{xx} (in^4)	y_S (in)	J (in^4)	C_ω (in^6)	I_{yr} (in^5)	I_{rr} (in^6)
36″ FIB	807	127,700	81,283	3.00	30,864	11,577,000	703,250	86,224,000
45″ FIB	870	226,810	81,540	3.46	31,885	21,835,000	1,521,200	167,760,000
54″ FIB	933	360,270	81,798	3.81	32,939	35,370,000	2,760,500	315,370,000
63″ FIB	996	530,790	82,055	4.07	33,973	52,203,000	4,471,300	562,480,000
72″ FIB	1059	741,060	82,314	4.27	35,041	72,337,000	6,693,800	951,390,000
78″ FIB	1101	904,610	82,484	4.38	35,693	87,610,000	8,473,400	1,314,600,000
84″ FIB	1143	1,087,800	82,657	4.46	36,421	104,350,000	10,504,000	1,781,400,000
96″ FIB	1227	1,516,200	83,002	4.56	37,859	142,280,000	15,336,000	3,107,900,000

APPENDIX B
DIMENSIONED DRAWINGS OF WIND TUNNEL TEST CONFIGURATIONS

This appendix includes dimensioned drawings of every girder configuration that was subjected to wind tunnel testing.

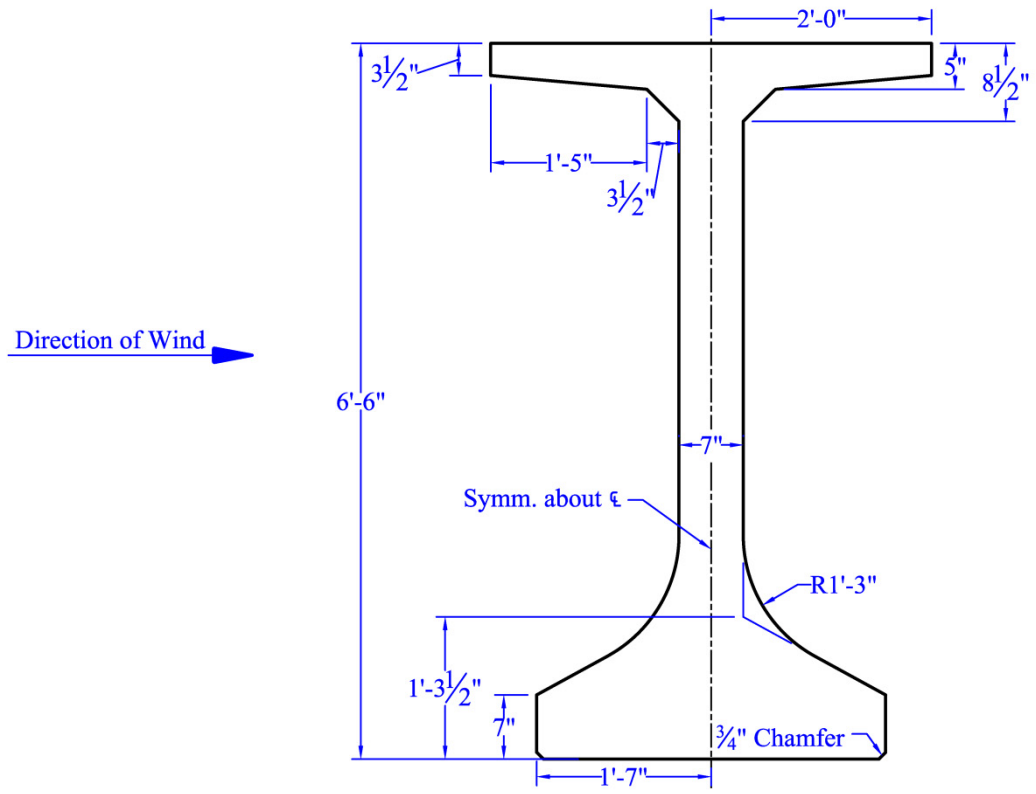

Girder Cross Section

REVISIONS			Determination of Brace Forces Caused by Construction Loads and Wind Loads During Bridge Construction		
Revision 1: 2012-12-17			University of Florida	78" Florida I-Beam Test Section	Sheet 1 of 7

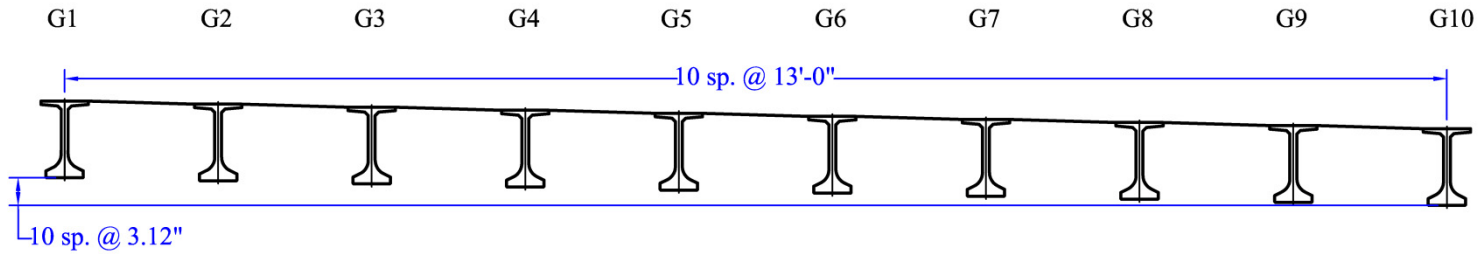

Set A1: 10 Girder Model (-2% Cross Slope)

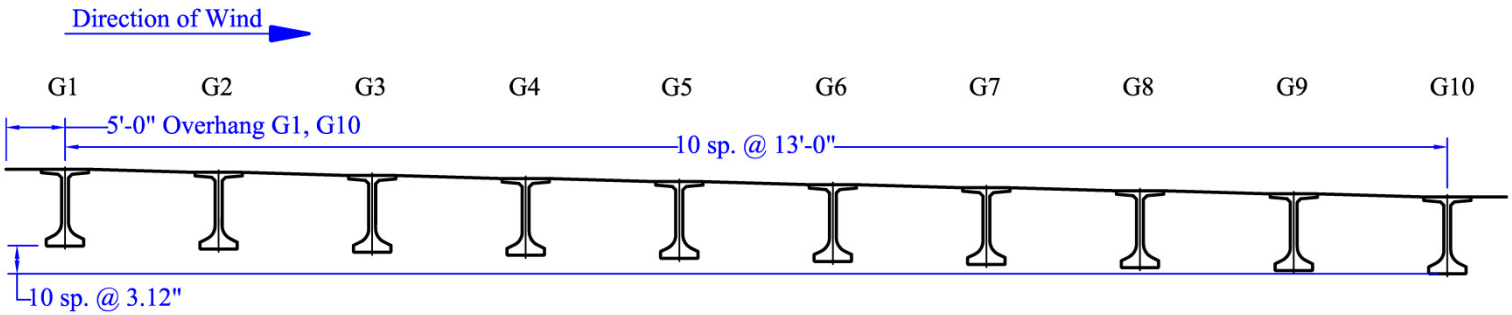

Set A2: 10 Girder Model (-2% Cross Slope, Overhangs Included)

REVISIONS			Determination of Brace Forces Caused by Construction Loads and Wind Loads During Bridge Construction		
Revision 1: 2012-12-17			University of Florida	78" Florida I-Beam Test Section	Sheet 2 of 7

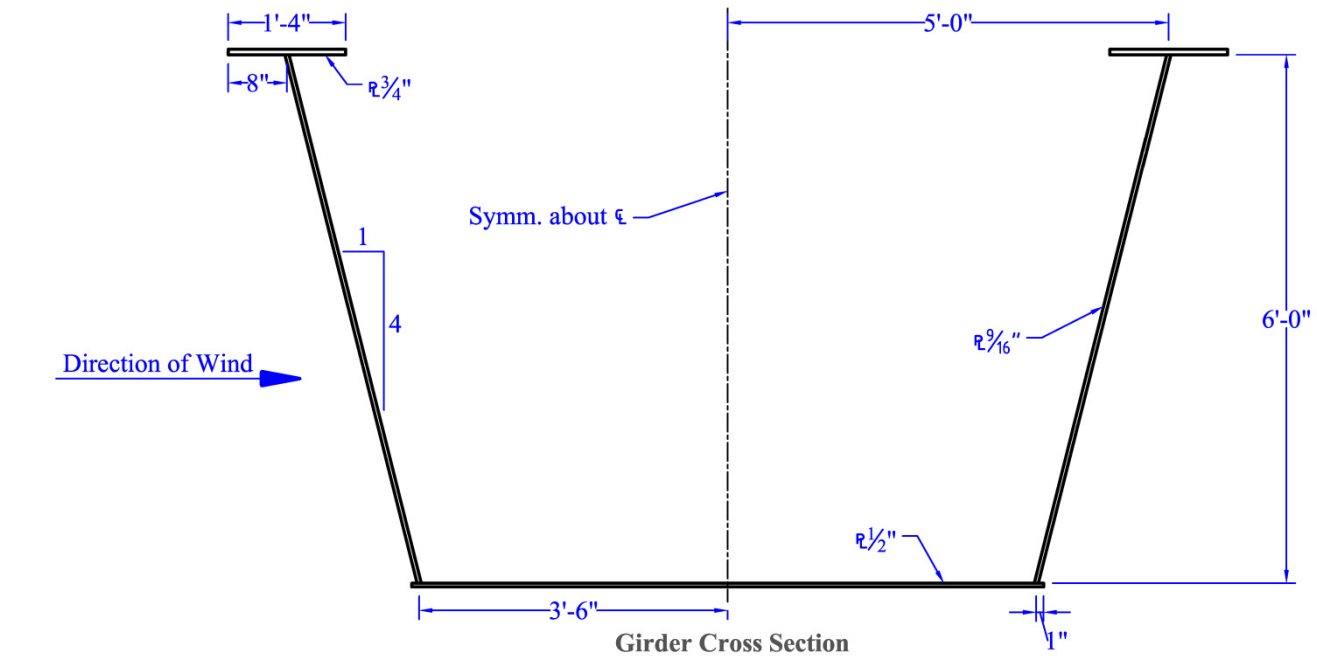

Girder Cross Section

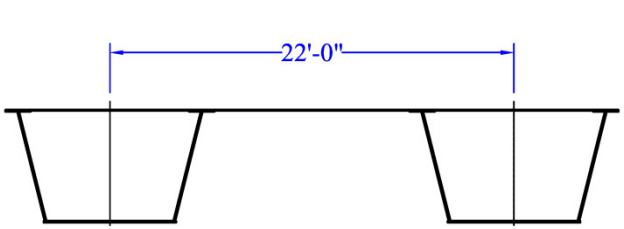

Set B1: 2 Girder Model
(0% Cross Slope)

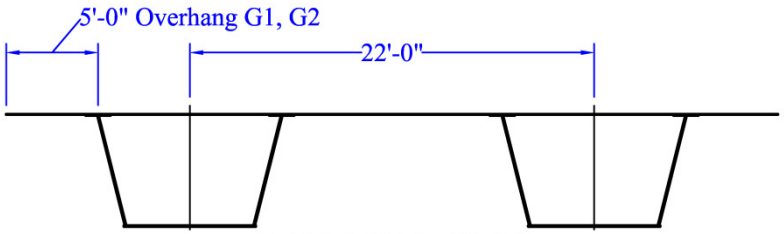

Set B2: 2 Girder Model
(0% Cross Slope, Overhangs Included)

REVISIONS			Determination of Brace Forces Caused by Construction Loads and Wind Loads During Bridge Construction		
Revision 1: 2012-12-17			University of Florida	Steel Box Girder Test Section	Sheet 3 of 7

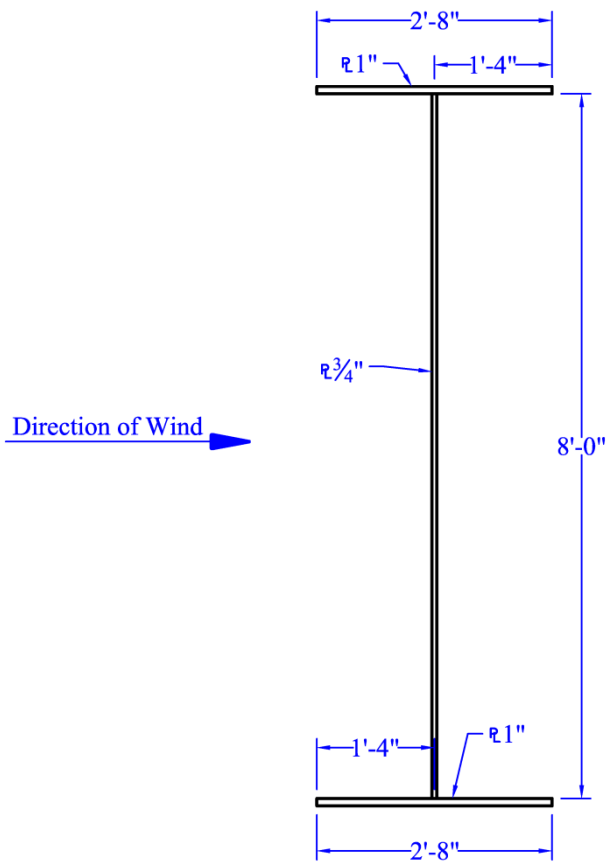

Girder Cross Section

REVISIONS			Determination of Brace Forces Caused by Construction Loads and Wind Loads During Bridge Construction		
Revision 1: 2012-12-17			University of Florida	Wide Flange Steel I-Girder Test Section	Sheet 4 of 7
Revision 2: 2013-07-30					

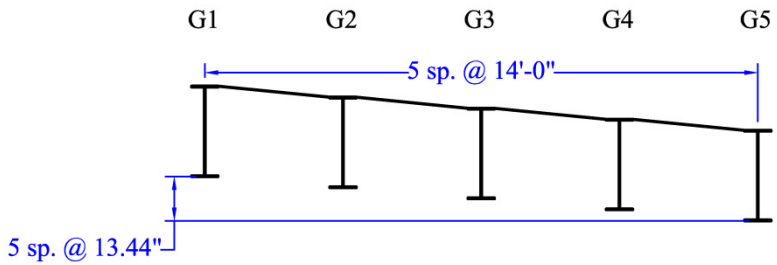

Set C1: 5 Girder Model (-8% Cross Slope)

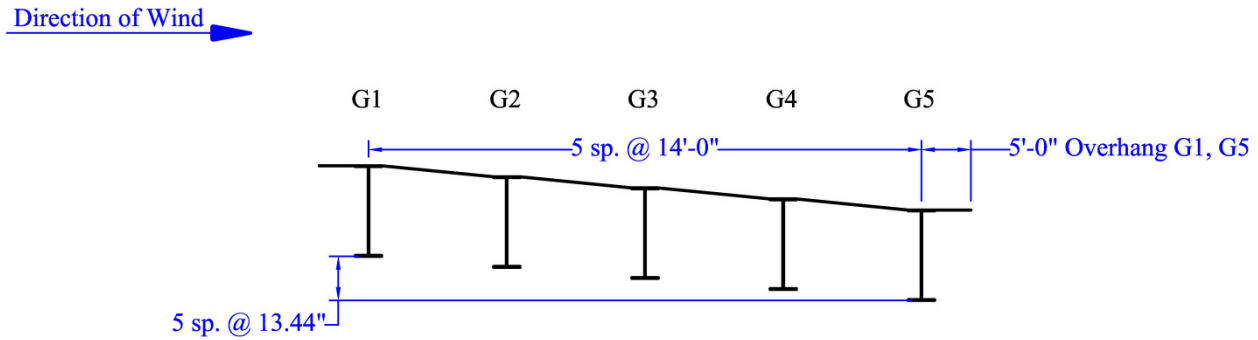

Set C2: 5 Girder Model (-8% Cross Slope, Overhangs Included)

REVISIONS			Determination of Brace Forces Caused by Construction Loads and Wind Loads During Bridge Construction		
Revision 1: 2012-12-17					
Revision 2: 2013-07-30			University of Florida	Wide Flange Steel I-Girder Test Section	Sheet 5 of 7

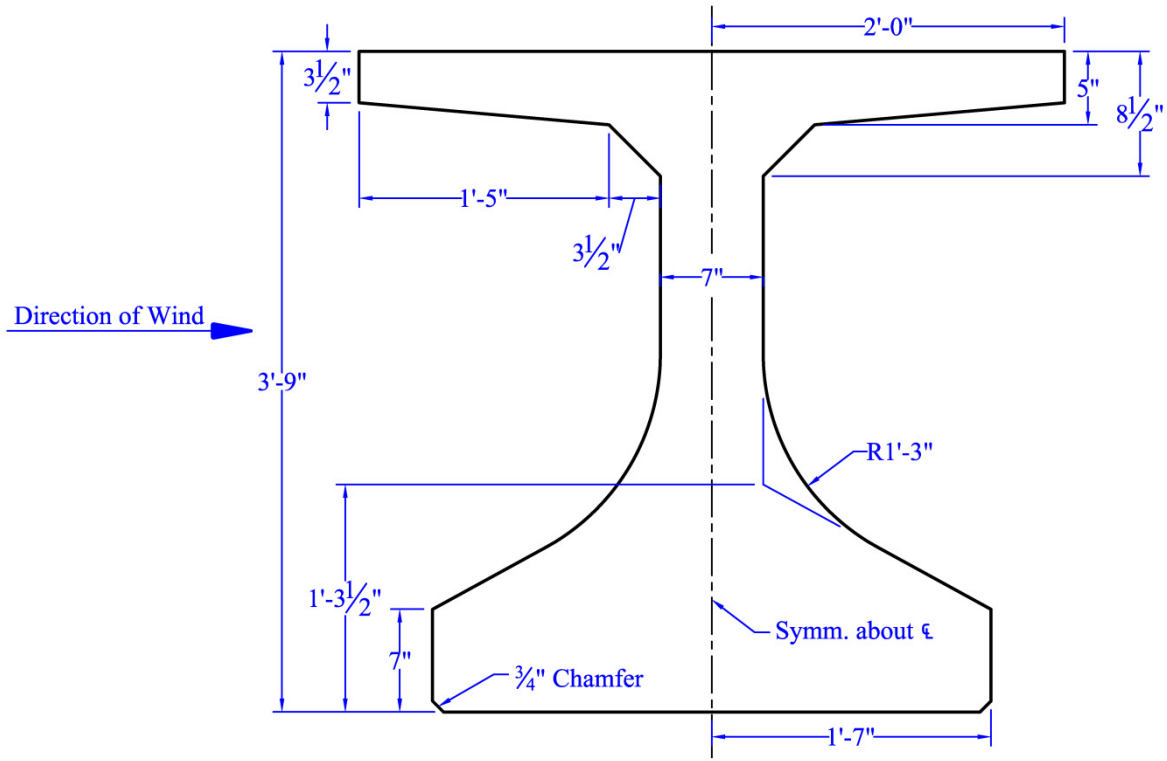

Girder Cross Section

REVISIONS			Determination of Brace Forces Caused by Construction Loads and Wind Loads During Bridge Construction		
Revision 1: 2012-12-17					
Revision 2: 2013-07-30			University of Florida	45" Florida I-Beam Test Section	Sheet 6 of 7

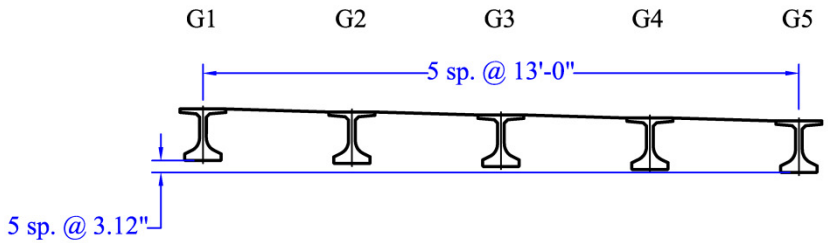

Set D1: 5 Girder Model (-2% Cross Slope)

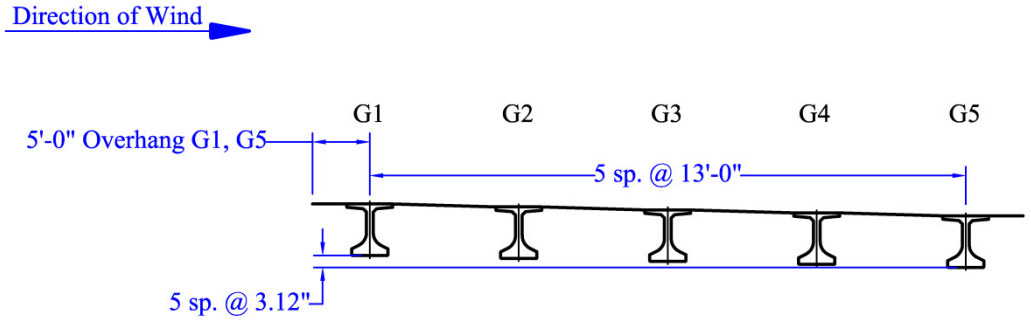

Set D2: 5 Girder Model (-2% Cross Slope, Overhangs Included)

REVISIONS			Determination of Brace Forces Caused by Construction Loads and Wind Loads During Bridge Construction		
Revision 1: 2012-12-17					
Revision 2: 2013-07-30			University of Florida	45" Florida I-Beam Test Section	Sheet 7 of 7

APPENDIX C
TABULATED RESULTS FROM WIND TUNNEL TESTS

This appendix contains results from all of the wind tunnel tests that were performed, including drag, lift, and torque coefficients. The wind tunnel testing scope is given in Table C.1. Note that the wind coefficients in this appendix are converted to measurements at the girder centroid. Results for each test configuration are given an ID code consisting of a letter and a number. The letter describes the cross-section of the girders, and the number indicates if overhangs were included. A second number following a dash is the girder being measured. For example, the designation A*2–5* refers to the fifth (5) 78" FIB girder with overhangs (indicated by 2) in a group of ten (10).

Table C.1 Summary of wind tunnel tests

Configuration Name	Section	Overhangs included	Cross-slope	Spacing (ft)	Number of girders	Instrumented girder position
A1	78" FIB	--	-2%	13	10	1,2,3
A2	78" FIB	Yes	-2%	13	10	1,2,3,5,10
B1	Box	--	0%	22	2	1,2
B2	Box	Yes	0%	22	2	1,2
C1	WF Plate	--	-8%	14	5	1,2,3
C2	WF Plate	Yes	-8%	14	5	1,2,3,4,5
D1	45" FIB	--	-2%	13	5	1,2
D2	45" FIB	Yes	-2%	13	5	1,2,3

Testing Configuration A1

Cross-section:	78″ FIB
Spacing:	13 ft
Cross-slope:	-2%
Overhangs:	No
Number of girders:	10
Instrumented girders:	1, 2, 3

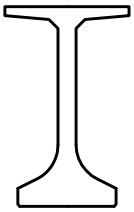

Drag coefficient (C_D)

Wind Angle	A1–1	A1–2	A1–3	A1–4	A1–5	A1–6	A1–7	A1–8	A1–9	A1–10
−5.0°	1.86	-0.02	-0.13	--	--	--	--	--	--	--
−2.5°	1.66	-0.10	-0.32	--	--	--	--	--	--	--
0°	1.47	-0.42	-0.17	--	--	--	--	--	--	--
2.5°	1.14	-0.52	0.08	--	--	--	--	--	--	--
5.0°	0.90	-0.31	0.09	--	--	--	--	--	--	--

Lift coefficient (C_L)

Wind Angle	A1–1	A1–2	A1–3	A1–4	A1–5	A1–6	A1–7	A1–8	A1–9	A1–10
−5.0°	-0.34	-1.96	-1.91	--	--	--	--	--	--	--
−2.5°	0.23	-0.28	-0.68	--	--	--	--	--	--	--
0°	0.69	1.07	1.53	--	--	--	--	--	--	--
2.5°	1.20	2.12	2.50	--	--	--	--	--	--	--
5.0°	1.44	2.69	2.70	--	--	--	--	--	--	--

Torque coefficient (C_T)

Wind Angle	A1–1	A1–2	A1–3	A1–4	A1–5	A1–6	A1–7	A1–8	A1–9	A1–10
−5.0°	0.41	0.10	-0.05	--	--	--	--	--	--	--
−2.5°	0.11	0.14	-0.07	--	--	--	--	--	--	--
0°	-0.10	-0.18	-0.01	--	--	--	--	--	--	--
2.5°	-0.36	-0.23	-0.01	--	--	--	--	--	--	--
5.0°	-0.48	-0.20	-0.04	--	--	--	--	--	--	--

Testing Configuration A2

Cross-section:	78″ FIB
Spacing:	13 ft
Cross-slope:	-2%
Overhangs:	Yes
Number of girders:	10
Instrumented girders:	1, 2, 3, 5, 10

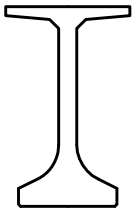

Drag coefficient (C_D)

Wind Angle	A2–1	A2–2	A2–3	A2–4	A2–5	A2–6	A2–7	A2–8	A2–9	A2–10
−5.0°	1.90	0.01	-0.10	--	-0.18	--	--	--	--	0.16
−2.5°	1.76	-0.05	-0.20	--	-0.10	--	--	--	--	0.21
0°	1.61	-0.11	-0.42	--	0.06	--	--	--	--	0.27
2.5°	1.43	-0.46	-0.12	--	0.03	--	--	--	--	0.34
5.0°	1.25	-0.53	0.06	--	0.01	--	--	--	--	0.46

Lift coefficient (C_L)

Wind Angle	A2–1	A2–2	A2–3	A2–4	A2–5	A2–6	A2–7	A2–8	A2–9	A2–10
−5.0°	0.14	-2.16	-1.95	--	-1.18	--	--	--	--	-0.06
−2.5°	1.47	-0.90	-1.10	--	-0.05	--	--	--	--	0.04
0°	2.07	0.56	1.03	--	0.62	--	--	--	--	0.04
2.5°	2.64	1.59	2.48	--	1.50	--	--	--	--	0.02
5.0°	2.85	2.05	2.75	--	2.41	--	--	--	--	0.24

Torque coefficient (C_T)

Wind Angle	A2–1	A2–2	A2–3	A2–4	A2–5	A2–6	A2–7	A2–8	A2–9	A2–10
−5.0°	1.47	0.01	-0.03	--	-0.04	--	--	--	--	0.11
−2.5°	1.11	0.18	-0.05	--	0.08	--	--	--	--	0.14
0°	0.98	-0.01	-0.11	--	0.09	--	--	--	--	0.15
2.5°	0.82	-0.26	-0.07	--	0.05	--	--	--	--	0.13
5.0°	0.67	-0.28	-0.03	--	-0.04	--	--	--	--	0.17

Testing Configuration B1

Cross-section:	Box
Spacing:	22 ft
Cross-slope:	0%
Overhangs:	No
Number of girders:	2
Instrumented girders:	1, 2

Drag coefficient (C_D)

Wind Angle	B1–1	B1-2
−10.0°	1.68	-0.05
−5.0°	1.74	-0.20
0°	1.71	-0.52
5.0°	1.67	-0.28
10.0°	1.55	0.22

Lift coefficient (C_L)

Wind Angle	B1–1	B1-2
−10.0°	-0.98	-1.34
−5.0°	0.01	-1.54
0°	1.04	-0.97
5.0°	1.19	0.88
10.0°	1.16	0.97

Torque coefficient (C_T)

Wind Angle	B1–1	B1-2
−10.0°	1.82	-0.71
−5.0°	1.56	-0.97
0°	0.64	-0.60
5.0°	0.53	0.29
10.0°	0.40	0.36

Testing Configuration B2

Cross-section:	Box
Spacing:	22 ft
Cross-slope:	0%
Overhangs:	Yes
Number of girders:	2
Instrumented girders:	1, 2

Drag coefficient (C_D)

Wind Angle	B2–1	B2–2
−10.0°	1.73	-0.01
−5.0°	1.80	-0.08
0°	1.80	-0.32
5.0°	1.92	-0.55
10.0°	1.88	-0.06

Lift coefficient (C_L)

Wind Angle	B2–1	B2–2
−10.0°	-0.83	-1.98
−5.0°	0.71	-1.77
0°	2.59	-1.34
5.0°	2.08	0.39
10.0°	1.89	0.75

Torque coefficient (C_T)

Wind Angle	B2–1	B2–2
−10.0°	2.76	-0.35
−5.0°	3.54	-0.41
0°	2.70	-0.42
5.0°	2.75	-0.08
10.0°	2.58	0.07

Testing Configuration C1

Cross-section:	WF Plate
Spacing:	14 ft
Cross-slope:	-8%
Overhangs:	No
Num. of girders	5
Instrumented girders:	1, 2, 3

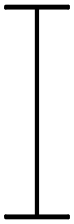

Drag coefficient (C_D)

Wind Angle	C1–1	C1–2	C1–3	C1–4	C1–5
−5.0°	1.97	-0.12	-0.40	--	--
−2.5°	1.88	-0.34	-0.25	--	--
0°	1.78	-0.47	0.12	--	--
2.5°	1.68	-0.47	0.25	--	--
5.0°	1.55	-0.42	0.39	--	--

Lift coefficient (C_L)

Wind Angle	C1–1	C1–2	C1–3	C1–4	C1–5
−5.0°	0.08	-0.06	-0.39	--	--
−2.5°	0.30	0.57	1.08	--	--
0°	0.38	0.91	1.49	--	--
2.5°	0.39	1.01	1.53	--	--
5.0°	0.45	1.31	1.50	--	--

Torque coefficient (C_T)

Wind Angle	C1–1	C1–2	C1–3	C1–4	C1–5
−5.0°	0.00	0.00	-0.03	--	--
−2.5°	-0.08	-0.09	0.01	--	--
0°	-0.12	-0.13	0.08	--	--
2.5°	-0.12	-0.13	0.09	--	--
5.0°	-0.15	-0.11	0.13	--	--

Testing Configuration C2

Cross-section:	WF Plate
Spacing:	14 ft
Cross-slope:	-8%
Overhangs:	Yes
Num. of girders	5
Instrumented girders:	1, 2, 3, 4, 5

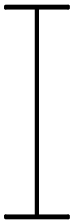

Drag coefficient (C_D)

Wind Angle	C2–1	C2–2	C2–3	C2–4	C2–5
−5.0°	2.20	-0.07	-0.30	-0.34	-0.02
−2.5°	2.12	-0.09	-0.40	-0.13	0.25
0°	2.06	-0.28	-0.30	0.28	0.40
2.5°	2.02	-0.41	-0.01	0.41	0.50
5.0°	1.95	-0.46	0.17	0.46	0.59

Lift coefficient (C_L)

Wind Angle	C2–1	C2–2	C2–3	C2–4	C2–5
−5.0°	1.44	-0.69	-1.30	-0.85	-0.11
−2.5°	1.76	0.33	0.13	0.12	0.06
0°	1.88	0.67	1.27	1.02	0.27
2.5°	1.79	0.81	1.52	1.24	0.37
5.0°	1.76	0.93	1.55	1.24	0.41

Torque coefficient (C_T)

Wind Angle	C2–1	C2–2	C2–3	C2–4	C2–5
−5.0°	0.83	0.10	-0.09	-0.10	-0.05
−2.5°	0.79	0.03	-0.04	0.03	0.05
0°	0.75	-0.09	-0.02	0.16	0.12
2.5°	0.72	-0.13	0.03	0.16	0.14
5.0°	0.69	-0.14	0.06	0.14	0.15

Testing Configuration D1

Cross-section:	45″ FIB
Spacing:	13 ft
Cross-slope:	-2%
Overhangs:	No
Num. of girders	5
Instrumented girders:	1, 2

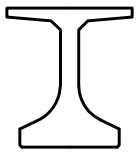

Drag coefficient (C_D)

Wind Angle	D1–1	D1–2	D1–3	D1–4	D1–5
−5.0°	1.65	-0.11	--	--	--
−2.5°	1.51	-0.23	--	--	--
0°	1.33	-0.38	--	--	--
2.5°	1.05	-0.22	--	--	--
5.0°	0.89	-0.01	--	--	--

Lift coefficient (C_L)

Wind Angle	D1–1	D1–2	D1–3	D1–4	D1–5
−5.0°	-1.09	-2.78	--	--	--
−2.5°	0.23	-1.60	--	--	--
0°	0.95	1.02	--	--	--
2.5°	1.68	2.86	--	--	--
5.0°	1.93	3.21	--	--	--

Torque coefficient (C_T)

Wind Angle	D1–1	D1–2	D1–3	D1–4	D1–5
−5.0°	1.44	-0.07	--	--	--
−2.5°	0.25	0.07	--	--	--
0°	-0.36	0.06	--	--	--
2.5°	-0.89	-0.32	--	--	--
5.0°	-1.14	-0.17	--	--	--

Testing Configuration D2

Cross-section:	45″ FIB
Spacing:	13 ft
Cross-slope:	-2%
Overhangs:	Yes
Num. of girders	5
Instrumented girders:	1, 2, 3

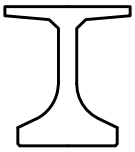

Drag coefficient (C_D)

Wind Angle	D2–1	D2–2	D2–3	D2–4	D2–5
−5.0°	1.69	-0.13	-0.18	--	--
−2.5°	1.66	-0.18	-0.20	--	--
0°	1.59	-0.28	-0.16	--	--
2.5°	1.49	-0.32	0.15	--	--
5.0°	1.41	-0.38	0.36	--	--

Lift coefficient (C_L)

Wind Angle	D2–1	D2–2	D2–3	D2–4	D2–5
−5.0°	-0.97	-2.96	-2.13	--	--
−2.5°	0.90	-2.34	-1.20	--	--
0°	2.63	-0.58	-0.16	--	--
2.5°	3.48	1.69	1.91	--	--
5.0°	3.64	2.30	2.86	--	--

Torque coefficient (C_T)

Wind Angle	D2–1	D2–2	D2–3	D2–4	D2–5
−5.0°	3.03	-0.01	-0.05	--	--
−2.5°	3.48	-0.18	-0.09	--	--
0°	2.59	0.19	-0.16	--	--
2.5°	2.27	-0.31	0.39	--	--
5.0°	2.06	-0.55	0.47	--	--

APPENDIX D
EXAMPLE CALCULATIONS:
GLOBAL PRESSURE COEFFICIENTS

This appendix contains example calculations for computing the global pressure coefficient for a multi-girder system with stay-in-place forms (discussed in Chapter 6).

Global pressure coefficient for bridge with stay-in-place (SIP) forms

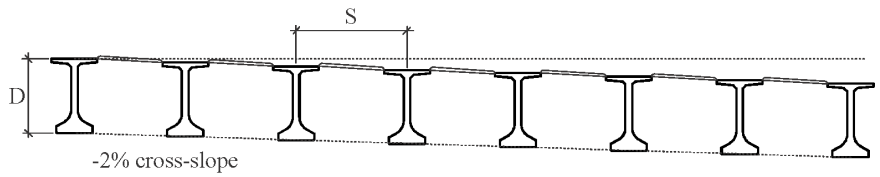

Section view

System parameters...

FIB78	... Girder type
$D := 78in$	... (in) Section depth
$n := 8$	... Number of girders
$S := 120in$	... (in) Girder spacing
$\theta_{cross\text{-}slope} := -2\%$	... (%) Girder cross-slope
$\theta_{wind} := 2.5deg$	... (deg) Assumed maximum wind angle
$L := 140ft$	... (ft) Span length

Wind parameters...

$V := 120mph$	... (mph) Wind velocity
$K_Z := 0.85$	... Velocity pressure exposure coefficient (2014 FDOT SDG, Section 2.4.1.D)
$G := 0.85$	... Gust effect factor (2014 FDOT SDG, Section 2.4.1.E)

Recommended pressure coefficient...

$C_{P,SIPF} := 1.4$	... Pressure coefficient for I-girders with SIP formwork (Table 6.4)

Calculation of global pressure coefficient...

$\theta_{max} := \lvert\theta_{wind}\rvert + \lvert\theta_{cross\text{-}slope}\rvert = 3.646 \cdot deg$	... (deg) Maximum angle between wind and cross-slope (Equation 6.14)
$\beta := 1.05 - 0.07\left(\frac{\theta_{max}}{deg}\right) = 0.795$	... Reduction factor for I-shaped girders (Equation 6.16)
$C_P := \beta \cdot C_{P,SIPF} = 1.11$	... Global pressure coefficient (Equation 6.15)
$D_{proj} := D + (n-1) \cdot S \cdot \tan(\theta_{max}) = 131.5 \cdot in$	... (in) Projected depth of bridge (Equation 6.18)
$P_Z := 2.56 \cdot 10^{-6} \frac{ksf}{mph^2} \cdot K_Z \cdot V^2 \cdot G \cdot C_P$	... (in), Design wind pressure (Equation 6.17)
$P_Z = 29.6 \cdot psf$	
$F_{substructure} := P_Z \cdot \left(\frac{L}{2}\right) \cdot (D_{proj}) = 22.7 \cdot kip$	... (kip) Unfactored wind-induced global lateral load on substructure

APPENDIX E
DETAILED REPORT FROM WIND TUNNEL TESTS

All wind tunnel testing, including model fabrication, wind load measurement, and data normalization, was performed by Boundary Layer Wind Tunnel Laboratory at the University of Western Ontario (UWO). This appendix consists of the full text of the final report from UWO detailing the tests that were performed and the results that were obtained.

Note that the UWO report is a self-contained document that uses its own terminology and naming conventions. Even fundamental terms such as *drag* and *lift* do not have the same meaning in the UWO report as they do in rest of this research report. In particular, do not use the raw data from the tables in the UWO report without reading them carefully to understand how the data should be interpreted. For a presentation of the UWO data that uses the terminology defined elsewhere in this report, see Appendix C.

Alan G. Davenport Wind Engineering Group

A Study of Wind Forces on

BRIDGE GIRDERS WITH STAY-IN-PLACE FORMWORK

Section Model Investigation

L. KONG / A. MUSA / J.P.C. KING

BLWT-SS30-2013 / OCTOBER 2013

The Boundary Layer Wind Tunnel Laboratory
The University of Western Ontario, Faculty of Engineering
London, Ontario, Canada N6A 5B9; Tel: (519) 661-3338; Fax: (519) 661-3339
Internet: www.blwtl.uwo.ca; E-mail: info@blwtl.uwo.ca

TABLE OF CONTENTS

LIST OF TABLES

LIST OF FIGURES

ACKNOWLEDGEMENTS

The study of wind forces for bridge girders while under construction was initiated by Dr. Gary R. Consolazio of the University of Florida (UF) as part of a major research project sponsored by the Florida Department of Transportation (FDOT). The study reported herein is the third component of a study of wind force measurements on typical bridge girder configurations used in the State of Florida and concentrates on the effect of stay-in-place formwork on the wind forces carried by individual girders. The assistance and continued co-operation and support of Dr. Consolazio are gratefully appreciated. The support of the Florida Department of Transportation of the umbrella UF research project is gratefully acknowledged.

Acknowledgment is also made of the contributions by various members of the technical staff of the Laboratory, particularly: Messrs. Gerry Dafoe, Anthony Burggraaff and Benjamin Brown who carried out the experimental phases of the study. The section models were constructed by members of the University Machine Shop under the direction of Mr. Ian Vinkenvleugel.

SUMMARY AND MAIN FINDINGS

This report on the study of "Wind Forces on Bridge Girders with Stay-In-Place Formwork" is an extension of previous studies performed for bridge girders while under construction. The previous reporting [1, 2], concentrated on the wind forces on individual girders within typical arrangements commonly used within the State of Florida for short to medium span highway bridges. The girder types examined were comprised of: a) wide flange plate girders, b) narrow flange plate girders, c) box girders, d) 78-inch "Florida" I-beams and e) 45-inch "Florida" I-beams. The current study addresses the condition where stay-in-place formwork bridges the gap between girders. The current report provides information from the section model testing of four of the previously studied types of bridge girders with stay-in-place formwork.

The current study examined: 1) 78-inch "Florida" I-Beams, 2) Box Girders, 3) Wide Flange Plate Girders, and 4) 45-inch "Florida" I-Beams. All tests in this study were performed on groupings of between two and ten girders with one instrumented girder placed at a specific position and the other non-instrumented dummy girders at the remaining positions. The details of the study are listed in the following table:

	78-inch "Florida" I-Beams		Box Girders		Wide Flange Plate Girders		45-inch "Florida" I-Beams	
Test Configuration	Without Overhang	With Overhang	Without Overhang	With Overhang	Without Overhang	With Overhang	Without Overhang	With Overhang
No. of Girders in Group	10	10	2	2	5	5	5	5
Instrumented Girder Position	1,2,3	1,2,3,5,10	1,2	1,2	1,2,3	1,2,3,4,5	1,2	1,2,3

The aim of this study was to evaluate the static force coefficients for each girder within the configuration for each of the four types of bridge girders.

The existing section models of the bridge girders were constructed at two geometric scales relative to the prototype dimensions in order to facilitate model construction and are as follows:

a) 1:25 scale for the box girders and wide flange plate girders;
b) 1:28 scale for the 78-inch and 45-inch "Florida" I-beams.

All tests were performed in smooth flow with turbulence intensities of less than 0.5%. The highlights and main findings of this study are as follows:

- The drag coefficients of the instrumented windward girder for each of the four girder types are larger with the deck overhang present. The drag coefficients with and without the overhang at 0^{o} and negative angles of attack are similar for the windward girder, while the difference in drag at positive angles of attack becomes much larger. The effect of the overhang on the drag coefficient is not as significant for the interior girders, due to the shielding effect from the upstream girders.

- The lift coefficients are generally much larger with the overhang for the windward girder.

- The attachment methodology employed to secure the formwork to the individual girders allowed for full moment transfer from the formwork to the girders. Should the formwork attachment permit only vertical shear transfer, then the torsional force effects on the girders will be minimal. Negative torque slopes are observed for the windward girder in most tests with and without the overhang present. The small torque coefficient at large positive angles of attack is as a result of the higher suction on the upper surface of the formwork. The torque coefficients of the instrumented windward girder are much larger with the overhang. The effect of the overhang on the torque coefficients of the interior girders is small.

DETAILS OF THE STUDY

Project Name:	Wind Forces on Bridge Girders With Stay-in-Place Formwork.
Project Location:	Florida.
Project Description:	The project is Phase 3 of an extension of previous projects performed by the Laboratory and reported in [1, 2]. This study is a critical component of a larger project with the Florida Department of Transportation (FDOT). The proper bracing of bridge girders for extreme wind during the construction process is the primary focus of this study. The critical component, as part of the FDOT Project, is an accurate quantification of wind loads on the girders during construction. This includes the windward girder, leeward girder and interior girders, including the influence of cross-slope and spacing. Previous studies have focused on the wind forces on bare girders while under construction. The current study addresses the condition where stay-in-place formwork bridges the gap between girders. Four different girder types have been selected for this investigation in groups of two girders to ten girders, with different spacing and cross slopes.
Test Dates:	Static Section Model Tests – September and October 2013
Preliminary Reporting:	Static Force Coefficients – September and October 2013
Report Scope:	The report is organized as follows: Section 1 – Introduction Section 2 – Section Model Study - Static Tests
General Reference:	Discussion and details of the general methodology used by the Alan G Davenport Wind Engineering Group can be found in “Wind Tunnel Testing – A General Outline” [Reference 3].

1 INTRODUCTION

1.1 General

The wind tunnel study of "Wind Forces on Bridge Girders With Stay-in-Place Formwork" is the Phase 3 study of an extension of a project previously performed at the Boundary Layer Wind Tunnel Laboratory, which has been reported in [1, 2]. This study is a critical component of a larger project with the Florida Department of Transportation (FDOT). The proper bracing of bridge girders for extreme wind during the construction process is the primary focus of the investigation. As a critical component of the FDOT Project, a primary focus of the current wind study is to have an accurate quantification of wind loads on typical types of girders during construction. This includes the windward girder and leeward girder as well as the interior girders, including the influence of cross-slope and spacing. Previous studies in [1, 2] performed by the Laboratory have focused on the wind forces on bare girders while under construction. The current study addresses the condition where stay-in-place formwork bridges the gap between girders. Four different girder types have been selected for this Phase 3 investigation, as described in Table 1.1.

In general, the drag force on an object is dependent upon the pressure on the windward face and the wind-induced suction on the leeward face of the object. The after-body length of an object is an important aerodynamic parameter which contributes to the lateral forces due to wind. In the case of a girder bridge while under construction, this after-body length is formed by the presence of downwind girders and is further enhanced through formwork at the upper surface. The lift and torsional forces are a consequence of pressure differences between the upper and lower surfaces of the formwork and are significant due to the relatively large lifting surface. In order to develop representative wind force coefficients which may be applied to multiple girder assemblies, a comprehensive test program in which measurements of the wind force on different girder types within an assembly of bridge girders in the presence of stay-in-place formwork was conducted. The configurations studied included girder assembles with and without deck (i.e. formwork) overhangs.

All tests in this study were performed on groupings of between two and ten girders with one instrumented girder placed at a specific position within the grouping. Non-instrumented girders completed the grouping of girders. The test details, including the test number, test conditions, test sequences, location of the instrumented girder and their corresponding file names, are given in Tables 1.2 to 1.5 and summarized below:

a) 78-inch "Florida" I-beam (Table 1.2): Comprised of a grouping of ten girders with the instrumented girder at five different positions from windward to the leeward position; girders spacing 13 ft.; cross slope -2%, test angles 0^o, $\pm 2.5^o$ and $\pm 5^o$, included 3 tests without deck overhangs and 5 tests with deck overhangs,
b) Box Girder (Table 1.3): Comprised of a grouping of two girders with the instrumented girder at the windward and leeward positions; girders spaced 22 ft.; cross slopes 0%; test angles 0^o, $\pm 5^o$ and $\pm 10^o$, included 2 tests without deck overhangs and 2 tests with deck overhangs,
c) Wide Flange Plate Girder (Table 1.4): Comprised of a grouping of five girders with the instrumented girder at five different positions from windward to the leeward position; girders spaced 14 ft.; cross slopes -8%; test angles 0^o, $\pm 2.5^o$ and $\pm 5^o$, included 3 tests without deck overhangs and 5 tests with deck overhangs
d) 45-inch "Florida" I-beam (Table 1.5): Comprised of a grouping of five girders with the instrumented girder at three different positions including windward and interior positions; girders spaced 13 ft.; cross slopes -2%; test angles 0^o, $\pm 2.5^o$ and $\pm 5^o$, included 2 tests without deck overhangs and 3 tests with deck overhangs

Rigid section models of the four girder cross sections (7 ft. in length) were made available from previous studies. The models were constructed at two geometric scales relative to prototype to facilitate model fabrication:

a) 1:25 scale for the box girders and wide flange plate girders
b) 1:28 scale for the 78-inch and 45-inch "Florida" I-beams

The 7 ft. long section models correspond to 175 ft. and 196 ft. long sections of the prototype girders at the geometric scales of 1 to 25 and 1 to 28, respectively. The length of model was chosen such that the lateral correlation effects of the wind are modeled properly and not to reflect any specific prototype girder length. Cross section details of the four girder types are given in Figures 1.1 to 1.4. Test configurations including girder arrangements, test number designations and test conditions are given schematically in Figures 1.5 to 1.8.

The modeling of the stay-in-place formwork presented several challenges. The prototype formwork spans between girder flanges and therefore the upper profile of the girder assemblies includes flat, horizontal portions over the girder flanges and a sloped portion between flanges. In the prototype, the formwork is a simply supported plate along the girder flanges and is therefore not continuous over each girder. It was impossible to provide this condition, while only measuring the force due to ½ of the span of formwork on each side of the girder; therefore, a compromise was developed to satisfy the primary goal of accurate drag force measurements, while minimizing the errors on the lift and torsional forces.

The primary objective of the measurements was to include the force generated by the pressures / suctions on the formwork as seen by the individual girders. The requirement of isolating the instrumented girder (and attached formwork) from the neighboring girders was achieved as follows:

- The formwork was constructed as discrete bent plates from the midpoint of the gap between girders to the midpoint of the adjacent gap. This allowed each girder to be isolated from neighboring girders, if required. Adjacent formwork plates for non-instrumented girders could be fully sealed / connected by adhesive tape to achieve the proper flow conditions.

- Each bent plate was secured to the top flange of each girder, resulting in the capturing of the forces on the plate (formwork) over either a full or half girder spacing, depending on whether an overhang was present.

- Loose-fitting, thin cellophane strips were adhered to cantilevered formwork sections, sealing the gap from air leakage, yet isolating the instrumented girder from the transfer of drag force to the adjacent non-instrumented girder and vice-versa. Lift force on the formwork is transferred directly to the instrumented girder with minimal impact of the cellophane strips, assuming the strips were not fully tensioned due to differential movements of adjacent girders.

- The method of attachment of the formwork to the top flange of the instrumented girder resulted in a full moment transfer between the formwork and girder top flange, which may not be present in the prototype girders. Therefore, caution should be exercised in the interpretation of torsional forces given in this report.

The section model study was performed at the inlet to the High Speed Test Section of the Boundary Layer Wind Tunnel II. Tests of the section models were performed in smooth, uniform flow conditions to evaluate the static forces on these sections. Figure 1.9 shows a sample set-up of the section model in the wind tunnel, while Figure 1.10 presents a close-up view of the static section model test rig.

Views of the model arrangements (with and without deck overhangs) and corresponding wind tunnel set-up (with the instrumented girder at different positions) are given in Figures 1.11 to 1.13 for the 78-inch “Florida” I-beams, in Figures 1.14 to 1.16 for the box girders, in Figures 1.17 to 1.19 for the Wide Flange Girders and in Figures 1.20 to 1.22 for the 45-inch “Florida” I-beams, respectively.

2 SECTION MODEL STUDY - STATIC TESTS

2.1 General

The section models were mounted on the BLWTL Bridge 3-component section model force balance, which is capable of measuring the total forces on the sections (X and Z body forces as well as the torque). The centers of measurement of the forces for the wide flange plate girders and both the 78-inch and 45-inch Florida I-beams are all at the mid-heights of the sections (as opposed to the centroid of the section), while the center of measurement for the box girder is at 2.46 ft. above the bottom plate.

The test rig was modified to permit the positioning of one instrumented girder in any desired position in a grouping of up to ten girders, with the remaining girders positioned either upwind or downwind of the instrumented girder. The test rig also permitted variable girder spacing and vertical offset to enable the simulation of any desired girder spacing and cross-slope.

Tests were performed adjusting the model inclination relative to the mean wind flow. The apparatus which rotates the test model also rotates the "dummy" model(s) situated either upwind or downwind of the instrumented model girder. Lift and D rag were calculated from the measured X and Z body force components. The sign conventions for the definition of the force coefficients for each of the four girder types are given in Figures 2.1 to 2.4 respectively.

A typical force coefficient is defined as follows:

$$C_{x,z,l,d} = \frac{F_{x,z,l,d}}{qD} \qquad (2.1)$$

in which: C is an aerodynamic coefficient,
F is the mean aerodynamic force per unit length,
$q = \frac{1}{2}\rho V^2$ is the mean wind velocity pressure,
ρ is the density of air (taken as 0.00238 slug/ft^3),
V is the mean wind velocity in ft/s, and
D is the overall depth of the section, see Table 2.1.

The subscripts *x,z,l,d* refer to the X and Z body force components and lift and drag respectively. It is important to note that C_x, C_z and C_m are "Body-Force Coefficients" and not aligned with the axis of the wind (i.e. as a "drag" coefficient) nor perpendicular to the wind (i.e. as a "lift" coefficient).

The torque coefficient is defined:

$$C_m = \frac{F_t}{qD^2} \qquad (2.2)$$

in which: F_t is the mean aerodynamic torque per unit length.

All tests were carried out in smooth flow (I_u< 0.5%) for angles of mean vertical inclination between -5 and +5 degrees in increments of 2.5 degrees for the 78-inch and 45-inch Florida I-beams as well as the wide flange plate girders, and between -10 to +10 degrees in increments of 5 degrees for the box girders.

2.2 Test Results

The static aerodynamic coefficients from the tests of the section models are summarized in the following tables:

1) Table 2.2 for the 78-inch "Florida" I-beams (cross slope of -2%);

2) Table 2.3 for the Box Girders (cross slope of 0%);

3) Table 2.4 for the Wide Flange Plate Girders (cross slope of -8%);

4) Table 2.5 for the 45-inch "Florida" I-beams (cross slope of -2%).

The corresponding summary plots of force coefficient vs. angle of attack are shown in the following figures:

1) Figures 2.5 and 2.6 for the 78-inch "Florida" I-beams without deck overhang and with a cross slope of -2%;

2) Figures 2.7 and 2.8 for the 78-inch "Florida" I-beams with deck overhang and with a cross slope of -2%;

3) Figures 2.9 and 2.10 for the Box Girders without deck overhang and with a cross slope of 0%;

4) Figures 2.11 and 2.12 for the Box Girders with deck overhang and with a cross slope of 0%;

5) Figures 2.13 and 2.14 for the Wide Flange Plate Girders without deck overhang and with a cross slope of -8%;

6) Figures 2.15 and 2.16 for the Wide Flange Plate Girders with deck overhang and with a cross slope of -8%;

7) Figures 2.17 and 2.18 for the 45-inch "Florida" I-beams without deck overhang and with a cross slope of -2%;

8) Figures 2.19 and 2.20 for the 45-inch "Florida" I-beams with deck overhang and with a cross slope of -2%.

The force coefficients are normalized by the section depth of the corresponding girder given in Table 2.1, in order to facilitate comparisons with published results of similar girder cross sections. The thickness of the plate (formwork) was considered to be negligible compared to the girder depth and therefore not included in this calculation.

The wind tunnel test wind speeds and corresponding Reynolds numbers for the four girder types tested are summarized in Table 2.6. Reynolds number is calculated based upon the test wind speed at girder height and the model girder depth.

A summary of the main results of the static section model tests is as follows:

- The drag coefficients of the instrumented windward girder for each of the four girder types are larger with the deck overhang present. The drag coefficients with and without the overhang at 0^o and negative angles of attack are similar for the windward girder, while the difference in drag at positive angles of attack becomes much larger. The effect of the overhang on the drag coefficient is not as significant for the interior girders, due to the shielding effect from the upstream girders.

- The lift coefficients are generally much larger with the overhang for the windward girder.

- The general trend of the lift coefficient vs. angle of attack with and without the overhang is similar for each of the four types of girders studied. Note that for some tested configurations, negative lift slopes are observed with the instrumented girder at the windward position.

- Negative torque slopes are observed for the windward girder in most tests either with or without the overhang present. The small torque coefficient at large positive angles of attack is as a result of the higher suction on the upper surface of the formwork. The torque coefficients of the instrumented windward girder are much larger with the overhang. The effect of the overhang on the torque coefficients of the interior girders is small.

- The attachment methodology employed to secure the formwork to the individual girders allowed for full moment transfer from the formwork to the girders. Should the prototype formwork attachment permit only vertical shear transfer, then the torsional force effects on the girders are likely to be minimal. Caution should therefore be exercised when considering the torsional data presented in this report.

- Since all sections tested have sharp edged corners, it is expected that the effects of Reynolds number on the force coefficients are minimal and that the force coefficients are applicable over a broad range of wind speeds. The "Reynolds number" is the ratio of the inertial force to viscous force of the fluid (i.e. air) and is computed as $\mathrm{Re} = VD/\gamma$, where V is the mean wind speed in ft/s, D is the overall section model depth in ft. as given in Table 2.1 and γ is the kinematic viscosity of air (1.615×10^{-4} ft^2/s). Tests were performed a two different wind speeds to verify that the coefficients were invariable with Reynolds number. The test wind speeds and corresponding Reynolds numbers are listed in Table 2.6.

2.3 Translation of Force Coefficients to the Section Centroid

The static force coefficients given in Section 2.2, which are referenced to the mid-height of the sections for the Florida I-beams, can be transformed to their centroid locations through a simple transformation of coordinates.

Figure 2.21 shows an example of the sign convention used in the transformation. Note that *o* is the mid-height location of the section and *o′* is the centroid. Assuming *h* is the distance between the mid-height and the centroid of the section, the body force coefficients to the centroid can be obtained as:

$$\begin{aligned} C_X^{'} &= C_X \\ C_Z^{'} &= C_Z \\ C_m^{'} &= C_m + C_X \times \frac{h}{D} \end{aligned} \tag{2.3}$$

The drag and lift coefficients relative to the centroid of the section are then calculated as:

$$\begin{aligned} C_D^{'} &= C_X^{'} \cos\alpha + C_Z^{'} \sin\alpha \\ C_L^{'} &= -C_X^{'} \sin\alpha + C_Z^{'} \cos\alpha \end{aligned} \tag{2.4}$$

REFERENCES

1. Kong, L. and King, J.P.C., “A Study of Wind Forces on Bridge Girders While Under Construction – Section Model Investigation”, The University of Western Ontario, Faculty of Engineering Research Report, BLWT-SS29-2011, London, Ontario, Canada 2011.
2. Kong, L. and King, J.P.C., “A Study of Wind Forces on Bridge Girders While Under Construction – Section Model Investigation”, The University of Western Ontario, Faculty of Engineering Research Report, BLWT-SS19-2012, London, Ontario, Canada 2012.
3. "Wind Tunnel Testing: A General Outline", The Boundary Layer Wind Tunnel Laboratory, The University of Western Ontario, May 2007.

TABLES

TABLE 1.1 SUMMARY OF STATIC SECTION MODEL TESTS

GIRDER TYPE AND CONFIGURATION		Spacing between Girders	Instrumented Girder Position	Cross-Slope	No. of Tests	Test Angles
A1) 78 inch "Florida" I-Beam	Ten Girders without deck overhangs	13 ft	1,2,3	-2%	3	0^o,$\pm2.5^o$, $\pm5^o$
A2) 78 inch "Florida" I-Beam	Ten Girders with deck overhangs	13 ft	1,2,3,5,10	-2%	5	0^o, $\pm2.5^o$, $\pm5^o$
B1) Box Girder	Two Girders without deck overhangs	22 ft	1,2	0%	2	0^o, $\pm5^o$, $\pm10^o$
B2) Box Girder	Two Girders with deck overhangs	22 ft	1,2	0%	2	0^o, $\pm5^o$, $\pm10^o$
C1) Wide Flange Plate Girder	Five Girders without deck overhangs	14 ft	1,2,3	-8%	3	0^o, $\pm2.5^o$, $\pm5^o$
C2) Wide Flange Plate Girder	Five Girders with deck overhangs	14 ft	1,2,3,4,5	-8%	5	0^o,$\pm2.5^o$, $\pm5^o$
D1) 45 inch "Florida" I-Beam	Five Girders without deck overhangs	13 ft	1,2	-2%	2	0^o,$\pm2.5^o$, $\pm5^o$
D2) 45 inch "Florida" I-Beam	Five Girders with deck overhangs	13 ft	1,2,3	-2%	3	0^o,$\pm2.5^o$, $\pm5^o$

TABLE 1.2 78-INCH "FLORIDA" I-BEAMS – TEST CONDITIONS

A) 78-INCH "FLORIDA" I-BEAMS		Spacing between Girders	Girder Tested	Cross-Slope	Test Sequence	File Name
A1 Without Overhang	Ten Girders	13 ft	1	-2%	1	F055a1E01R001 ~ F055a1E01R005
	Ten Girders	13 ft	2	-2%	4	F055a1E01R006 ~ F055a1E01R011
	Ten Girders	13 ft	3	-2%	6	F055a1E01R012 ~ F055a1E01R016
A2 With Overhang	Ten Girders	13 ft	1	-2%	2	F055a2E01R001 ~ F055a2E01R005
	Ten Girders	13 ft	2	-2%	3	F055a2E01R006 ~ F055a2E01R010
	Ten Girders	13 ft	3	-2%	5	F055a2E01R011 ~ F055a2E01R015
	Ten Girders	13 ft	5	-2%	7	F055a2E01R016 ~ F055a2E01R020
	Ten Girders	13 ft	10	-2%	8	F055a2E01R001 ~ F055a2E01R005

Angles of Attack：0^o, $\pm 2.5^o$, $\pm 5^o$: Smooth Flow, 1:28 Scale

TABLE 1.3 BOX GIRDER – TEST CONDITIONS

B) BOX GIRDER		Spacing between Girders	Girder Tested	Cross-Slope	Test Sequence	File Name
B1 Without Overhang	Two Girders	22 ft	1	0%	4	F055b1E01R006 ~ F055b1E01R010
	Two Girders	22 ft	2	0%	1	F055b1E01R001 ~ F055b1E01R005
B2 With Overhang	Two Girders	22 ft	1	0%	3	F055b2E01R006 ~ F055b2E01R010
	Two Girders	22 ft	2	0%	2	F055b2E01R001 ~ F055b2E01R005

Angles of Attack：0^o, $\pm5^o$, $\pm10^o$: Smooth Flow, 1:25 Scale

TABLE 1.4 WIDE FLANGE PLATE GIRDER – TEST CONDITIONS

C) WIDE FLANGE PLATE GIRDER		Spacing between Girders	Girder Tested	Cross-Slope	Test Sequence	File Name
C1 Without Overhang	Five Girders	14 ft	1	-8%	1	F055c1E01R010 ~ F055c1E01R014
	Five Girders	14 ft	2	-8%	4	F055c1E01R015 ~ F055c1E01R019
	Five Girders	14 ft	3	-8%	5	F055c1E01R020 ~ F055c1E01R024
C2 With Overhang	Five Girders	14 ft	1	-8%	2	F055c2E01R001 ~ F055c2E01R005
	Five Girders	14 ft	2	-8%	3	F055c2E01R008 ~ F055c2E01R012
	Five Girders	14 ft	3	-8%	6	F055c2E01R013 ~ F055c2E01R017
	Five Girders	14 ft	4	-8%	7	F055c2E01R018 ~ F055c2E01R022
	Five Girders	14 ft	5	-8%	8	F055c2E01R023 ~ F055c2E01R027

Angles of Attack：0^o, $\pm 2.5^o$, $\pm 5^o$: Smooth Flow, 1:25 Scale

TABLE 1.5 45-INCH "FLORIDA" I-BEAM – TEST CONDITIONS

D) 45-INCH "FLORIDA" I-BEAM		Spacing between Girders	Girder Tested	Cross-Slope	Test Sequence	File Name
D1 Without Overhang	Five Girders	13 ft	1	-2%	2	F055d1E01R036 ~ F055d1E01R040
	Five Girders	13 ft	2	-2%	4	F055d1E01R046 ~ F055d1E01R050
D2 With Overhang	Five Girders	13 ft	1	-2%	1	F055d2E01R021 ~ F055d2E01R025
	Five Girders	13 ft	2	-2%	3	F055d2E01R026 ~ F055d2E01R030
	Five Girders	13 ft	3	-2%	5	F055d2E01R031 ~ F055d2E01R035

Angles of Attack：0^o, $\pm 2.5^o$, $\pm 5^o$: Smooth Flow, 1:28 Scale

TABLE 2.1 OVERALL DEPTHS OF PROTOTYPE GIRDERS

PROTOTYPE CONFIGURATION	PROTOTYPE OVERALL DEPTH* (ft)	MODEL SCALE
A) 78-inch “Florida” I-Beam	6+6/12 = 6.5	1:28
B) Box Girder	6+(3/4)/12+(1/2)/12 = 6.104	1:25
C) Wide Flange Plate Girder	8+1/12+1/12 = 8.167	1:25
D) 45-inch “Florida” I-Beam	3+9/12 = 3.75	1:28

* Overall depth of the corresponding girder was used for normalization to obtain the force coefficients. The thickness of the deck plate (i.e. the stay-in-place formwork) is not included in the calculation.

TABLE 2.2 STATIC FORCE COEFFICIENTS:- 78-INCH "FLORIDA" I-BEAM, 13FT SPACING, -2% CROSS SLOPE, SMOOTH FLOW

			Angle of Attack (deg)	-5	-2.5	0	2.5	5
Without Overhang	F055a1E01 R005 ~ R010	78-in I-beam, -2% slope, 10 I-beams, 13ft spacing, first	Cx (X Body Force)	1.86	1.66	1.47	1.14	0.90
			Cz (Z Body Force)	-0.34	0.23	0.69	1.20	1.44
			Ct (Torque)	0.31	0.02	-0.18	-0.42	-0.53
			Cd (Drag)	1.88	1.65	1.47	1.19	1.02
			Cl (Lift)	-0.18	0.30	0.69	1.15	1.35
	F055a1E01 R006 ~ R011	78-in I-beam, -2% slope, 10 I-beams, 13ft spacing, second	Cx (X Body Force)	-0.02	-0.10	-0.42	-0.52	-0.31
			Cz (Z Body Force)	-1.96	-0.28	1.07	2.12	2.69
			Ct (Torque)	0.10	0.15	-0.15	-0.20	-0.18
			Cd (Drag)	0.15	-0.09	-0.42	-0.43	-0.08
			Cl (Lift)	-1.96	-0.28	1.07	2.14	2.70
	F055a1E01 R012 ~ R016	78-in I-beam, -2% slope, 10 I-beams, 13ft spacing, third	Cx (X Body Force)	-0.13	-0.32	-0.17	0.08	0.09
			Cz (Z Body Force)	-1.91	-0.68	1.53	2.50	2.70
			Ct (Torque)	-0.05	-0.05	0.00	-0.02	-0.05
			Cd (Drag)	0.04	-0.29	-0.17	0.19	0.32
			Cl (Lift)	-1.92	-0.69	1.53	2.49	2.68
With Overhang	F055a2E01 R001 ~ R005	78-in I-beam, -2% slope, 10 I-beams, 13ft spacing, first	Cx (X Body Force)	1.90	1.76	1.61	1.43	1.25
			Cz (Z Body Force)	0.14	1.47	2.07	2.64	2.85
			Ct (Torque)	1.37	1.01	0.89	0.74	0.60
			Cd (Drag)	1.88	1.70	1.61	1.55	1.49
			Cl (Lift)	0.30	1.55	2.07	2.57	2.73
	F055a2E01 R006 ~ R010	78-in I-beam, -2% slope, 10 I-beams, 13ft spacing, second	Cx (X Body Force)	0.01	-0.05	-0.11	-0.46	-0.53
			Cz (Z Body Force)	-2.16	-0.90	0.56	1.59	2.05
			Ct (Torque)	0.01	0.18	0.00	-0.23	-0.25
			Cd (Drag)	0.20	-0.01	-0.11	-0.39	-0.35
			Cl (Lift)	-2.15	-0.90	0.56	1.61	2.09
	F055a2E01 R011 ~ R015	78-in I-beam, -2% slope, 10 I-beams, 13ft spacing, third	Cx (X Body Force)	-0.10	-0.20	-0.42	-0.12	0.06
			Cz (Z Body Force)	-1.95	-1.10	1.03	2.48	2.75
			Ct (Torque)	-0.03	-0.04	-0.09	-0.07	-0.03
			Cd (Drag)	0.07	-0.15	-0.42	-0.01	0.30
			Cl (Lift)	-1.95	-1.10	1.03	2.48	2.74
	F055a2E01 R016 ~ R020	78-in I-beam, -2% slope, 10 I-beams, 13ft spacing, fifth	Cx (X Body Force)	-0.18	-0.10	0.06	0.03	0.01
			Cz (Z Body Force)	-1.18	-0.05	0.62	1.50	2.41
			Ct (Torque)	-0.03	0.08	0.09	0.05	-0.04
			Cd (Drag)	-0.08	-0.10	0.06	0.09	0.22
			Cl (Lift)	-1.19	-0.05	0.62	1.50	2.40
	F055a2E01 R023 ~ R027	78-in I-beam, -2% slope, 10 I-beams, 13ft spacing, tenth	Cx (X Body Force)	0.16	0.21	0.27	0.34	0.46
			Cz (Z Body Force)	-0.06	0.04	0.04	0.02	0.24
			Ct (Torque)	0.10	0.13	0.13	0.11	0.14
			Cd (Drag)	0.16	0.20	0.27	0.34	0.47
			Cl (Lift)	-0.04	0.05	0.04	0.01	0.20

TABLE 2.3 STATIC FORCE COEFFICIENTS:- BOX GIRDER, 22FT SPACING, 0% CROSS SLOPE, SMOOTH FLOW

			Angle of Attack (deg)	-10	-5	0	5	10
Without Overhang	F055b1E01 R006 ~ R010	Box, 0% slope, 2 girders, 22ft spacing, first	Cx (X Body Force)	1.68	1.74	1.71	1.67	1.55
			Cz (Z Body Force)	-0.98	0.01	1.04	1.19	1.16
			Ct (Torque)	1.88	1.61	0.70	0.58	0.45
			Cd (Drag)	1.82	1.74	1.71	1.77	1.73
			Cl (Lift)	-0.67	0.16	1.04	1.04	0.87
	F055b1E01 R001 ~ R005	Box, 0% slope, 2 girders, 22ft spacing, second	Cx (X Body Force)	-0.05	-0.20	-0.52	-0.28	0.22
			Cz (Z Body Force)	-1.34	-1.54	-0.97	0.88	0.97
			Ct (Torque)	-0.71	-0.97	-0.61	0.28	0.37
			Cd (Drag)	0.18	-0.06	-0.52	-0.20	0.38
			Cl (Lift)	-1.33	-1.55	-0.97	0.90	0.92
With Overhang	F055b2E01 R006 ~ R010	Box, 0% slope, 2 girders, 22ft spacing, first	Cx (X Body Force)	1.73	1.80	1.80	1.92	1.88
			Cz (Z Body Force)	-0.83	0.71	2.59	2.08	1.89
			Ct (Torque)	2.81	3.60	2.76	2.81	2.64
			Cd (Drag)	1.85	1.73	1.80	2.09	2.18
			Cl (Lift)	-0.52	0.86	2.59	1.90	1.53
	F055b2E01 R001 ~ R005	Box, 0% slope, 2 girders, 22ft spacing, second	Cx (X Body Force)	-0.01	-0.08	-0.32	-0.55	-0.06
			Cz (Z Body Force)	-1.98	-1.77	-1.34	0.39	0.75
			Ct (Torque)	-0.35	-0.41	-0.43	-0.09	0.07
			Cd (Drag)	0.33	0.07	-0.32	-0.51	0.08
			Cl (Lift)	-1.95	-1.77	-1.34	0.44	0.75

TABLE 2.4 STATIC FORCE COEFFICIENTS:- WIDE FLANGE PLATE GIRDER, 14FT SPACING, -8% CROSS SLOPE, SMOOTH FLOW

			Angle of Attack (deg)	-5	-2.5	0	2.5	5
Without Overhang	F055c1E01 R010 ~ R014	Wide, -8% slope, 5 girders, 14ft spacing, first	Cx (X Body Force)	1.97	1.88	1.78	1.68	1.55
			Cz (Z Body Force)	0.08	0.30	0.38	0.39	0.45
			Ct (Torque)	0.00	-0.08	-0.12	-0.12	-0.15
			Cd (Drag)	1.96	1.86	1.78	1.70	1.59
			Cl (Lift)	0.25	0.38	0.38	0.31	0.31
	F055c1E01 R015 ~ R019	Wide, -8% slope, 5 girders, 14ft spacing, second	Cx (X Body Force)	-0.12	-0.34	-0.47	-0.47	-0.42
			Cz (Z Body Force)	-0.06	0.57	0.91	1.01	1.31
			Ct (Torque)	0.00	-0.09	-0.13	-0.13	-0.11
			Cd (Drag)	-0.11	-0.37	-0.47	-0.43	-0.31
			Cl (Lift)	-0.07	0.56	0.91	1.03	1.35
	F055c1E01 R020 ~ R024	Wide, -8% slope, 5 girders, 14ft spacing, third	Cx (X Body Force)	-0.40	-0.25	0.12	0.25	0.39
			Cz (Z Body Force)	-0.39	1.08	1.49	1.53	1.50
			Ct (Torque)	-0.03	0.01	0.08	0.09	0.13
			Cd (Drag)	-0.37	-0.30	0.12	0.32	0.52
			Cl (Lift)	-0.42	1.06	1.49	1.51	1.46
With Overhang	F055c2E01 R001 ~ R005	Wide, -8% slope, 5 girders, 14ft spacing, first	Cx (X Body Force)	2.20	2.12	2.06	2.02	1.95
			Cz (Z Body Force)	1.44	1.76	1.88	1.79	1.76
			Ct (Torque)	0.83	0.79	0.75	0.72	0.69
			Cd (Drag)	2.07	2.04	2.06	2.10	2.09
			Cl (Lift)	1.63	1.85	1.88	1.70	1.59
	F055c2E01 R008 ~ R012	Wide, -8% slope, 5 girders, 14ft spacing, second	Cx (X Body Force)	-0.07	-0.09	-0.28	-0.41	-0.46
			Cz (Z Body Force)	-0.69	0.33	0.67	0.81	0.93
			Ct (Torque)	0.10	0.03	-0.09	-0.13	-0.14
			Cd (Drag)	-0.01	-0.10	-0.28	-0.37	-0.38
			Cl (Lift)	-0.69	0.32	0.67	0.83	0.97
	F055c2E01 R013 ~ R017	Wide, -8% slope, 5 girders, 14ft spacing, third	Cx (X Body Force)	-0.30	-0.40	-0.30	-0.01	0.17
			Cz (Z Body Force)	-1.30	0.13	1.27	1.52	1.55
			Ct (Torque)	-0.09	-0.04	-0.02	0.03	0.06
			Cd (Drag)	-0.18	-0.41	-0.30	0.05	0.30
			Cl (Lift)	-1.32	0.11	1.27	1.52	1.53
	F055c2E01 R018 ~ R022	Wide, -8% slope, 5 girders, 14ft spacing, fourth	Cx (X Body Force)	-0.34	-0.13	0.28	0.41	0.46
			Cz (Z Body Force)	-0.85	0.12	1.02	1.24	1.24
			Ct (Torque)	-0.10	0.03	0.16	0.16	0.14
			Cd (Drag)	-0.26	-0.14	0.28	0.46	0.57
			Cl (Lift)	-0.88	0.11	1.02	1.22	1.20
	F055c2E01 R023 ~ R027	Wide, -8% slope, 5 girders, 14ft spacing, fifth	Cx (X Body Force)	-0.02	0.25	0.40	0.50	0.59
			Cz (Z Body Force)	-0.11	0.06	0.27	0.37	0.41
			Ct (Torque)	-0.05	0.05	0.12	0.14	0.15
			Cd (Drag)	-0.01	0.24	0.40	0.51	0.63
			Cl (Lift)	-0.11	0.08	0.27	0.34	0.36

TABLE 2.5 STATIC FORCE COEFFICIENTS:- 45-INCH "FLORIDA" I-BEAM, 13FT SPACING, -2% CROSS SLOPE, SMOOTH FLOW

			Angle of Attack (deg)	-5	-2.5	0	2.5	5
Without Overhang	F055d1E01 R036 ~ R040	45" Florida girders, -2% slope, 5 girders, 13ft spacing, First Girder	Cx (X Body Force)	1.65	1.51	1.33	1.05	0.89
			Cz (Z Body Force)	-1.09	0.23	0.95	1.68	1.93
			Ct (Torque)	1.36	0.17	-0.42	-0.94	-1.19
			Cd (Drag)	1.74	1.50	1.33	1.12	1.05
			Cl (Lift)	-0.94	0.30	0.95	1.63	1.85
	F055d2E01 R041 ~ R045	45" Florida girders, -2% slope, 5 girders, 13ft spacing, Second Girder	Cx (X Body Force)	-0.11	-0.23	-0.38	-0.22	-0.01
			Cz (Z Body Force)	-2.78	-1.60	1.02	2.86	3.21
			Ct (Torque)	-0.06	0.08	0.08	-0.31	-0.17
			Cd (Drag)	0.13	-0.16	-0.38	-0.09	0.27
			Cl (Lift)	-2.78	-1.60	1.02	2.87	3.20
With Overhang	F055d2E01 R021 ~ R025	45" Florida girders, -2% slope, 5 girders, 13ft spacing, First Girder	Cx (X Body Force)	1.69	1.66	1.59	1.49	1.41
			Cz (Z Body Force)	-0.97	0.90	2.63	3.48	3.64
			Ct (Torque)	2.94	3.40	2.51	2.20	1.99
			Cd (Drag)	1.77	1.62	1.59	1.64	1.73
			Cl (Lift)	-0.82	0.97	2.63	3.41	3.50
	F055d2E01 R026 ~ R030	45" Florida girders, -2% slope, 5 girders, 13ft spacing, Second Girder	Cx (X Body Force)	-0.13	-0.18	-0.28	-0.32	-0.38
			Cz (Z Body Force)	-2.96	-2.34	-0.58	1.69	2.30
			Ct (Torque)	-0.01	-0.17	0.21	-0.29	-0.53
			Cd (Drag)	0.13	-0.08	-0.28	-0.25	-0.18
			Cl (Lift)	-2.96	-2.35	-0.58	1.70	2.33
	F055d2E01 R031 ~ R035	45" Florida girders, -2% slope, 5 girders, 13ft spacing, Third Girder	Cx (X Body Force)	-0.18	-0.20	-0.16	0.15	0.36
			Cz (Z Body Force)	-2.13	-1.20	-0.16	1.91	2.86
			Ct (Torque)	-0.04	-0.08	-0.15	0.38	0.46
			Cd (Drag)	0.01	-0.14	-0.16	0.23	0.61
			Cl (Lift)	-2.14	-1.21	-0.16	1.90	2.82

TABLE 2.6 TEST WIND SPEED (MAXIMUM) AND CORRESPONDING REYNOLDS NUMBER

PROTOTYPE CONFIGURATION	TEST WIND SPEED (ft/s)	REYNOLDS NUMBER
A) 78-inch “Florida” I-Beam	37.4	56000
B) Box Girder	37.1	58000
C) Wide Flange Plate Girder	37.0	77000
D) 45-inch “Florida” I-Beam	37.7	33000

FIGURES

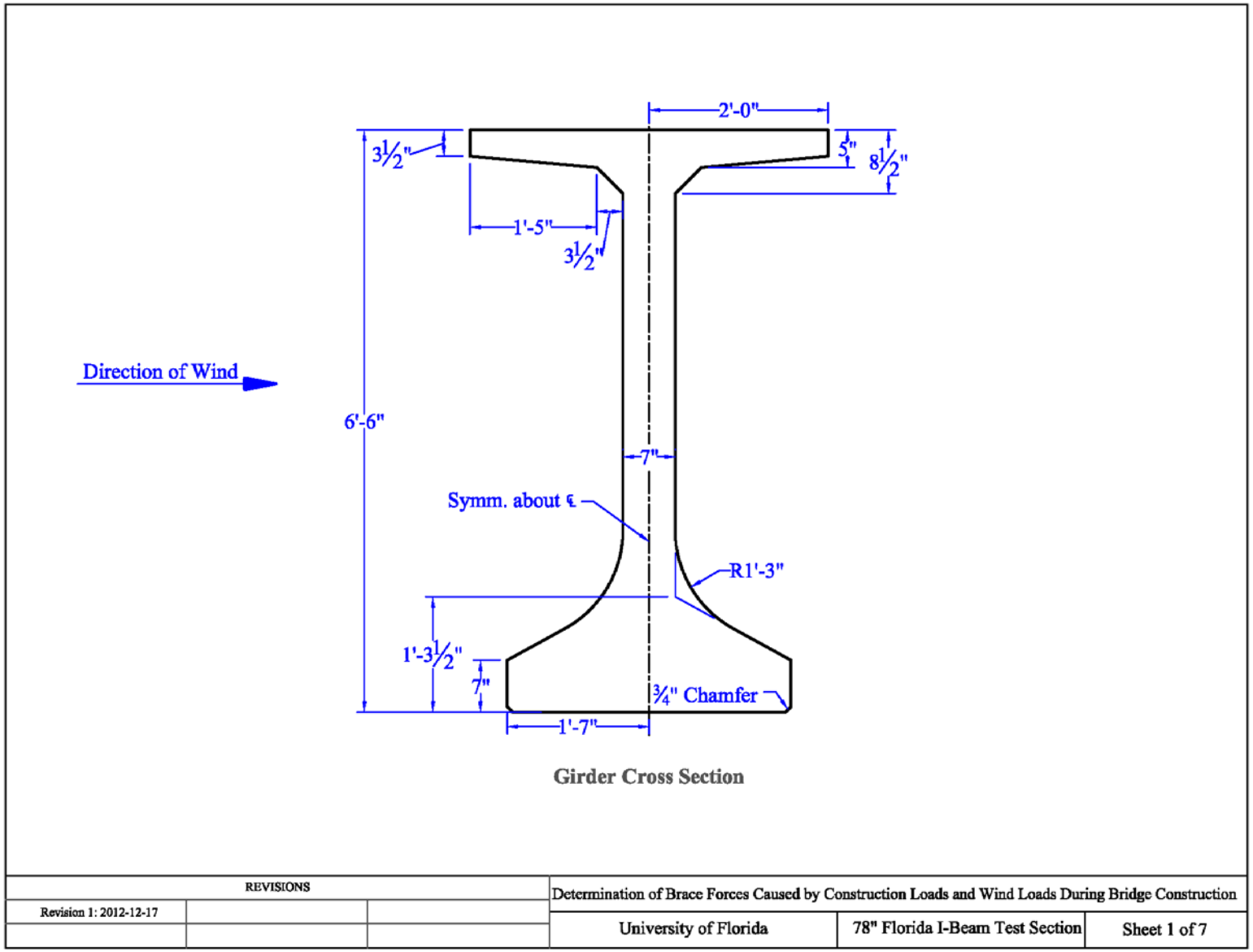

FIGURE 1.1 PROTOTYPE DIMENSIONS AND CONFIGURATIONS OF 78-INCH "FLORIDA" I-BEAM

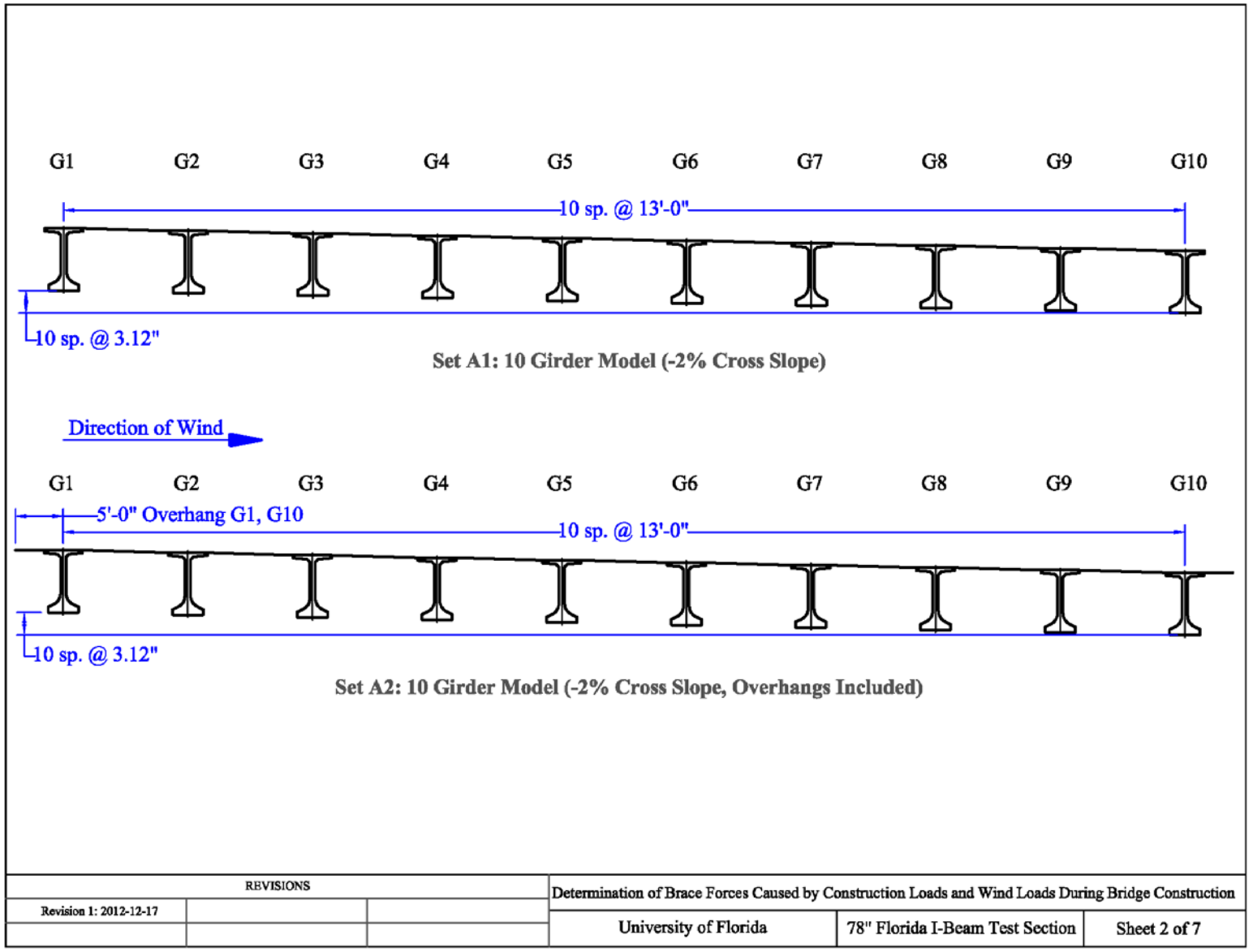

FIGURE 1.1 (CONT.) PROTOTYPE DIMENSIONS AND CONFIGURATIONS OF 78-INCH "FLORIDA" I-BEAM

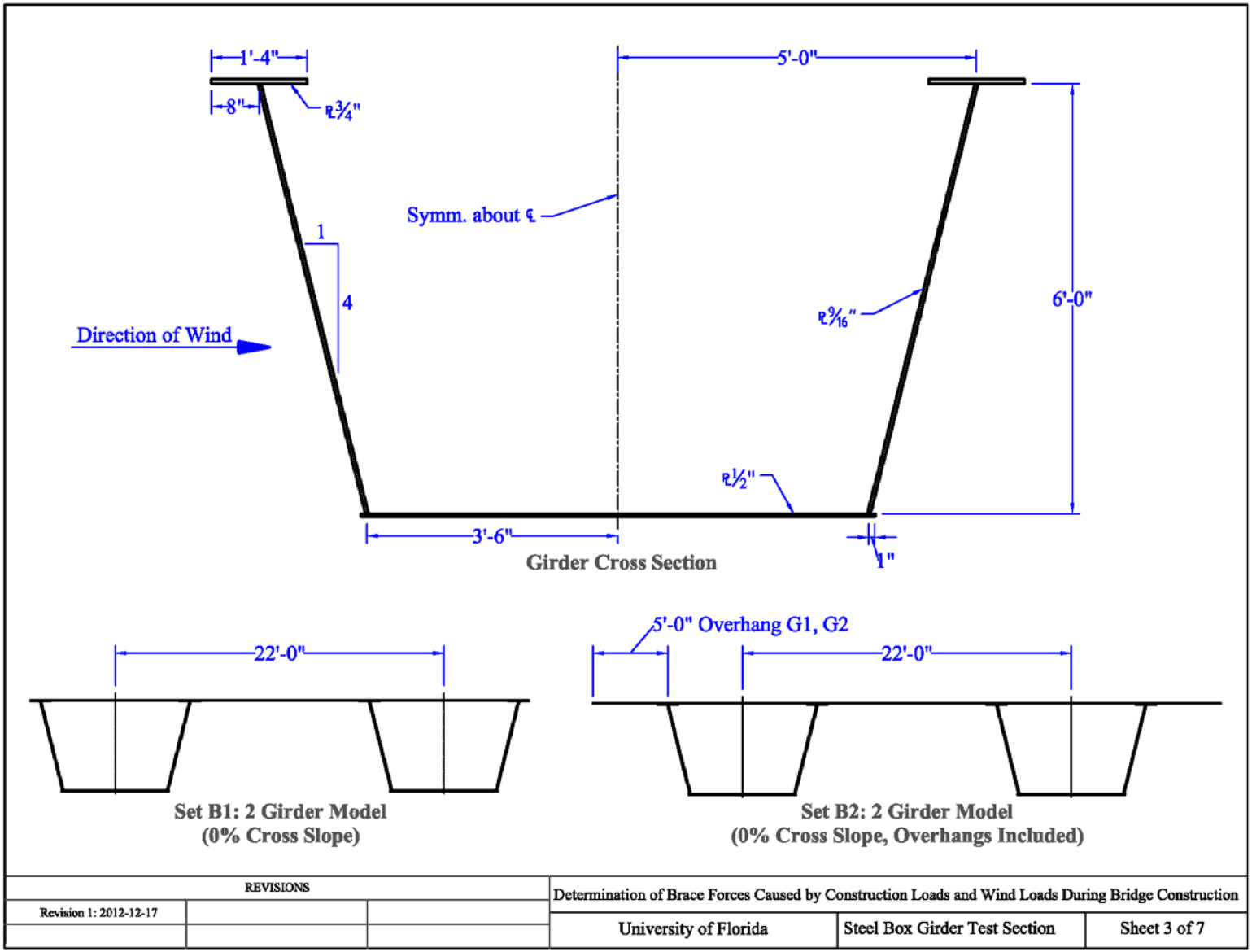

FIGURE 1.2 PROTOTYPE DIMENSIONS AND CONFIGURATIONS OF BOX GIRDERS

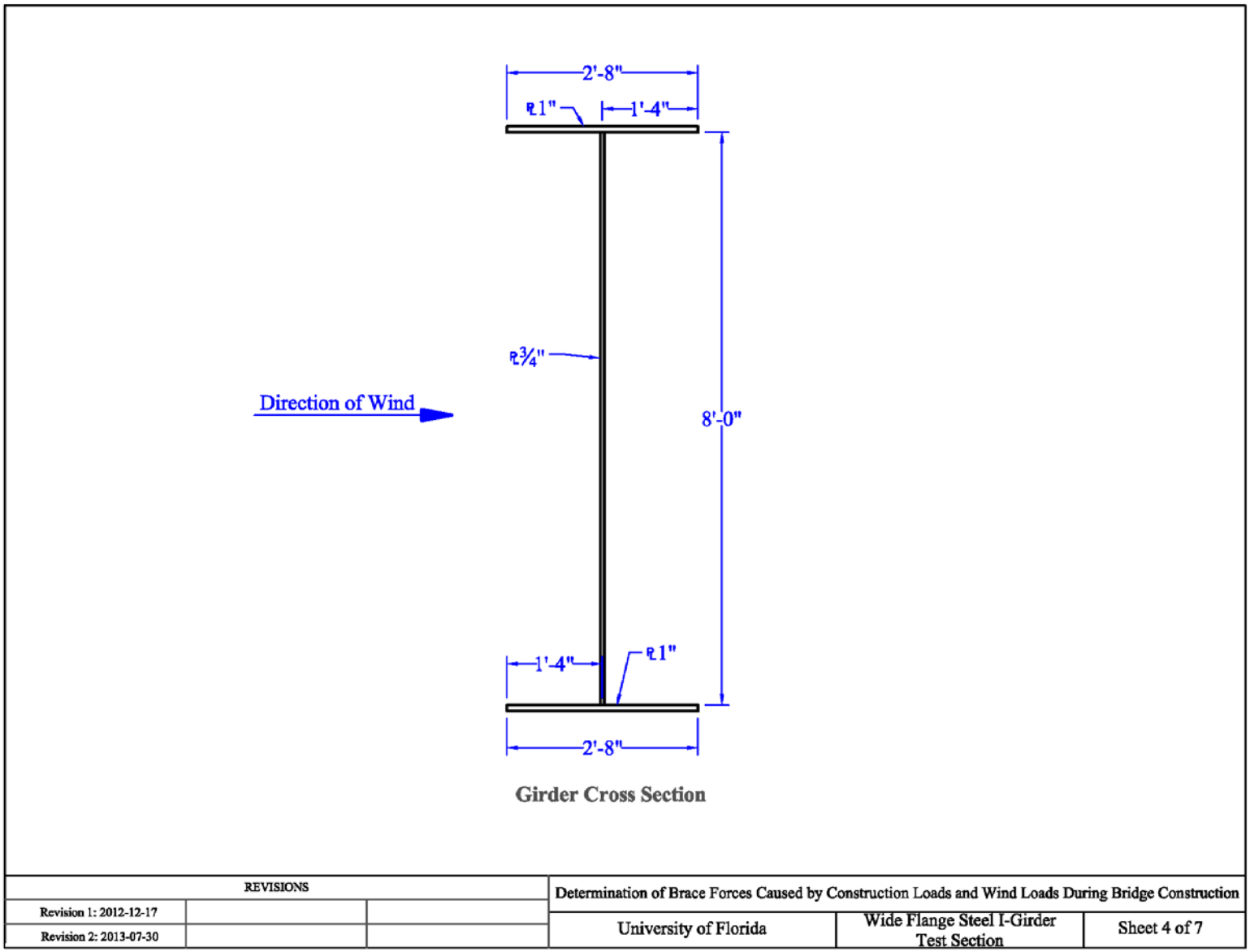

FIGURE 1.3 PROTOTYPE DIMENSIONS AND CONFIGURATIONS OF WIDE FLANGE PLATE GIRDERS

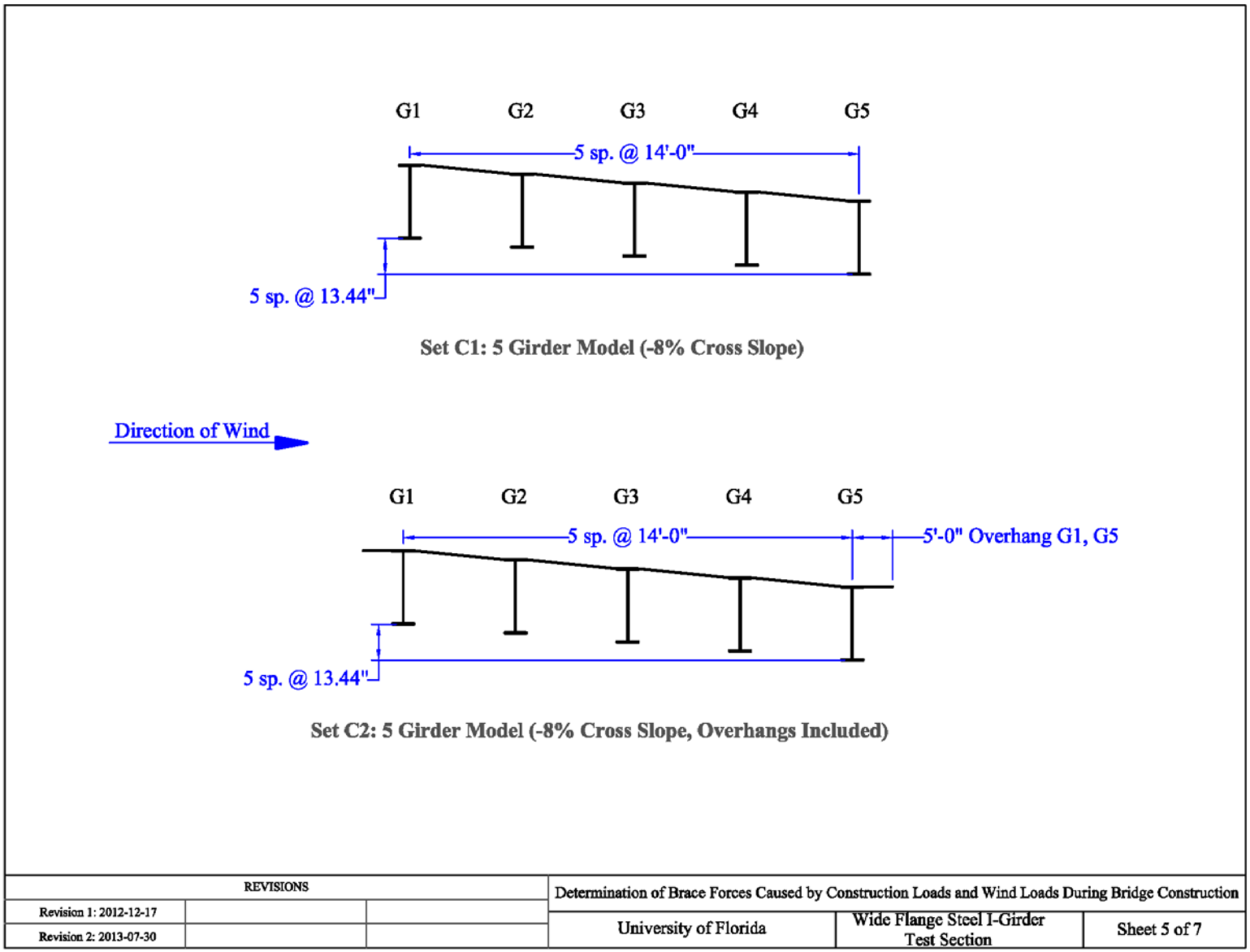

FIGURE 1.3 (CONT.) PROTOTYPE DIMENSIONS AND CONFIGURATIONS OF WIDE FLANGE PLATE GIRDERS

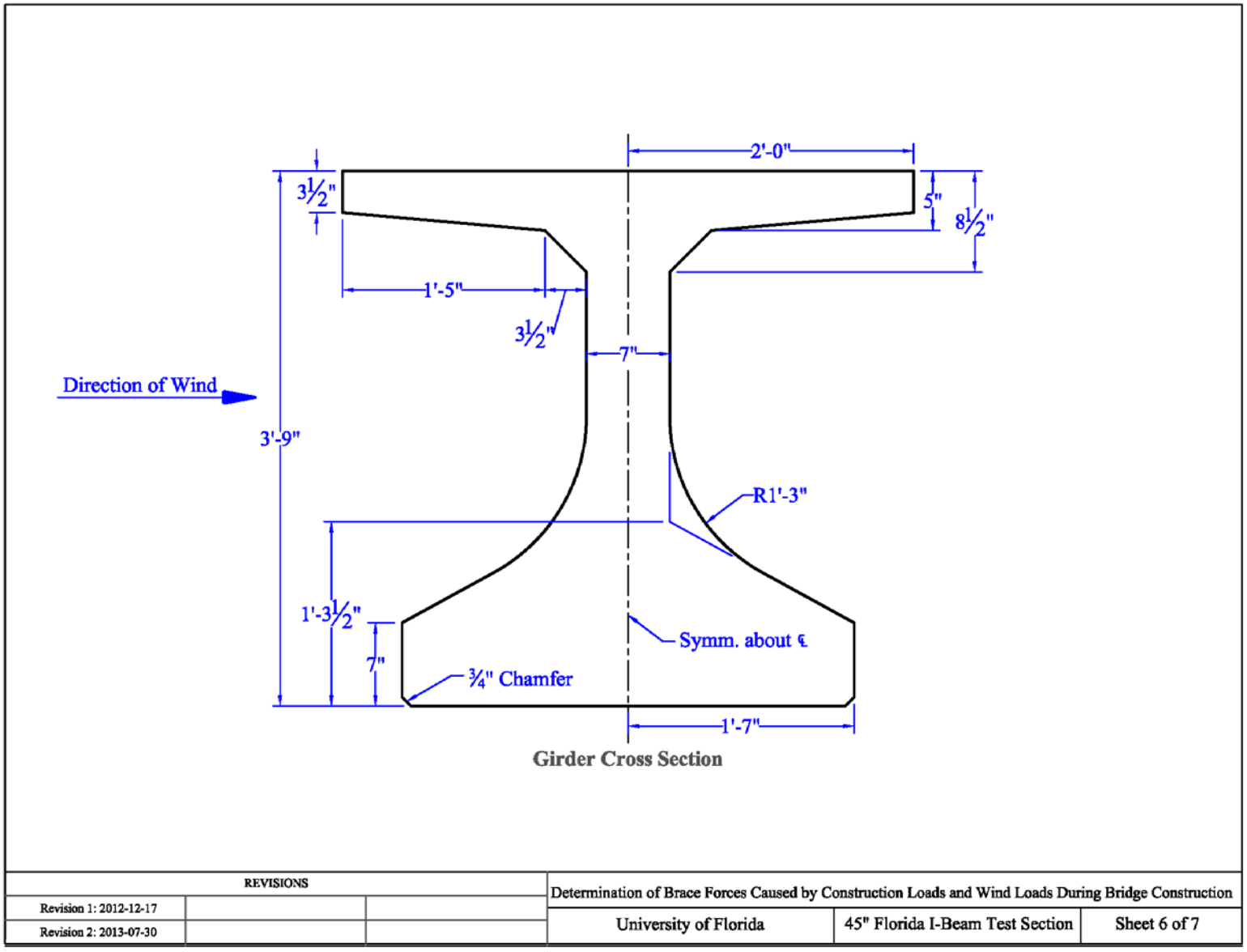

FIGURE 1.4 PROTOTYPE DIMENSIONS AND CONFIGURATIONS OF 45-INCH "FLORIDA" I-BEAM

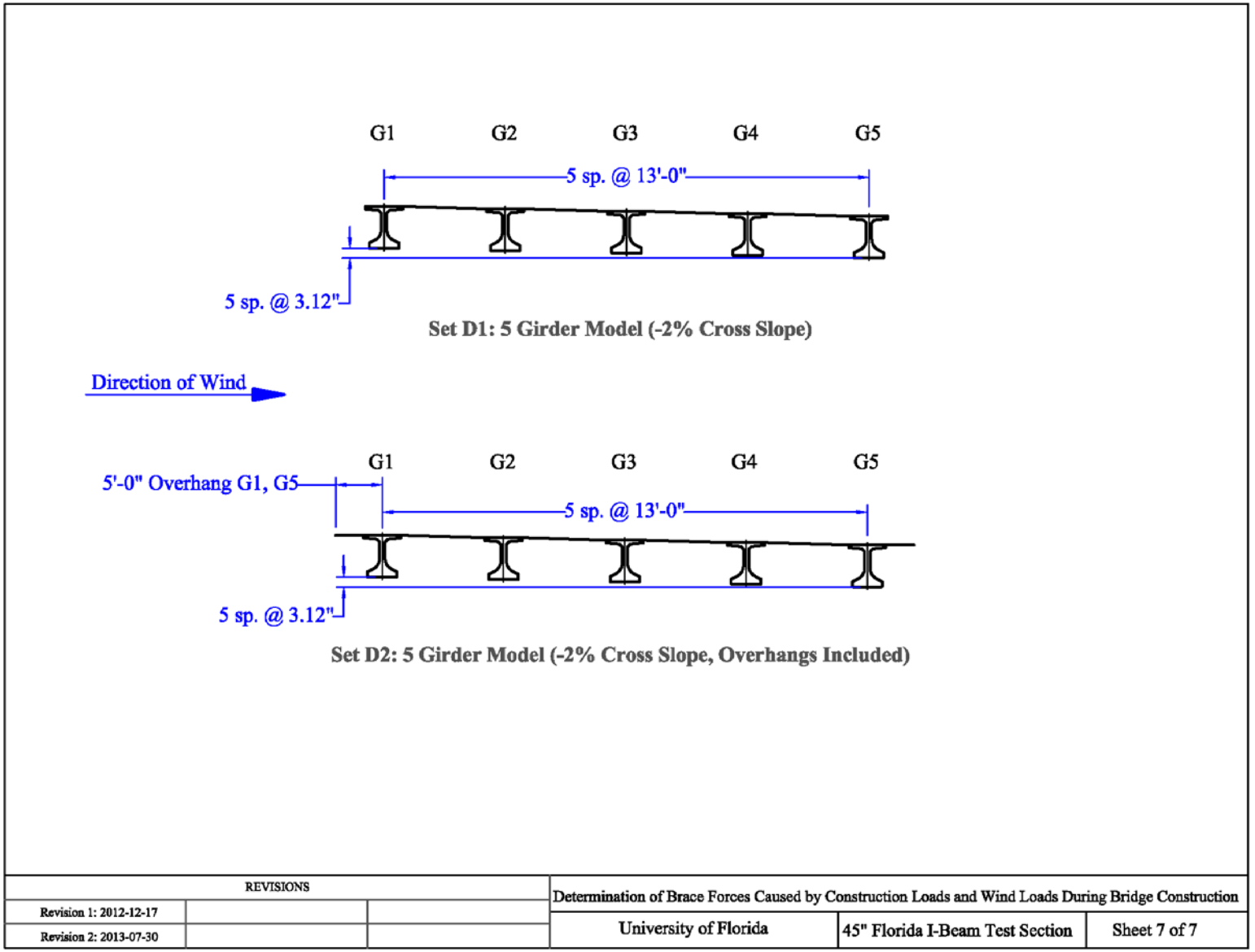

FIGURE 1.4 (CONT.) PROTOTYPE DIMENSIONS AND CONFIGURATIONS OF 45-INCH "FLORIDA" I-BEAM

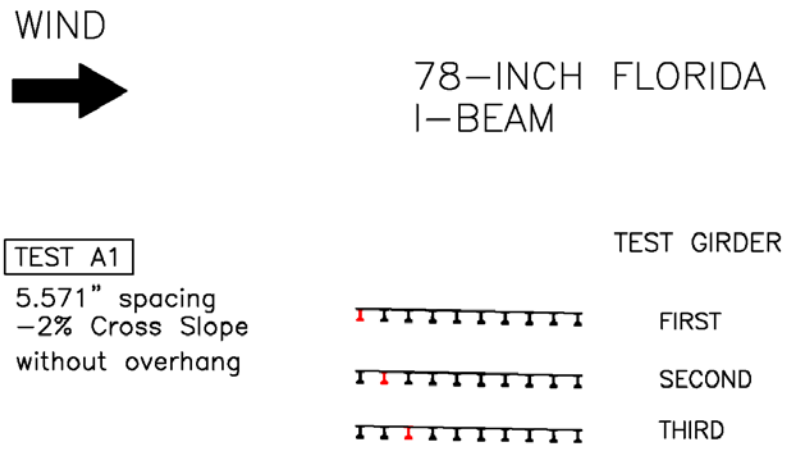

TEST A1 WITHOUT OVERHANG

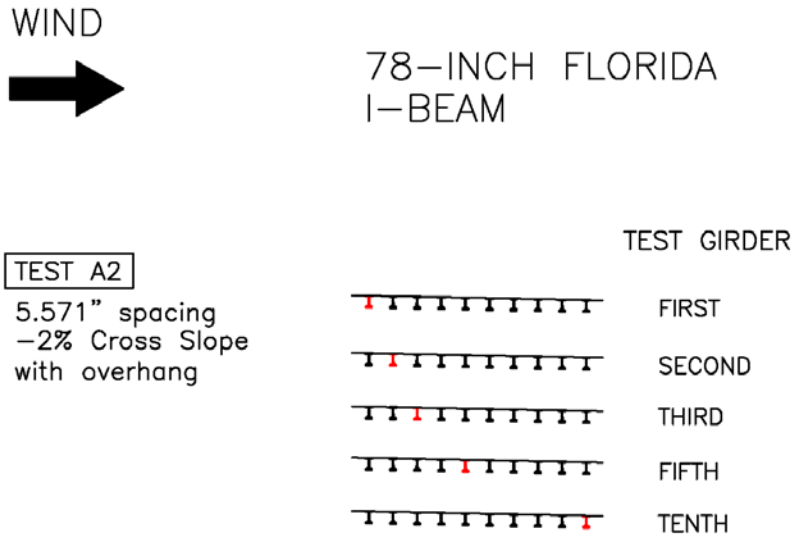

TEST A2 WITH OVERHANG

FIGURE 1.5 TEST CONFIGURATIONS AND DESIGNATIONS – 78-INCH "FLORIDA" I-BEAM (1:28 SCALE, RED – INSTRUMENTED I-BEAM)

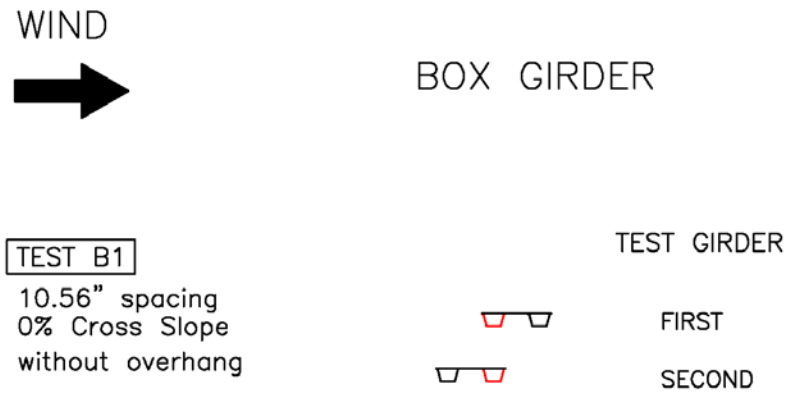

TEST B1 WITHOUT OVERHANG

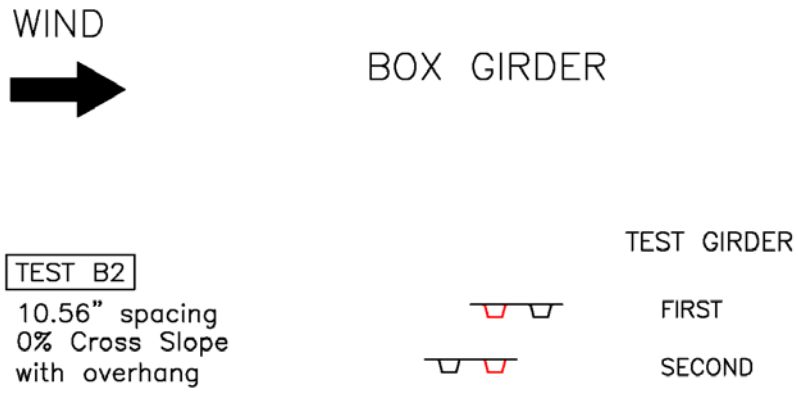

TEST B2 WITH OVERHANG

FIGURE 1.6 TEST CONFIGURATIONS AND DESIGNATIONS – BOX GIRDERS (1:25 SCALE, RED – INSTRUMENTED GIRDER)

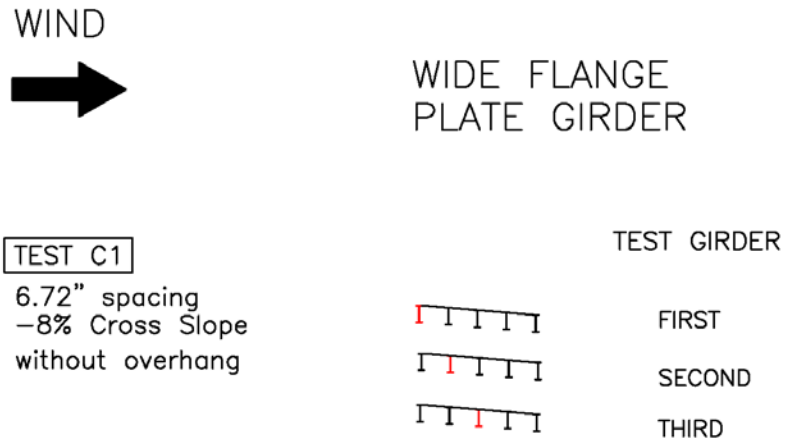

TEST C1 WITHOUT OVERHANG

TEST C2 WITH OVERHANG

FIGURE 1.7 TEST CONFIGURATIONS AND DESIGNATIONS – WIDE FLANGE PLATE GIRDERS (1:25 SCALE, RED – INSTRUMENTED GIRDER)

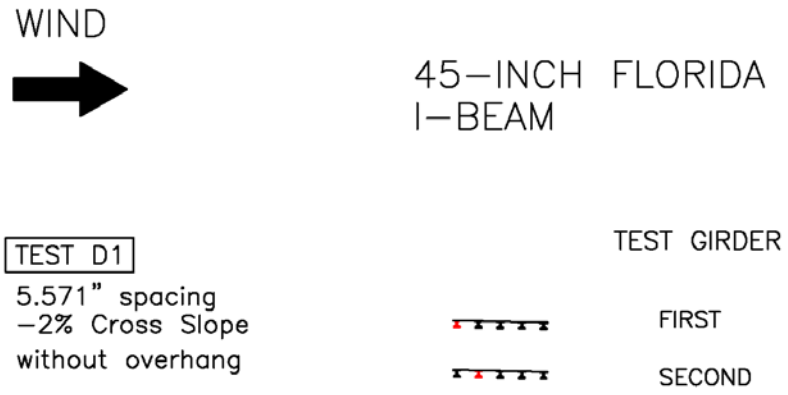

TEST D1 WITHOUT OVERHANG

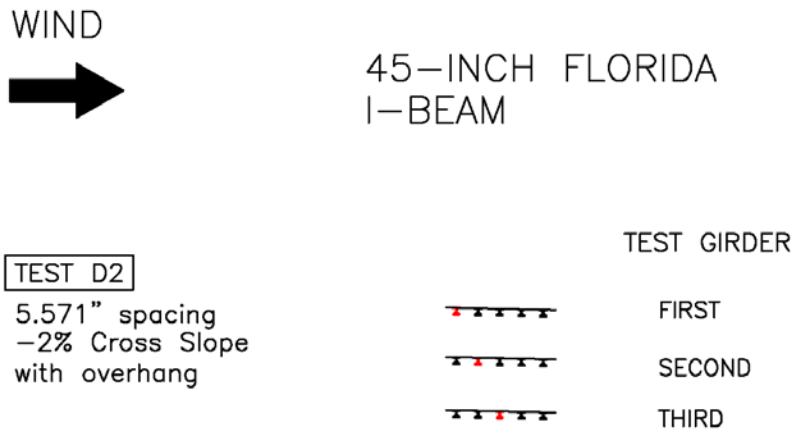

TEST D2 WITH OVERHANG

FIGURE 1.8 TEST CONFIGURATIONS AND DESIGNATIONS – 45-INCH "FLORIDA" I-BEAM (1:28 SCALE, RED – INSTRUMENTED I-BEAM)

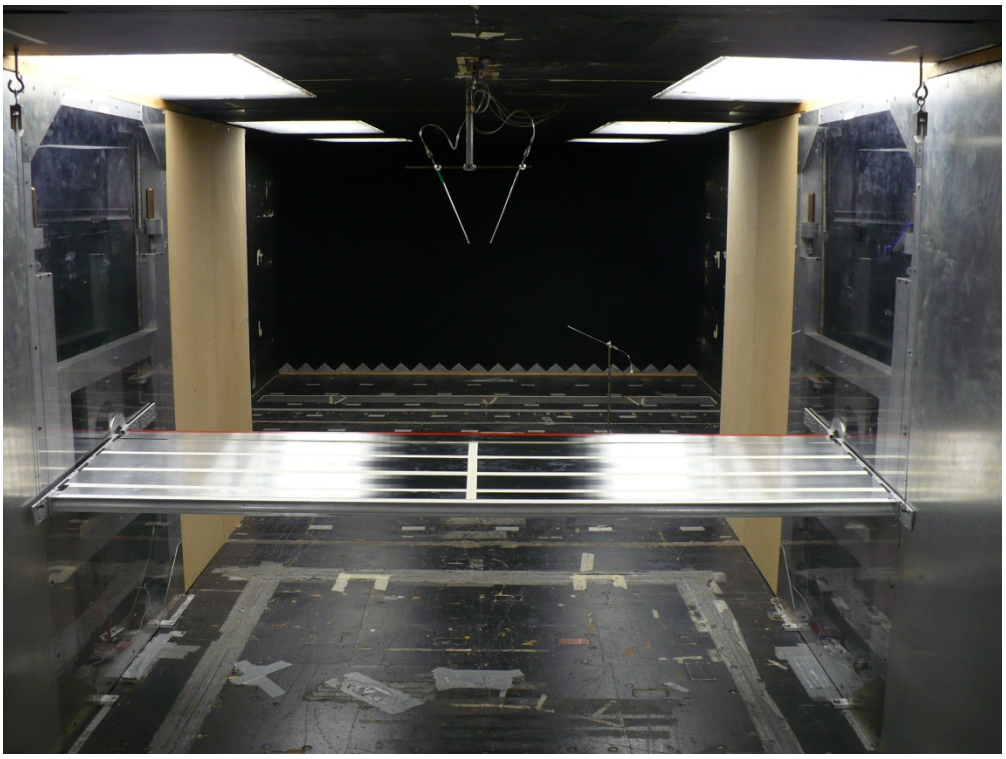

FIGURE 1.9 STATIC SECTION MODEL TEST SET-UP

FIGURE 1.10 STATIC SECTION MODEL TEST RIG

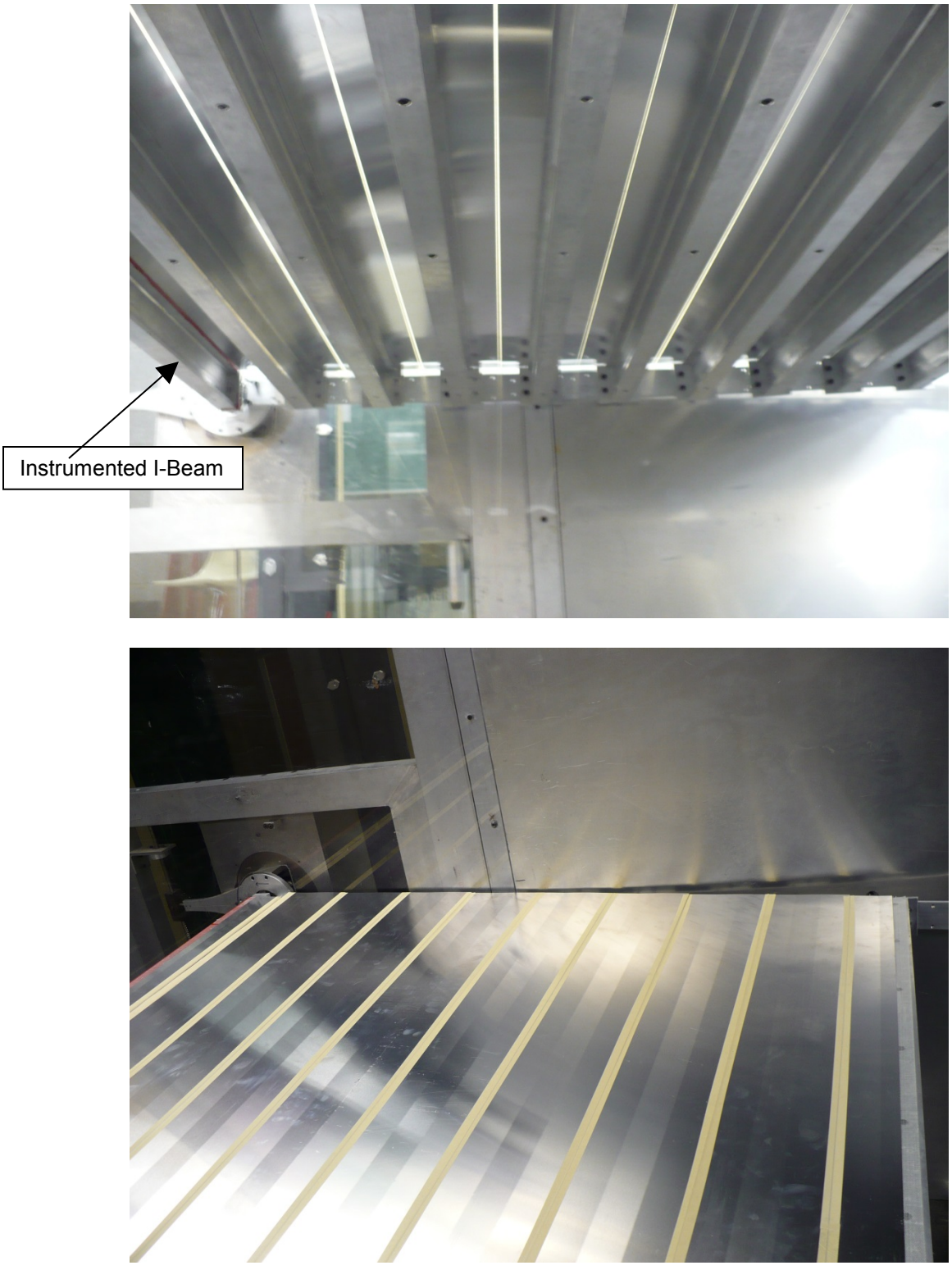

INSTRUMENTED I-BEAM AT 1st POSITION

FIGURE 1.11 78-INCH "FLORIDA" I-BEAM, -2% CROSS SLOPE, WITHOUT OVERHANG

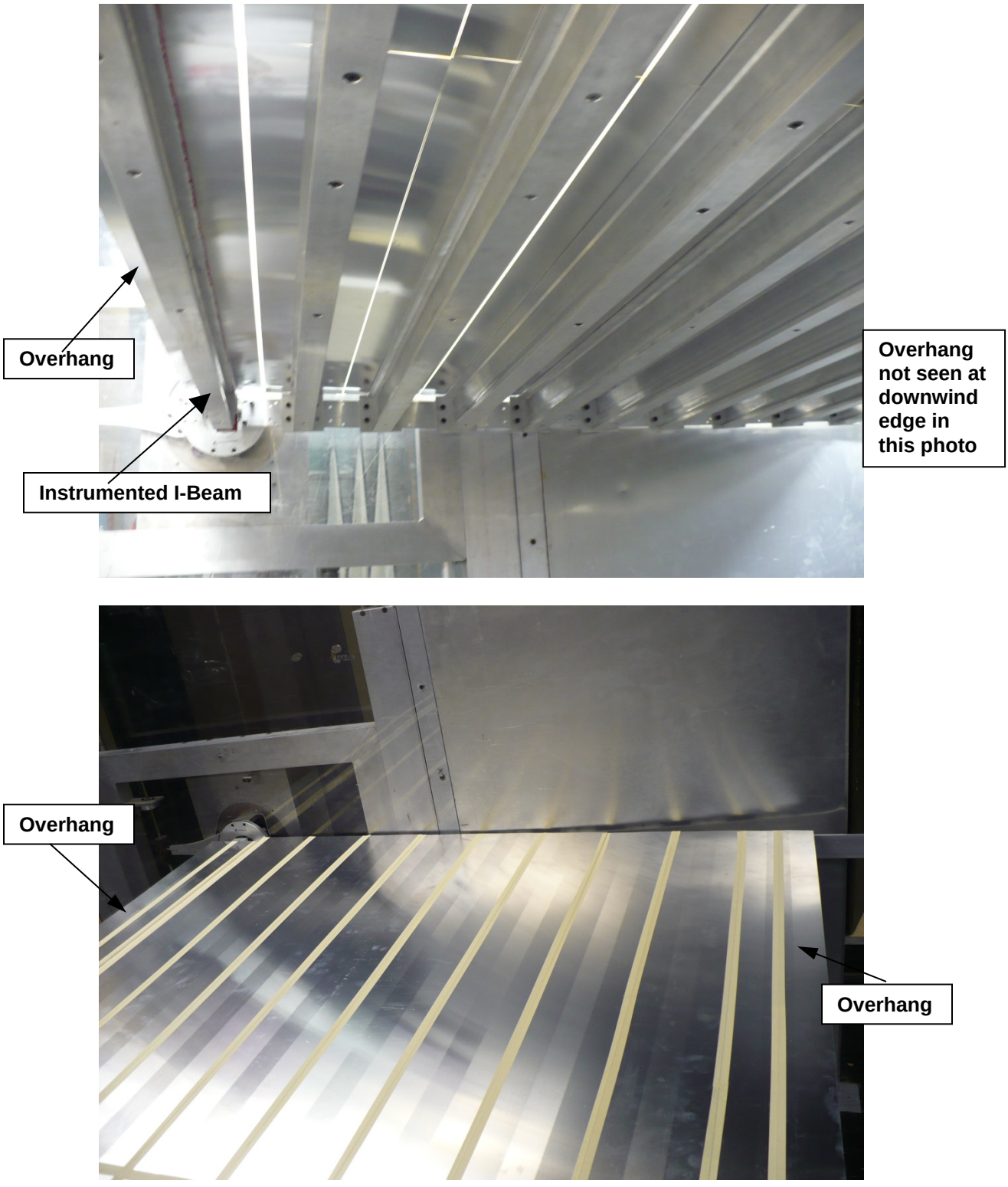

INSTRUMENTED I-BEAM AT 1st POSITION

FIGURE 1.12 78-INCH "FLORIDA" I-BEAM, -2% CROSS SLOPE, WITH OVERHANG

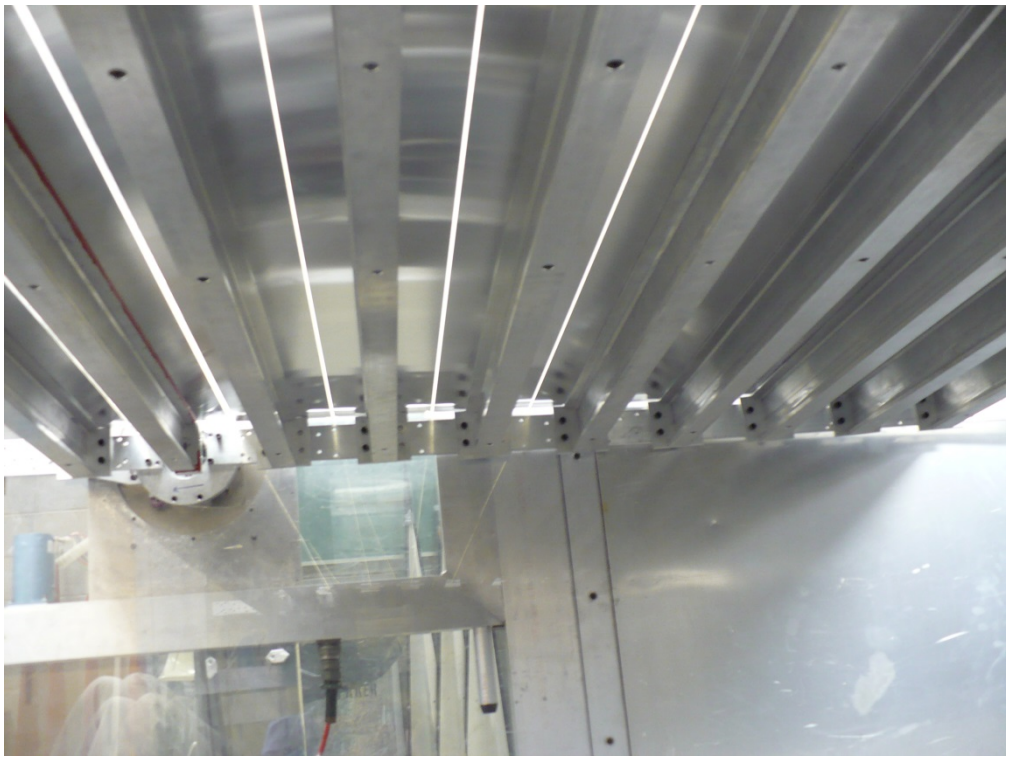

a) INSTRUMENTED I-BEAM AT 2nd POSITION

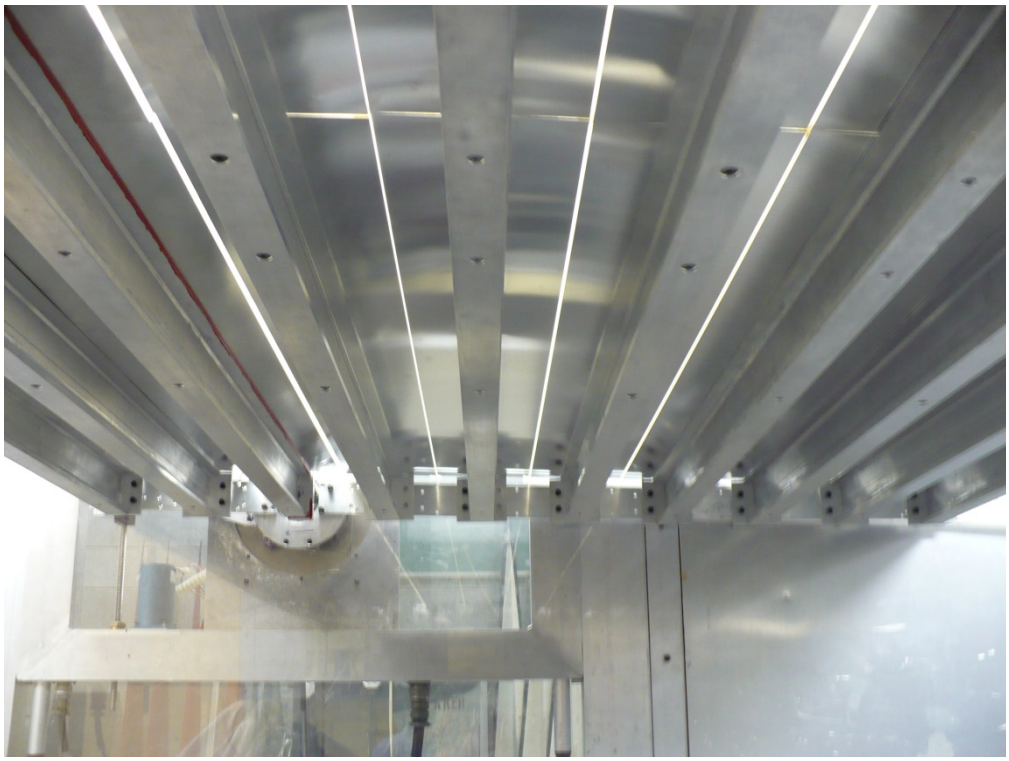

b) INSTRUMENTED I-BEAM AT 3rd POSITION

FIGURE 1.13 SECTION MODEL TEST SET-UP – 78-INCH "FLORIDA" I-BEAM, -2% CROSS SLOPE

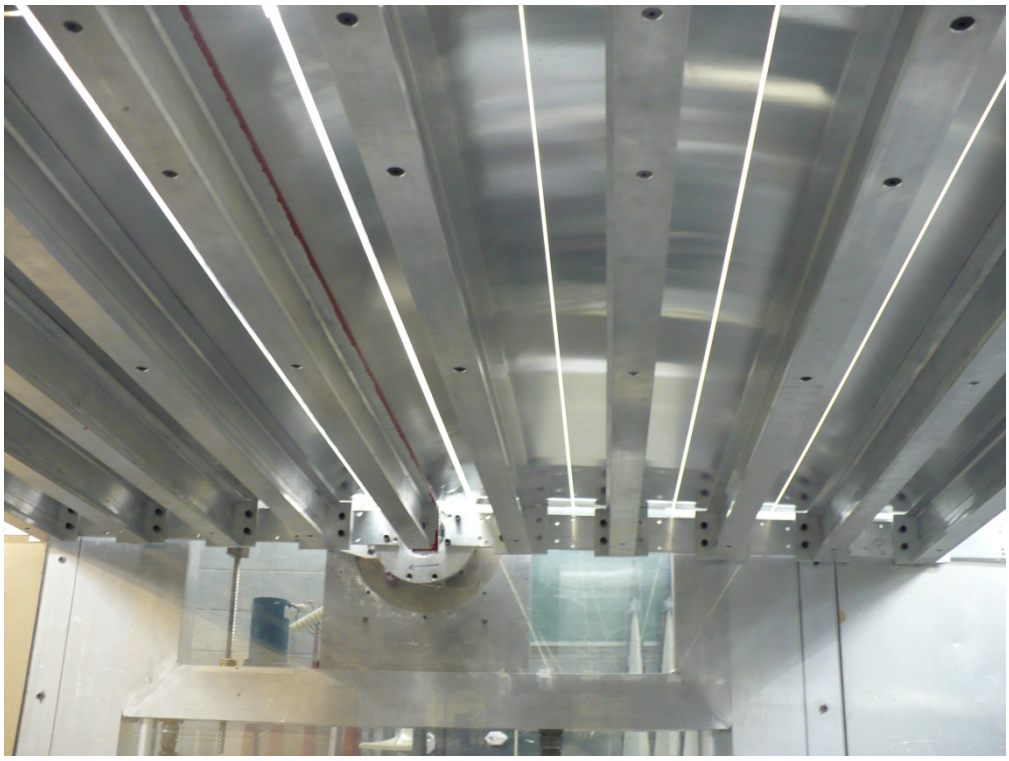

c) INSTRUMENTED GIRDER AT 5th POSITION

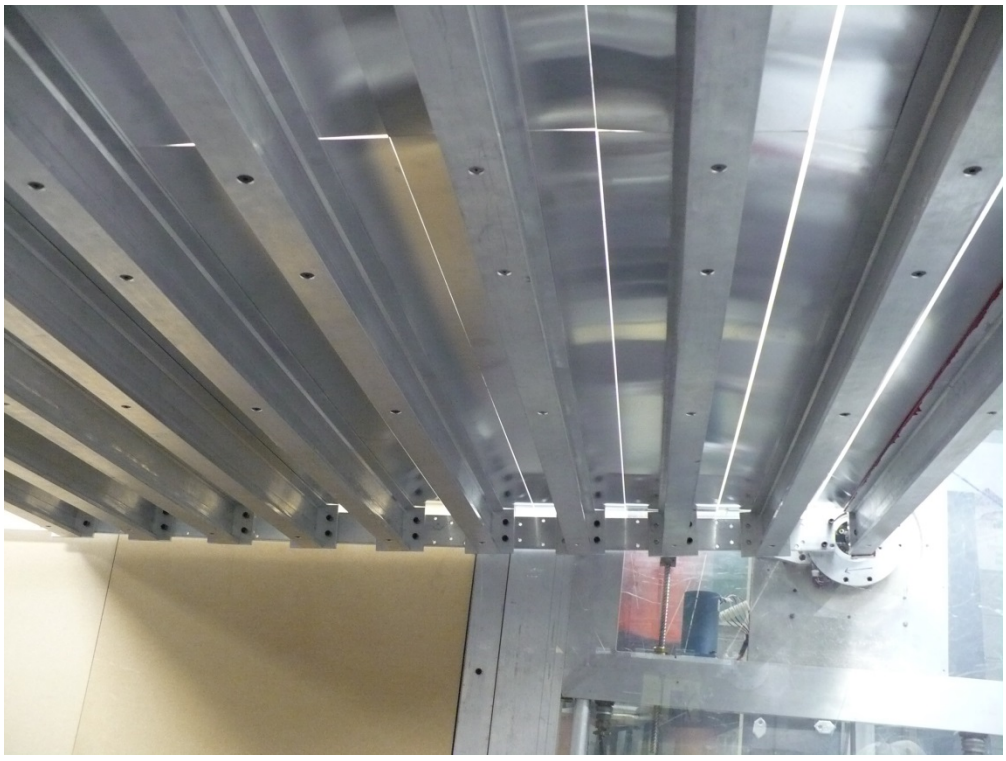

d) INSTRUMENTED GIRDER AT 10th POSITION

FIGURE 1.13 (CONT.) **SECTION MODEL TEST SET-UP – 78-INCH "FLORIDA" I-BEAM, -2% CROSS SLOPE**

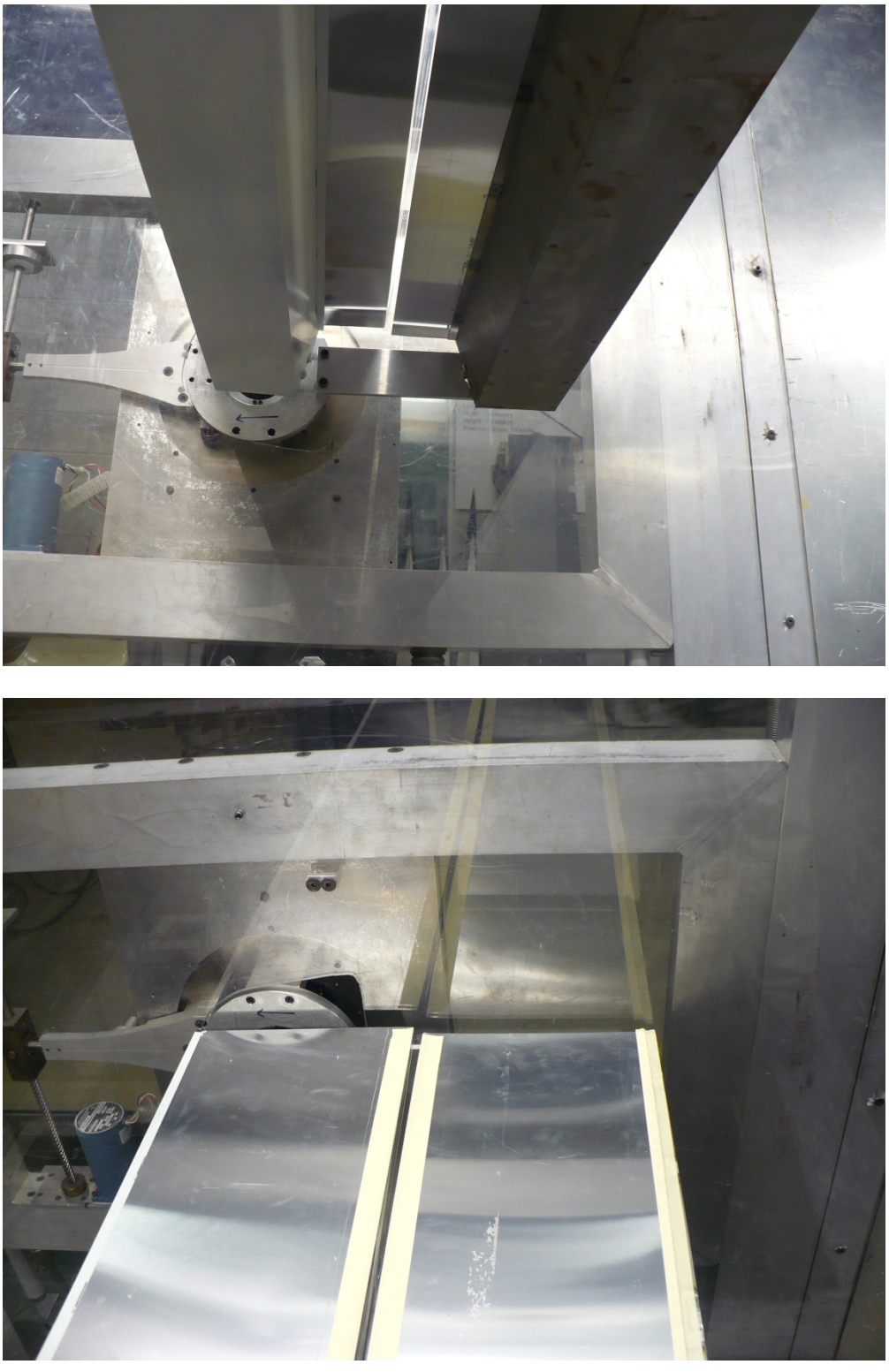

INSTRUMENTED GIRDER AT 1st POSITION

FIGURE 1.14 BOX GIRDER, 0% CROSS SLOPE, WITHOUT OVERHANG

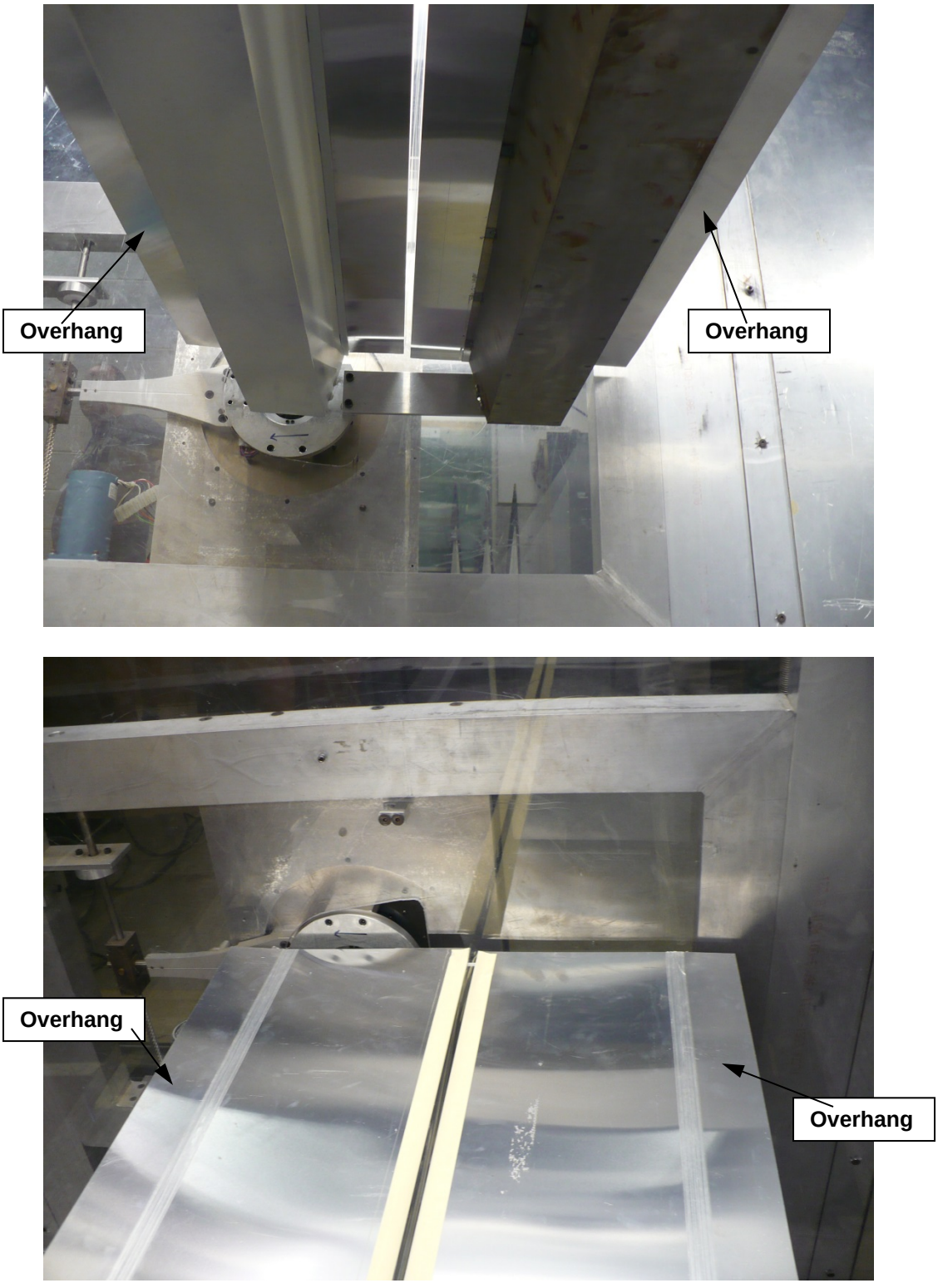

INSTRUMENTED GIRDER AT 1st POSITION

FIGURE 1.15 BOX GIRDER, 0% CROSS SLOPE, WITH OVERHANG

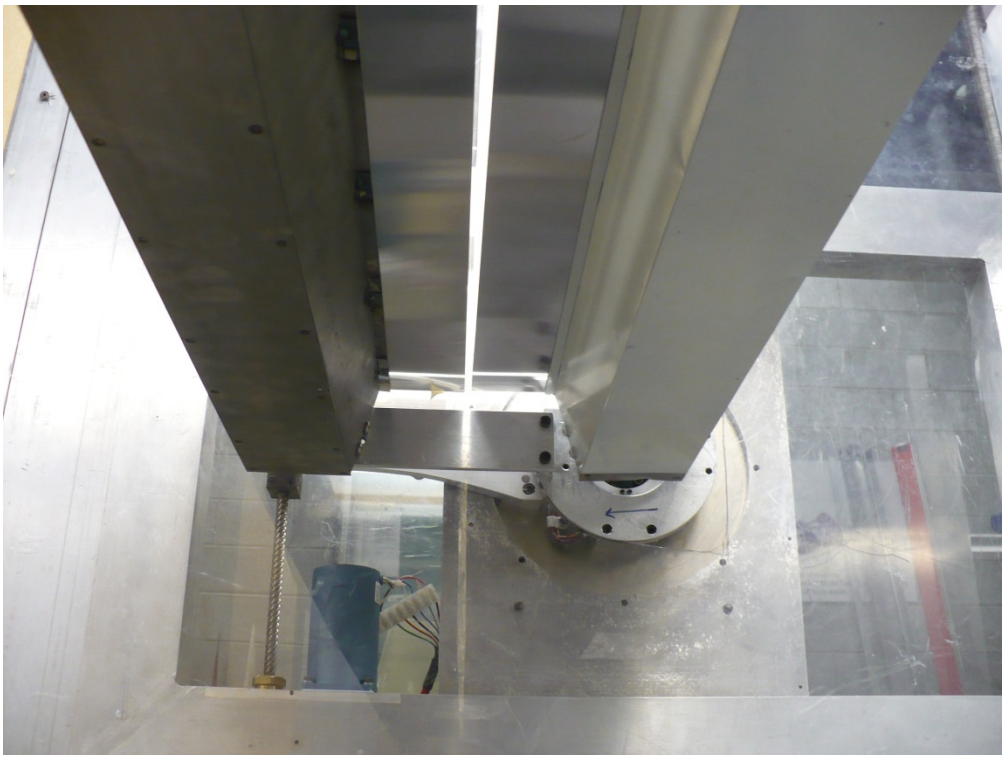

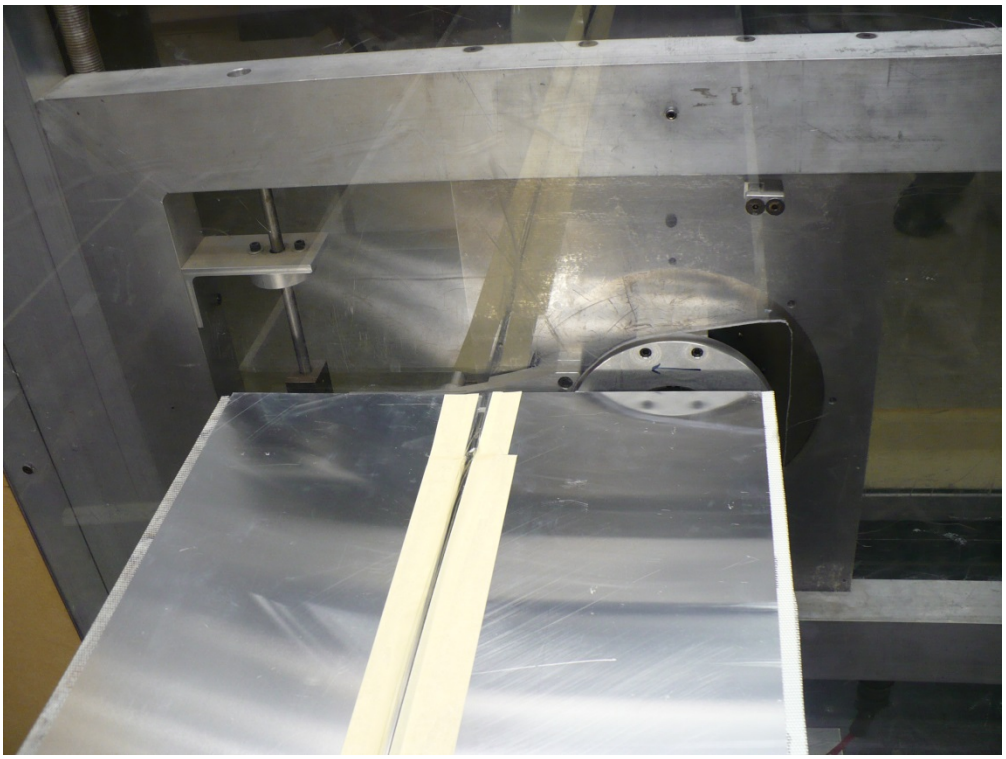

INSTRUMENTED GIRDER AT 2nd POSITION, WITHOUT OVERHANG

FIGURE 1.16 SECTION MODEL TEST SET-UP – BOX GIRDER, 0% CROSS SLOPE

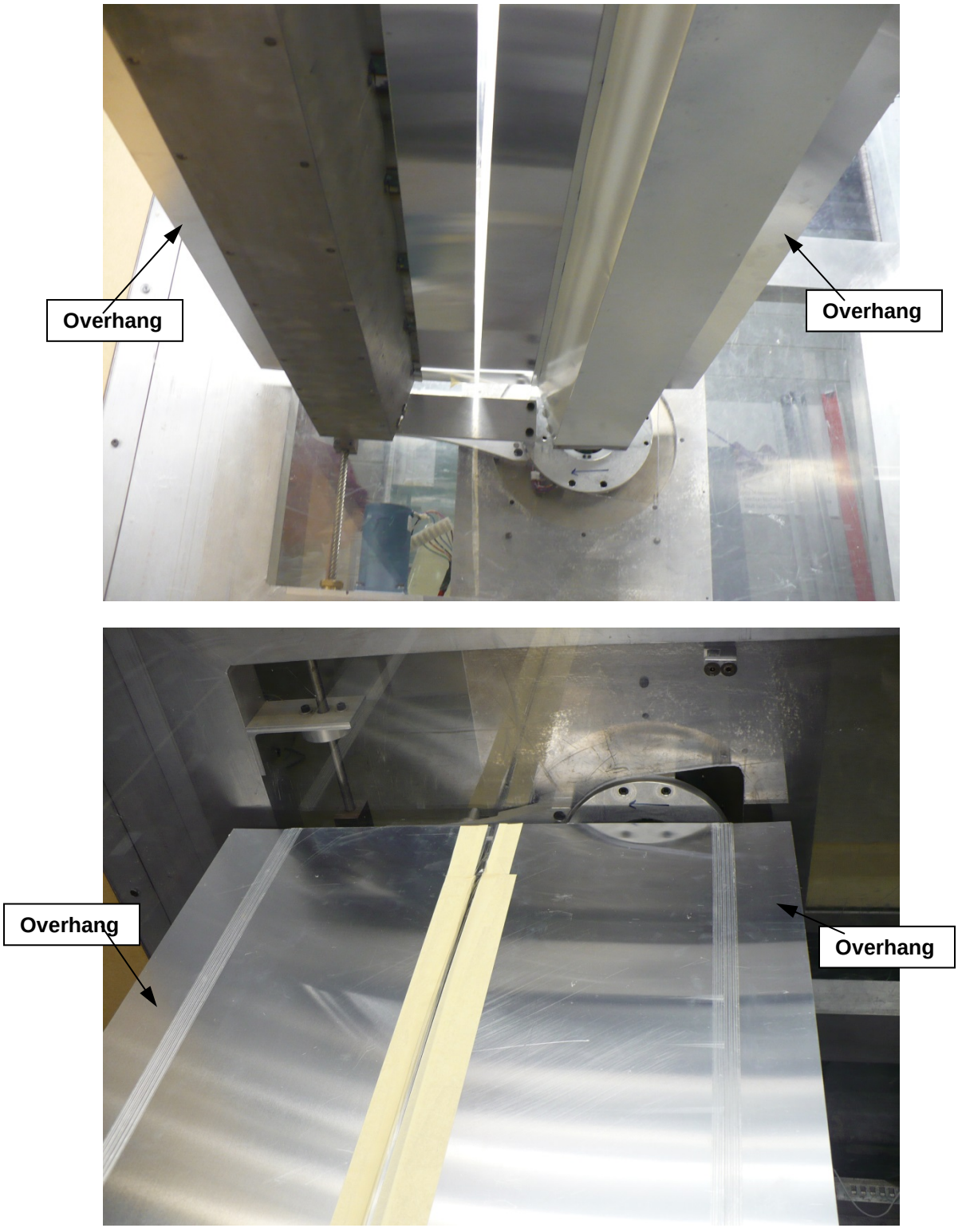

INSTRUMENTED GIRDER AT 2nd POSITION, WITH OVERHANG

FIGURE 1.16 (CONT.) SECTION MODEL TEST SET-UP – BOX GIRDER, 0% CROSS SLOPE

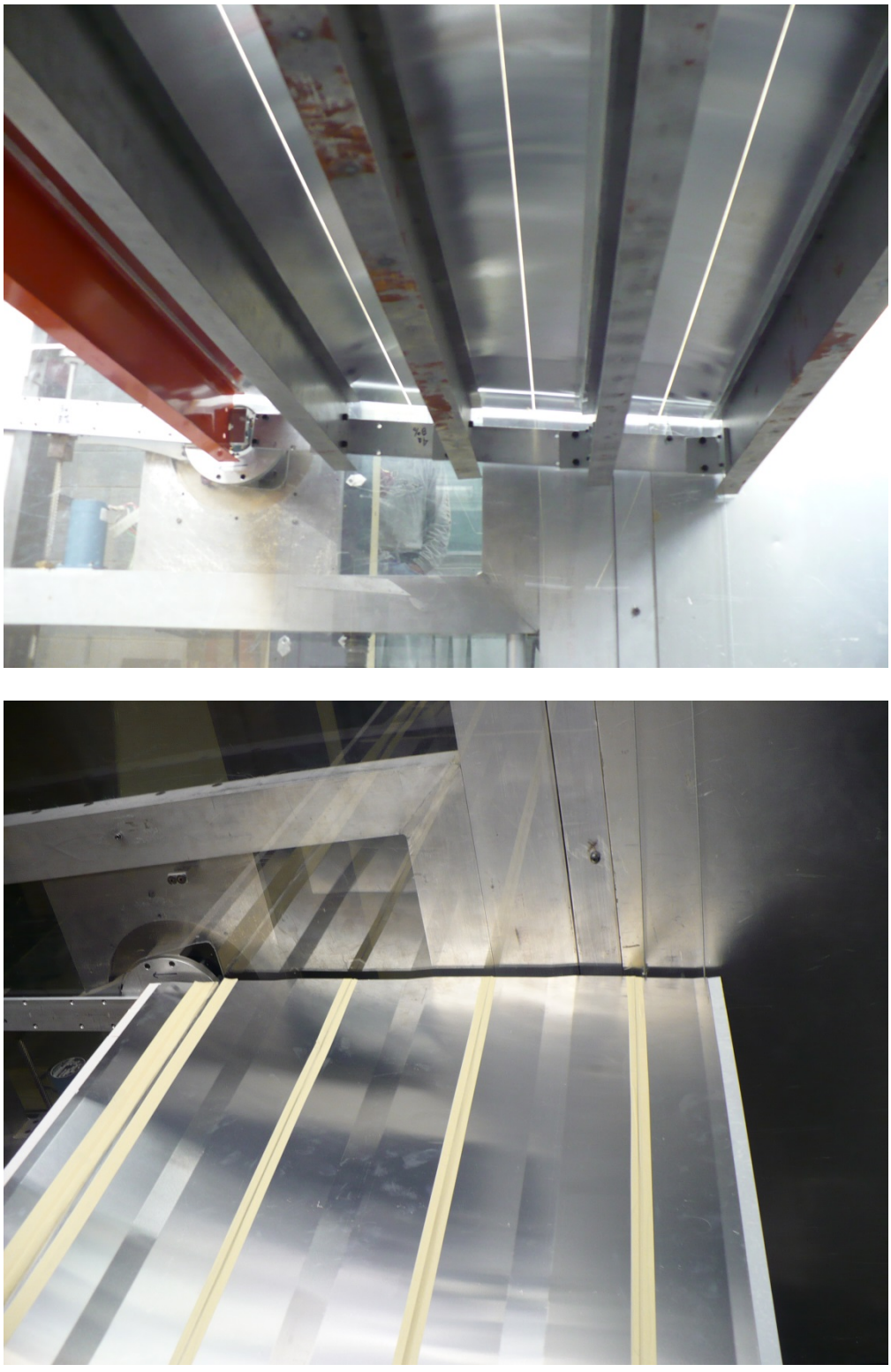

INSTRUMENTED GIRDER AT 1st POSITION

FIGURE 1.17 WIDE FLANGE PLATE GIRDER, -8% CROSS SLOPE, WITHOUT OVERHANG

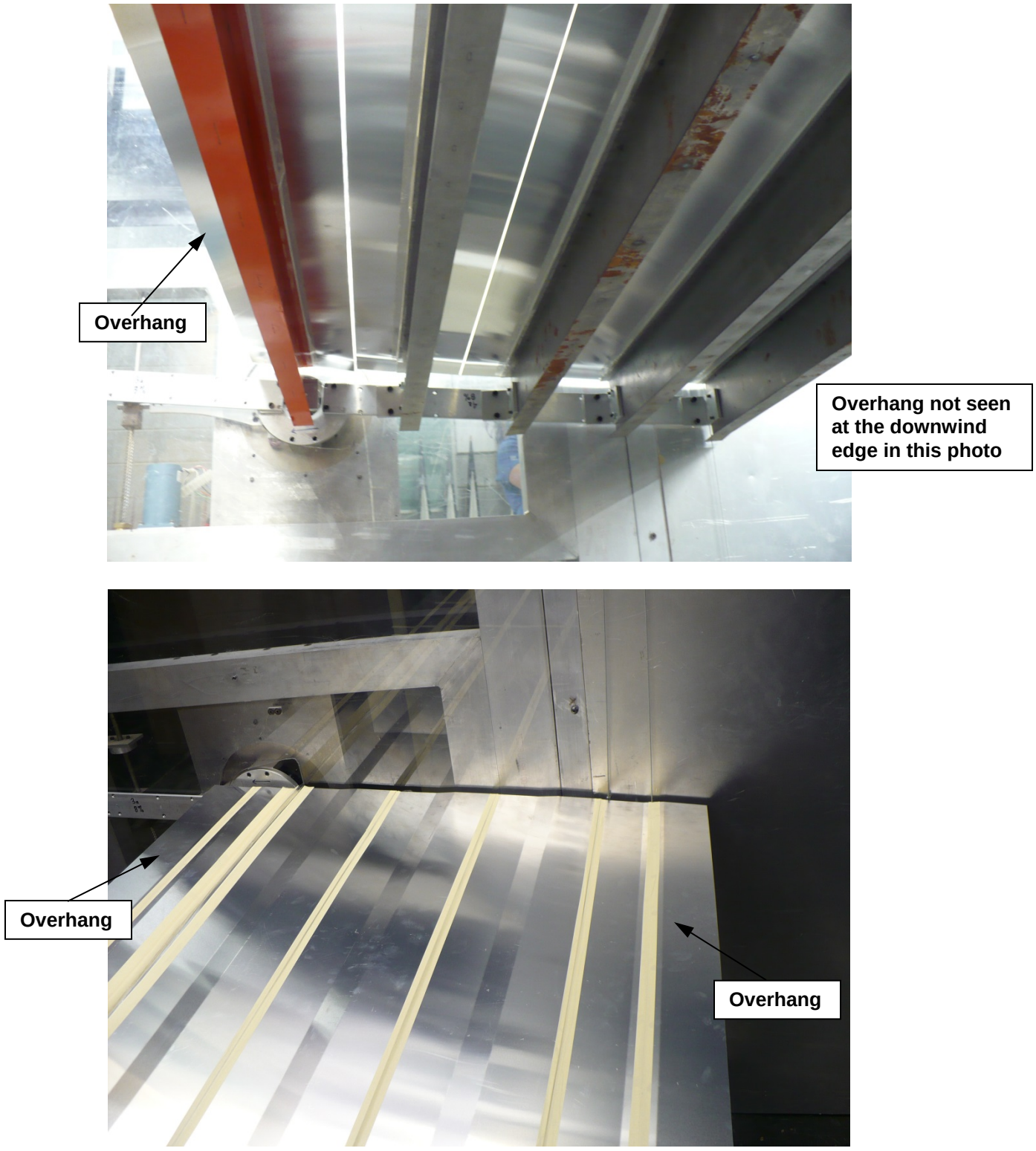

INSTRUMENTED GIRDER AT 1st POSITION

FIGURE 1.18 WIDE FLANGE PLATE GIRDER, -8% CROSS SLOPE, WITH OVERHANG

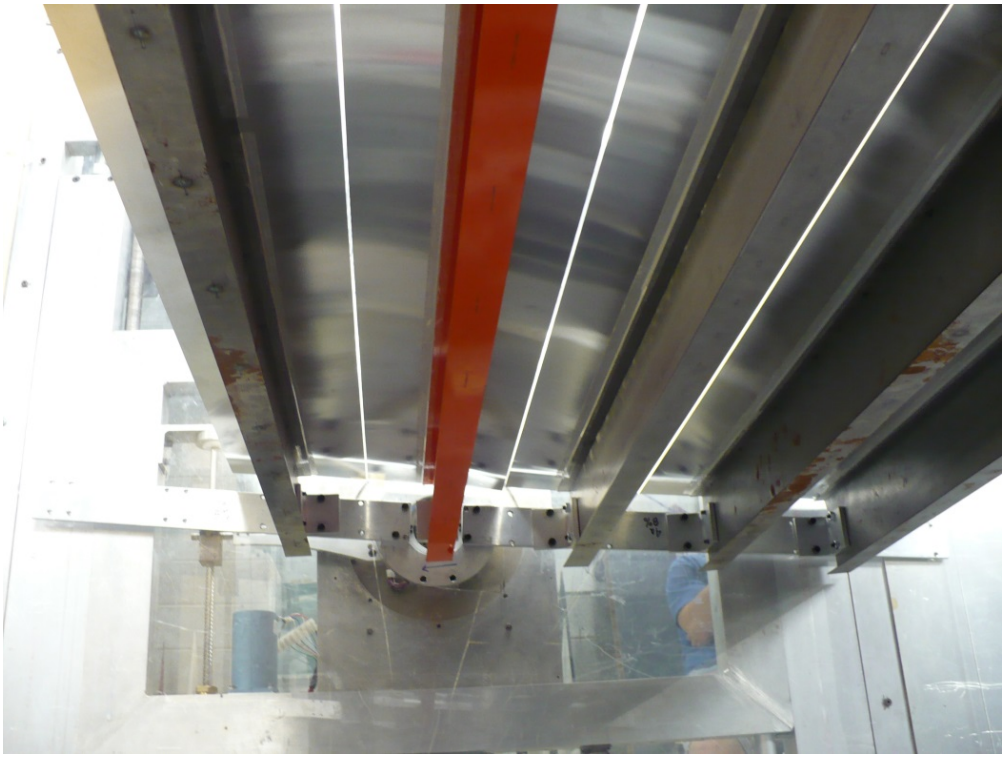

a) INSTRUMENTED GIRDER AT 2nd POSITION

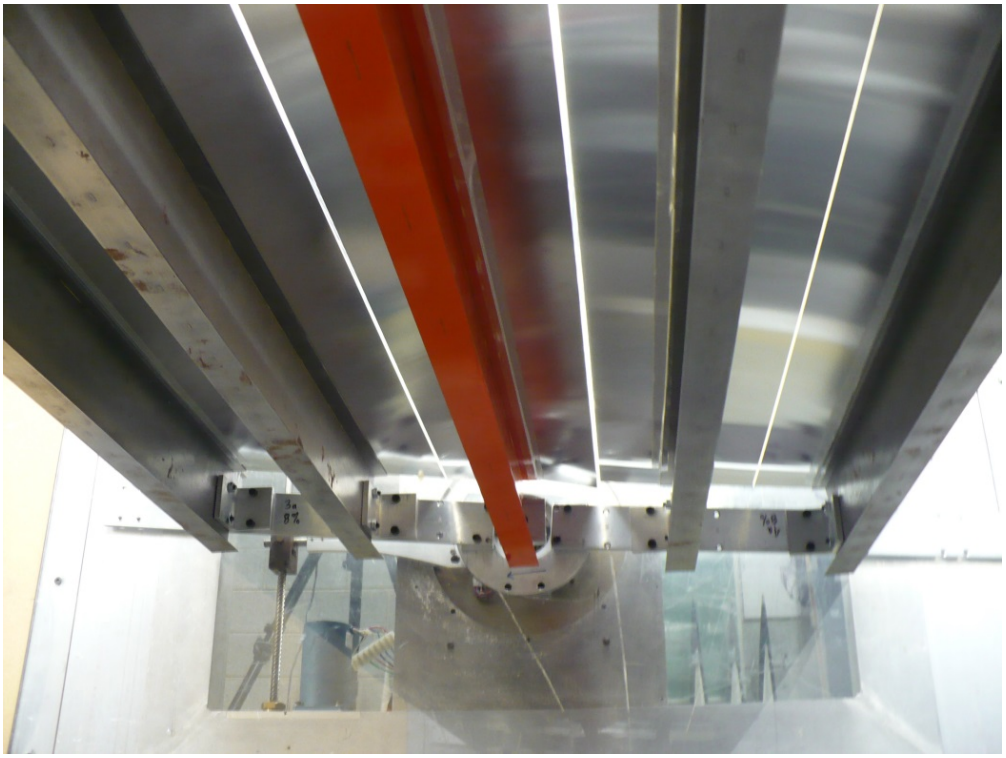

b) INSTRUMENTED GIRDER AT 3rd POSITION

FIGURE 1.19 SECTION MODEL TEST SET-UP – WIDE FLANGE PLATE GIRDER, -8% CROSS SLOPE

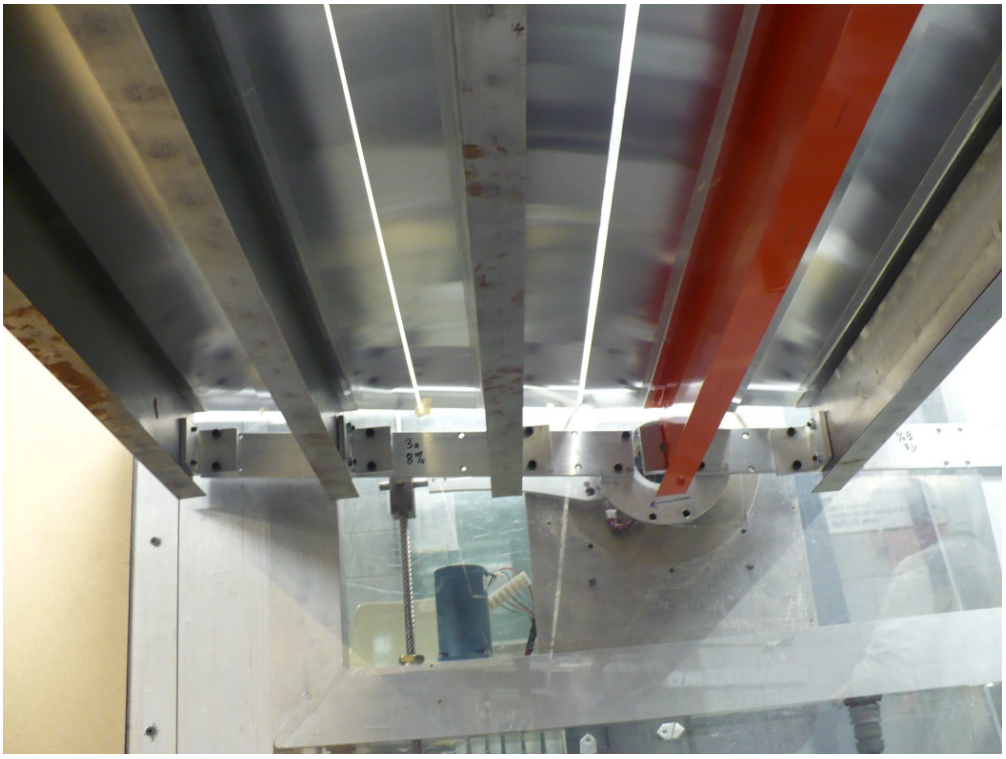

c) INSTRUMENTED GIRDER AT 4TH POSITION

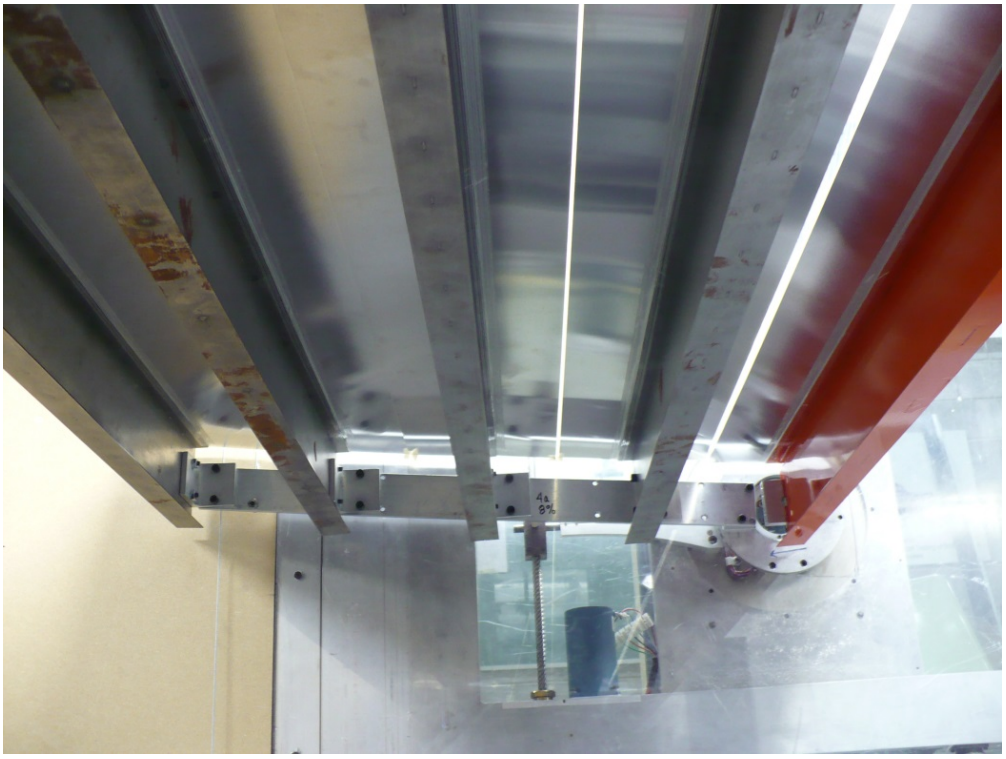

c) INSTRUMENTED GIRDER AT 5TH POSITION

FIGURE 1.19 (CONT.) **SECTION MODEL TEST SET-UP – WIDE FLANGE PLATE GIRDER, -8% CROSS SLOPE**

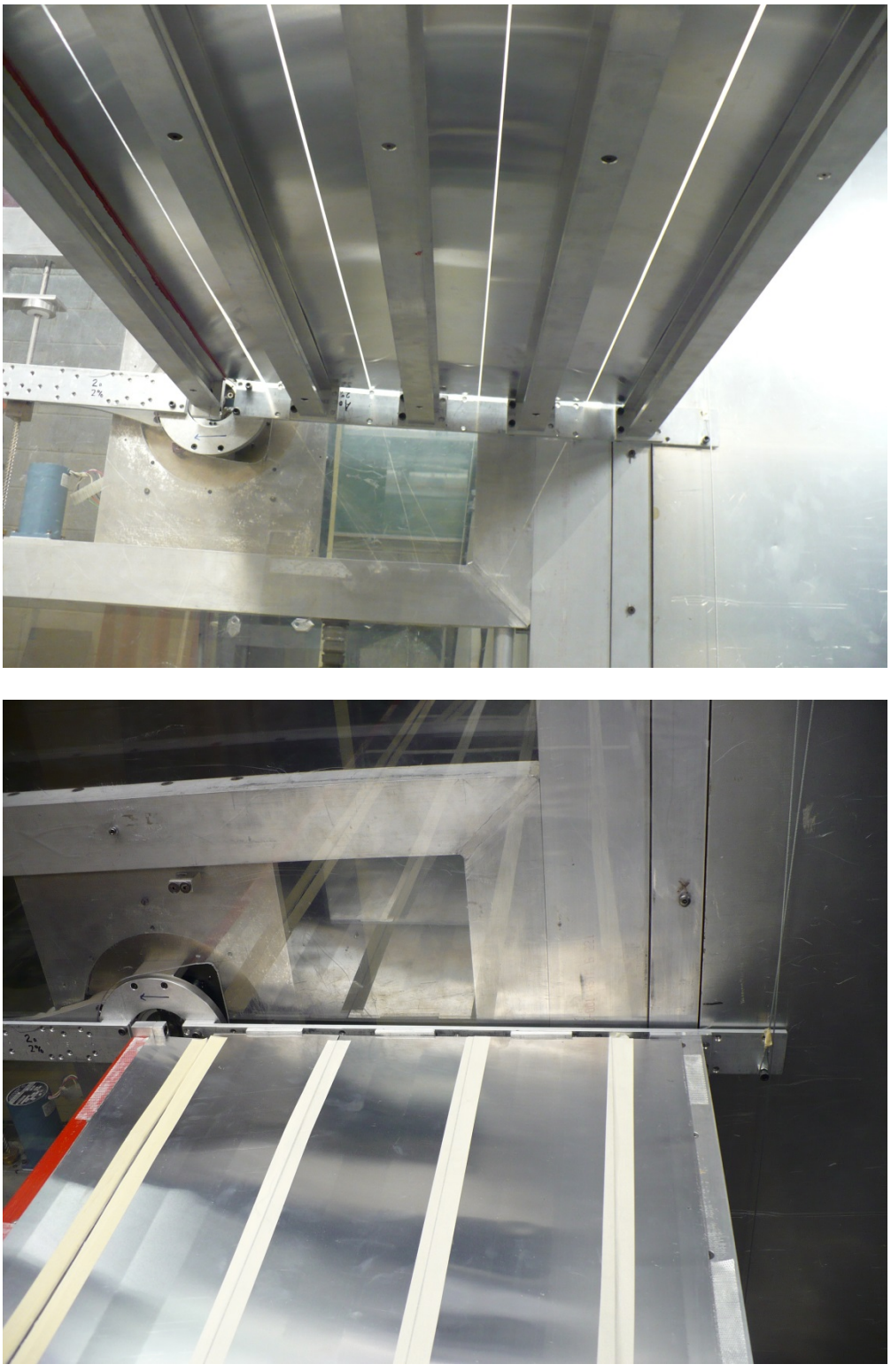

INSTRUMENTED I-BEAM AT 1st POSITION

FIGURE 1.20 **45-INCH "FLORIDA" I-BEAM, -2% CROSS SLOPE, WITHOUT OVERHANG**

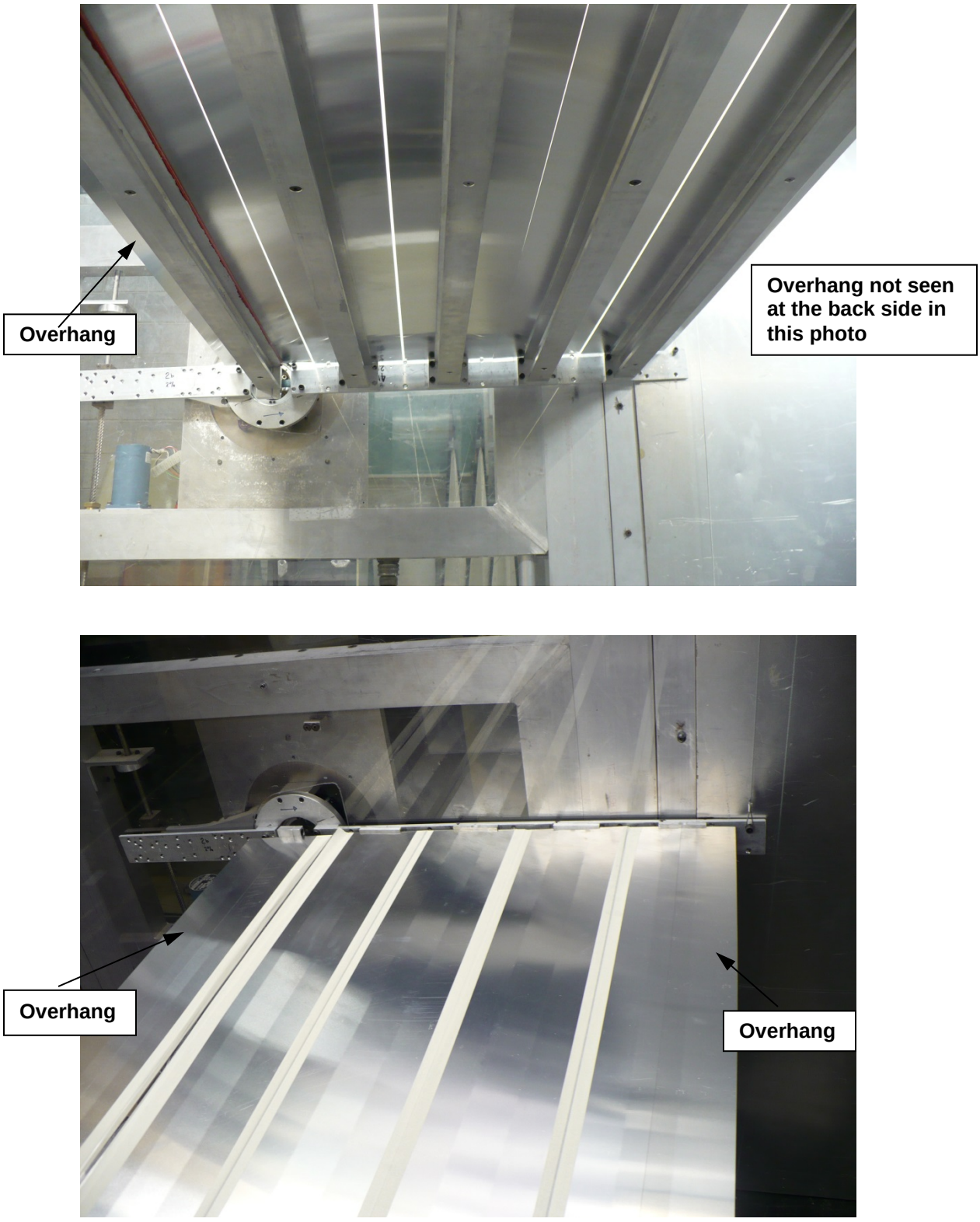

INSTRUMENTED I-BEAM AT 1st POSITION

FIGURE 1.21 45-INCH "FLORIDA" I-BEAM, -2% CROSS SLOPE, WITH OVERHANG

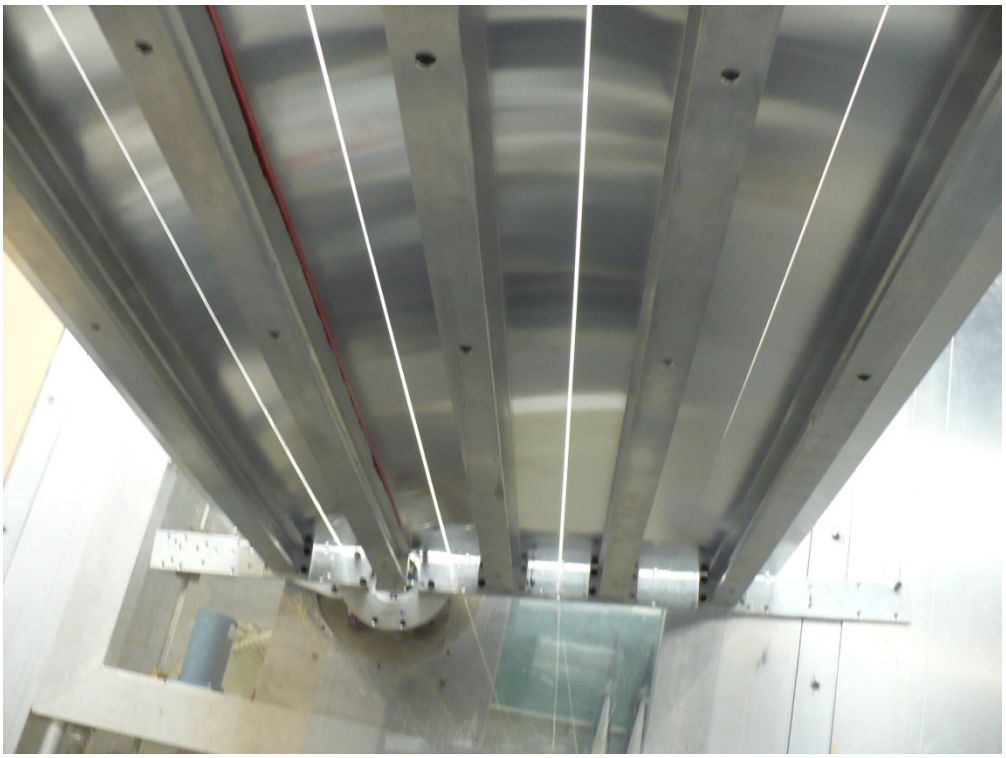

a) INSTRUMENTED I-BEAM AT 2nd POSITION

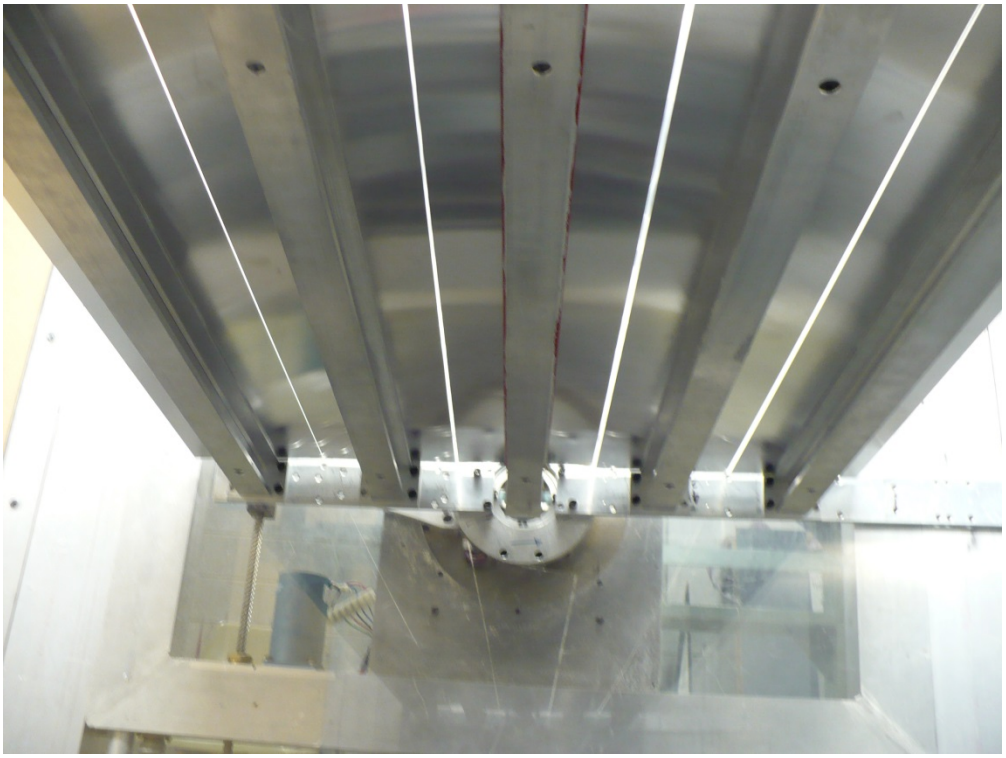

b) INSTRUMENTED I-BEAM AT 3rd POSITION

FIGURE 1.22 SECTION MODEL TEST SET-UP – 45-INCH "FLORIDA" I-BEAM, -2% CROSS SLOPE

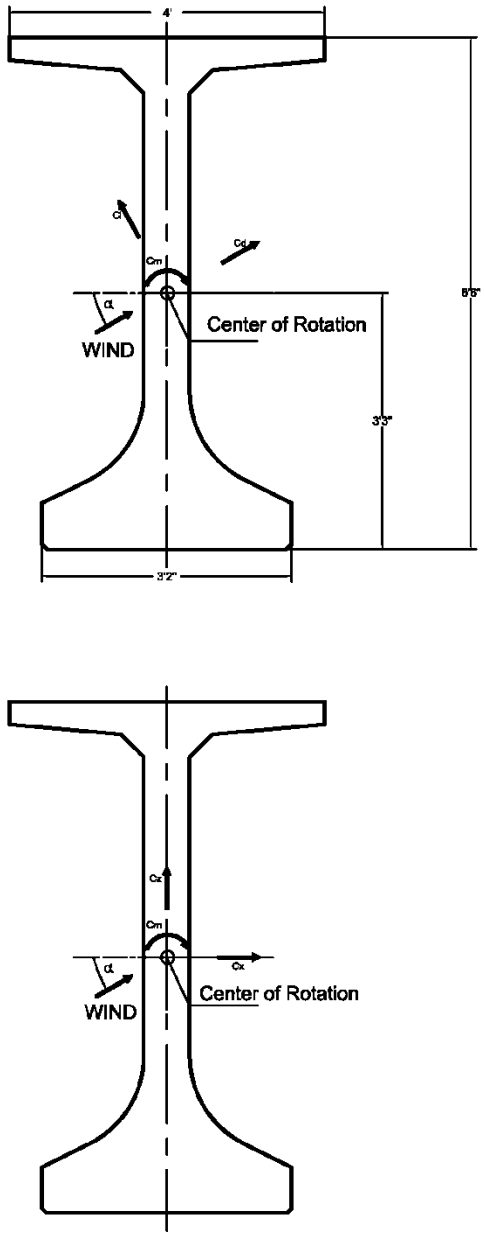

FIGURE 2.1 SIGN CONVENTION OF FORCES – 78-INCH "FLORIDA" I-BEAM

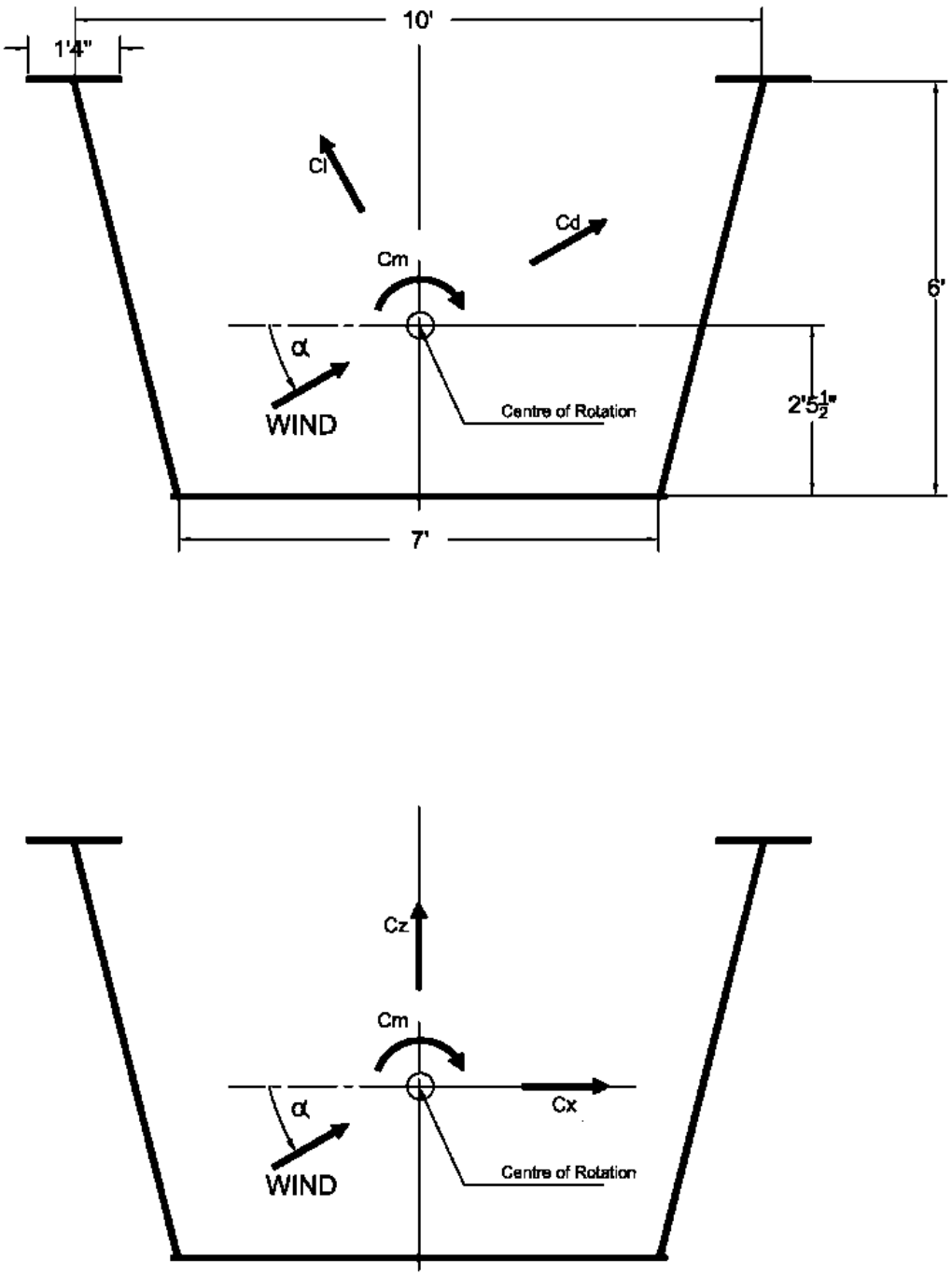

FIGURE 2.2 SIGN CONVENTION OF FORCES – BOX GIRDER

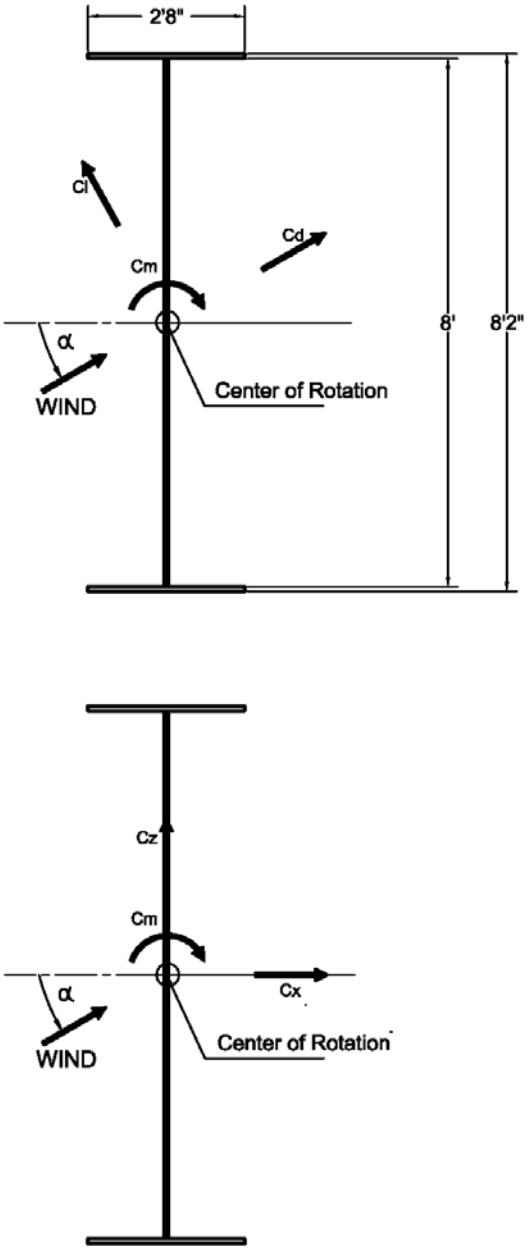

FIGURE 2.3 SIGN CONVENTION OF FORCES – WIDE FLANGE PLATE GIRDER

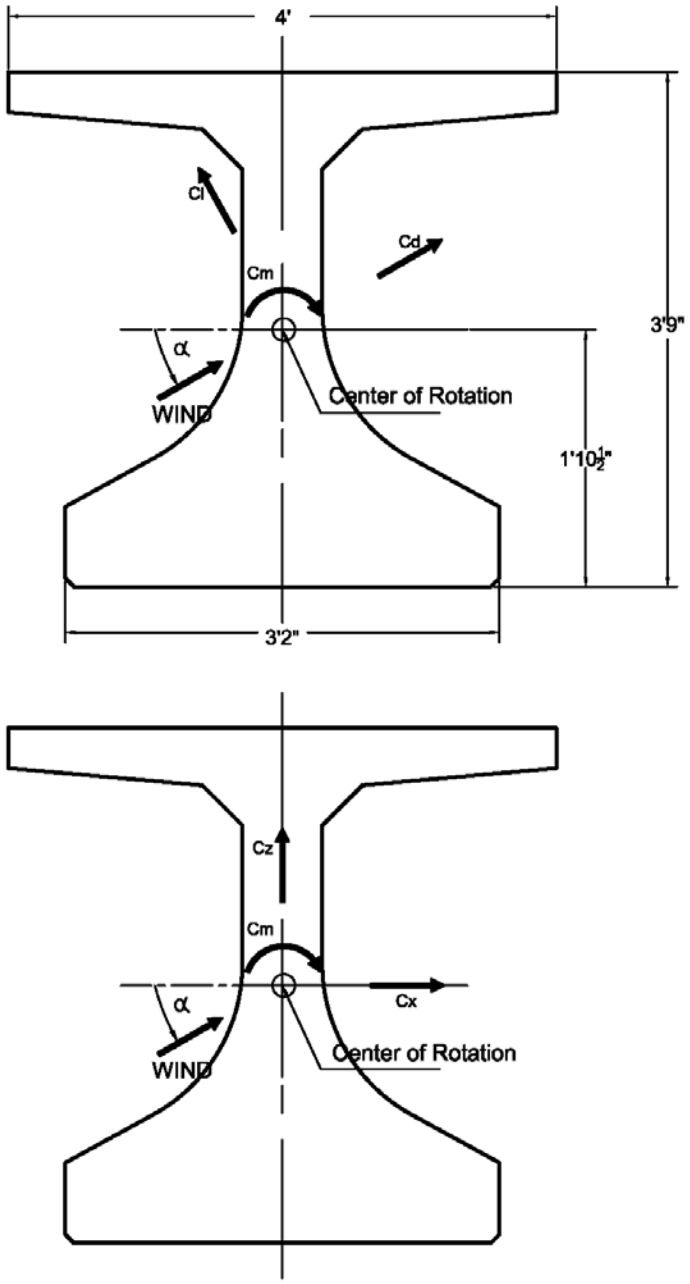

FIGURE 2.4 SIGN CONVENTION OF FORCES – 45-INCH "FLORIDA" I-BEAM

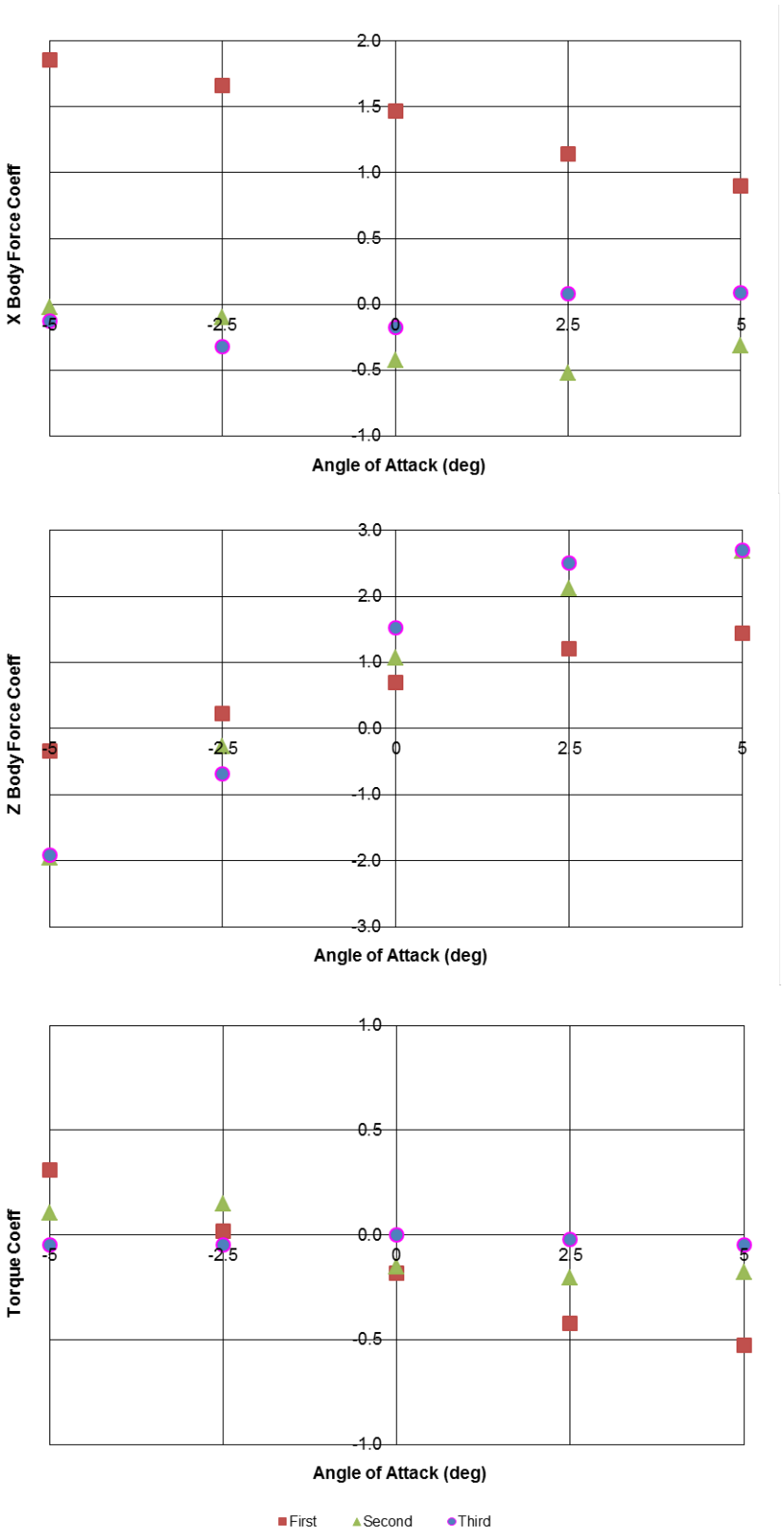

FIGURE 2.5 STATIC FORCE COEFFICIENTS (BODY FORCES) – 78-INCH "FLORIDA" I-BEAMS, -2% CROSS SLOPE, 13FT SPACING, WITHOUT OVERHANG

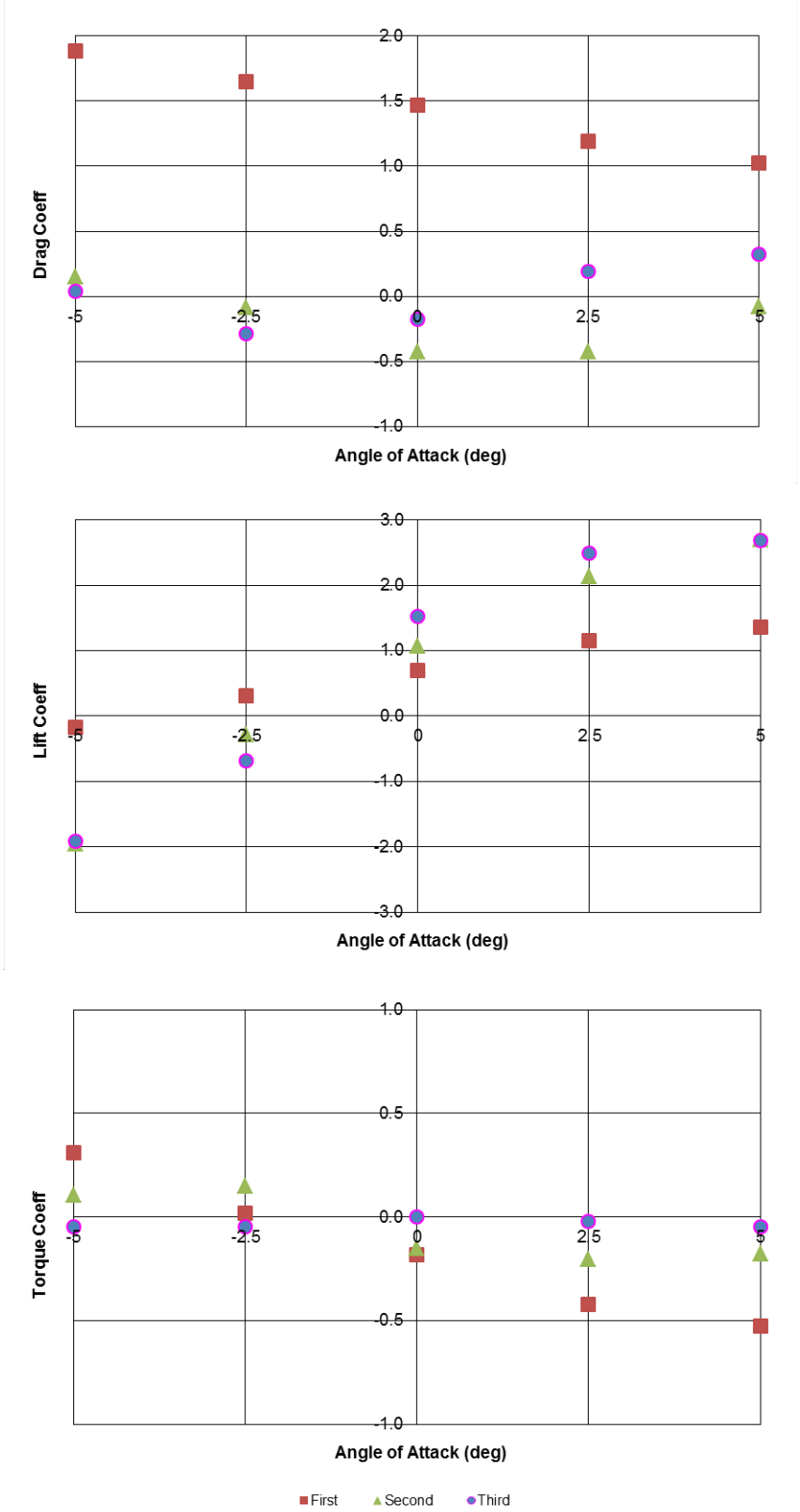

FIGURE 2.6 STATIC FORCE COEFFICIENTS (WIND AXIS FORCES) – 78-INCH "FLORIDA" I-BEAMS, -2% CROSS SLOPE, 13FT SPACING, WITHOUT OVERHANG

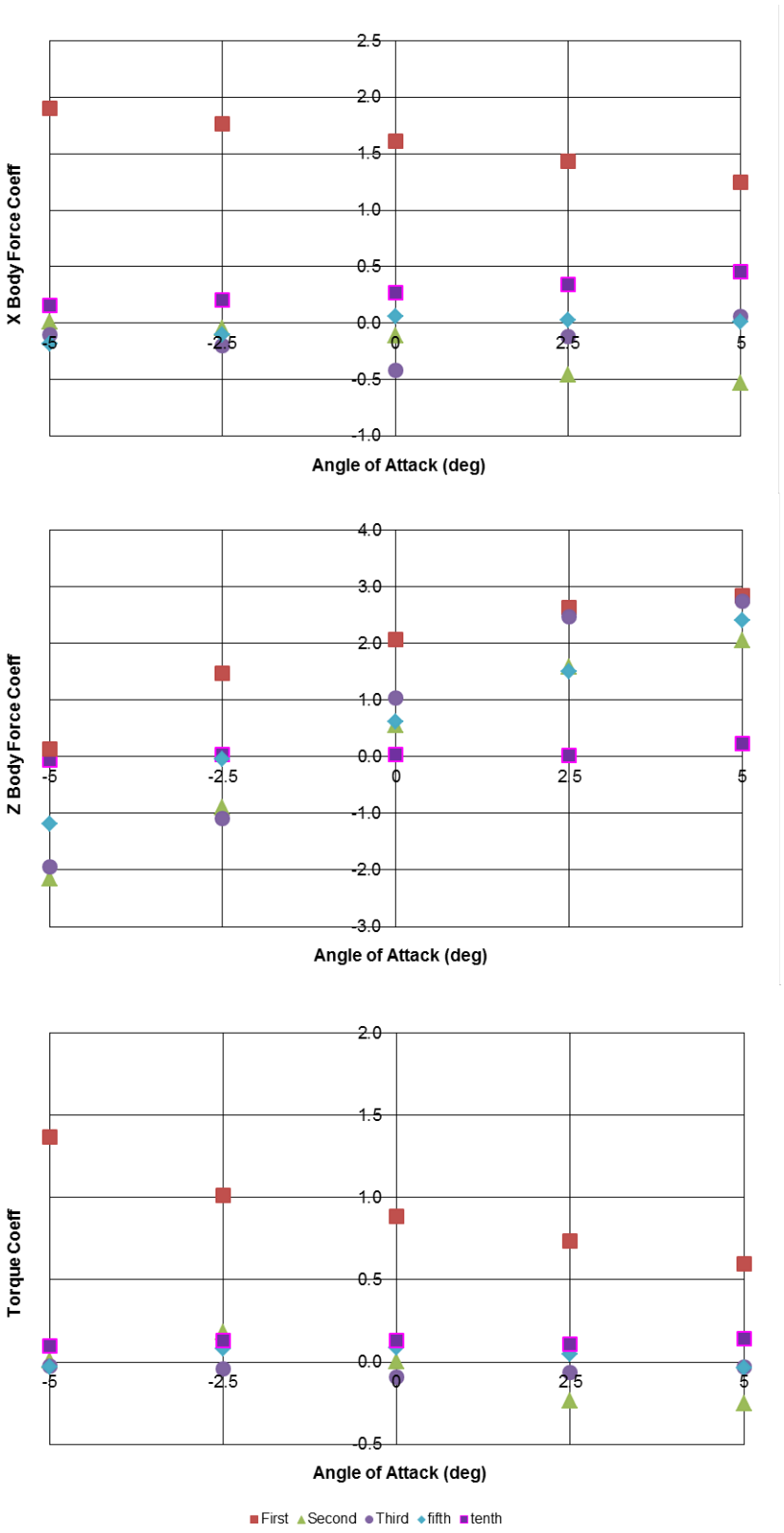

FIGURE 2.7 STATIC FORCE COEFFICIENTS (BODY FORCES) – 78-INCH "FLORIDA" I-BEAMS, -2% CROSS SLOPE, 13FT SPACING, WITH OVERHANG

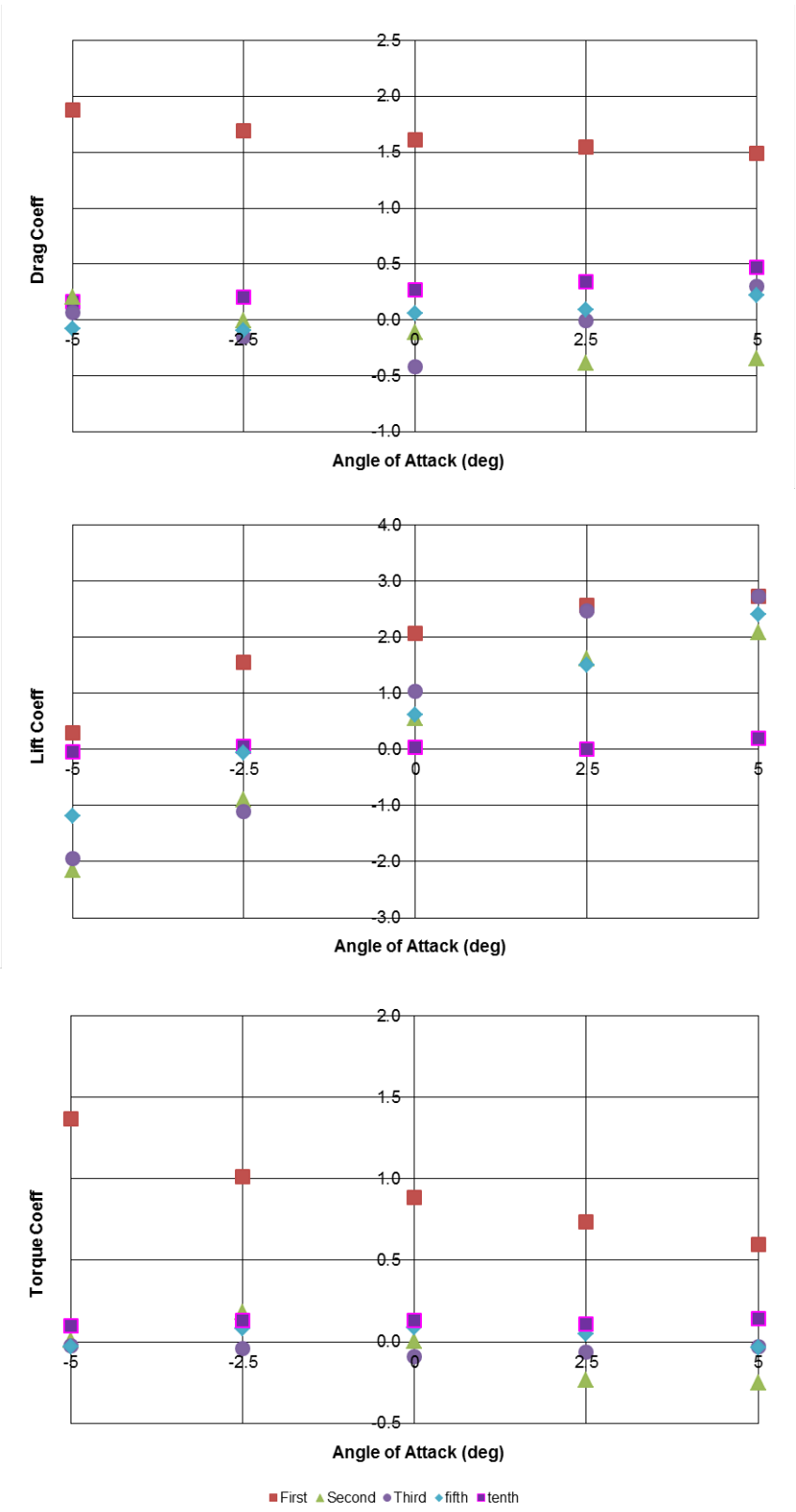

FIGURE 2.8 STATIC FORCE COEFFICIENTS (WIND AXIS FORCES) – 78-INCH "FLORIDA" I-BEAMS, -2% CROSS SLOPE, 13FT SPACING, WITH OVERHANG

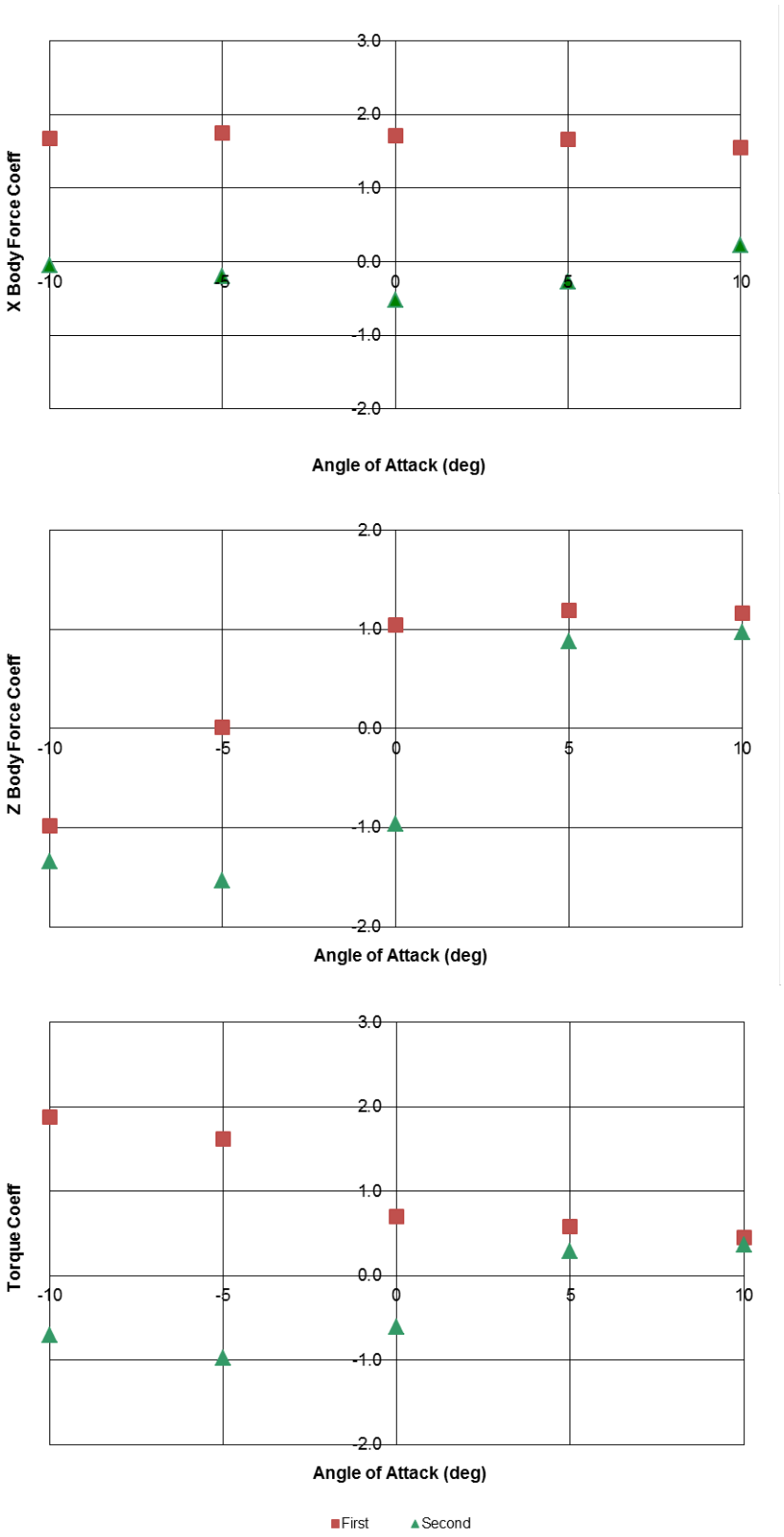

FIGURE 2.9 STATIC FORCE COEFFICIENTS (BODY FORCES) – BOX GIRDER, 0% CROSS SLOPE, 22FT SPACING, WITHOUT OVERHANG

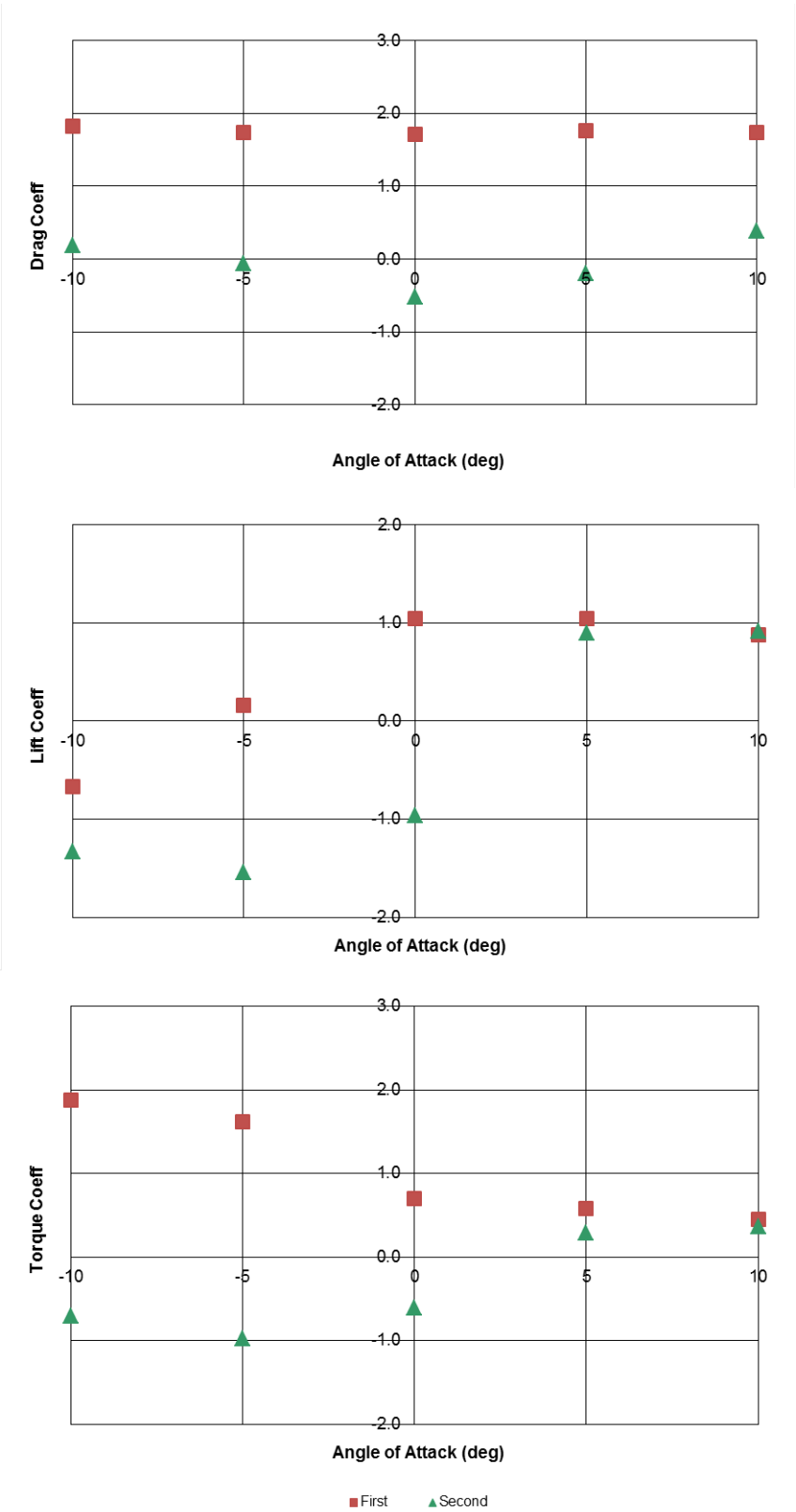

FIGURE 2.10 STATIC FORCE COEFFICIENTS (WIND AXIS FORCES) – BOX GIRDER, 0% CROSS SLOPE, 22FT SPACING, WITHOUT OVERHANG

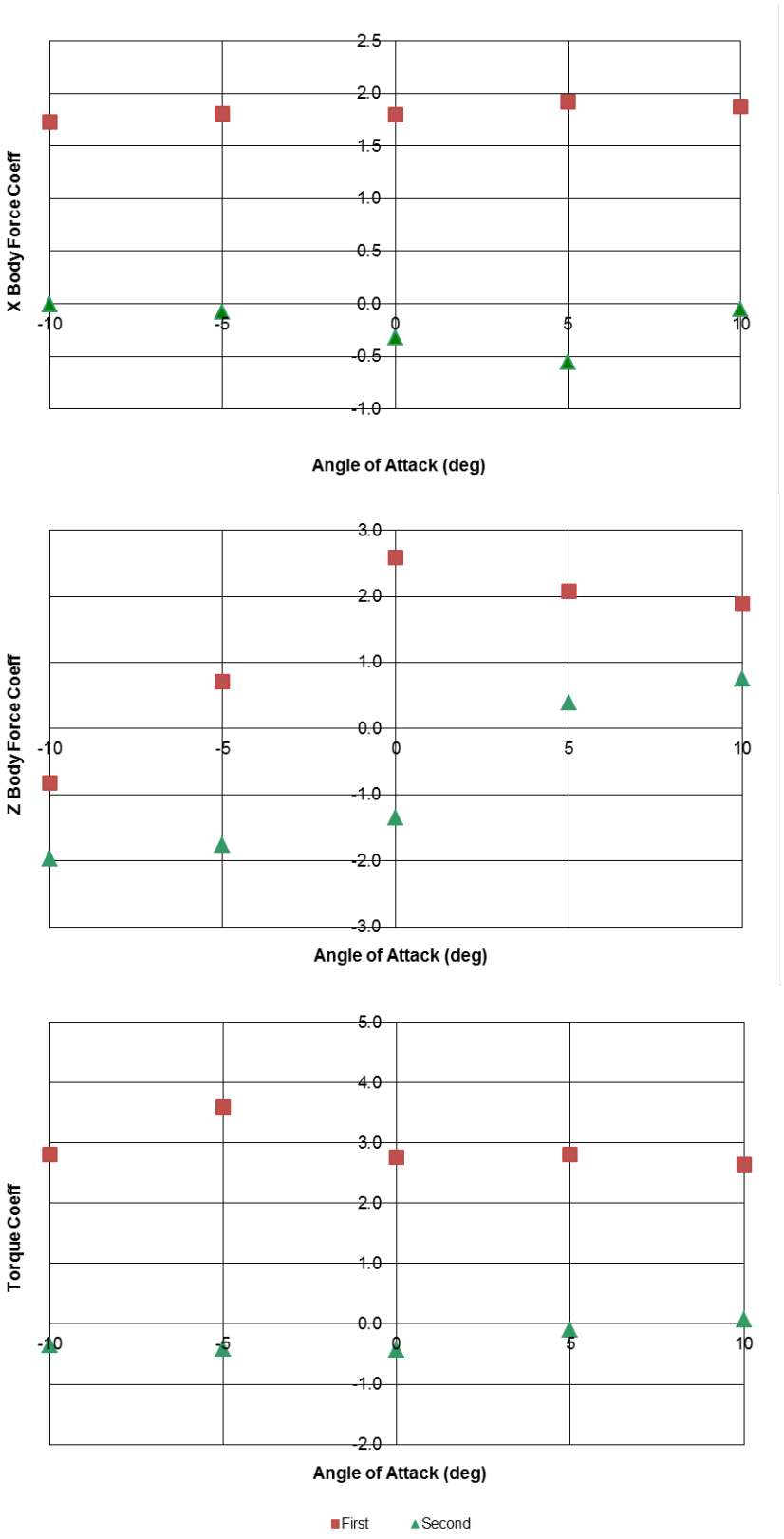

FIGURE 2.11 STATIC FORCE COEFFICIENTS (BODY FORCES) – BOX GIRDER, 0% CROSS SLOPE, 22FT SPACING, WITH OVERHANG

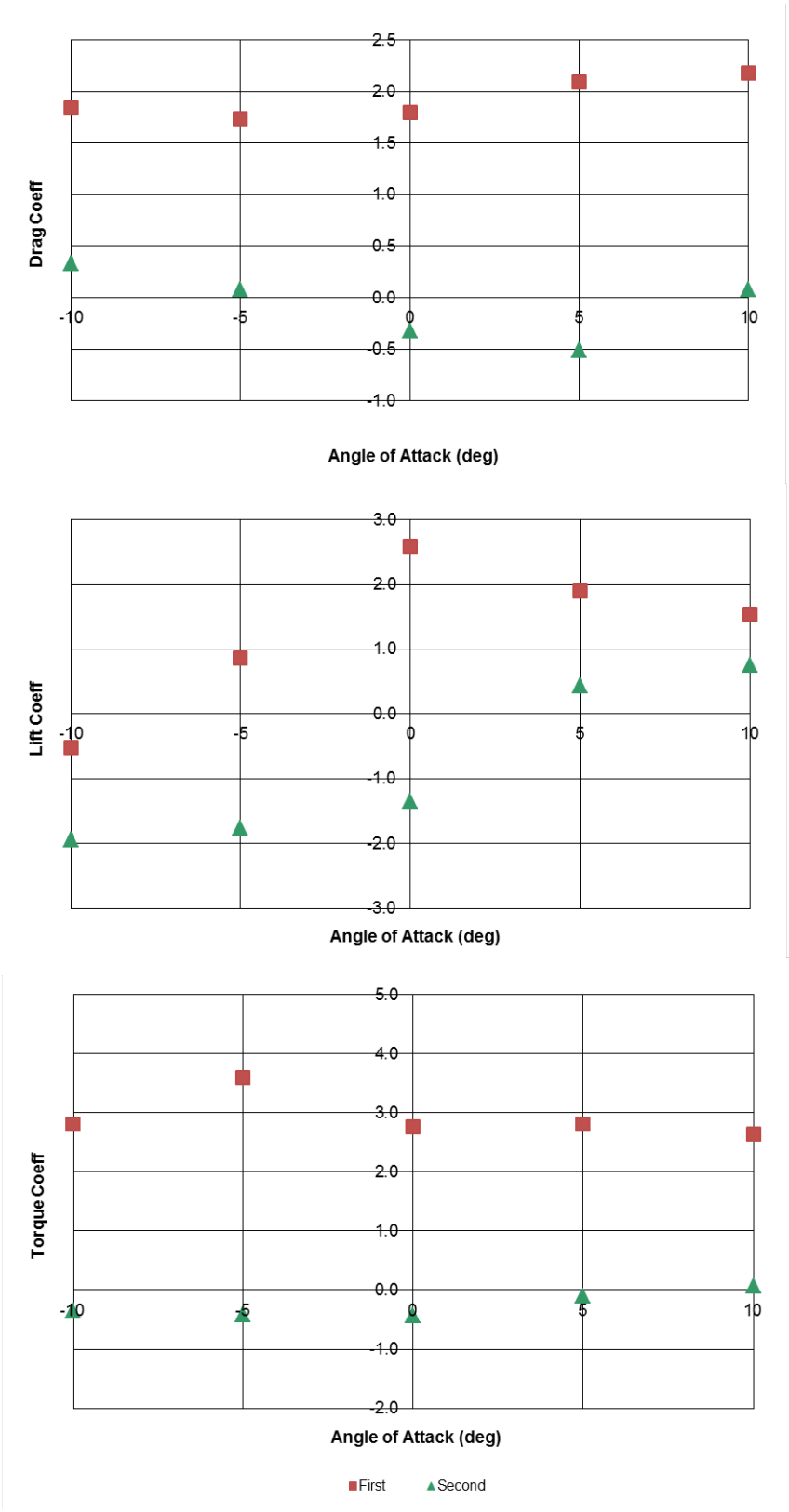

FIGURE 2.12 STATIC FORCE COEFFICIENTS (WIND AXIS FORCES) – BOX GIRDER, 0% CROSS SLOPE, 22FT SPACING, WITH OVERHANG

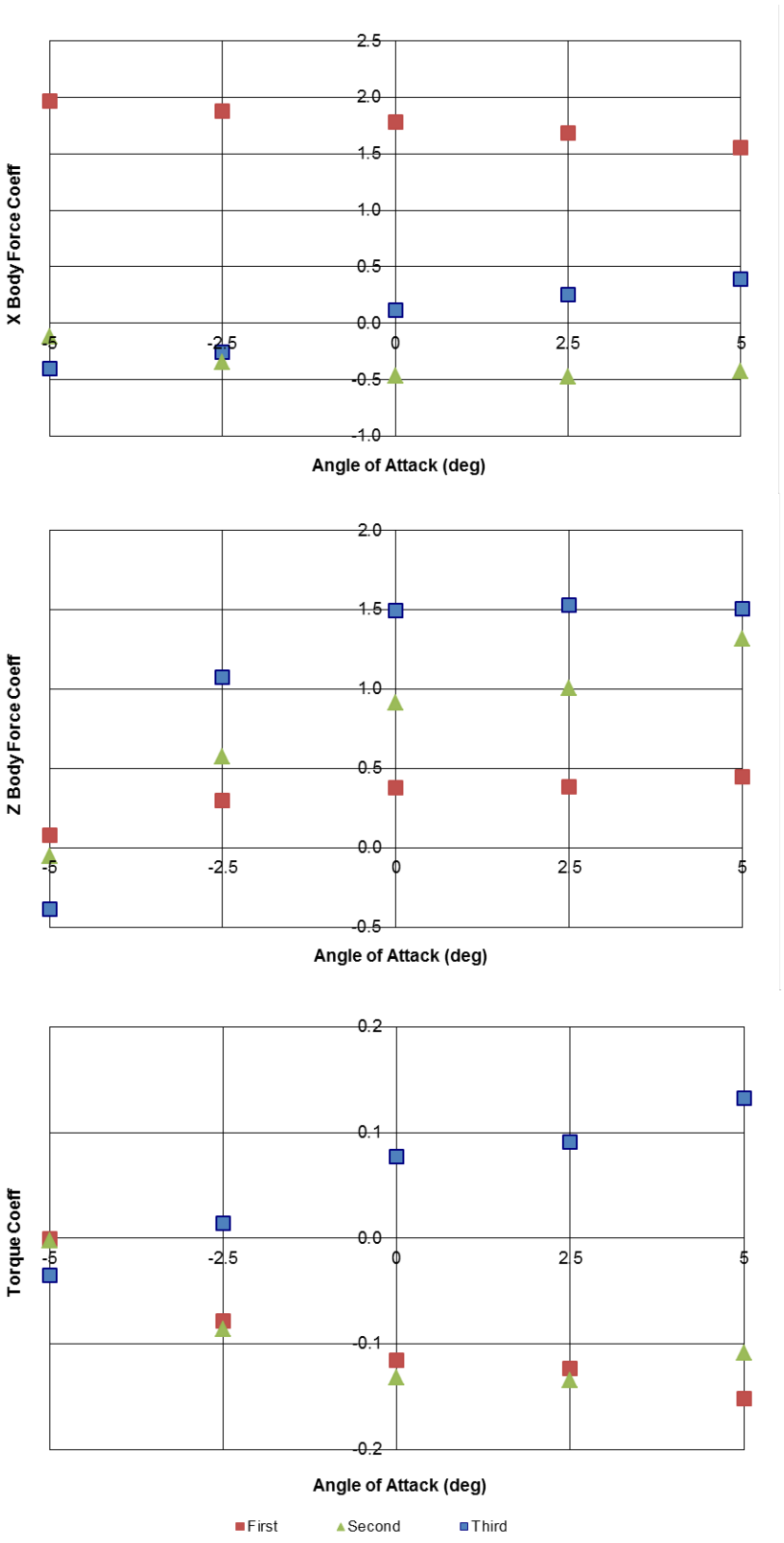

FIGURE 2.13 STATIC FORCE COEFFICIENTS (BODY FORCES) – WIDE FLANGE GIRDER, -8% CROSS SLOPE, 14FT SPACING, WITHOUT OVERHANG

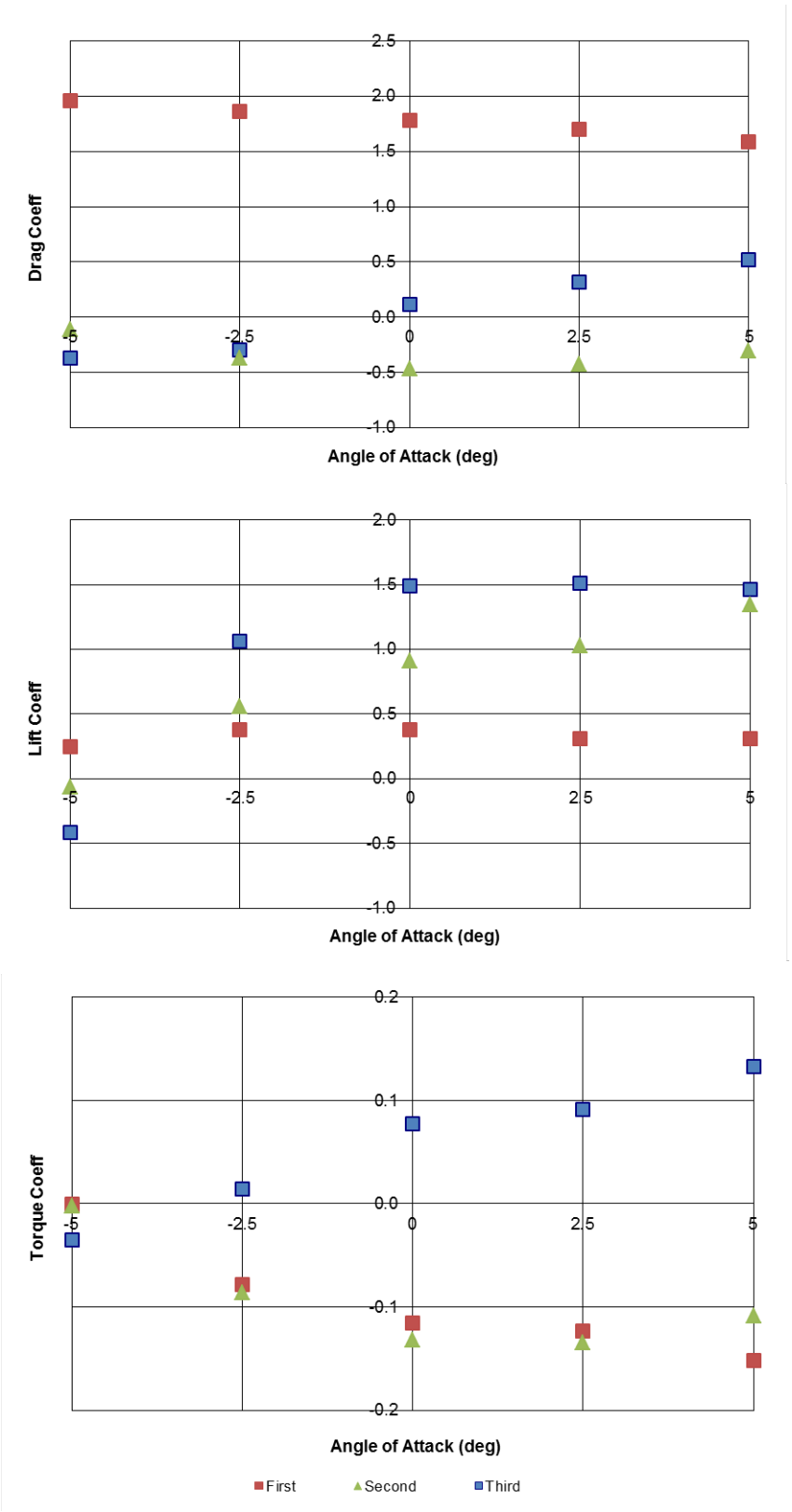

FIGURE 2.14 STATIC FORCE COEFFICIENTS (WIND AXIS FORCES) – WIDE FLANGE GIRDER, -8% CROSS SLOPE, 14FT SPACING, WITHOUT OVERHANG

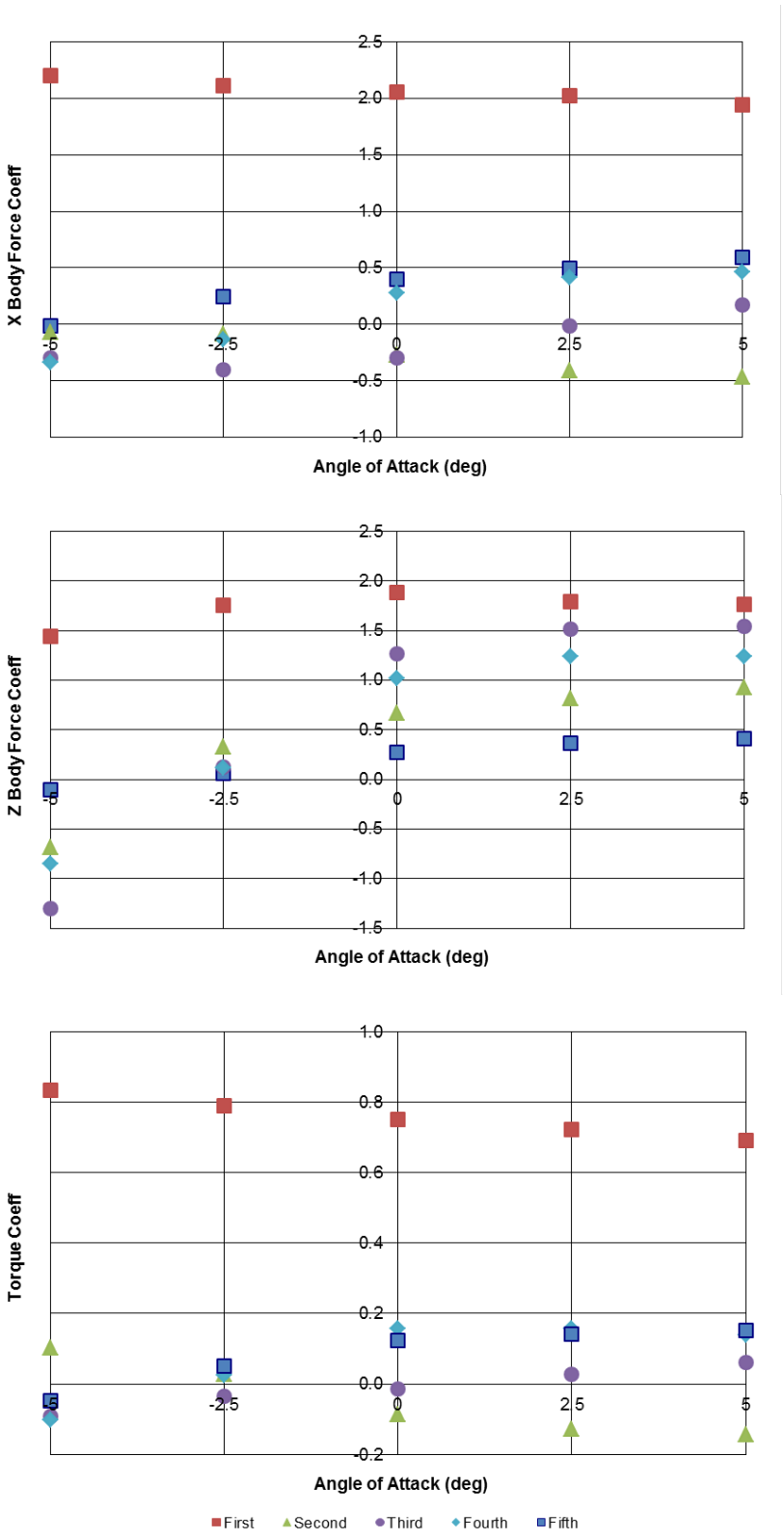

FIGURE 2.15 STATIC FORCE COEFFICIENTS (BODY FORCES) – WIDE FLANGE GIRDER, -8% CROSS SLOPE, 14FT SPACING, WITH OVERHANG

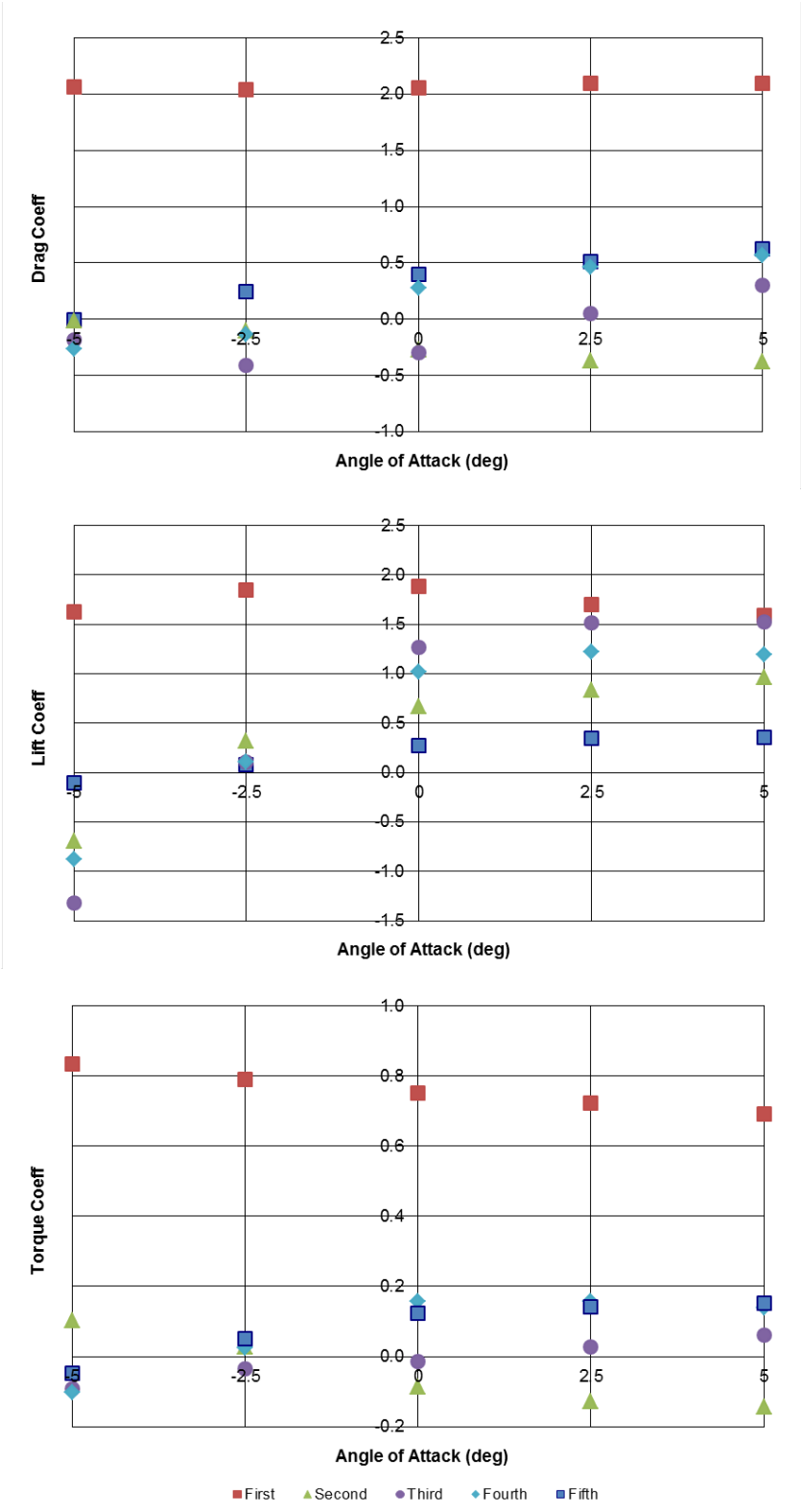

FIGURE 2.16 STATIC FORCE COEFFICIENTS (WIND AXIS FORCES) – WIDE FLANGE GIRDER, -8% CROSS SLOPE, 14FT SPACING, WITH OVERHANG

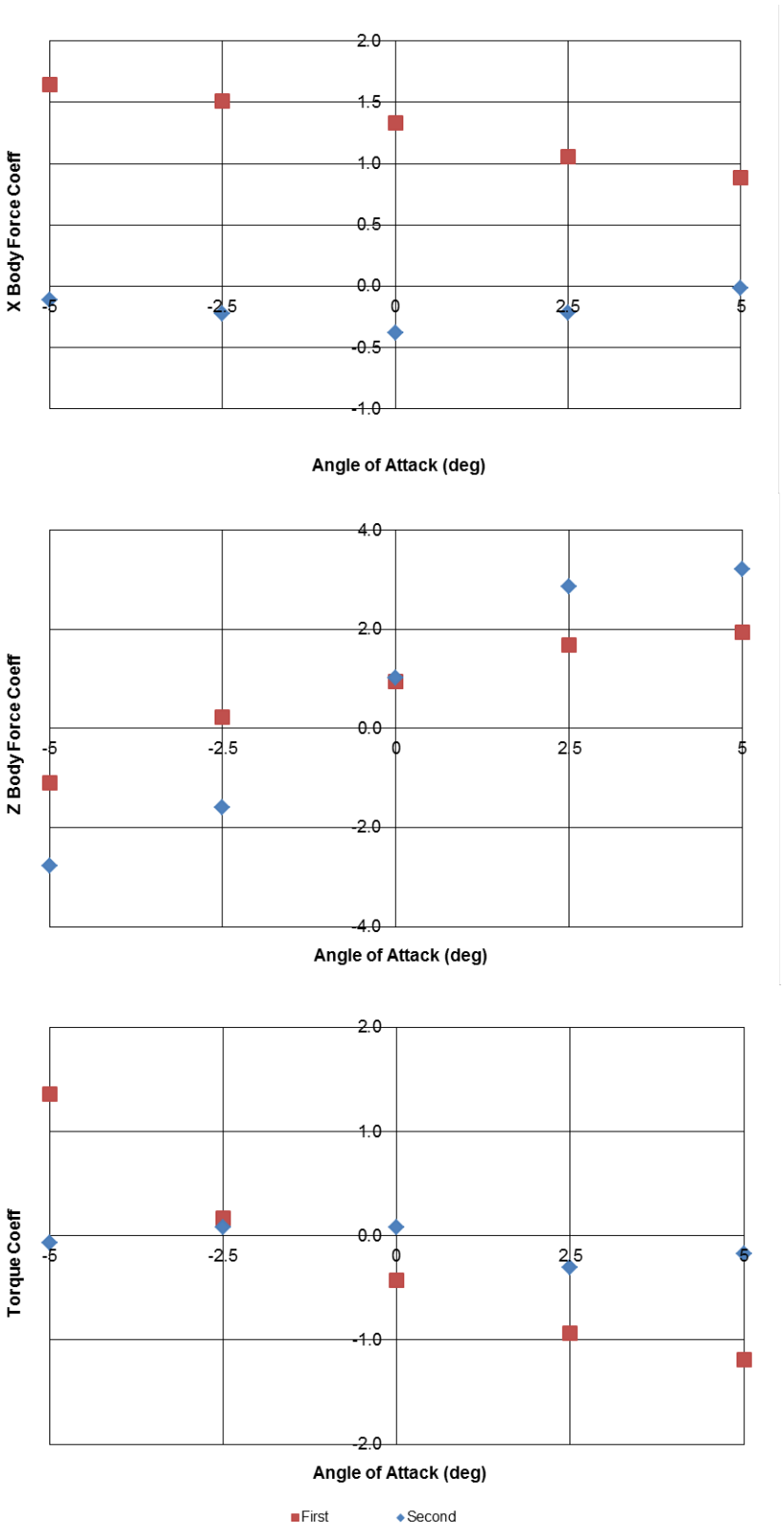

FIGURE 2.17 STATIC FORCE COEFFICIENTS (BODY FORCES) – 45-INCH "FLORIDA" I-BEAMS, -2% CROSS SLOPE, 13FT SPACING, WITHOUT OVERHANG

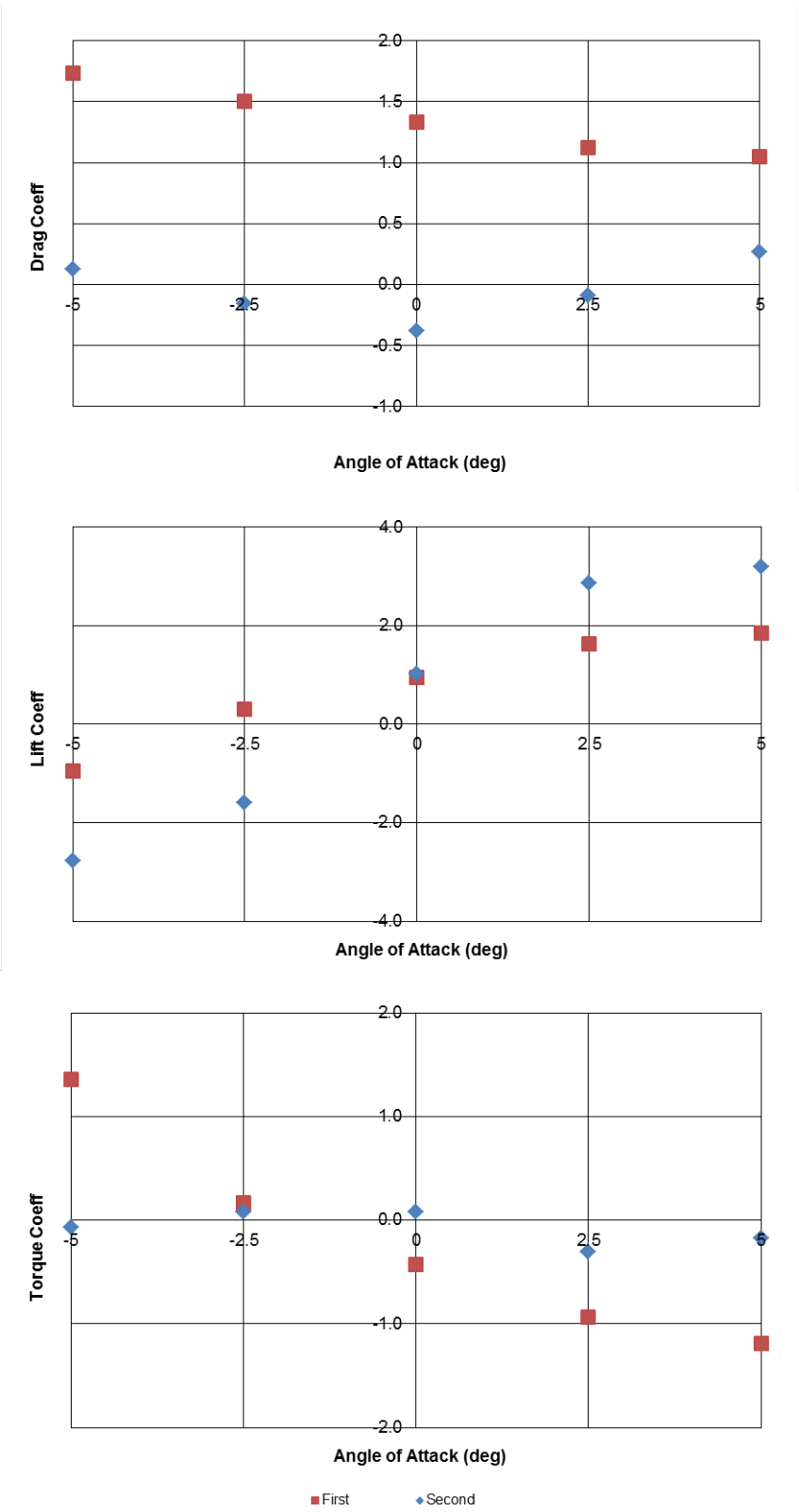

FIGURE 2.18 STATIC FORCE COEFFICIENTS (WIND AXIS FORCES) – 45-INCH "FLORIDA" I-BEAMS, -2% CROSS SLOPE, 13FT SPACING, WITHOUT OVERHANG

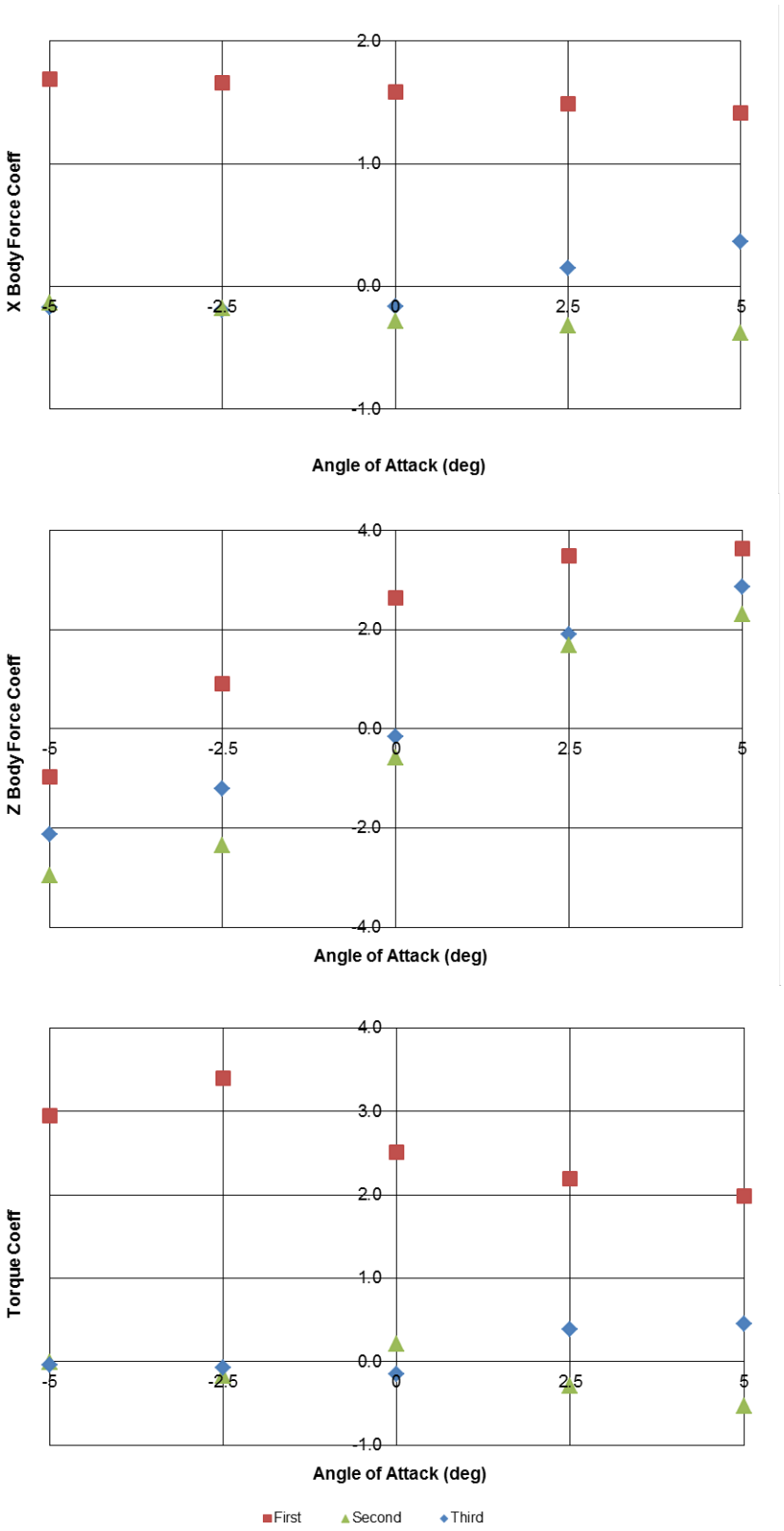

FIGURE 2.19 STATIC FORCE COEFFICIENTS (BODY FORCES) – 45-INCH "FLORIDA" I-BEAMS, -2% CROSS SLOPE, 13FT SPACING, WITH OVERHANG

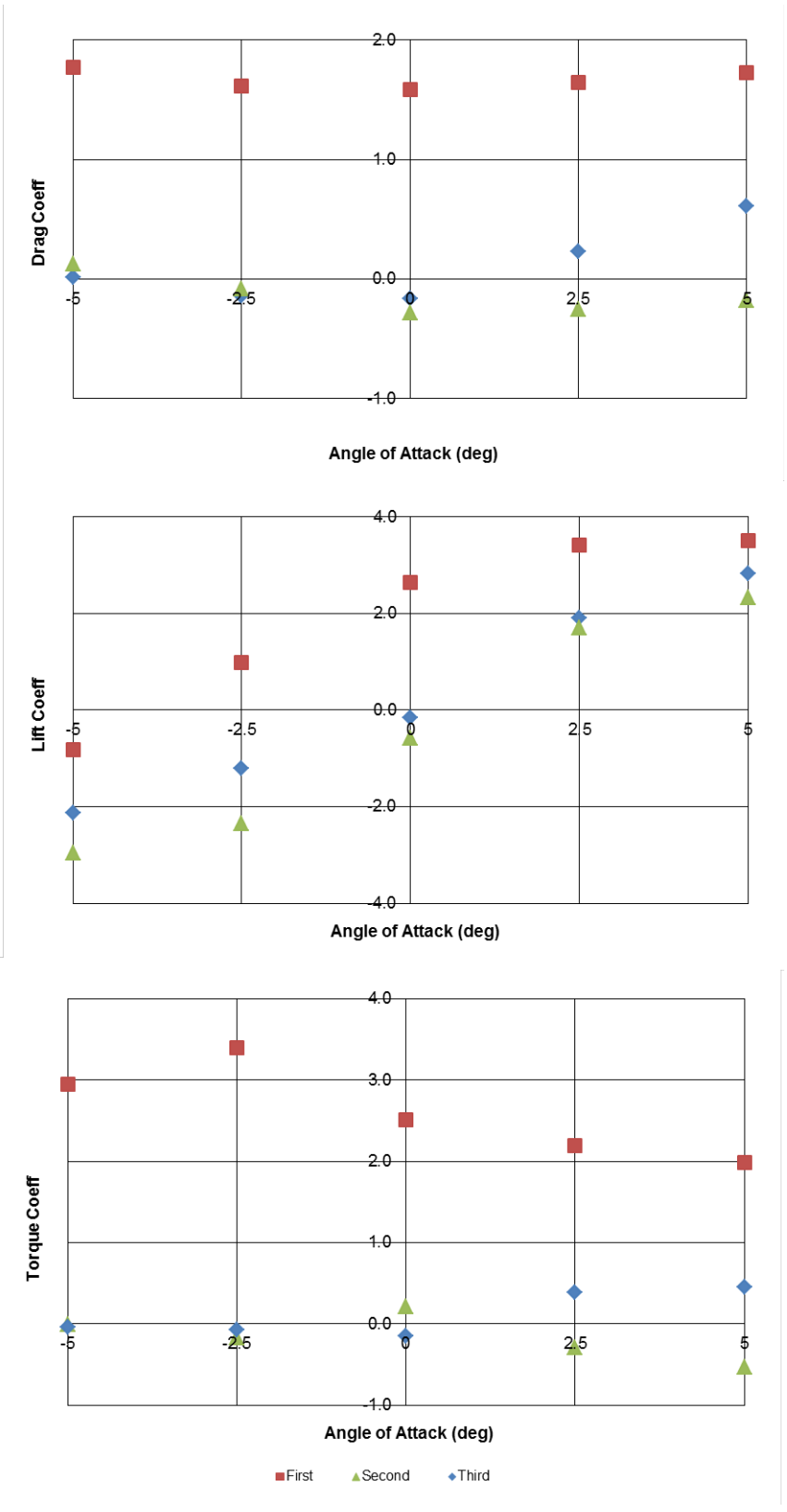

FIGURE 2.20 STATIC FORCE COEFFICIENTS (WIND AXIS FORCES) – 45-INCH "FLORIDA" I-BEAMS, -2% CROSS SLOPE, 13FT SPACING, WITH OVERHANG

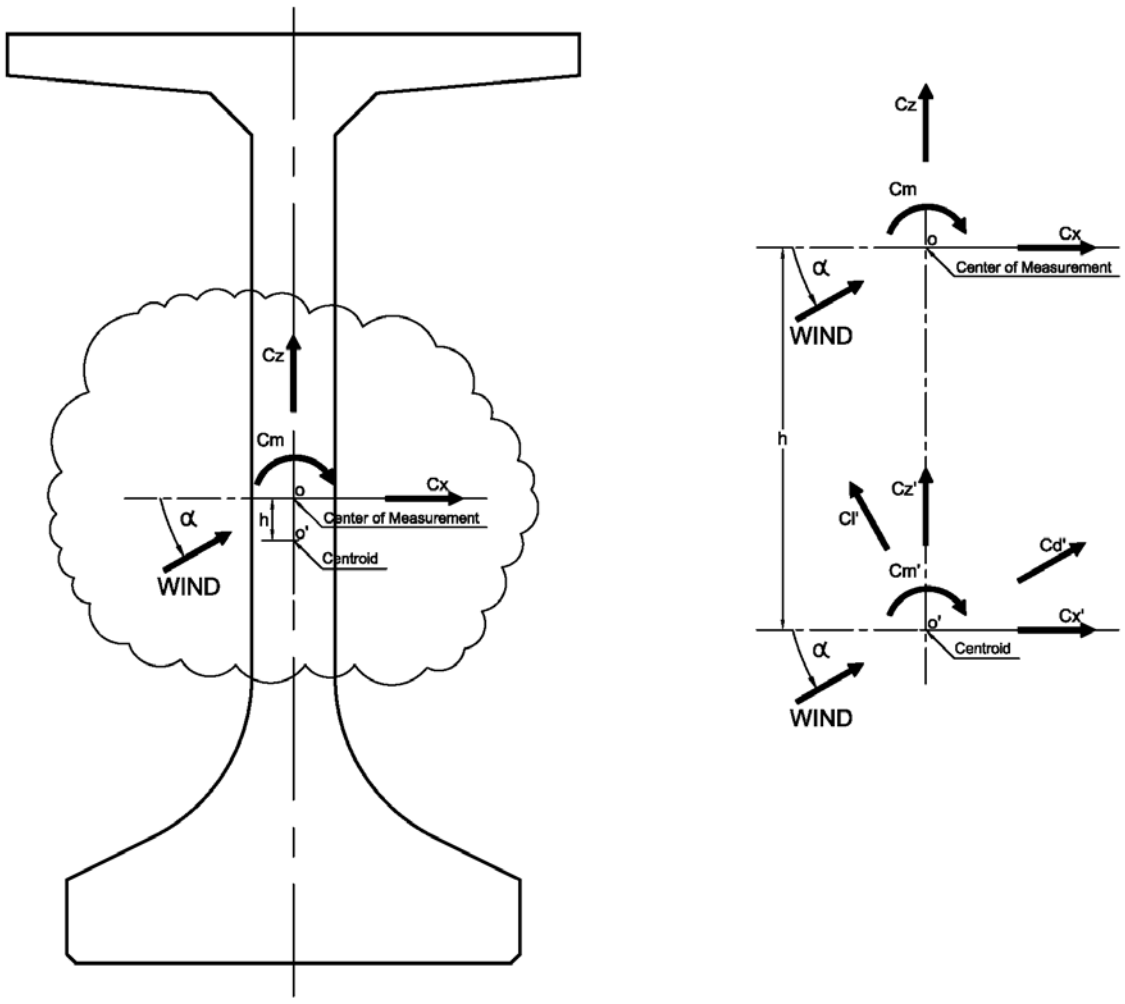

FIGURE 2.21 SIGN CONVENTION OF FORCES – CENTROID LOCATION